Louvain Drug Research Institute

Pharmaceutics and Drug Delivery

Targeted chitosan-based delivery systems of siRNA

Héloïse Ragelle

Thèse présentée en vue de l'obtention du grade de
Docteur en Sciences Biomédicales et Pharmaceutiques

Promoteur : Véronique Préat

Co-Promoteur : Gaëlle Vandermeulen

2013

Au terme de ce travail, je tiens à remercier…

Mon promoteur, le Professeur Véronique Préat, pour les discussions scientifiques, son soutien constant et la confiance qu'elle m'a témoignée tout au long de ce travail de recherche.

Mon co-promoteur et amie, le Docteur Gaëlle Vandermeulen, auprès de qui j'ai énormément appris, toujours disponible, de bonne humeur et d'excellent conseil.

Le Professeur Olivier Feron, de m'avoir soutenue à la fois dans mon travail de recherche et dans mes projets à l'étranger.

Kevin Vanvarenberg pour son aide, son efficacité et son professionnalisme lors de la réalisation des expériences.

Les docteurs Caroline Bouzin et Cyril Corbet pour leurs judicieuses remarques et leur compétence.

Le Professeur Jacqueline Marchand et Vincent Pourcelle pour leur précieuse collaboration, leur temps et les discussions, toujours très bénéfiques.

Le Professeur Christine Jérôme, membre du Jury et le Docteur Raphaël Riva de nous avoir fait bénéficier de leur expertise concernant la synthèse du chitosan et de leur disponibilité pour répondre à mes questions.

The Professeur Camilla Foged, member of the thesis committee, for having hosting me in her laboratory in Copenhagen. This was a rewarding and great experience. Many thanks to Stefano Colombo for the learning of the RT-PCR technique and his wise advices.

Les Professeurs Géraldine Piel, Jean-Pierre Benoit et Bernard Gallez d'avoir accepté de faire partie de mon Jury de thèse. Merci pour les remarques et les discussions qui m'ont permis d'améliorer ce travail.

Murielle Callier pour son aide inestimable dans la mise en page de ce manuscrit et sa gentillesse.

Je tiens à remercier de tout cœur toute l'équipe FARG auprès de qui j'ai passé ces quatre belles années. Un grand merci à tous pour cette bonne ambiance qui règne dans le laboratoire et pour tous les moments passés ensemble. Un merci particulier à Salomé, Régis, Nicolas, Julie, Patrick pour leur amitié et leur complicité ; à Bernard, Jean-Pierre et Nathalie L pour leur bonne humeur, leur aide et leur soutien quotidiens ; aux anciens Edith, Claudia et Eduardo ; à Anne pour ses conseils et enfin à Cristina, Fabienne, Pauline, Damien, Nathalie S, Kiran, Sravan, Julian, Rita que j'ai eu la chance de croiser au cours de mes années de thèse.

Merci à mes parents et mon frère pour leurs encouragements et leur soutien. Et bien sûr à Maxime, d'avoir toujours été là.

LIST OF ABBREVIATIONS

AFM	:	atomic force microscopy
ApoB	:	apolipopotein B
ASCT2	:	amino acid transporter 2
CD	:	cyclodextrin
CPP	:	cell-penetrating peptide
DD	:	deacetylation degree
DLS	:	dynamic light scattering
DNA	:	deoxyribonucleic acid
dsRNA	:	double stranded RNA
DsiRNA	:	Dicer substrate siRNA
ECM	:	extracellular matrix
e.g.	:	exempli gratia
EGF(R)	:	epidermal growth factor (receptor)
EGFP	:	enhanced green fluorescent protein
endo-siRNA	:	endogenous siRNA
EphA2	:	erythropoietin-producing human hepatocellular receptor
EPR	:	enhanced permeability and retention
FDA	:	food and drug administration
FGF	:	fibroblast growth factor
FFS	:	fluorescence fluctuation spectroscopy
GFP	:	green fluorescent protein
GRAS	:	generally recognized as safe
HA	:	hyaluronic acid
IC_{50}	:	half-maximal inhibitory concentration
i.e.	:	id est

IFN	:	interferon
Ig	:	immunoglobulin
IL	:	interleukine
I.V.	:	intravenous
KSP	:	kinesin spindle protein
LD_{50}	:	lethal dose, 50% or median lethal dose
LDL	:	low density lipoprotein
LNA	:	locked nucleic acid
LNP	:	lipid nanoparticles
MAA	:	methacrylic acid
MCT	:	monocarboxylate transporter
MDM2	:	murine double minute
MDR	:	multiple-drug resistant
miRNA	:	micro RNA
mRNA	:	messenger RNA
MW	:	molecular weight
NC	:	nanocarrier
NP	:	nanoparticle
Nt	:	nucleotide
OTEs	:	off-target effects
PAMAM	:	polyamidoamine
PDGF(R)	:	plateled derived growth factor (receptor)
PDI	:	polydispersity index
PEG	:	poly(ethylene glycol)
PEI	:	poly(ethylene imine)
PGA	:	poly(γ glutamic acid)
piRNA	:	piwi-interacting RNA

PKN3	:	protein kinase N3
PLGA	:	poly(lactide-co-glicolide)
PLK1	:	polo-like kinase 1
PLL	:	poly-L-lysine
PLR	:	poly-L-arginine
pSP	:	phosphorylatable short peptide
RFP	:	red fluorescent protein
RGD	:	arginine-glycine-aspartic acid
RGDp	:	RGD peptidomimetic
RIG-1	:	retinoic acid-inducible gene 1
RISC	:	RNA-induced silencing complex
RNA	:	ribonucleic acid
RNAi	:	RNA interference
RT-qPCR	:	reverse transcription quantitative polymerase chain reaction
shRNA	:	short hairpin RNA
siRNA	:	small interfering RNA
SNALP	:	stable nucleic acid-lipid nanoparticles
SPT	:	single particle tracking
TLR	:	toll-like receptor
TMC	:	trimethyl chitosan
TNF-α	:	tumor necrosis factor α
TPP	:	tripolyphosphate
UNA	:	unlocked nucleic acid
UTR	:	untranslated region
VEGF(R)	:	vascular endothelial growth factor (receptor)

FOREWORD

The mechanism of RNA silencing has first been evidenced in plants [1]. Then, studies on the nematode *Caenorhabditis elegans* identified a similar phenomenon, called RNA interference (RNAi). RNAi was described as a naturally occurring mechanism that induced sequence-specific post-transcriptional gene silencing and that was mediated by long double stranded RNAs [2]. Few years later, the administration of exogenous small interfering RNA (siRNA) of 21-22 nucleotides in mammalian cells successfully induced the silencing of endogenous and heterologous genes [3].

This discovery has created new perspectives for the development of gene medicines, especially for the treatment of diseases that are characterized by an overexpression of specific proteins. The RNAi technology promised the rapid development of highly specific therapeutics that could theoretically silence any gene, thus overcoming the issue of undruggable targets. However, after the initial enthusiasm, it clearly appeared that the delivery of small RNAs molecules required precisely engineered nanosystems. Although recent progresses have been made in the understanding of the siRNA delivery modalities, as well as in the design of siRNA delivery systems, the translational development of RNAi-based drugs remains challenging and researchers are still looking for powerful delivery approaches.

This work investigated the biopolymer chitosan as the basis material for the elaboration of a siRNA delivery system and was done in collaboration with different academic and industrial partners. The group of the Professor Marchand-Brynaert *(Molecules, Solid and Reactivity, Institute of Condensed Matter and Nanosciences, Université Catholique de Louvain)* was involved in the synthesis and the characterization of the targeting moieties. The synthesis of the copolymer *i.e.* the PEGylated chitosan was performed in the laboratory of the Professor Jérôme *(Center for Education and Research on Macromolecules, Université de Liège)*. The industrial company Kitozyme was in charge of providing chitosan batches derived from fungal sources.

Our work was first to formulate the nanoparticles for the delivery of siRNA based on the copolymer. This implies the physico-chemical characterization of the nanoparticles as well as their optimization in order to meet the requirements of a potential future I.V. administration. Secondly, we investigated and characterized the *in vitro* biological activity of the nanoparticles, especially in terms of their gene silencing efficiency and their cellular internalization. We worked in close collaboration with the group of the Professor Feron *(Angiogenesis and Cancer Research Lab, Pole of Pharmacology and Therapeutics, Université Catholique de Louvain)*, for its expertise in tumor models and therapeutic targets.

[1] C. Napoli, C. Lemieux, and R. Jorgensen, Introduction of a Chimeric Chalcone Synthase Gene into Petunia Results in Reversible Co-Suppression of Homologous Genes in trans, Plant Cell, 2 (1990) 279-289.

[2] A. Fire, S. Xu, M. K. Montgomery, S. A. Kostas, S. E. Driver, and C. C. Mello, Potent and specific genetic interference by double-stranded RNA in Caenorhabditis elegans, Nature, 391 (1998) 806-811.

[3] S. M. Elbashir, J. Harborth, W. Lendeckel, A. Yalcin, K. Weber, and T. Tuschl, Duplexes of 21-nucleotide RNAs mediate RNA interference in cultured mammalian cells, Nature, 411 (2001) 494-498.

TABLE OF CONTENTS

CHAPTER I.
INTRODUCTION

TABLE OF CONTENTS

I. RNA INTERFERENCE

I.1. AN INTRINSIC NATURAL MECHANISM

The discovery of RNA interference (RNAi) in 1998 revolutionized the understanding of gene regulation. RNAi is a fundamental pathway in eukaryotic cells in which a short piece of RNA blocks the translation or induces the destruction of mRNA with sequence complementarities, inhibiting the production of the corresponding protein [1]. This mechanism allows the regulation of gene networks and biological processes and is mediated by small RNAs. In animals, three types of small RNA have been described: micro RNA (miRNA), small interfering RNA (siRNA) and piwi-interacting RNA (piRNA).

Higher eukaryotes contain a few hundred genes that encode miRNAs. In the cell nucleus, long primary hairpin miRNA transcripts (pri-miRNA) are processed by an RNase class III nuclease Drosha into a 70 nucleotide (nt) stem-loop structure called the pre-miRNA that lacks perfect Watson-Crick complementarity. Subsequently, the pre-miRNA are exported by exportin-5 to the cell cytoplasm, where RNase III Dicer removes the loop, producing mature double-stranded miRNA of 21-23 nt with 2 nt 3'-overhangs. The miRNA binds to a multifunctional protein complex called RNA-induced silencing complex (RISC) and guides the complex to a specific region in the targeted messenger RNA (mRNA), called the 3' untranslated region (UTR) (Fig. 1). The antisense strand (or guide strand) is implicated in mRNA binding, while the sense strand (or passenger strand) is cleaved following RISC binding by a helicase associated with RISC. Nucleotides 2-7 from the 5'-end of the antisense strand, also called the seed region, are responsible for hybridizing to target mRNA with partial complementarity. As a result, translation arrest or mRNA destabilization occurs [2]. Each miRNA possesses multiple mRNA targets and leads to the silencing of a large variety of genes. The miRNA have been found in all tissues and regulate more than 30% of the genes in mammals. Some genes are more susceptible to miRNA regulation than others. For example, genes implicated in basic cellular processes exhibit short 3' UTRs or the loss of miRNA-binding sites, thus avoiding or limiting miRNA regulation. In contrast, enrichment for miRNA sites has been shown in genes involved in developmental processes, suggesting that miRNAs may improve the fitness of the organism [3]. Furthermore, the expression of miRNAs is disturbed in cancers, with some being downregulated in tumor tissues, suggesting that they function as tumor suppressors. Conversely, other miRNAs, called oncomiRs, have been shown to act as oncogenes.

Endogenous siRNA (endo-siRNA) are double stranded RNAs that are 19-23 nt in length (7,5 nm) with a 2-base 3'-overhang on each strand [4]. They originate from different genomic sites, such as transposons, pseudogenes or endo-siRNA clusters [5]. Unlike miRNA, their biogenesis does not

involve Drosha [6]. Long double stranded RNA (dsRNA) or hairpin-type dsRNA that are perfectly base-paired are processed by Dicer to produce endo-siRNA. They utilize a similar mechanism to that of miRNA in their binding to the transcript. However, due to the perfect complementarity between the siRNA seed region and the 3'UTR of the target, the catalytic part of RISC, Argonaute 2, is activated, thus leading to the enzymatic cleavage of the target transcript [1]. In contrast to ubiquitous miRNAs, endo-siRNAs are found in specific tissues, such as ovary and somatic tissues. They act as gene regulators and transposon suppressors in the soma and germline [6,7].

The final class of endogenous small RNA are the piwi-interacting RNA (piRNA), which are 24-32 nt in length. They are encoded within cellular genomes and their biogenesis remains unclear. However, it has been demonstrated that they bind to a subtype of Ago proteins called Piwi. They possess an essential role during gametogenesis by suppressing the potentially hazardous mobility of transposons [3]. They were found to collaborate with endo-siRNA to repress transposons in the germline. Mutations of the piwi pathway results in severe effects on fertility [7].

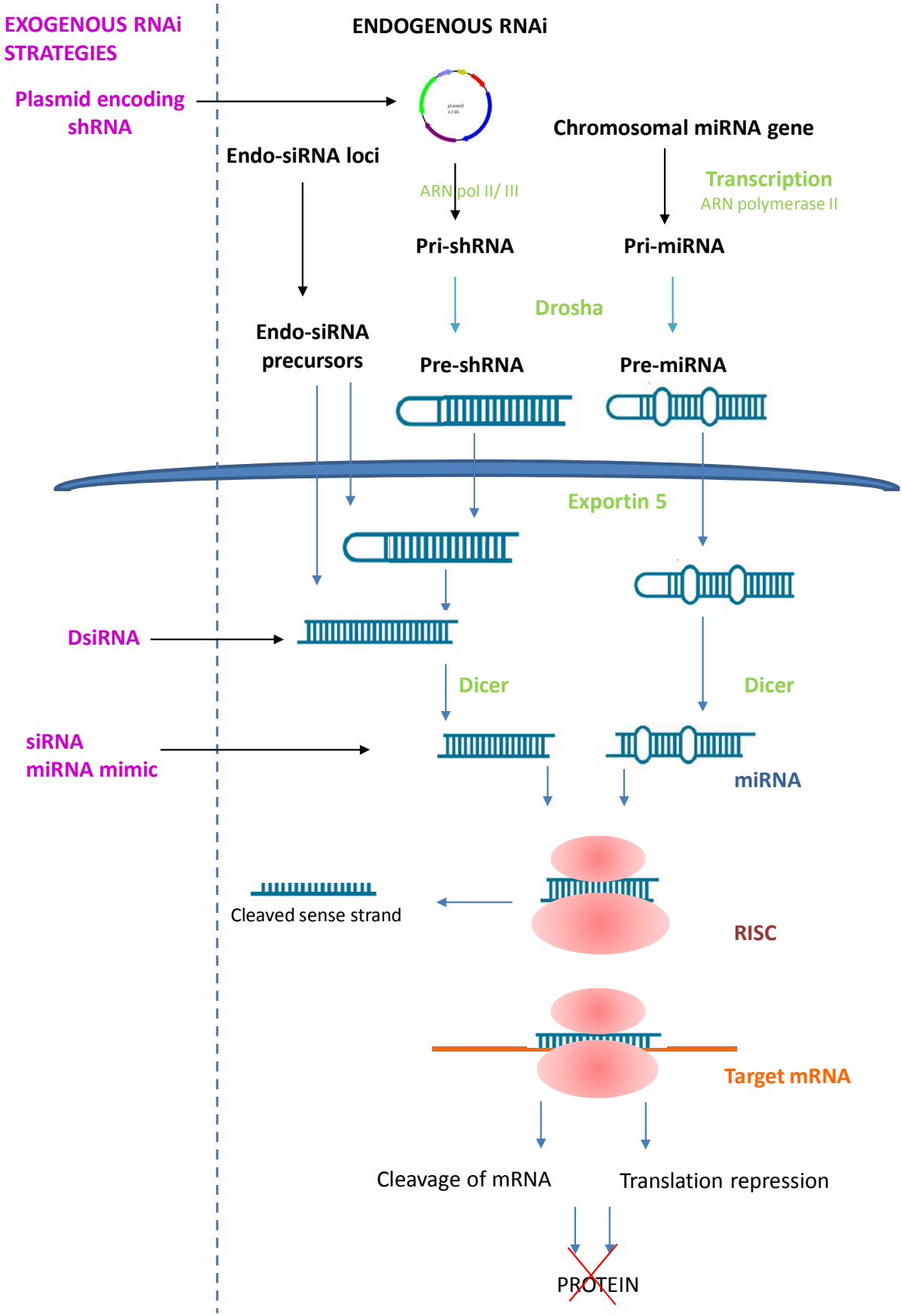

Figure 1: Schematic representation of endogenous and exogenous RNAi mechanisms

I.2. RNAi AS A THERAPEUTIC TOOL: EXOGENOUS STRATEGIES

a. Actors

It was found that synthetic exogenous siRNA can be used to effectively silence mRNA in mammalian cells [8]. This discovery opened the way for new therapeutic applications. Since then, the number of publications has continuously increased (Fig. 2).

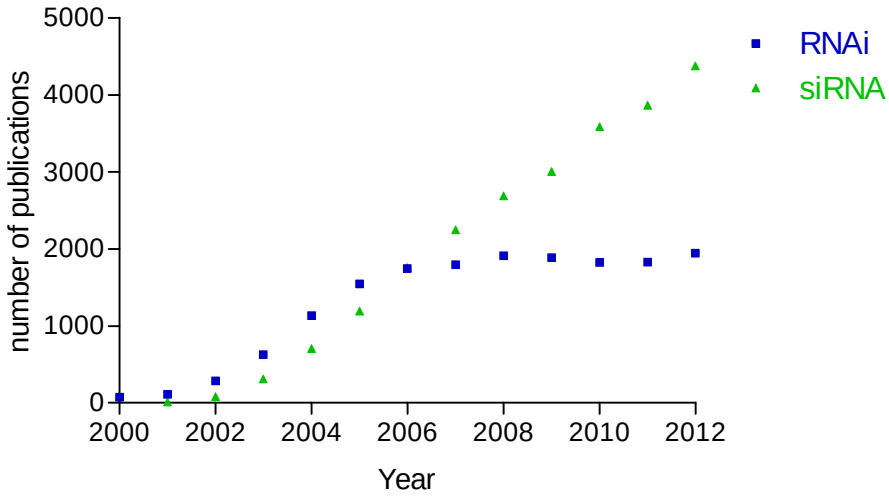

Figure 2: Number of publications for RNAi and siRNA from 2000 to 2012 (Pubmed search in title/abstract)

As the endo-siRNA, synthetic siRNA duplexes are typically 19-23 nt long with 2-base 3'-overhangs. The antisense strand of siRNA is designed to perfectly match the targeted mRNA sequence. As a result, the production of the protein encoded by the mRNA is inhibited. The duration of the inhibition ranges from 3 to 7 days in dividing cells and 3 to 4 weeks in non-dividing cells [4]. SiRNA is designed for one mRNA target. The antisense strand can be recycled and re-used [9].

RNAi can also be mediated by agents other than 19-23-mer synthetic siRNA. These mediation strategies can occur at different levels of the RNAi machinery (Fig. 1). Some studies have demonstrated that longer double stranded (dsRNA) are more efficient mediators than siRNA. In the cell cytoplasm, long dsRNA are first processed by Dicer to generate siRNA. They are also called dicer-substrate siRNA (DsiRNA). The processing by Dicer enhances the loading into RISC, improving the rate and efficiency of the duplex entry into RISC and resulting in more efficient RNAi [10]. However, dsRNA longer than 30 nt are thought to mediate a stronger immune response than smaller duplexes. DsiRNA of 27 nt have demonstrated higher or similar gene silencing compared with conventional 19-23-mer siRNA, depending on the target [11,12]. Furthermore, 27-mer duplexes were more resistant

to nuclease degradation compared with 21-mers [13]. By using an asymmetric duplex with a 25-nt sense strand and a 27-nt antisense strand with a 2-base 3'-overhang, it is possible to generate a predictable 21-mer siRNA following Dicer cleavage. Moreover, the presence of two DNA residues at the 3'end of the sense strand was shown to improve the reliability of Dicer cleavage [14].

Plasmid-encoding short hairpin RNA (shRNA) can be introduced into cells to generate siRNA. The primary transcript is processed into pre-shRNA by Drosha then exported to the cell cytoplasm by exportin-5, where it is further processed into siRNA (Fig. 1). Plasmids encoding shRNA are easy to produce and manipulate. Moreover, they are lower in cost than siRNA. Once inside the cell, the plasmid can produce large numbers of shRNA molecules, producing a potentially longer-lasting effect compared with siRNA, which is 99% eliminated after 48 h [15]. Furthermore, compared with siRNA, the loading of shRNA onto RISC is more efficient, and the potency was demonstrated to increase 250-fold in a luciferase model [15]. However, it has been shown that the overexpression of shRNA induces the saturation of exportin-5, which ensures transport out of the nucleus. Consequently, the endogenous pre-miRNA pathway can be repressed, leading to lethality. For example, the transfection of plasmid-encoding shRNA using viral vectors caused morbidity in mice and was related to the down-regulation of two liver-derived miRNA [16]. However, when shRNA are produced in lower quantities, neither oversaturation nor lethality occurs [17] and in general non-viral vectors are not efficient enough to promote an overexpression of shRNA. Nevertheless, the initiation of gene silencing can be delayed due to nuclear processing, and some of the essential processes to generate mi/siRNA are saturable [18,19]. Moreover, the efficient delivery of shRNA necessitates an additional step, *i.e.*, the nucleus delivery.

b. Importance of siRNA and mRNA properties

The efficiency of RNAi is primarily dependent on the molecules implicated in the pathway. The sequence of the siRNA duplex as well as the target mRNA characteristics play an important role and must be considered to maximize efficiency. The siRNA sequence determines the duplex conformation and its stability. A number of guidelines and design criteria have been described to increase the potency of siRNA duplexes. Moreover, algorithms compiling most of the criteria can be used for duplex selection [20].

Of primary importance in determining efficiency is the selection of a strand presenting a 5' end with the lowest hybridization stability that will be loaded into RISC, namely the antisense strand (Fig. 3). Therefore, a thermodynamic asymmetry between the two strands is required. To achieve such asymmetry, A-U base pairs in the 5'end of the antisense strand are recommended along with unlocked nucleic acids that are known to induce local destabilization [20]. In all cases, a 5'phosphate

on the antisense strand is mandatory for activity. It is also possible to modify the 3'end of the sense strand with a 2'-O-aminoethyl or a methyl group to obtain the same effect [21].

The global stability of the duplex, characterized by its free enthalpy, is a predictive factor for activity. Destructured siRNA containing wobble links instead of van der Waals links has demonstrated higher potency. Moreover, the sum of the guanine and cytosine (GC) content should be between 36-52%. At higher contents the inhibition of RISC can occur, and at lower contents the hybridization between the duplex and mRNA is weakened [20].

Finally, the presence of nucleotides in specific positions is required. For example, the presence of A or U at position 1 of the antisense strand is recommended for asymmetry as well as at position 10, which is the substrate cleavage site [20]. Generally, the 3'end of the antisense strand is more G/C rich.

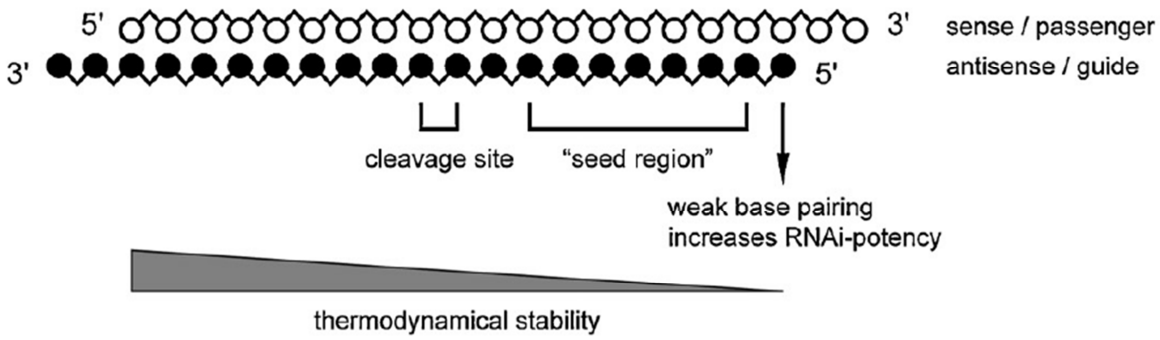

Figure 3: 21-mer siRNA from [21].

SiRNA efficiency is also influenced by inherent parameters of the target mRNA, such as its accessibility, structure and half-life. For example, it has been reported that increasing the accessibility of the mRNA target leads to a 40% increase in efficiency. In comparison, siRNA sequence optimization produces only a 26% increase [22]. Self-folding of the mRNA 3'end can be an issue, as this region is responsible for siRNA fixation and because activated RISC cannot unfold the mRNA secondary structures. A structural analysis of the target mRNA has been proposed along with a more precise screen for the absence of alternative foldings that could occlude the 3'end [23,24]. Algorithms such as Oligo Walk are also available to predict the self-folding of mRNA.

The mRNA turnover rate, which can be extremely variable in mammalian cells, with half-lives ranging from minutes to days, is also a necessary consideration. It has been demonstrated that mRNA transcripts with high turnover rates (< 200 min) are poorly silenced by exogenous siRNA [25]. Therefore, in theory, metabolic-related genes could be more easily repressed than apoptosis-related genes or transcription factors, which typically exhibit shorter half-lives. This study suggests that the

half-life of the targeted mRNA could be a supplementary factor in choosing the therapeutic target [25].

I.3. LIMITATIONS OF SIRNA-MEDIATED SILENCING

RNAi has been reported to induce side-effects. These include specific off-target effects (OTE) that silence non-target genes and non-specific OTEs, such as the induction of an innate immune response and the saturation of the RNAi pathway.

Specific OTEs, also called miRNA-like OTEs, are gene perturbations due to unintended interactions between siRNA and mRNA transcripts. More precisely, they are due to a partial sequence homology between the seed region of the siRNA and the 3'UTR region of mRNA transcripts. Both the sense and antisense strands of siRNA duplexes can be involved if poorly designed. OTEs result in undesirable gene knockdown. As a consequence, changes in gene expression as well as toxicity may occur [26] [18]. In general, the silencing efficiency induced by OTEs is approximately two-fold lower than that observed for the targeted gene. Nevertheless, in some cases this reduction can have important consequences [27]. Predictive bioinformatic approaches can be used to design highly effective and selective siRNA, thus avoiding or limiting OTEs. Chemical modifications have been shown to avoid complementarity with mRNA and thus decrease OTEs as well.

Synthetic siRNA duplexes are potent activators of the innate immune response, which is characterized by the release of pro-inflammatory cytokines, including interleukins (IL), type I interferons (IFN) and tumor necrosis factor-α (TNF-α). The immune response to siRNA can be induced either by a toll-like receptor (TLR) or cytoplasmic receptor pathways (Fig. 4). TLRs are a family of receptors involved in identifying pathogens, including TLR3, TLR7 and TLR8, which are implicated in the immune response to siRNA [26]. TLR7/8 are the most involved in the siRNA immune response and are located in intracellular vesicles, especially endosomes. They recognize single-stranded siRNA (ssRNA), unlike TLR3, which identifies double-stranded RNA (dsRNA). It has been reported that TLR7/8 activation is determined by the siRNA sequence and ribonucleotide structure. For example, the 'danger motif' (5'-GUCCUUCAA-3') and similar GU-rich sequences often mediate activation, resulting in the induction of IFN-α and IFN-γ as well as IL-6 or TNF-α. Therefore, the careful design of siRNA is crucial in avoiding the occurrence of sequences that induce TLR7/8 activation. TLR3 is located both in the endosomes and on the cell surface, is implicated in the siRNA-mediated immune response to a smaller extent, and its activation is less dependent on the siRNA sequence. However, during the phase I clinical trials of the first RNAi molecule (bevasiranib, against age-related macular

degeneration), TLR3 activation was responsible for anti-angiogenic effects through the release of IFN-γ and IL-12, necessitating the termination of the clinical trial.

Cytoplasmic receptors are involved in the immune response to siRNA as well: protein kinase PKR and helicase RIG-1 (retinoic acid-inducible gene 1) can cause a strong IFN response when activated [20]. These receptors recognize particular dsRNA that are longer than the classic 21-mer, and, more specifically, longer than 30 for PKR [14].

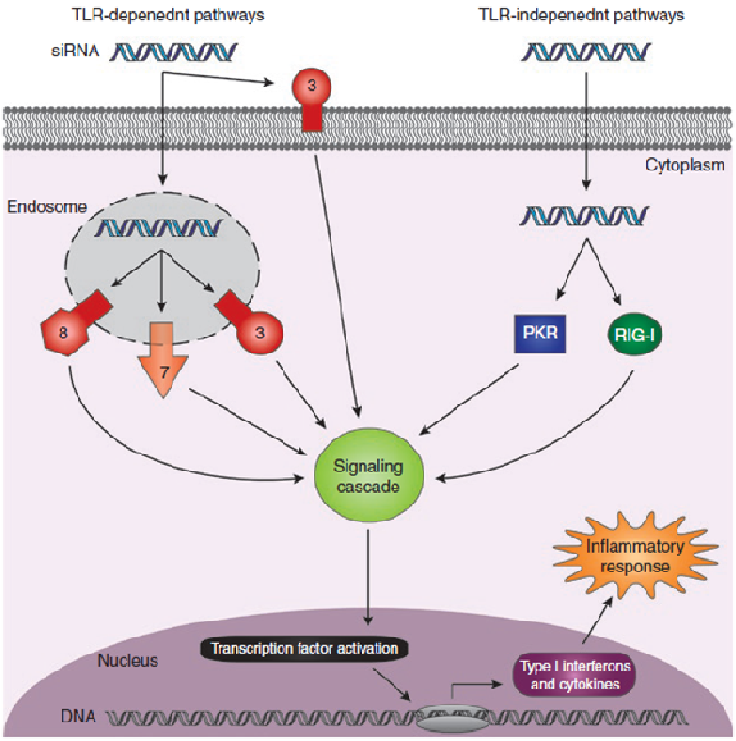

Figure 4 : Immune responses induced by siRNA (from [20])

As shRNA are expressed in the nucleus and processed by the endogenous RNAi machinery, they become less potent activators of the innate immune response compared with siRNA. However, they can activate TLR9 if they have an unmethylated CpG motif, which is typically found in bacterial DNA. The careful design of plasmid-encoding shRNA can prevent TLR9 activation [15].

Another notable limitation of exogenous RNAi is its potential competition with endogenous small RNA pathways. Some studies have reported the deleterious effects of RNAi saturability, which resulted in the disruption of potentially critical regulatory functions [16]. For example, shRNA processing is closely related to miRNA genesis, and both mechanisms involve exportin-5 for nucleus export, which is a saturable transport pathway [28]. The overexpression of shRNA can inhibit gene regulation by competing with miRNA for exportin-5, resulting in morbidity [26]. Saturation can also occur downstream from exportin-5. Indeed, the co-administration of multiple synthetic siRNA has

been shown to decrease the efficacy of each individual siRNA and to inhibit miRNA functions. The same effect was reported for the co-administration of shRNA and siRNA. As siRNA processing does not rely on exportin-5, these results suggested saturation at the level of incorporation into RISC [28]. Apparently, the competition of exogenous si/shRNA with each other is correlated with their potency and therefore sequence. Moreover, it has been suggested that the lack of competition of endogenous miRNA may be due to their slower kinetic incorporation into RISC compared with exogenous nucleic acids [28].

A new generation of RNA silencing actors has recently been demonstrated to overcome the limitations of the commonly used RNAi mediators [2]. To reduce OTEs by eliminating sense strand activity, asymmetric interfering RNA (aiRNA) and small internally segmented RNA (sisiRNA) were developed. AiRNA are composed of a shortened sense strand (15 nt), while sisiRNA a fragmented sense strand. These modifications prevent the sense strand from acting as a RISC substrate. Substitutions of RNA with DNA at precise positions, so called RNA-DNA chimeras, were found to exert the same effect. Finally, multiple effectors, such as the pri-miRNA cluster mimics or tandem siRNA, are able to generate multiple small RNA within a single construct. This approach could be advantageous in targeting biological pathways by silencing multiple genes [2]. Although further design improvements are necessary, this new generation of small RNA represents an interesting approach and a potential solution to common RNAi hurdles.

II. UNDERSTAND RNAI TO DEVELOP A SIRNA DELIVERY SYSTEM TO TREAT CANCER

Although siRNA have demonstrated excellent potential *in vitro*, their *in vivo* delivery presents considerable challenges. The barriers to siRNA administration are of course dependent on the delivery modality and on the targeted tissue. In the case of cancer therapy, intravenous (I.V.) injection is usually required [29]. Therefore, the following sections focus on intravenous siRNA delivery.

II.1. THE CHALLENGES OF EFFECTIVE SIRNA DELIVERY *IN VIVO*

Due to their intrinsic properties, siRNA cannot be administered directly. siRNA exhibit high molecular weights and anionic charges and are hydrophilic, preventing their diffusion across cellular membranes. Furthermore, siRNA molecules are extremely labile and are degraded by nucleases, which are found in biological fluids and tissues. In blood, the primary nuclease involved is a 3' exonuclease, but the cleavage of internucleotide links can occur as well [30]. Naked exogenous siRNA are 99% degraded in blood within a few minutes. Thus, delivery systems are required to encapsulate and efficiently protect the siRNA to deliver intact siRNA molecules to the tumor. In recent years, different types of delivery systems have been investigated. First, viral vectors were developed that presented high transfection efficiency but strong immunogenicity. Subsequently, numerous non-viral vectors were synthesized. These are usually composed of lipids or polymers and can be generically designated as nanocarriers. In comparison with the viral vectors, they present a better safety profile but lower transfection efficiency. From I.V. administration to cytoplasmic delivery, nanocarriers face numerous barriers. For all nanocarriers, these barriers are (i) potential instability in blood, (ii) phagocytic capture, (iii) tumor distribution, (iv) cellular internalization and (v) endosomal escape (Fig. 5). A better understanding of these barriers is required for the development of powerful siRNA delivery systems.

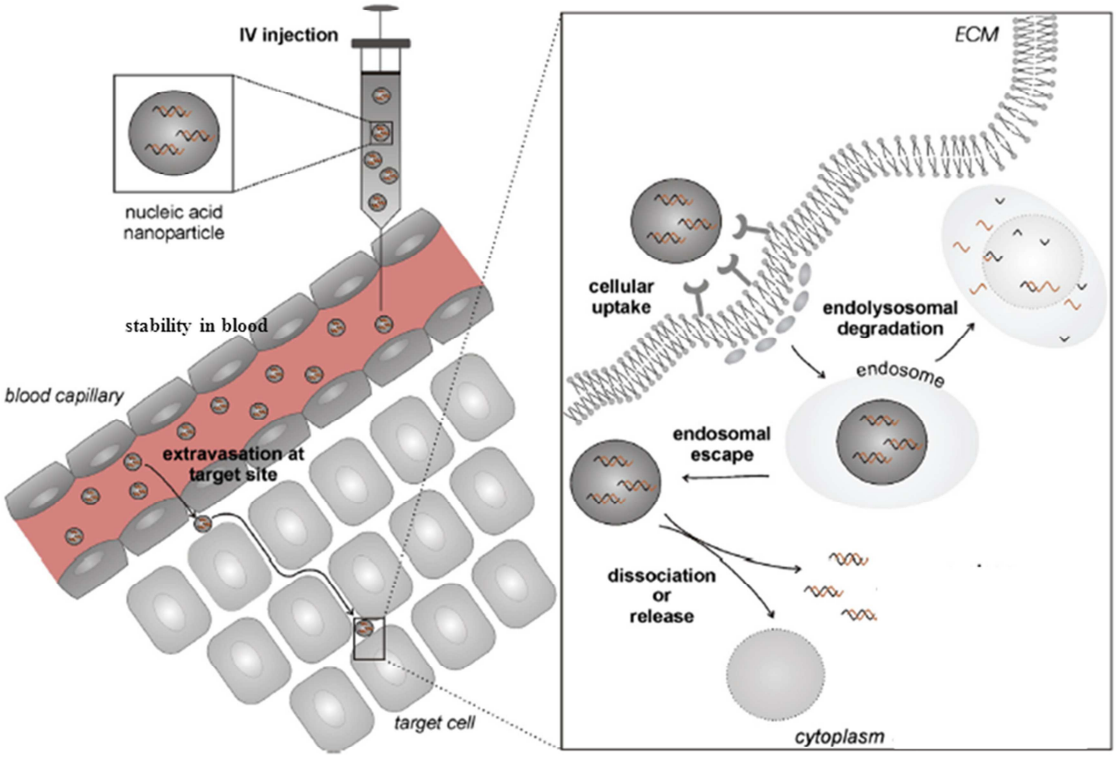

Figure 5: Biological barriers to siRNA delivery after I.V. administration adapted from [31].

II.1.1. Blood transit: stability and immune system evasion

The stability of nanocarriers in blood is a crucial parameter. Immediate dilution can be hazardous for the integrity of the formulation. Moreover, blood components can destabilize the delivery vehicle [32]. Due to the binding of proteins such as albumin or fibrinogen, the aggregation of nanocarriers can occur, leading to embolism and toxicity. Conversely, negatively charged components can compete with siRNA for binding to cationic lipids or polymers. As a result, nanocarriers will disassemble in the bloodstream, inducing siRNA release followed by its renal filtration [33].

If the nanocarrier is unstable or partially destabilized, interactions with blood components can nonetheless induce changes in the vehicle charge or composition, affecting the nanocarrier biodistribution, its interactions with cells and consequently its cellular uptake.

Numerous techniques are used to study the behavior of the delivery vehicle in biological fluids and can aid the optimization of formulations. Fluorescence fluctuation spectroscopy (FFS) is a microscopy-based technique that can monitor the integrity of the delivery system (Fig. 6A). The siRNA is labeled with a fluorophore and fluctuations in the fluorescence intensity in plasma are monitored over time. In the case of free siRNA, a constant signal is detected, which is proportional to

the siRNA concentration. Upon complexation with the nanocarriers, variations in the signal intensity occur, with peaks corresponding to nanocarriers bearing a high quantity of siRNA. The baseline signal between peaks is proportional to the amount of free siRNA in the medium. By measuring the background fluorescence, it is thus possible to quantify the amount of siRNA released from the delivery system over time [34].

In addition to its integrity, the size of the delivery vehicle is another crucial factor, as it can affect the biodistribution of the siRNA delivery system and/or cause toxicity. Nanoparticle size measurements in solution are most commonly made using a NanoSizer (Malvern UK), which functions based on dynamic light scattering. However, this technique is incompatible with biological fluids, such as plasma, as the laser light will be scattered by the biological components. Thus, the measurements obtained will not be representative only of the nanocarrier size but rather of a mix between the plasma components and the nanocarriers. Fluorescence Single Particle Tracking (fSPT) is a microscopy technique that can track the movement of individual fluorescently labeled particles (Fig. 6B). The motion trajectory of every single particle diffusing in the fluid is recorded and analyzed. The diffusion coefficient of each trajectory can then be calculated, providing a distribution of diffusion coefficients that can be converted to a size distribution using the Stokes-Einstein equation [35]. Recently, the commercially available apparatus Nanosight, which is based on the principle of particle tracking, has been used for size measurements in biological fluids.

As mentioned previously, interactions of the nanocarrier with the blood components can alter the stability as well as the biodistribution of the delivery system. Conversely, these contacts can affect the blood cell viability. Hemocompatible formulations can be defined as formulations which do not result in any form of toxicity and remain efficacious after being exposed to the blood [36]. Besides the standard hemolysis assay (which measures the release of hemoglobin from damaged erythrocytes) or the platelet aggregation method, new approaches have been developed for the evaluation of the hemocompatibility of a delivery system. SPT has been used to determine the fraction of the nanocarriers that have interacted with the blood cells. In addition, flow cytometry was employed to quantify the amount of fluorescently-labeled nanocarriers that were internalized by the blood cells and thus potentially affected their viability. The results showed that the PEGylated dextran nanogels strongly interacted with the erythrocytes as well as with the leukocytes and the platelets but to a lower extent. The negatively charged nanogels appeared to be the safest formulation. More data about the hemocompatibility of polymeric delivery systems would be very useful for the future translational development of such systems.

A

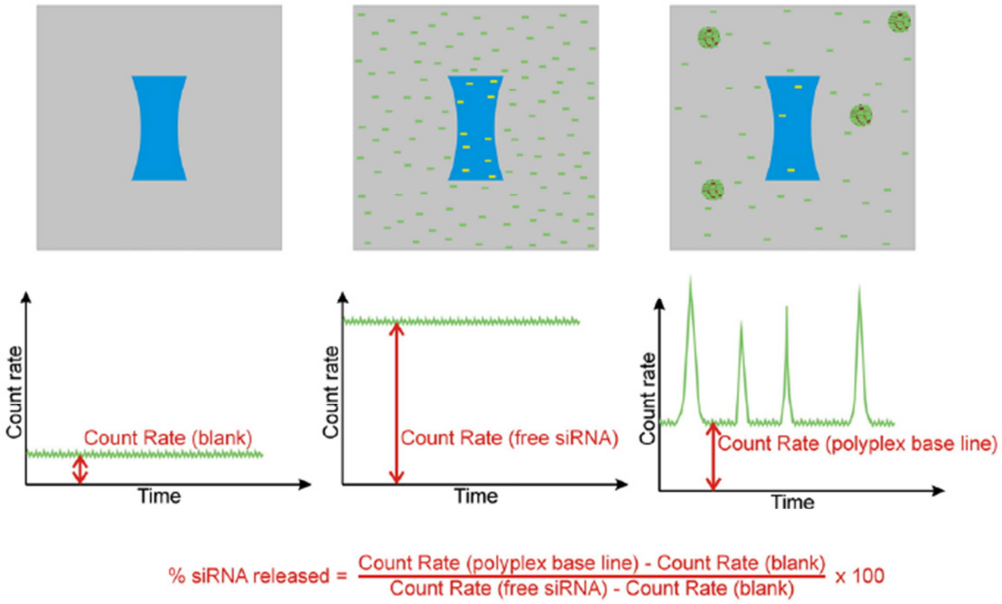

B

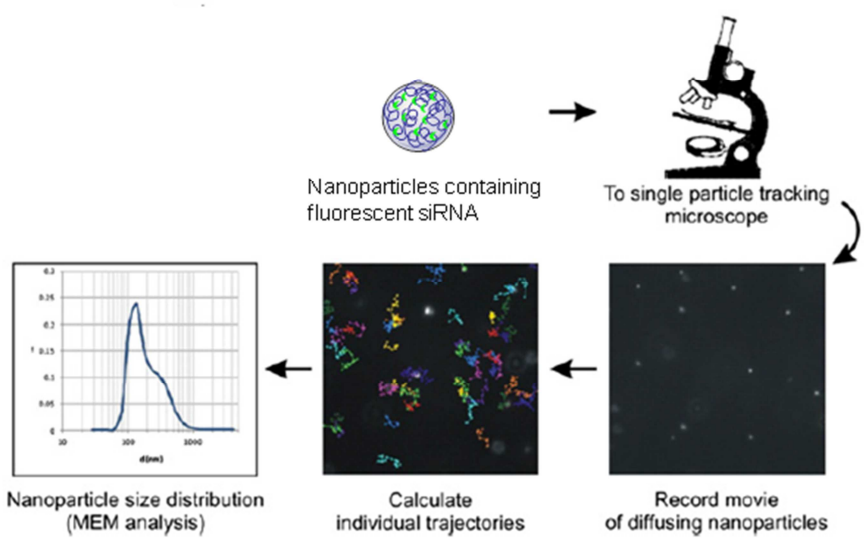

Figure 6: Principle of (A) fluorescence fluctuation spectroscopy FFS and (B) single particle tracking SPT from [34] and [35].

Another critical step is the adsorption of opsonins (immunoglobulins Ig, complement-related components) to the nanocarrier surface, which results in uptake by the macrophages of the mononuclear phagocyte system (MPS) and the subsequent clearance of the nanocarrier. Highly charged nanocarriers, regardless of the type of charge, preferentially fix the complement proteins. Surface hydrophobicity is a major factor for opsonization; indeed, IgG and fibronectin possess a high

affinity for hydrophobic regions. For example, nanocarriers made of hydrophobic polymers such as poly(lactide-co-glicolide) (PLGA) or poly(alkylcyanoacrylate) (PACA) are subject to important opsonization [37]. Thus, to reduce adsorption, the design of stealth nanocarriers is mandatory. For this purpose, hydrophilic polymers, usually poly(ethylene glycol) (PEG), are grafted onto the nanocarrier surface. This PEG shielding provides a steric barrier to the nanocarrier. Moreover, it will confer long circulation properties to the delivery vehicle. PEG shielding is thought to change the opsonization pattern, with a decrease in opsonin binding and an increase in dysopsonin adsorption, the latter preventing recognition and phagocyte uptake, likely due to changes in the protein conformation [38]. However, the mechanisms are still unclear and under debate [32]. The PEG molecular weight and density must be optimized because insufficient or inhomogeneous PEGylation will result in clearance [39]. In addition, a 'brush-like' conformation is preferred [32]. High molecular weight hyaluronic acid has been suggested as an alternative to PEG [40]. Indeed, this polymer possesses hydrated hydrogel-like mobile molecular chains that can act as a steric barrier [41].

Recently, two different types of positively charged nanocarriers that were 10-100 nm size and self-assembled by electrostatic forces were subjected to renal clearance [39,42]. The first carrier, a cyclodextrin-based delivery system, remained stable in blood but accumulated in the glomerular basement membrane where the negatively charged proteoglycans compete with siRNA for binding and lead to vehicle disassembly. The residence time in kidneys was increased compared with the injection of free siRNA. The second type of carriers, polymeric nanogels, were cleared from circulation *via* different mechanisms, including renal clearance. To avoid this phenomenon, negatively charged nanocarriers can be designed [42]. However, partial disassembly in blood can reveal positive charges and lead to renal clearance as well. Heparan sulfate stability tests can help to predict eventual renal clearance [39].

II.1.2. Tumoral delivery

Usually, molecules larger than 45 Å (corresponding to the size of an immunoglobulin) cannot cross the capillary endothelium and thus are not able to reach the targeted tissue [43]. However, in tumors, structural changes in the vascular endothelium that result in increased permeability have been reported. Open fenestrae are approximately 100-400 nm and can permit nanoparticle extravasation, provided that the particles present a suitable size. Moreover, tumors are characterized by inefficient drainage. This passive phenomenon is called the enhanced permeability and retention effect (EPR) and can be exploited for nanoparticle delivery to tumors. In the interstitial space, the delivery vehicle has to survive in the extracellular fluids and to diffuse into the extracellular matrix, which is a tight network of polysaccharides and proteins produced by the cell [44].

The adherence of the nanocarrier to the cell surface is the first step in enabling further cellular uptake. Usually, attachment to cells is mediated by non-specific hydrophobic or electrostatic interactions. Thus, nanocarriers with high cationic charges or a hydrophobic surface are believed to interact more strongly with cells. Cationic nanocarriers can interact with the anionic glycosaminoglycans that compose the extracellular matrix (Fig. 7A). However, because of their cationic charges, these nanocarriers are quite toxic and are more prone to opsonization and clearance. Furthermore, they interact with cells in an unspecific manner and can deliver their payload to non-targeted cells [45]. For these reasons, a more selective method for facilitating adhesion to cells would be preferred. The grafting of targeting ligands onto the nanocarrier surface that will recognize specific cell receptors is an interesting strategy (Fig. 7B and 9). The nanocarriers are then preferentially taken up by the cells bearing the receptor, allowing specific targeting of the desired tissue. This approach is called active targeting. The choice of ligand is based on the degree of its receptor expression in the targeted tissue and on its limited presence or even absence in other tissues [46]. Various types of ligands have been investigated for tumor targeting, such as monoclonal antibodies, antibody fragments or non-antibody ligands. Non-antibody ligands present the advantages of being readily manipulated and less expensive than antibodies [46]. The most commonly described ligands are the tripeptide Arginine-Glycine-Aspartic acid (RGD), which targets the cellular adhesion molecules integrins, folate and transferrin, which in turn target growth factor receptors.

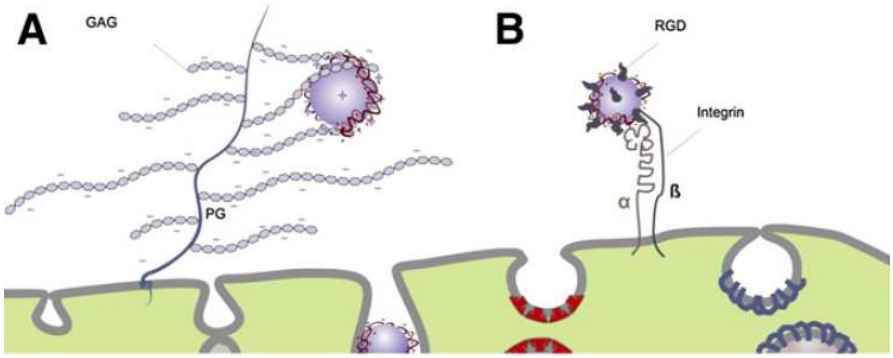

Figure 7: (A) Non-specific binding to glycosaminoglycans through electrostatic interactions and (B) active targeting *via* integrins, from [45].

The RGD sequence has been identified as the cellular attachment site of natural ligands and binds to multiple integrin receptors *i.e.* all five α_v integrins ($\alpha_v\beta_1$, $\alpha_v\beta_3$, $\alpha_v\beta_5$, $\alpha_v\beta_6$, $\alpha_v\beta_8$), two β_1 integrins ($\alpha_5\beta_1$ and $\alpha_8\beta_1$) and $\alpha_{IIb}\beta_3$, however, with various degrees of affinity [47]. Small molecules that mimic the RGD sequence and called RGD peptidomimetic (RGDp) have been designed to increase the affinity towards the integrin receptors as well as to enhance the *in vivo* stability of such ligands (Fig. 8A-B)

[48,49]. The RGD or the RGDp binds at the interface of the α and β subunits. X-ray crystal structures of the RGD ligand complexed with the extracellular segments of the $\alpha_v\beta_3$ and the $\alpha_{IIb}\beta_3$ integrins have demonstrated identical interactions between the integrin active site and the ligand [47]: the R residue is docked to the α subunit while the D residue is paired with metal ions and other modules from the β subunit (Fig. 8C).

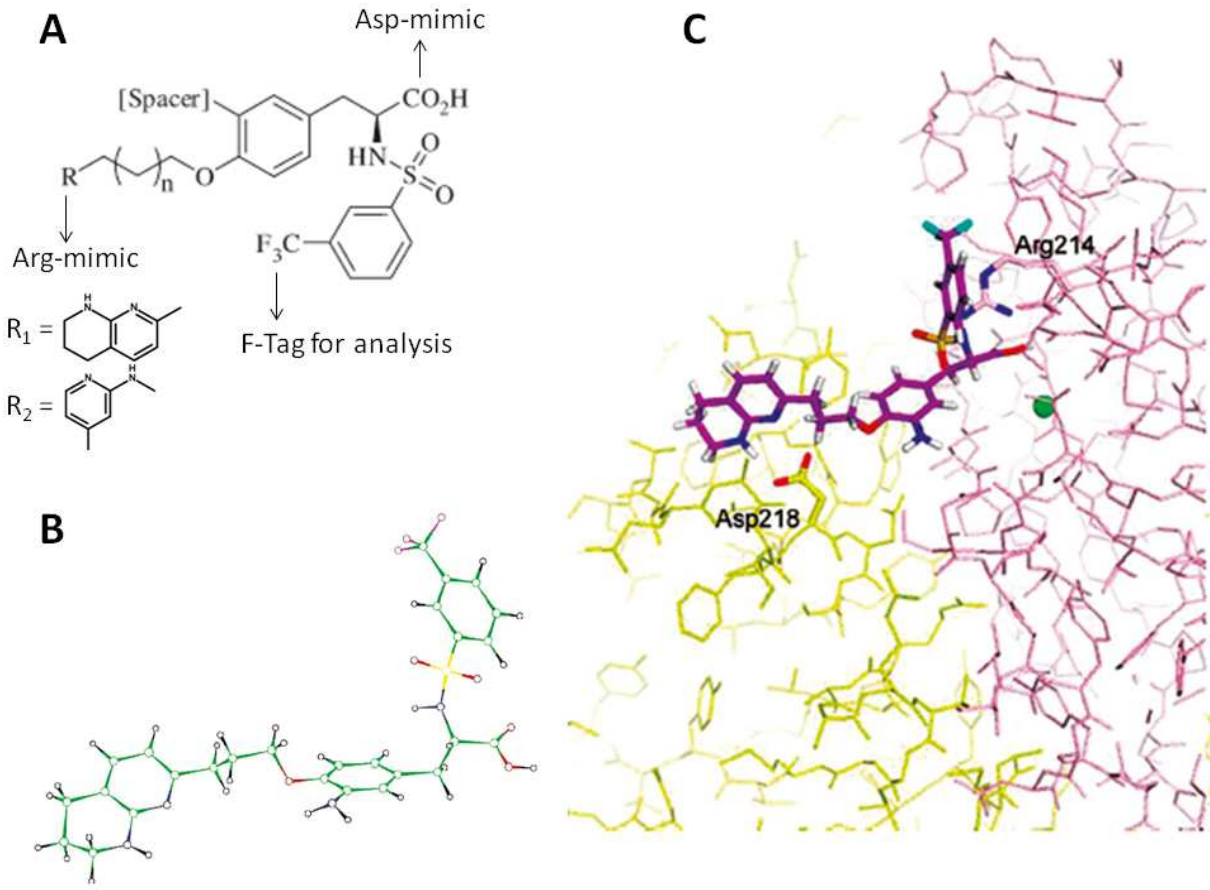

Figure 8: A: Schematic representation of the structure of a RGDp *(n=1-2)* B: Conformational representation of RGDp with R= R_1, n=1 and spacer = NH_2. C: Docking of the RGDp presented in B in the active site of the $\alpha_v\beta_3$ integrin (where α subunit is colored in yellow and β subunit in pink). The RGDp is colored is purple. Oxygen atoms are in red, nitrogen atoms are in blue, hydrogen atom are in white and fluorine atoms are in cyan. The Mn^{2+} ion is shown as a green sphere. Adapted from [48].

The $\alpha_v\beta_3$ integrins represent an interesting target as they are upregulated in many types of tumor and as they are overexpressed by in endothelial tumor cells as well [50]. Therefore, the targeting approach can be dual, increasing the uptake efficiency (Fig. 8). Moreover, endothelial cells are more accessible to nanocarriers than to tumor cells [51]. PEGylated liposomes were decorated with cyclic RGD and loaded with a cocktail of three siRNA-targeting c-myc, Vascular Endothelial Growth Factor (VEGF) and murine double minute (MDM2). After systemic injection in lung-metastasized B16F10-bearing mice, the accumulation of the targeted liposomes was greater in the tumor compared than

in the non-targeted ones. This resulted in a 62.5% tumor growth reduction, while only 35.3% tumor growth inhibition was observed with the non-targeted formulation [52].

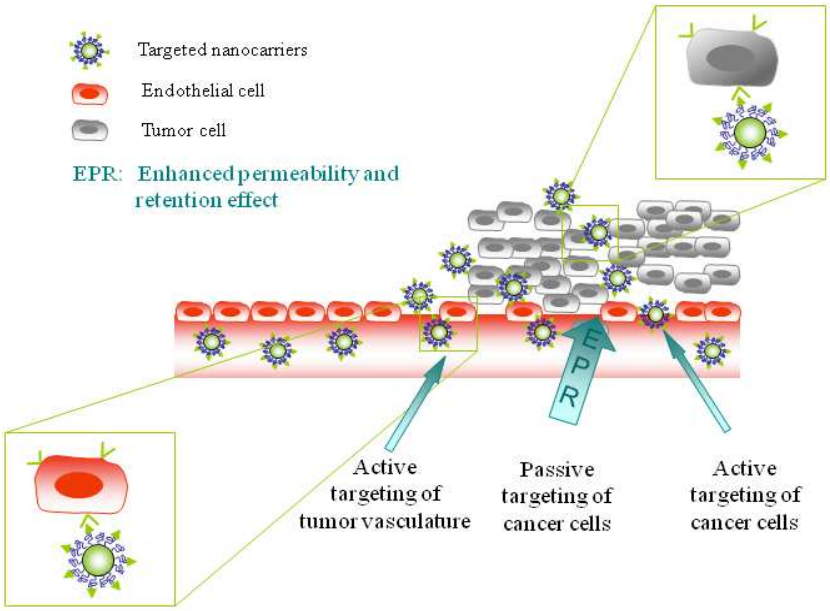

Figure 9: Schematic representation of integrin-targeting mechanisms using nanocarriers adapted from [53].

II.1.3. <u>At the cellular level</u>

Nanocarriers are generally internalized in the cell *via* endocytosis. Different endocytic pathways have been described in mammalian cells. In addition to phagocytosis, non-phagocytic pathways exist and are referred to as pinocytosis. They are not restricted to specialized cells, contrary to phagocytosis. Four main pathways can be cited: (i) clathrin-mediated endocytosis, (ii) caveolae-mediated endocytosis, (iii) macropinocytosis and (iv) other clathrin-independent and caveolae-independent endocytosis [37]. Clathrin-mediated endocytosis is implicated in the uptake of numerous macromolecules and nanocarriers 100 nm in diameter and is most likely the best-studied endocytic mechanism [4] [45]. The internalization pathway of the nanocarrier has been shown to impact the final cytoplasmic delivery of its cargo: chitosan-alginate DNA complexes taken up *via* the caveloae pathway remained entrapped in the caveosomes, which did not undergo acidification, while internalization *via* the clathrin-route in other cell lines allowed escape from the endosomes and resulted in high transfection [54].

II.1.4. Cytoplasmic release

Following internalization, the nanocarrier must escape the endocytic vesicle to release the siRNA into the cytoplasm. At the beginning of the endocytosis, the nanocarrier is located in early endosomes that progressively mature into late endosomes. This maturation is accompanied by acidification to pH 5-6 due to proton accumulation *via* the proton pump ATPase. Usually, this ends with fusion with the lysosomes, where the pH is 4-5 and the enzymatic environment is hazardous for the nanocarrier. Thus, the nanocarrier must evade the endosomes prior to their fusion with lysosomes. Different mechanisms have been proposed for the endosomal escape mediated by the nanocarrier. These mechanisms differ depending on the nature of the delivery system. For polymeric nanocarriers, the proton-sponge effect and the umbrella hypothesis are the most generally accepted mechanisms to explain endosomal escape [55]. Typically, cationic polymers possess a high number of primary amines with a pKa of approximately 6. During the acidification of the endosomes, the amines are progressively protonated, leading to an influx of chloride ions in the endosomes to maintain charge neutrality and increasing the ionic strength in the endosomes. This results in an influx of water, leading to osmotic swelling and the physical rupture of the endosome (Fig. 10A). Moreover, the tertiary amines of the polymer will be protonated as well, leading to electrostatic repulsion of the neighboring amine groups and thus to polymer expansion. This mechanism is called the umbrella hypothesis and is thought to contribute to the rupture of the endosomes for some polymers [55]. The proton sponge mechanism was observed for PEI [56] but it is still debated. Recently, it was suggested that this mechanism was not the dominant contributor to endosomal escape and was concomitant with evasion through membrane pores or holes [57]. Moreover, the release of the lysosome content in the cytoplasm could be deleterious for the cell. Nevertheless, regardless of the type of evasion mechanism, the use of polymers with abundant amino groups and a flexible structure that can increase volumetrically is extremely advantageous.

For lipidic formulations, endosomal escape arises due to interactions of the cationic lipids with the phospholipids of the endosomes. These interactions destabilize the endosome membrane, resulting in siRNA release (Fig. 10B).

After the endosomal release, the siRNA has to be dissociated from the polymer in order to reach the RNAi machinery. Once delivered to the cell cytoplasm, siRNA molecules must reach RISC. Some authors have demonstrated that these complexes are concentrated in particular areas of the cytoplasm and thus suggested that the location of the siRNA delivery to the cytoplasm should be optimized [55].

A

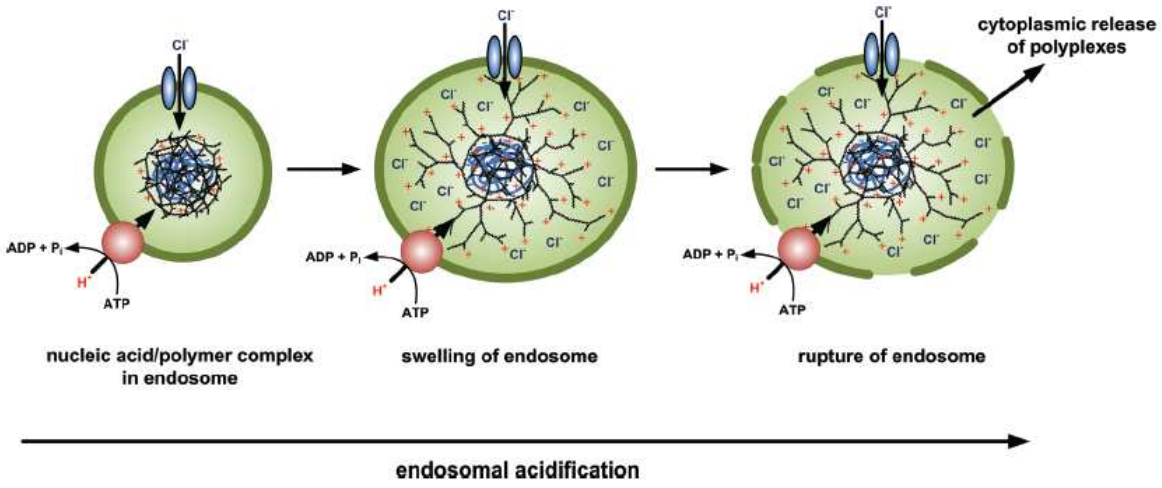

B

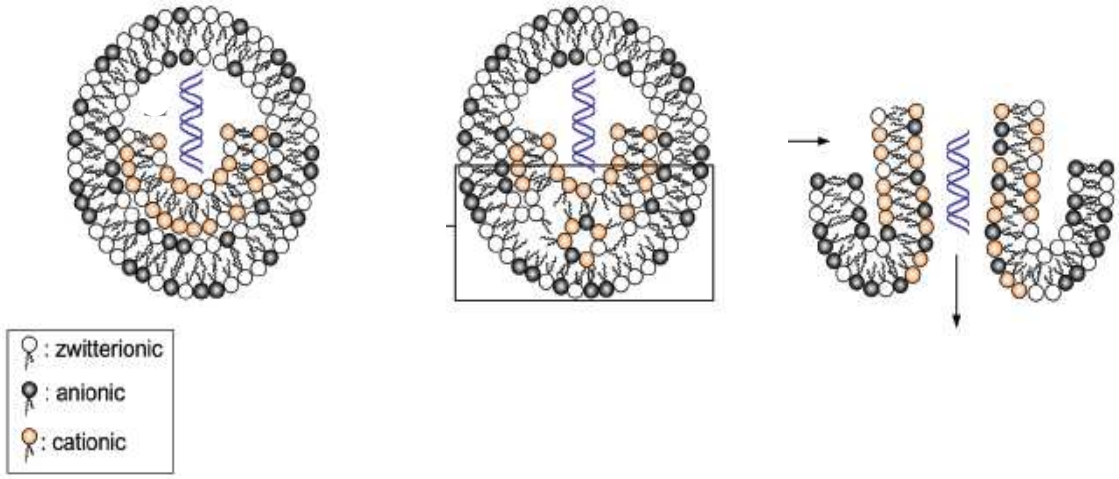

Figure 10: Schematic representation of the mechanism of endosomal escape for (A) polymeric and (B) lipidic nanocarriers (adapted from [55]).

II.1.5. Quantifying the intracellular delivery of siRNA

The efficacy of a siRNA-based therapy strongly depends on the delivery of therapeutic siRNA concentrations in the desired cells, tissues or organs. Usually, fluorescently-labelled siRNA are used to estimate the delivery efficiency and the siRNA localization, both *in vitro* (flow cytometry, microscopy) and *in vivo* (imaging techniques). However, these methods are not fully quantitative for the delivery of the active compound, as they detect the fluorophore and not the siRNA itself. Thus, the stem-loop reverse transcription quantitative polymerase chain reaction (RT-qPCR) approach has

been developed to quantify the amount of small RNA delivered in the cells (Fig. 11). First described for the quantification of miRNA [58,59], this approach has also been applied to siRNA, both for *in vitro* [60] and *in vivo* quantification [61,62]. Because of the short length of siRNA and miRNA, the use of stem-loop RT primers is necessary. Indeed, the stem loop primers provide higher specificity and enables better sensitivity than conventional linear primers because of the base stacking and spatial constraint of the stem-loop structure [58].

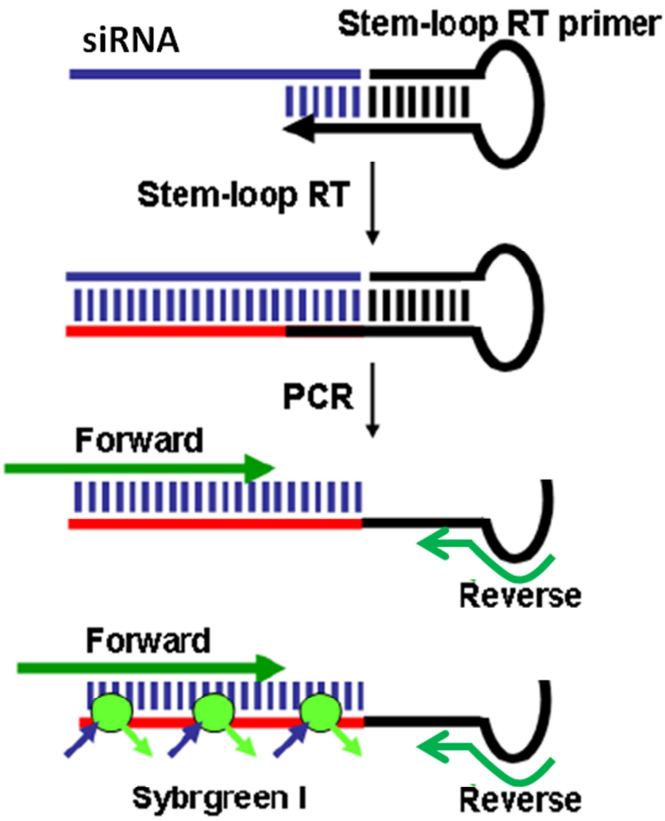

Figure 11: Schematic representation of the stem-loop RT-qPCR method adapted from [63]: the stem-loop RT primer binds to the 3'end of the siRNA antisens strand, initiating reverse transcription. The RT product is then amplified using a specific forward PCR primer. The universal reverse primer is designed on the loop region to avoid formation of primer dimers. The quantification is done by using SYBR Green I assay.

Table I: SiRNA delivery: hurdles, causes and potential solutions

Hurdles	Causes											Potential solutions						
	Nature of siRNA				Instability in blood		Tumoral delivery	At the cellular level										
	Hydrophilic	Anionic	High MW	Nuclease sensitivity	Disassembly of the NC	Interactions with blood components	Extravasation	Non-specific or insufficient endocytosis	Insufficient endosomal escape	RISC loading	Interactions with TLR , PKR or RIG-1	Encapsulation into NC	siRNA chemical modifications	Stability tests and optimization of the formulation	Hydrophilic polymer coating	Targeting ligands	Endosomal disrupting agents	Optimization of sequence and choice of target
siRNA cannot diffuse across cell membranes	x	x	x									x	x					
siRNA is easily degraded				x								x	x					
Aggregation of the NC						x								x	x			
siRNA releasefrom the NC					x	x								x				
Rapid clearance						x						x	x		x			
Failure to reach the therapeutic dose in the targeted cells							x	x								x		
Delivery in other organs								x								x		
Lysosomal degradation									x								x	
Triggering immune response											x		x					
Inefficient mRNA silencing									x	x							x	x

NC : nanocarrier, TLR : toll-like receptor, PKR: protein kinase, RIG-1: retinoic acid-inductible gene 1

II.2. CONSIDERATIONS IN THE DESIGN OF AN EFFECTIVE RNAI THERAPEUTIC

Many efforts have been made to develop an effective siRNA delivery system that could bypass the aforementioned *in vivo* barriers. Various methods have been employed to modify the chemical structure of siRNA or to encapsulate them into smart nanocarriers. A combination of both approaches will be advantageous in conferring optimal properties to the delivery system.

II.2.1. Improvements of siRNA features through chemical modifications

Modifications to the siRNA structure have been intensively studied in an attempt to overcome the primary siRNA drawbacks, including its (i) low stability, (ii) poor pharmacokinetic behavior and (iii) immune stimulant properties. Moreover, it was shown that some modifications can improve siRNA potency by providing better loading into RISC or preventing specific OTEs [21]. In general, the sense strand tolerates more modifications than the antisense strand or the extremities relative to the central region. An ideal modification should impart new properties to the siRNA duplex without decreasing its silencing activity [64]. Therefore, an optimal balance must be found.

II.2.1.1. Modifications within the nucleotide

Chemical modifications to the nucleotide structure can be used to address the instability of siRNA, to reduce OTEs or to avoid an *in vivo* immune response [30]. Common chemical modifications are made to the backbone or to the sugar of siRNA (Fig. 12).

Modifications to the sugar are most commonly used. The 2'-OH group of the ribose is sensitive to many RNases. For example, ribonucleases are known to provoke nucleophilic attack *via* a 2'-3' cyclic phosphate intermediate followed by water hydrolysis [21]. Therefore, blocking the 2'-OH group is a powerful strategy to avoid degradation. The addition of a 2'-O-methyl (2'-OMe) or 2'-deoxy-2'-fluoro is commonly employed. Furthermore, 2'-OMe modifications at the second position of the sense or antisense strand decrease the OTEs [65]. Moreover, a 2'-OMe modified 23-mer siRNA was able to abolish immunostimulatory effects [66] and the same modification, especially when made to a uridine base, blocked the immune response to siRNA delivered using cationic lipid vehicles [14].

Locked Locked Nucleic Acids (LNA) are novel RNA derivative nucleotide analogs that contain a methylene bridge linking the 2'-oxygen and 4'-carbon of the ribose sugar rings. This bridge locks the ribose ring in the 3'endo conformation, which is characteristic of RNA [67]. An appropriate introduction of LNA residues into the oligonucleotides stabilizes the duplex without altering its function [67]. In addition, it has been shown that LNA oligonucleotides can reside for long periods in

several organs, such as the liver, kidneys and skin [68]. The systemic administration of naked LNA oligonucleotides is currently being investigated in Phase I clinical trials. Moreover, LNA and 2'-deoxy-2'-fluoro modifications can lead to significantly increased target binding affinity [69].

UNA or unlocked nucleic acids are ring-opened derivatives of ribose lacking the C2'-C3' link. They exert the opposite effect of LNA, inducing a local destabilization of the duplex [70]. UNA can be exploited to improve the strand selection [21]. For example, if placed at position 7 of the antisense strand, UNAs can weaken the binding between the siRNA strand and the semi-complementary mRNA, thus reducing OTEs [65].

The stabilization of internucleotide phosphates is another strategy for decreasing the susceptibility to nucleases. Moreover, phosphodiester groups found on the linkages between sugars can be crucial to exonucleases. Backbone modifications such as the addition of boranophosphate have been demonstrated to be highly effective in protecting siRNA against nuclease degradation (10-fold more than unmodified siRNA) and were better tolerated in the sense strand [69]. Phosphorothioate (PS) modifications can result in enhanced stability and increased cell uptake as well [9] [20]. However, PS nucleotides can cause toxicity by nonspecifically binding to proteins [30].

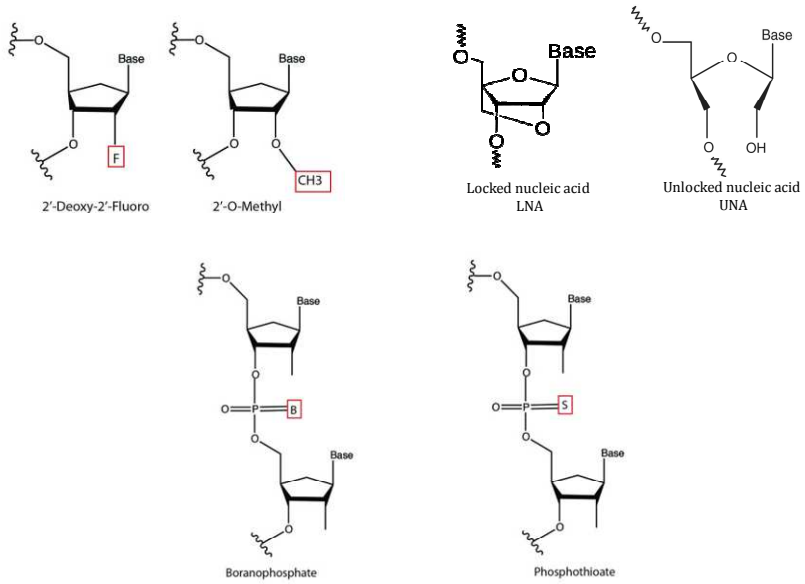

Figure 12 : Chemical modifications to the siRNA structure (adapted from [9]).

II.2.1.2. Termini modifications

The ability of termini modifications to increase the cellular uptake of siRNA has been investigated. Because the 5'-phosphate of the antisense strand is crucial for RNAi activity, termini modifications

are commonly made to the sense strand or to the 3'end of the antisense strand. Most of these modifications use cleavable linkages such as acid-labile bonds or disulfide links to allow facile release of the siRNA following cellular internalization. Another possibility is to exploit cleavage by the Dicer enzyme [71].

The conjugates thus obtained are usually administered directly in their conjugated form. Therefore, they can be considered to be a type of delivery system.

The conjugation of lipophilic moieties such as cholesterol [72] or α-tocopherol (vitamin E) [73] was shown to enhance the *in vivo* pharmacokinetic profile compared with unmodified siRNA and could be exploited for liver targeting. For example, the elimination half-life was prolonged to 95 min using cholesterol conjugation [72]. Moreover, cholesterol-siRNA was shown to bind to serum proteins or lipoproteins, resulting in increased liver uptake *via* the low-density lipoprotein receptor [30]. In another study, α-tocopherol was covalently bound to the 5'end of the antisense strand of DsiRNA and was released in the cytoplasm during Dicer processing. The conjugation resulted in increased liver accumulation when administered to mice, efficiently silencing Apolipoprotein B without triggering an immune response [73].

The conjugation of cell penetrating peptides (CPP) has been demonstrated to improve siRNA internalization by cells [71]. CPPs are small cationic peptides (<30 amino acids) that bind to glycosaminoglycans on the cell surface, allowing uptake by the cells [43]. CPPs include TAT, Penetratin and Transportan. Despite promising *in vitro* results, the intra-tracheal administration of a Penetratin-siRNA conjugate induced a strong immune response in mice, possibly through the activation of TLR3, 7 and/or TLR8 [74,75].

II.2.2. Encapsulating siRNA into nanocarriers

Among the non-viral vectors, the two most developed approaches are lipidic and polymeric nanocarriers. Although of different compositions, they share certain features, including the condensation of the siRNA into nanoscale structures, the use of cationic components and the need for improvements such as PEGylation or ligand grafting to meet the requirements of *in vivo* use.

II.2.2.1. Lipidic formulations

The most frequently described lipidic nanocarriers are lipoplexes and liposomes. Lipoplexes possess a multi-lamellar structure of cationic lipid bilayers separated by anionic siRNA, while liposomes are spherical uni- or multi-lamellar vesicles with an aqueous core containing siRNA surrounded by lipid bilayers. Lipoplexes present some heterogeneity in shape and size. Various morphologies have been

reported, including the lamellar phase, in which the lipoplexes complex the siRNA and exhibit an inverted hexagonal structure during cell uptake [76]. Due to their highly positive charges, lipoplexes often induce toxicity. They tend to form aggregates when intravenously administered due to the binding of blood proteins [77]. Moreover, cationic lipids can also activate the complement system [20,78].

Regarding liposome formulations, the most commonly used lipids are 1,2-di-O-octadecenyl-3-trimethylammonium propane (DOTMA) and 1,2-dioleoyl-3-trimethylammonium-propane (DOTAP) as well as some lipid-like molecules called lipidoids ($98N_{12}$-5) that have recently emerged. They possess a cationic polar head that is primarily composed of amino groups that interact with the siRNA molecules [79]. Generally, some neutral lipids or helper lipids, such as 1,2-dioleoyl-*sn*-glycero-3-phosphoethanolamine (DOPE), are incorporated to reduce the repulsion between similar charges in the bilayer. Cholesterol is usually added to the hydrophobic component of the formulation to facilitate cell fusion or endosomal internalization. PEG-lipids are also commonly found in these formulations because they endow stealth properties to the lipid nanocarrier [4]. However, multiple injections of PEGylated liposomes have induced an antibody immune response (IgG and IgM) against PEG, resulting in the rapid clearance of the liposomes upon re-administration. New PEG-derivatized lipids, such as sheddable PEG-lipids or serum esterase sensitive PEG-lipids, can limit this adverse PEG effect [77]. The major limitation of cationic liposomes is their failure to release the siRNA contents due to their stable intracellular properties [80]. Thus, pH-sensitive liposomes have been described in which the acidic endosomal environment is exploited to induce liposomal membrane destabilization and siRNA release. For example, citraconyl-DOPE can be incorporated into the formulation as a pH-responsive phospholipid. In acidic environments, the degradation of this lipid will provoke the destabilization of the delivery system and siRNA release [4]. Liposomal formulations called SNALP (for stable nucleic acid-lipid particles) are currently being investigated in clinical trials.

II.2.2.2. Polymeric formulation

Different varieties of polymeric delivery systems exist (Fig.13). The majority of nanocarriers are composed of cationic polymers and are based on electrostatic interactions with the anionic siRNA. Other systems can form nanoparticles (NPs) or nanogels *via* the chemical or physical crosslinking of polymers in addition to electrostatic interactions. The major advantage of polymers is their versatility. Indeed, they offer numerous possibilities for chemical modification and can be found in a variety of molecular weights and geometries. Moreover, a large variety of moieties can be easily

grafted [81]. In addition, they offer good protection against nucleases. However, some of them are non-biodegradable, which is a detriment for *in vivo* use.

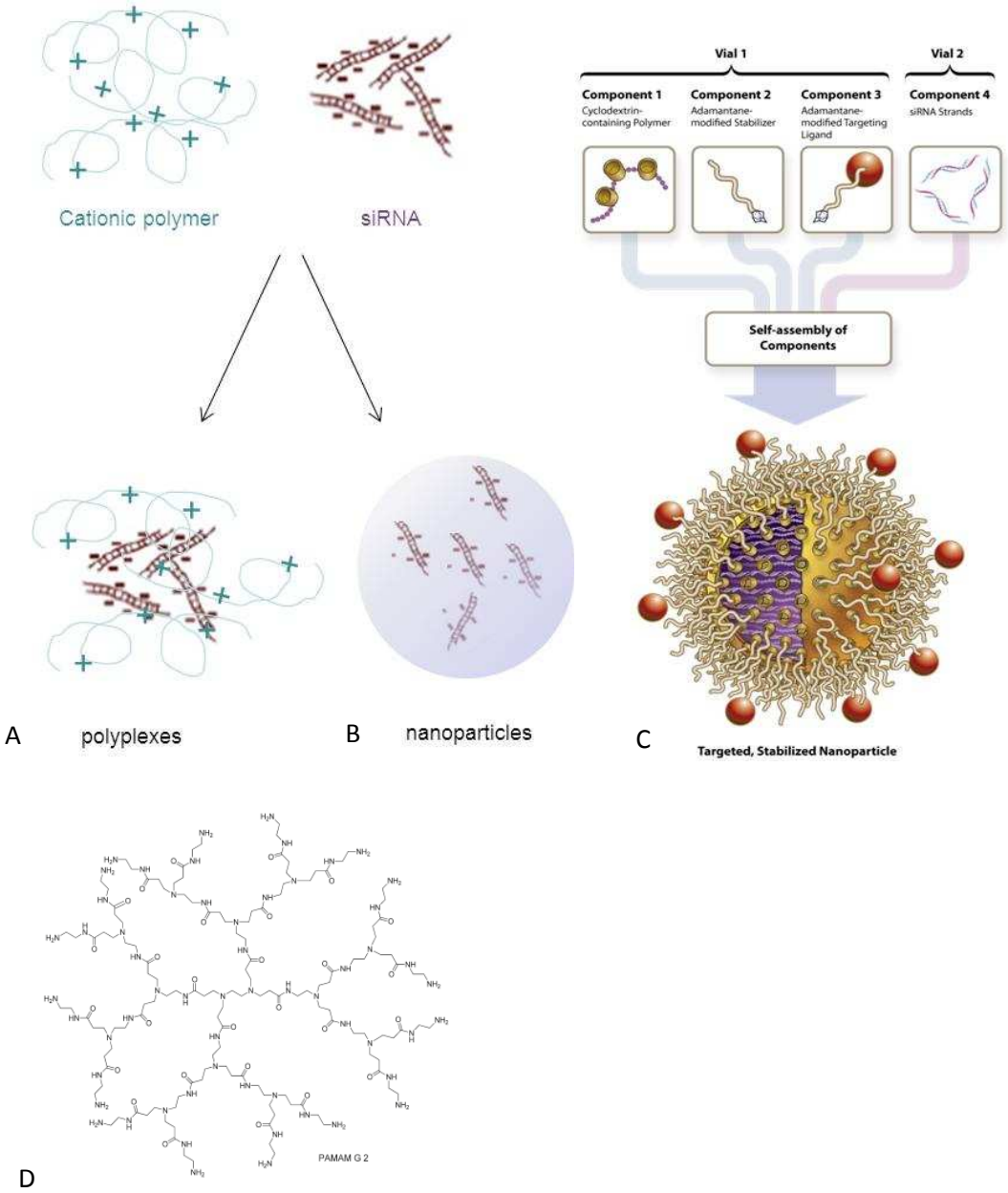

Figure 13: Some examples of the most described polymeric nanocarriers: polyplexes (A), nanoparticles (NPs) (B), cyclodextrin-based NPs [82] (C) and dendrimers [83] (D)**.**

Cationic polymers are able to complex anionic siRNA into structures called polyplexes through electrostatic interactions. To obtain monodisperse polyplexes in the nanometer range, the amount of polymer and siRNA must be finely balanced. For that matter, the N/P ratio (the molar ratio of the amino groups [N] of the cationic polymer to the phosphate groups [P] of siRNA) is calculated. In general, the cationic polymer is present in excess in the formulation. Usually, the cationic polymers possess amino groups that can bind to the nucleic acid. The presence of these amino groups can

mediate endosomal escape *via* the proton sponge mechanism. We can distinguish synthetic polymers, such as PEI, poly-L-lysine (PLL), polyamidoamine (PAMAM) or cyclodextrin-based polymers, from natural polymers, such as chitosan and its derivatives, atelocollagen or polypeptides [80]. Compared with liposomes, the formulation process is straightforward, as polyplexes can be obtained through a simple mixing procedure [29].

Polymers presenting polyamine structures, such as PEI, PLL or PAMAM dendrimers, have been widely described. Despite good transfection properties, PEI/siRNA polyplexes have been shown to be highly toxic due to mitochondrial membrane depolarization and strong interactions with the cell membrane, especially for branched PEI [14]. Therefore, formulation improvements such as PEGylation, conjugation to other polymers or the incorporation of biodegradable bonds have been made [76]. Dendrimers are branched molecules exhibiting a high charge density extending outward from an inner core (Fig. 13) [83]. PAMAM dendrimers can self-assemble with siRNA *via* electrostatic interactions to form spherical nanoscale structures that exhibit good efficiency [81]. Nevertheless, surface chemistry modifications must be made to decrease the cytotoxicity of dendrimers [84]. In general, these polyamine structures present heterogenous molecular weights and isomers, which could influence the physico-chemical characteristics of the nanocarriers as well as their biological activity. Therefore, the development of well-defined polymeric systems with low polydispersity, for example, has emerged [83].

Cyclodextrin-based polymers have been successfully used for siRNA delivery, with clinical trials ongoing (Fig. 13) [82]. Briefly, these polymers are composed of a polycation that assembles with siRNA through electrostatic interactions. Cyclodextrins (CD), which are grafted within the polymer chains, reside at the surface of the NPs and allow the addition of the stabilizing agent (PEG adamentane) and the targeting agent (transferrin grafted on PEG adamentane). Adamentane, which is hydrophobic, is encapsulated in the core of the CD, while the PEG chains are on the hydrophilic surface of the CD [85].

Atecollagen, a water soluble pepsin digestion product of collagen, can be used to efficiently form NPs with siRNA through electrostatic interactions. The major advantage of this polymer is its biodegradability, as it is eliminated by similar processes as endogenous collagen. Chitosan and trimethylchitosan are biodegradable polymers that are widely studied for their ability to complex siRNA. Moreover, upon the addition of cross-linking agents, they can form NPs that are more stable than polyplexes owing to the combination of electrostatic interactions and ionic cross-linking (see section III).

PLGA is a biodegradable and biocompatible copolymer of glycolic acid and lactic acid. PLGA can form NPs with siRNA that allow the controlled release of the siRNA through the erosion of the polymer matrix. Moreover, compared with cationic polymers, PLGA exhibits lower toxicity [86]. However, due to its hydrophobic and anionic nature, PLGA can only encapsulate siRNA to a small extent, resulting in a very low loading efficiency. Moreover, due to its slow degradation rate, the intracellular release of siRNA from PLGA particles often leads to poor gene silencing efficiency. Therefore, the addition of cationic compounds such as PEI, PLL, chitosan or DOTAP has been shown to successfully increase the efficiency of these NPs [76].

Finally, dextran nanogels have been recently designed for siRNA delivery. They are formed by the physical or chemical crosslinking of polymers. Biodegradable cationic dextran nanogels can encapsulate high quantities of siRNA using electrostatic interactions. A mini-emulsion is first prepared, followed by UV polarization to induce crosslinking. The nanogels are then incubated in a solution of siRNA. This formulation demonstrated good gene silencing *in vitro* without toxicity [87]. Hybrid systems, with poly- or lipoplexes incorporated into a matrix, have also been described.

II.3. THERAPEUTIC POTENTIAL OF SIRNA DELIVERY SYSTEMS IN CANCER TREATMENT

II.3.1. Potential of siRNA

Cancer is a disease in which the mutational and/or epigenetic changes in a genome lead to the stepwise deregulation of cell proliferation and cell death mechanisms [88]. Over the last few years, intense studies on genes that mediate cancer progression have been conducted and have aided the identification of multiple therapeutic gene targets [89]. SiRNA can be designed to silence any gene, thus broadening the possibilities of druggable targets to the entire genome [27]. Moreover, once a target is identified, it requires only a few months to obtain its sequence and to design a specific siRNA. In comparison, the identification and elaboration of a potent drug candidate requires several years. Furthermore, siRNA are highly selective and possess an extremely high inhibitory activity, exhibiting activity at only picomolar concentrations [89]. Finally, siRNA are not processed by drug efflux systems, which are typically responsible for chemoresistance. Therefore, there are several reasonable rationales for exploiting siRNA in cancer therapy.

The administration of multiple siRNA in the same formulation offers an interesting approach to silencing various targets and thus increases treatment efficiency. For example, a cocktail of siRNA that targets several genes implicated in the same cancer-promoting pathway or that targets genes that interfere simultaneously within different pathways could be highly beneficial [27]. However, the

combination of multiple siRNA must be carefully designed to avoid competition between the RNAi pathways that would result in toxicity and/or loss of efficiency.

With the continual progress in tumor characterization and diagnostic tools as well as advances in siRNA-based therapeutics, there is the potential to develop personalized therapies or treatments for specific patient cohorts in the near future [51]. The combination of the siRNA would be adjusted depending on the genetic characteristics of the patient's tumor [27]. However, to achieve this objective, the complexity, heterogeneity and genomic instability of cancers must first be better understood.

II.3.2. Therapeutic targets

Hanahan and Weinberg have described 10 hallmarks of cancer (Fig. 14). Some of the key molecules implicated in these processes, which are generally overexpressed in tumor cells, can be targeted by siRNA. Thus, therapeutic siRNA can be used to knock down gene products involved in tumor growth, tumor-host interactions and/or resistance to conventional cancer therapies, all of these processes being inherently linked. Examples of therapeutic targets are presented in Table II, and a more detailed study can be found in [90].

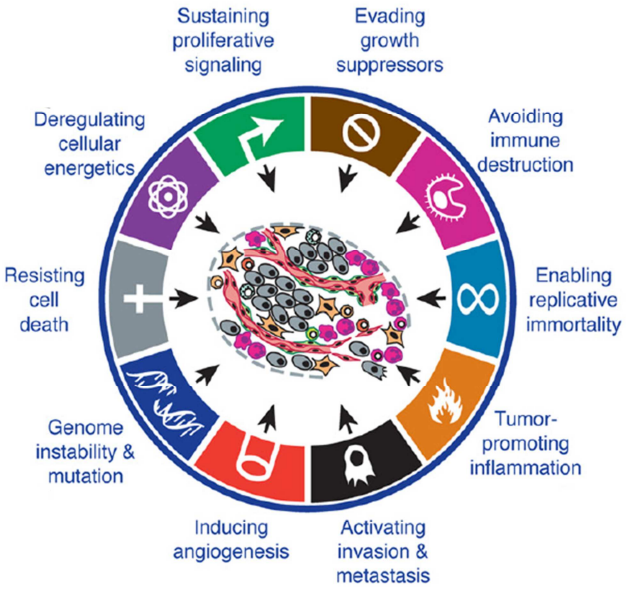

Figure 14: Hallmarks of cancer [91].

SiRNA can silence the gene products directly implicated in tumor growth, such as the growth factors (epidermal growth factor (EGF), platelet derived growth factor (PDGF)) and their receptors (EGFR, PDGFR) involved in cell proliferation and survival [90]. Cancer cells possess the ability to resist

programmed cell death due to the expression of anti-apoptotic proteins such as Bcl-2 or survivin, which are interesting targets for RNAi as well. Yano *et al.* revealed that Bcl-2 silencing using cationic liposomes led to the significant inhibition of tumor growth both in murine liver metastasis and prostate cancer models following I.V. and subcutaneous administrations, respectively [92]. Moreover, because the majority of chemotherapeutic agents exert a pro-apoptotic action, the simultaneous silencing of anti-apoptotic proteins may increase the efficacy of the treatment [93].

Molecules that are indirectly implicated in tumor growth also represent attractive targets for siRNA. This is true for oncoproteins that act as negative regulators of growth suppressors, proteins that disrupt the function of cell cycle regulators or molecules that prevent cellular senescence (Table II).

Another hallmark of tumors is their deregulated energetic metabolism. Indeed, cancer cells meet their energy needs through increased glucose consumption, producing large quantities of lactate *via* glycolysis. This lactate is employed as an energy substrate by oxidative tumor cells, thus preserving the glucose for use by the hypoxic tumor cells. Monocarboxylate transporters (MCTs) are therefore commonly overexpressed in cancer to mediate the lactate transport into and out of tumor cells. Targeting MCTs constitutes an interesting approach to inducing tumor regression by depriving the tumor cells of their essential fuel [94]. The metabolic profile of some tumors is strongly dependent on glutamine, which enters the cells through the amino acid transporter 2 (ASCT2) [95-97]. Thus, ASCT2 is an attractive target for siRNA and its silencing was found to induce significant tumor regression [98].

Tumor cells proliferate in the context of the host environment and develop mechanisms to bypass the host vigilance to grow and propagate. Thus, tumor cells can avoid destruction by the host immune system, generate new vessels to obtain sufficient oxygen and nutrients, invade neighboring tissues and consequently metastasize. Therefore, the inhibition of the molecules implicated in tumor-host interactions, *i.e.*, angiogenesis, invasion, metastasis and/or immune evasion, represents a powerful strategy for cancer treatment. Thus, siRNA targeting of the angiogenic activator VEGF or its receptor (VEGFR2) induces a strong inhibition of tumor growth [99,100]. However, the knockdown of several pro-angiogenic factors is preferred for long-term treatment, as tumors can circumvent the inhibition of one pro-angiogenic molecule by the alternative expression of other pro-angiogenic factors, such as bFGF (basic Fibroblast Growth Factor) [51]. Because tumor growth and metastasis are angiogenesis-dependent, this approach can be highly effective. By conferring motility and altered attachment features to other cells and to the extracellular matrix (ECM), cancer cells can escape the primary tumor mass and metastasize. This progression is governed by multiple factors that can be targeted by siRNA (Table II). For example, the silencing of EphA2 (erythropoietin-producing human

hepatocellular receptor), which is a tyrosine kinase receptor overexpressed in many cancers, induced the inhibition of gastric cell proliferation and invasion [101] and a reduction in tumor growth in an ovarian xenograft model compared with a control group [102]. Tumor growth was even more dramatically reduced when an EphA2 siRNA was combined with paclitaxel (82%).

Finally, the administration of siRNA has exhibited interesting effects in combination with conventional therapies, *i.e.*, chemotherapy and radiotherapy, circumventing their limitations that allow tumor resistance due to the drug-efflux by multiple-drug resistant (MDR) proteins or to the restoration of therapy-induced DNA damages [90]. Therefore, MDR proteins, as well as the molecules related to DNA repair mechanisms, which are both overexpressed in cancer cells, represent potential targets for RNAi. In combination with chemodrugs or irradiaton, these siRNA improve treatment efficacy [103,104].

Small nucleic acids can be designed not only to inhibit a specific protein but also to mimic certain miRNA known as tumor suppressors that are generally inactivated in cancer. Because miRNA possess multiple targets, thereby affecting various oncogenic pathways, the restoration of tumor suppressor miRNA levels might be highly effective [105]. Thus, miRNA mimics of let-7 and miR34 encapsulated in neutral emulsions were injected intravenously and compared for their anti-tumoral effect. Both led to reduced cell proliferation (60% reduction in tumor area for miR34) through cell cycle arrest in a K-RAS^{G12D} transgenic mouse model of lung cancer. In addition, miR34 induced apoptosis [106]. Conversely, because some miRNA that are overexpressed in tumors have been found to be oncogenic, small nucleic acids can be used to silence them. These so-called antago-miRs possess a complementary sequence to the targeted miRNA as well as specific chemical modifications (LNA, 2'-O-methyl). Their structure allows miRNA trapping in a configuration that makes them inaccessible to processing by RISC. The systemic administration of miR10b antago-miR, known as metastasis inducers, resulted in an 86% decrease in pulmonary metastases in a 4T1 mouse mammary carcinoma metastasis model [107].

Table II: Examples of potential targets for siRNA in cancer therapy

Hallmarks	Types of targets	Examples	References
TUMOR GROWTH/ONCOGENESIS			
Sustaining proliferative signaling	Growth factors and their receptors, oncoproteins transmitting growth-promoting signals	EGFR, PDGF-Rβ,EphA2, K-ras,	[108,109]
Resisting cell death	Anti-apoptotic proteins	Bcl-2, Bcl-xL, survivin	[92,110]
Evading growth suppressors	Negative regulators or molecules disrupting p53 and pRb pathways	E7 HPV, Hdmx	[111]
Deregulating cellular energetics	Lactate and amino acid transporters	MCT 1-4, ASCT 1-2	[112] [96]
Enabling replicative immortality	Molecules avoiding cellular senescence	Telomerase	[113] [114]
TUMOR-HOST INTERACTIONS			
Inducing angiogenesis	Proangiogenic factors and their receptors, molecules involved in basement membrane and ECM degradation, hypoxia factors	VEGF, VEGFR, FGF, MMP,HIF-1α	[99,100,115]
Activating invasion and metastasis	Molecules involved in cell mobility, cell-to-cell/matrix adhesion	RhoA, EphA2 , EpCAM	[101,116,117]
Evading immune destruction	Immunosupressive cytokines, negative regulators of T-cells	IL-10, Galectin-1	[118]
TUMOR RESISTANCE TO CHEMOTHERAPY OR RADIOTHERAPY			
	Multidrug resistance (MDR) proteins	MDR1 (P-gp), MDR3	[119]
	Molecules related to DNA repair mechanisms	ERCC1, RRM2, DNA damage sensors ATR/ATM	[104,120-122]

EGFR: epidermal growth factor receptor, PDGF-Rβ: platelet-derived growth factor receptor β, EphA2: erythropoietin-producing hepatocellular A2,Bcl-2: B-cell lymphoma2, Bcl-xL: B-cell lymphoma xL, E7 HPV: E7 oncoprotein from human papillomavirus, Hdmx: human double minute X, MCT: monocarboxylate transporters, ASCT: amino acid transporter, VEGF(R): vascular endothelial growth factor (receptor), FGF: fibroblast growth factor, MMP: matrix metalloprotease, HIF-1α: hypoxia-inducible factor 1-alpha, EpCAM: epithelial cell adhesion molecule, IL-10: interleukine-10, MDR: multi-drug resistance protein, ERCC1: Excision repair cross-complementing 1, RRM2: ribonucleotide reductase subunit M2, ATM : ataxia-telangiectasia mutated , ATR: ATM- and Rad3-related

II.3.3. Overview of clinical trials using siRNA

Due to promising preclinical results, clinical trials of siRNA administration have been conducted or are currently ongoing (Table III). To date, siRNA delivery systems have been shown to be well-tolerated, and no significant dose-limiting or toxicity has been observed. Moreover, some early reports revealed promising results.

The first RNAi-based delivery system (CALAA-01) investigated in clinical trials was a PEGylated cyclodextrin-based polymer 70 nm in diameter that targeted the transferrin receptor (TfR), which is overexpressed in many tumor cells. The siRNA was directed against the M2 subunit of ribonucleotide reductase (RRM2), which is essential for DNA synthesis and replication. The overexpression of this enzyme contributes to drug-resistance and malignant progression. Pre-clinical studies in head and neck squamous cell carcinoma xenograft models exhibited a 2.9-fold reduction in tumor growth. Neither liver toxicity nor complement activation were detected in a pilot safety study on non-human primates [85,122]. Currently, this delivery system is in a phase Ib trial (NCT00689065) using a dose-escalating study in adults with solid tumors refractory to standard-of-care therapies. By biopsy, the authors were able to provide proof of mRNA silencing using an exogenous siRNA in humans [82].

The administration of polymeric NPs in clinical trials is still limited. The majority of delivery vehicles are lipidic. Stable nucleic acid-lipid nanoparticles (SNALP) were developed by Tekmira (TKM-080301). Their formulation consists of PEGylated liposomes that encapsulate an siRNA against polo-like kinase 1 (PLK1), which is a cell cycle protein involved in tumor cell proliferation. The inhibition of PLK1 prevents the tumor cell from completing cell division, resulting in cell cycle arrest and cell death [123]. Phase I preliminary results revealed that the treatment is generally well tolerated (NCT01262235). One patient's disease was stabilized following 6 months at 0.6 mg/kg, and another patient experienced a partial response following 5 months of treatment at 0.7 mg/kg. Patient enrollment is continuing at 0.75 mg/kg [124,125].

A similar SNALP formulation (ALN-VSP02) was investigated by Anylam Pharmaceuticals for liver cancer treatment. In preclinical studies on non-human primates, the SNALP demonstrated good effectiveness for liver disease. Indeed, 65% cholesterol and 85% LDL inhibition in the liver were obtained using SNALP loaded with siRNA directed against the Apolipoprotein B after 11 days. Here, two siRNA targeting the kinesin spindle protein (KSP) and VEGF were encapsulated to induce cell cycle arrest and angiogenesis inhibition, respectively. In phase I clinical trials (NCT00882180), the chronic administration of SNALP (the average length of treatment time was 10.5 months) was well tolerated by patients with primary hepatocellular cancer or liver metastases up to a dose of 1 mg/kg.

Liver tumor biopsies revealed preliminary signs of efficacy, such as efficient SNALP liver delivery and VEGF mRNA knockdown (but not KSP mRNA silencing). In an extension study (NCT01158079), one patient achieved a complete response after 20 months of treatment (bi-weekly injection at a dose of 0.7 mg/kg) and a dose-dependent increase in the number of stable patients was highlighted (Alnylam Pharmaceuticals). However, a decrease in spleen volume, likely an on-target anti-KSP effect and not associated with any adverse events, occurred to a greater degree in the extension study than in the phase I trial and was most pronounced in patients receiving 12 or more doses [126].

A liposomal formulation (Atu027) comprising an siRNA directed against protein kinase N3 (PKN3) encapsulated in neutral fusogenic lipids and PEG-modified lipid components was developed by Silence Therapeutics. PKN3 has been identified as an appropriate therapeutic target for anti-metastatic approaches. Pre-clinical studies reported effective PKN3 mRNA silencing in different animal species as well as tumor growth inhibition and metastasis reduction in a prostate cancer model [66]. Phase I clinical trial results revealed a favorable safety profile without dose-limiting toxicities or signs of immune stimulation (NCT00938574).

The I.V. administration of naked nucleic acids is currently being investigated by the pharmaceutical company Enzon. The delivery systems developed by Enzon are oligonucleotides composed of 16 monomeric units containing 6 or 7 LNA nucleotides. Different targets are currently being examined in phase I clinical trials. Escalating-dose studies demonstrated that LNA was generally well-tolerated by the patients: the dose-limiting toxicity was 8 mg/kg and the maximum tolerated dose was 6.5 mg/kg. The first target investigated (EZN-2968) was hypoxia-induced factor (HIF 1α), which is activated in response to hypoxia-induced stress. HIF 1α is a key transcription regulator of a large number of genes important in cellular adaptation to low-oxygen conditions. Therefore, HIF 1α silencing results in the inhibition of angiogenesis and tumor cell proliferation as well as apoptosis [68]. In phase I clinical trials (NCT00466583), the best overall response was prolonged disease stabilization in 39% of the patients. For 2 patients with renal cell cancer and hepatocellular carcinoma, tumor shrinkage was observed at 1 mg/kg and 1.5 mg/kg, respectively. For the first patient, a 14% decrease in the sum of the tumor sizes was achieved 239 days after the first dose. For the second patient, the sum of the tumor sizes decreased 21% after cycle 1 (36 days after first dose) and increased less than 1% after cycle 3 (120 days) [127].

The knockdown of survivin is being investigated in phase I trials (EZN-3042). Survivin belongs to the inhibitors of the apoptosis gene family and is upregulated in a variety of human cancers but absent in most normal adult cells. Its expression in tumors is associated with a more aggressive phenotype, decreased survival and increased resistance to chemotherapy. In preclinical studies, a 60% inhibition

of survivin mRNA in a xenografted model of human lung cancer was obtained, resulting in a 37-45% tumor growth inhibition. In a phase I escalating-dose study, LNA against survivin was investigated as a single agent as well as in combination with docetaxel (NCT01186328). The best LNA response as a single agent was disease stabilization in 21% of patients with advanced malignancies. When combined with docetaxel, one patient achieved a partial response at 2.5 mg/kg [128-130].

Whereas the previous delivery systems are administered *via* I.V. infusion, one system is intended to be implanted within the tumor. This biodegradable polymeric matrix is inserted in the tumor using a 19 gauge endoscope ultrasound biopsy needle and allows the prolonged release of an siRNA over 12-16 weeks. Pancreatic cancers are targeted by this system, known as LODER (for Local Drug Eluter), which encloses an siRNA against the K-ras oncogene with the G12D mutation that is commonly mutated in pancreatic cancer [131]. Due to promising phase I results (NCT01188785) that indicated a favorable safety profile and the halting of tumor progression, a phase II study (NCT01676259) will begin in the next months to assess the response rate of LODER in patients (Silenseed).

Table III: Ongoing clinical trials with siRNA from clinicaltrial.gov.

Name	Targets	siRNA	Delivery system	Route	Dose schedule	Type of cancer	Status	Sponsor
siRNA-EphA2-DOPC	EphA2	Not mentionned	Neutral liposomes	I .V infusion	Twice weekly (D1, D4) for 3 weeks Starting dose 450 µg/m²	Advanced solid tumors	Phase I – not yet recruiting	MD Anderson Cancer Center
CALAA-01	RRM2	Unmodified	TfR-Targeted PEG-cyclodextrin	I.V. infusion	D1, D3, D8, D10, 11 days of rest. If safe, 2nd cycle	Solid tumors	Phase Ib on going	Calando
Atu027	PK N3	blunt-ended 23-mer, alternating 2'O-methyl	PEGylated lipoplexes	I.V. infusion	Single treatment followed by repeated treatment twice a week for 4 weeks	Solid tumors	Phase I completed	Silence Therapeutics AG
SiG12D LODER	K-RAS ^{G12D}	Not mentionned	LODER	implantation	One to 8 LODERs/ tumor Prolonged release of 12-16 weeks	Pancreas adenocarcinoma	Phase I ongoing	Silenseed Ltd
SiG12D LODER	K-RAS ^{G12D}	Not mentionned	LODER + Gemcitabine or Folfirinox	implantation	Eight LODERs (375 µg each)	Advanced pancreatic cancer	Phase II - not yet recruiting	Silenseed Ltd
TKM-080301	PLK1	2'O-methyl, 2'-F, DNA and PS bond)	SNALP	I.V. infusion	Once a week for 3 weeks followed by 1 week of rest	Primary and secondary liver cancers	Phase I completed	Tekmira
ALN-VSP02	VEGF + KSP	Modified	SNALP	I.V. infusion	One dose (0.4 to 1 mg/kg) every 2 weeks (up to 25 cycles)	Liver cancer	Phase I completed	Alnylam
EZN 2968	HIF-1α	LNA	Naked	I.V. infusion	Once a week for 3 weeks followed by a 3-week period without the drug (6-week cycle)	Solid tumors or lymphoma	Phase I completed	Enzon
EZN 3042	Survivin	LNA	Naked	I.V. infusion	D-5, D-2, D8, D15, D22 ,D29: 2 doses before syst therapy with vincristine, doxorubicin, prednisolone, PEG asparaginase	ALL relaped acute lymphoblastic leukemia (children)	Phase I terminated	Enzon

III. CHITOSAN AS NANOCARRIER FOR SIRNA

Parts of this chapter are adapted from the review 'Chitosan-based siRNA delivery systems' Ragelle, Vandermeulen and Préat, published in Journal of Controlled Release.

III.1. A VERSATILE BIOPOLYMER

Polymers have attracted considerable attention in the formulation of delivery systems for pharmaceutical compounds such as proteins, drugs and nucleic acids. Among them, biodegradable polymers are highly recommended. Indeed, upon delivery, the polymer must undergo chemical or enzymatic degradation to be eliminated from the body. Moreover, the use of biocompatible polymers avoids side effects and carrier-associated-toxicity, especially when the carrier is intravenously injected. For all of these reasons, natural polymers such as polysaccharides, polypeptides or phospholipids are generally used as building blocks for the formulation [132].

III.1.1. Production and basic properties of chitosan

Chitosan is a linear polysaccharide of randomly distributed *N*-acetylglucosamine and glucosamine units (Fig. 15). The primary amines of chitosan exhibit a pKa of 6.5, making it soluble only under slightly acidic conditions. In this case, the presence of positive charges on the chitosan skeleton increases the repulsion between different polymer chains, facilitating their solubilization.

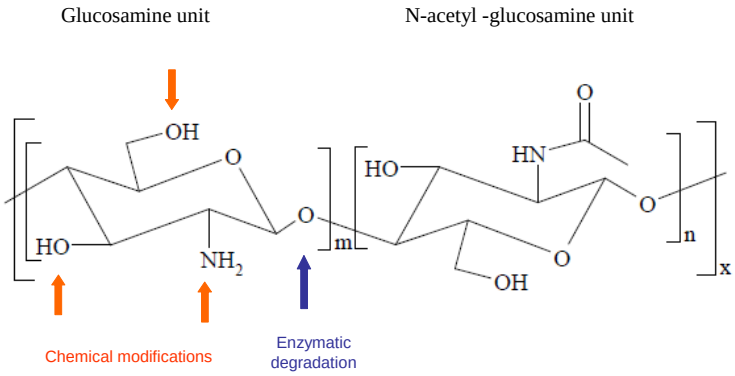

Figure 15: Chitosan chemical structure and reactive sites for chemical modifications.

Chitosan is not largely present as such in nature and thus cannot be directly extracted from natural materials. Indeed, chitosan is a derivative of natural chitin, the second most abundant polysaccharide in nature after cellulose [133]. Typically, chitosan is obtained through the deacetylation of the *N*-

acetyl glucosamine units of chitin, generally *via* hydrolysis under alkaline conditions at high temperature. The deacetylation of chitin is rarely complete. When the acetylation degree falls below 60 mol%, chitin becomes chitosan. In nature, chitin is present in life forms including insects and crustaceans, where it is the primary component of their exoskeleton. Chitin can be obtained from non-animal biomass, in particular from the cell walls of fungal mycelium (Agarics, Pleurotus, Boletus and Lentinula species) or yeasts from several groups, including Zygomycetes, Basidiomycetes, Ascomycetes and Deuteromycetes [134,135].

Figure 16 depicts the production process for chitosan from crustaceans and mushrooms. Generally, vegetal chitosans present a narrow molecular weight (MW) distribution compared with chitosans produced from crustaceans. Indeed, the chitin produced from crustacean biomass often contains high levels of minerals, primarily calcium carbonate, whose amount can reach up to 90% of the chitin dry weight. The quality of chitin and chitosan is therefore often non-uniform and dependent on seasonal variation and the crustacean species [136]. Moreover, the chitosan from non-animal sources is considered safer for biomedical and healthcare uses. For example, these chitosans are less prone to induce allergies in comparison with those obtained from crustacean shells.

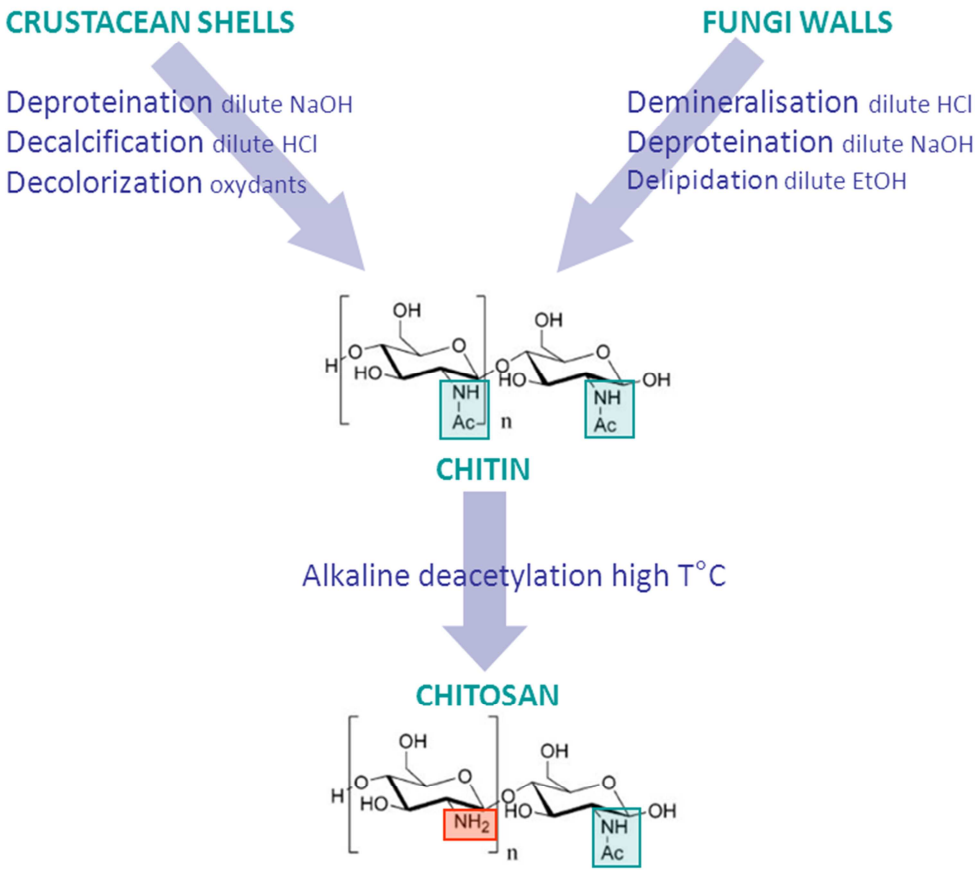

Figure 16: Production of chitosan from animal and vegetal sources.

III.1.2. Chitosan for pharmaceutical and biomedical uses

III.1.2.1. Safety aspect

Chitosan is biodegradable [137,138] and biocompatible [139] [140]. Chitosan is generally eliminated by renal clearance. When its MW is too high, chitosan is subject to enzymatic degradation, which decreases its MW to a suitable size for renal elimination. Hydrolytic enzymes such as lysozymes or chitinases have been found to mediate chitosan degradation to oligosaccharides by catalyzing the hydrolysis of 1,4-β linkages. These enzymes can be found in blood or in the human intestine. In humans, three chitinases are responsible for chitosan degradation. The efficiency of degradation is thought to be dependent on the acetylation degree as well as the chitosan MW. Moreover, some chemical modifications can impact the degradation fate [141].

In vitro, chitosan presents a half-maximal inhibitory concentration (IC_{50}) ranging from 0.2 to 2 mg/mL [142]. Table IV presents toxicology data for chitosan and chitosan-oligosaccharides following administration *via* different routes. Chitosan presents an LD_{50} of 16 g/kg for oral administration in mice, which is nearly equivalent to sugar or salt [143,144]. In comparison, a solution of PEI (30% in water) exhibited an LD_{50} of 1.15 g/kg (TCI America). Moreover, the oral administration of chitosan up to 6.75 g/day to healthy human volunteers was found to be safe, without any relevant clinical side effects [145]. Chitosan is currently used as a common dietary supplement for preventing fat absorption and has been designated as Generally Recognized As Safe (GRAS) by the FDA [142]. Nevertheless, high dose effects were observed in rabbits following the I.V. administration of 50 mg/kg/day, most likely due to blood cell aggregation, but doses of 4.5 mg/kg/day were found to be safe. The subcutaneous administration of 10 mg/kg in dogs provoked cytokine activation, and clinical signs, such as anorexia and vigor loss, were observed at 50 mg/kg [146].

The toxicity profile of chitosan might be altered by chemical modifications or by administration in a micro- or nanoparticulate form. Although pre-clinical studies demonstrated that chitosan NPs are well-tolerated [147], clinical data remain limited. The intra-arterial administration of a ^{166}Holmium-chitosan complex, used as a radiopharmaceutical for cancer therapy, was investigated in patients with hepatocellular carcinoma. The results demonstrated a durable complete response with an acceptable safety profile (no grade III/IV toxicity observed) [148]. Several clinical trials of chitosan-based formulations are currently underway, varying from chewing-gum for chronic kidney diseases, eye drops to treat dry eye syndromes or particulate vaccines for intranasal administration. This will certainly provide more information about the safety of chitosan delivery systems in the near future.

Table IV: Toxicity of chitosan from [146].

Study[a]	Results	
Single dose various species		
LD_{50} value of chitosan	Oral rat: >1500 mg/kg Intraperitoneal rat: 3000 mg/kg Subcutaneous mouse: >10,000 mg/kg Intraperitoneal mouse: 5200 mg/kg Oral mouse: >16,000 mg/kg	[149] [150]
LD_{50} value of chitooligomers (produced by depolymerisation of chitosan)	Oral mouse: >10,000 mg/kg (no deaths or clinical signs of toxicity in dose range of 1000–10,000 mg/kg)	[151]
Repeat dose rat		
Dietary administration of *N*-acetylglucosamine (a copolymer of chitosan) to groups of 10 male and 10 female rats at 0%, 0.625%, 1.25%, 2.5% or 5% (corresponding to 0, 302–351, 588–695, 1218–1412 or 2476–2834 mg/kg/day) for 13 weeks	No obvious toxicity seen (among males, there was a increase in bodyweights along with daily food intake, perhaps due to the sweet flavour of *N*-acetylglucosamine)	[152]
Dietary administration with glucosamine (another copolymer of chitosan) in rats at 300–2700 mg/kg/day for 52 weeks and dogs at 159–2149 mg/kg/day for 26 weeks	No adverse findings reported	[153]
Dietary administration of chitooligomers (produced by depolymerisation of chitosan) at 0%, 0.75%, 1.5% or 3% (corresponding to levels of 0, 750, 1500 or 3000 mg/kg/day) to in groups of 10 male and 10 female rats over 30 days	No study findings seen	[151]
Oral gavage administration of either 0, 500, 1000 or 2000 mg/kg/day chitosan oligosaccharide (also known as oligoglucosamine and prepared by hydrolysis of chitosan) to groups of 9 male and 9 female rats for 4 weeks or to groups of 10 male and 10 female rats using 0%, 0.04%, 0.2% or 1% (corresponding to 0, 25–27, 124–142 or 653–720 mg/kg/day) in the diet over 90 days	Oral gavage dosing showed no study findings. Dietary administration had findings confined to the high dose level and included erythema and swelling of the snout and forelimbs and, loss of fur on the forelimbs along with macroscopic emaciation, swelling of the snout, auricles and forelimbs and, alopecia of the forelimbs. Other findings were decreased bodyweight gain and food consumption, increased platelet count, lymphocyte count and differential neutrophil count abnormalities in urinalysis (including proteinuria) and blood chemistry (including decreased blood protein, creatinine, glucose, total cholesterol and triglyceride), as well as a small thymus, small spleen, dark spots or areas on the glandular stomach mucosa, pale Harderian glands and small testes along with vacuolised Sertolic cells and decreased germ cells. A dietary level of 0.2% produced no signs of toxicity	[154,155]
Dietary administration of oligo-*N*-acetylglucosamine (consists of the monomer and oligomers of *N*-acetyl-D-glucosamine) to groups of 10 male and 10 female rats at 0.2%, 1% or 5% for 90 days (with the latter 2 dose levels reported as corresponding to 641 or 3640 mg/kg/day)	No obvious toxicity was seen and study findings were limited to occasional increases in food consumption (perhaps due to the sweet nature of oligo-*N*-acetylglucosamine in the diet) in males at the high dose level	[156]
Dietary administration of *N*-acetylglucosamine to groups of 10 male and 10 female rats at 0%, 1.25%, 2.5% or 5% (corresponding to 0, 580–647, 1159–1269 and 2323–2545 mg/kg/day) for 52 weeks	No obvious toxicity (a slight suppression of bodyweight gain at the higher dose levels was attributed to slight reduction of caloric intake due to high concentration of test material)	[157]
Repeat dose mouse, rabbit and dog		
Intraperitoneal and subcutaneous dosing of 5 mg chitosan to mice every 2 weeks over a 12-week period and dietary administration of up to 5% over 4 weeks	Intraperitoneal dosing resulted in decreased bodyweights along with clinical signs of emaciation, pilomotor, depilation around the rostrum and eyelids, oedema of the auricle, rostrum and eyelids and photophobia and, histological changes of macrophages with hyperplasia in the mesenterium. Following subcutaneous injection, the dose site was swollen and contained polymorphonuclear cells and cell debris. Dietary administration at 5% resulted in decreased bodyweight as well as a reduction in the number of *Bifidobacterium* and *Lactobacillus* in normal flora of the intestinal tract, although there was no effect with a 0.5% diet	[158]
Repeat dosing of chitosan (10 days with a solution formulation and 14 days with a powder formulation) to rabbits (no further details are given)	No macroscopic or histopathological changes in organs and tissues (no further details are given)	[159]
Intravenous injection of chitosan to rabbits at 4.5 and 50 mg/kg/day for 10 days and oral dosing at 700–800 mg/kg/day for 34 weeks	Intravenous injection at 4.5 mg/kg/day produced no abnormal changes, while 50 mg/kg/day caused death. Oral dosing produced no evidence of toxicity	[149,160,161]
Subcutaneous dosing of chitosan to mongrel dogs for 1 month at 0, 10, 30, 50, 100, 150 and 200 mg/kg/day	Vigour loss and anorexia were seen from 50 mg/kg/day (transient at 30 mg/kg/day), with deaths from 150 mg/kg/day and evidence of severe dyspnoea. Increased white blood cell count (due to neutrophilia) was seen from 50 mg/kg/day, while raised lactate dehydrogenase and creatine kinase (notably at 200 mg/kg/day) occurred. Severe pneumonia was noted in dogs that died	

III.1.2.2. Biological properties

Chitosan presents remarkable biological properties, which has paved the way to its application in the pharmaceutical and biomedical fields [159,162] as a novel delivery system and as a biomaterial. First, its hemostatic properties make chitosan a good candidate for wound dressing [163,164], and it has been approved by the FDA for this application. Several clinical trials have been conducted using chitosan-based systems for knee injuries, dental dressings or wound debridements (clinicaltrials.gov). Chitosan plays an important role in the nutritional supplement market as a weight-loss aid and cholesterol lowering agent, even though its clinical efficiency remains controversial. Chitosan is thought to bind free fatty acids and bile salt components, thus preventing fat absorption in the gut [146]. Moreover, chitosan presents antimicrobial properties [165] [166]. Although the exact mechanism remains unclear, it has been suggested that due to its cationic nature, chitosan binds to microbial cell membranes, leading to the leakage of the intracellular constituents. In addition, its chelating property allows the binding of metal ions, inhibiting toxin production and microbial growth [167]. Furthermore, chitosan possesses superior mucoadhesive properties by facilitating electrostatic interactions with the glycoproteins of the mucus, either *via* hydrogen bonds or ionic interactions [168,169]. Finally, chitosan exhibits penetration enhancement properties. The mechanism of action is thought to be a transitory opening of tight junctions in the cell membrane in response to the chitosan positive charges.

Over the last decades, the interesting biological properties of chitosan have promoted its use in the development of drug delivery systems and biomaterials [169]. Recently, a commercial DNA transfection reagent based on a chitosan oligomer has been developed (Novafect, Novamatrix).

III.1.3. Chitosan as a nanocarrier

The potential of chitosan as a nanocarrier is based on (i) its biocompatibility, (ii) its easy formulation in nanosystems and (iii) its cationic properties.

The combination of the mucoadhesive and penetration-enhancement properties of chitosan is highly advantageous for topical delivery applications [169]. Indeed, chitosan-based nanocarriers have been widely investigated for ocular, nasal or buccal delivery of various drugs. The prolonged contact of the delivery system with the mucosa that is associated with the absorption-enhancing effect of chitosan has been shown to increase drug efficacy. The nasal administration of insulin incorporated into chitosan NPs in rabbits resulted in increased insulin absorption compared with standard formulations [170]. Moreover, chitosan offers powerful applications for immunization. Chitosan-based antigen carriers have been described for intranasal administration [171]. Indeed, chitosan is used as an

excipient of an intranasal Virus-Like-Particle Vaccine currently being evaluated in clinical trials by Norwalk (clinicaltrials.gov). In addition, ocular chitosan-based delivery systems of nucleic acids have shown great potential [169].

Chitosan has been used for the oral delivery of peptides, either as the main excipient or as a coating material of liposomes or nanocapsules, to increase their residence time in the gastrointestinal tract and enhance transmucosal transport [144].

Finally, the I.V. administration of chitosan-based nanocarriers was investigated for the delivery of DNA [172], contrast agent [173], chemotherapeutics [174,175] and various other drugs [176,177], with encouraging results.

III.2. CHITOSAN-BASED SIRNA DELIVERY SYSTEMS

Because of its cationic nature, chitosan offers attractive possibilities for siRNA delivery, allowing siRNA complexation into NPs in a fast and relatively easy process. Furthermore, chitosan can readily be chemically modified on its amine and hydroxyl functional groups. Here, the parameters influencing the formulation process and the improvements of chitosan/siRNA NPs are reviewed, as well as their *in vivo* applications.

III.2.1. Parameters influencing the chitosan/siRNA NPs and their impact

To achieve high gene silencing efficiency of siRNA/chitosan NPs, some parameters have to be optimized including (i) the characteristics of the chitosan itself, such as its molecular weight or deacetylation degree, (ii) the formulation method, (iii) the addition of efficiency enhancers and (iv) targeting ligands.

III.2.1.1. Chitosan characteristics

III.2.1.1.1 Chitosan molecular weight (MW)

The MW of chitosan is an important parameter to consider for the formulation of NPs. Chitosan chains form the NP structure. It is comprehensible that the lengths of these chains will have an impact on NP stability. To protect siRNA before internalization, NPs need to have appropriate stability that is high enough to protect siRNA before internalization but low enough to permit its release in the cell cytoplasm [178]. Chitosan MW not only influences the physico-chemical and morphological characteristics of NPs but also affects their biological activity *in vitro*.

The different types of chitosan can be classified according to their MW. For better comprehension, we suggest the following classification: very low MW (< 10 kDa), low MW (from 10 to 80 kDa), high MW (80-300 kDa) and very high MW chitosan (> 300 kDa).

First, chitosan MW impacts NP formation. Liu and colleagues showed that very low MW chitosan was not able to condense siRNA to form discrete NPs because of the short chain length of the polymer [179]. Similarly, large and unstable NPs were obtained with 2 kDa chitosan [180]. Complete siRNA binding could only be observed with 25 and 50 kDa chitosan and not with 10 kDa MW [180]. Finally, low MW chitosan (40 or 80 kDa) offered better protection against enzyme degradation than 10 kDa chitosan, thus confirming that the formulation of stable NPs is difficult to achieve with very low MW chitosan [181]. Kong and colleagues are the only ones to report the formation of 130-nm diameter NPs with very low MW chitosan (2 and 5 kDa). However, these NPs demonstrated low gene silencing efficiency *in vitro* on MDA-MB-231 cells [182]. A minimum MW and binding affinity is required to efficiently complex siRNA, thereby forming NPs in the nanometer range. Various publications have demonstrated the formation of discrete NPs with high MW chitosan and, more recently, with low MW chitosan. For instance, NPs with a diameter of 200 nm were obtained with low MW chitosan (70 kDa) [179]. More recently, Fernandes reported the formation of NPs with mean diameters of 150 and 400 nm using chitosans of 25 and 50 kDa, respectively [180]. High MW chitosans have been widely used to complex siRNA [179,183]. However, beyond a certain MW, chitosan chains may be too long to form NPs with a mean diameter of 100-300 nm. Indeed, Liu and colleagues mentioned that chitosan molecules (MW 64.8–170 kDa) that were 5–10 times the length of siRNA (MW of 13.36 kDa) could form suitable NPs [184]. Generally, the mean diameter of the NPs increases with the chitosan MW [181,182,185]. NPs with diameters of 200, 250 and 330 nm were obtained with chitosan MWs of 20, 40 and 80 kDa, respectively [182]. Likewise, a smaller particle size was obtained with a 110 kDa chitosan than with a 270 kDa chitosan [185]. On the contrary, Holzerny and colleagues did not report any influence of MW on the size, but rather on the NP morphology: spherical NPs were formulated with 44 kDa chitosan in contrast to 143 kDa, which formed elongated and irregular NPs [186].

By affecting the size, morphology and/or stability of the NPs, chitosan MW indirectly influences the NP biological activity. Indeed, major differences in the levels of *in vitro* transfection can be observed depending on the MW. GFP silencing increased up to 65% with high MW chitosan of 114 and 170 kDa, whereas less than 5% GFP extinction was observed for the low MW chitosans (9 and 12 kDa) [179]. Similarly, chitosans of 55 and 142 kDa were more efficient than the 16 and 35 kDa chitosans [187]. In another study, 25 kDa chitosan demonstrated almost no silencing in three cell lines, whereas the silencing was slightly increased when using 50 kDa (50% in OV3 cells and 10% in HeLa cells) [180]. The same trend was observed by Kong and colleagues: the percentage of luciferase

silencing in MDA-MB-231 was slightly increased (from 60% to 70%) when increasing the MW from 20 to 40 or 80 kDa [182]. Unlike the above-cited publications, Holzerny and colleagues showed that NPs made of 44 kDa chitosan were more efficient (80% silencing) than NPs of 143 kDa chitosan (60%) on H1299 cells. The authors explained this difference by referring to the increased uptake of 44 kDa NPs due to the NP morphology [186].

Because of the lack of uniformity in the transfection protocols, it is difficult to draw a general conclusion from the literature about the influence of MW (as shown in Table VI). However, some trends emerge and are summarized in Table V.

Table V: Performance of chitosans according to their MW.

Chitosan denomination	MW (kDa)	NP formation [a]	*In vitro* gene silencing efficiency [b]
Very low MW chitosan	< 10	-/+	-
Low MW chitosan	10 - 80	++	-/++
High MW chitosan	80 - 300	++	++
Very high MW chitosan	> 300	+	+

[a]: monodisperse NPs with a mean diameter < 300 nm and [b]: ++ > 50%, + 30-50% and - < 30% protein silencing, considering a DD of approximately 80%.

III.2.1.1.2 Chitosan deacetylation degree (DD)

The percentage of deacetylated primary amine groups represents the charge density of chitosan in acidic conditions and determines the ability of chitosan to complex siRNA. Because of its stiff molecular topology and short length, siRNA needs a high number of positive charges to remain efficiently bound. Therefore, high DD (≥ 80%) is mandatory to complex siRNA and form efficient NPs [178]. Liu et al. managed to formulate NPs of approximately 200 nm with high MW (173 kDa) and low DD (54%) chitosan; however, these NPs yielded low transfection efficiency on H1299 GFP cells because of their lack of stability [179]. Recently, Malmo and colleagues used a fully de-N-acetylated chitosan, which formed NPs of approximately 30-80 nm and mediated more efficient silencing than the conventional partially de-N-acetylated chitosan [187]. Fully de-N-acetylated chitosan exhibited more effective endosomal escape than partially de-N-acetylated chitosan because of the high number of charges. Moreover, the use of this type of chitosan eliminated the need for a cross-linker agent.

III.2.1.1.3 Methods of formulating siRNA/chitosan NPs

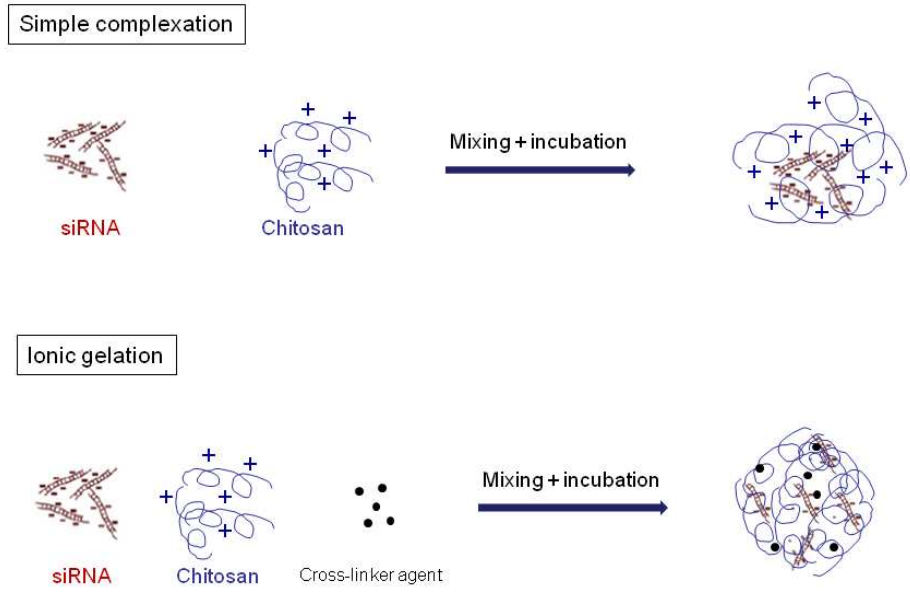

Figure 17: Schematic representation of the two main methods of formulating chitosan NPs for siRNA delivery.

The first method of NP formulation described in the literature was the simple complexation, where siRNA is mixed with chitosan [183] (Fig. 17). The formation of NPs through this method occurs at a specific chitosan/siRNA ratio. Usually, the N/P ratio (the molar ratio of the amino groups [N] of the chitosan to the phosphate groups [P] of siRNA) is calculated, but the weight ratio is also used. These ratios have to be optimized depending on the characteristics of the chitosan and the formulation process.

Some publications have highlighted a clear influence of the N/P ratio on NP size. Increasing the N/P ratio allows a better complexation of the siRNA, resulting in smaller particles [183]. Kong and colleagues reported that a higher N/P ratio (50-100) tends to form NPs in the 100 nm-range, whereas 200 nm NPs were obtained at a lower N/P ratio (5-10) [182]. In other publications, the N/P ratio influenced the transfection efficiency: for example, Liu and Howard demonstrated an increased efficiency of the NPs formulated at high N/P ratios (50-150). However, formulations with N/P ratios greater than 70 showed enhanced toxicity [179,183]. In this case, the large excess of free chitosan can interact with membrane components or interfere with cellular processes and thus reduces cell viability [184]. To address this toxicity issue, NPs formulated at low N/P ratios (4 and 8) have recently shown good luciferase silencing on H1299 cells [186]. However, the use of low N/P ratio might impact NP stability, which is crucial for *in vivo* administration. Indeed, NPs formulated at N/P ratios lower than 2 were unstable at pH 6.5. At pH 8, a complete release of siRNA occurred for N/P ratios lower than 10, whereas only a partial release was observed at N/P ratio of 10 [181].

Some authors reported a poor efficiency of NPs that were formulated using the simple complexation method, with less than 20% gene silencing [185]. These results were related to the weak interactions between siRNA and chitosan, resulting in poor stability in the transfection medium and NP dissociation before their uptake by the cells. By adding a cross-linker agent in the formulation, such as sodium tripolyphosphate (TPP), the interactions between siRNA and the polymer are strengthened (Fig. 17). This approach, called ionic gelation, permits higher NP stability [185,188]. For example, Katas and colleagues obtained 82% luciferase silencing on CHO K1 cells using the ionic gelation method. Another group used thiamine pyrophosphate to consolidate the NP structure and was able to silence GFP in HepG2 cells up to 70% 5 days after transfection [189].

III.2.1.1.4 The type of chitosan

The type of chitosan is also a factor that might influence NP formation or biological activity. Chitosan comes from chitin, which can be extracted from crustacean shells or from fungi cell walls (Fig. 16). Chitin is linked to proteins and glucans in crustaceans and fungi, respectively. Because of the different extraction or purification methods, the nature of the impurities can be different, which may contribute to variations in the NP formation or efficacy [186]. However, the influence of chitosan origin has not been studied and is rarely considered.

Some publications have studied the influence of chitosan salt type. Different types of chitosan salts (hydrochloride Cs-HCl, glutamate Cs-Glu, aspartate Cs-Asp and acetate Cs-Ac) were compared for their ability to form NPs *in vitro*. The type of salts highly influenced both the size and the zeta potential of the NPs at fixed weight ratios. The binding of siRNA onto Cs-HCl and Cs-Ac was slightly increased in comparison with Cs-Glu and Cs-Asp. Interestingly, regardless of the type of salt, the GFP silencing was enhanced with low MW chitosan salts in comparison with high or very high MW chitosan salts. Among these chitosan salts, Cs-Ac demonstrated the lowest efficiency *in vitro*, likely because of the large particle size. The authors conclude that the MW and the N/P ratio tend to influence gene silencing rather than the salt form. A GFP silencing of 50% was observed in HeLa cells with Cs-Asp, Cs-Glu and Cs-HCl five days after transfection [190]. Another group evaluated different chitosan salt form *in vitro* and showed that Cs-Glu was more efficient than Cs-HCl [185].

Finally, Malmo and colleagues synthesized self-branched chitosan and compared it with the linear counterpart. No difference was observed regarding siRNA transfection efficiency contrary to what was noticed for pDNA [191].

Table VI summarizes the different formulations described above and lists their *in vitro* transfection efficiencies. Some differences in biological activity can be observed depending on the cell model used. It has been shown that the internalization mechanisms of chitosan NPs are highly cell-line

dependent. For example, similar chitosan/siRNA NPs were taken up more readily by A549 or HEK293 cells (95% uptake) than Raw 264.7 or HepG2 cells (only 50%) [181,192]. Moreover, the same formulation mediated different gene silencing efficiencies depending on the cell type [185]. Therefore, the biological activity variability observed in each article with similar formulations might be due to different cell lines, cell density, transfection medium, target proteins and/or doses.

Table VI : Chitosan-based NPs: *in vitro* efficiency.

Chitosan/siRNA					
MW (kDa)	**DD (%)**	**Protein /mRNA silencing (%)**	**Cell model**	**Transfection conditions**	**Ref**
50	92	< 10	HEK 293 GFP	0.5 µg siRNA in complete medium for 4 h (24-well plate)	[184]
114	84	78 89	H1299 GFP Peritoneal macrophages from GFP transgenic mice	50 nM siRNA serum-free medium for 4 h 100 nM siRNA serum-free medium for 4 h	[183]
114	84	60	Peritoneal macrophages	50 nM siRNA serum-free medium for 4 h	[193]
9, 12 65, 114, 170	95, 77 78, 84, 84	< 5 45-65	H1299 GFP	50 nM siRNA serum-free medium for 4 h	[179]
173	54	< 5	H1299 GFP	50 nM siRNA serum-free medium for 4 h	[179]
190-310	75-85	70	Lovo FHL2	100 nM siRNA serum-free medium for 4 h	[194]
67/ 50-150/ 150-400	84 86	< 20	HEK 293 GFP	50 nM siRNA overnight in serum-free medium	[195]
Cs Glu 160/470	86	51	CHO K1 previously transfected with pLuc	4 pmol siRNA/well in serum-free medium for 24 h or 48 h (96-well plate)	[185]
10	92	56 (72 mRNA)	HepG2 DPP-IV	100 nM siRNA in high glucose medium 10% FBS pH 6.5 for 24 h	[192]
10	92	50 80	HepG2 (SSB silencing) LS174 T (SSB silencing)	100 nM siRNA in high glucose medium 10%FBS pH6.5 for 24 h	[181]
44, 63, 93 143	86, 84, 81 78	80 60	H1299 luc	150 nM in complete medium for 48 h	[186]
54.6, 74.5, 100.3, 141.6	100	> 90	H1299 GFP	45 nM siRNA in serum-free medium supplemented with mannitol and Hepes for osmolarity for 5 h, pH 7.2	[187]
25 50	96	< 1% in all cell lines 10% in HeLa 50% in OV-3 < 1% in MG 63	HeLa, OV-3, MG 63	5 µg siRNA/well in complete medium for 6 h (24-well plate)	[180]

Chitosan/siRNA/TPP or thiamine pyrophosphate						
Cross-linker	**MW (kDa)**	**DD (%)**	**Protein /mRNA silencing (%)**	**Cell model**	**Transfection conditions**	**Ref**
TPP	Glu 160/470	86	82	CHO K1 previously transfected with pLuc	4 pmol siRNA/well in serum-free medium for 24 h or 48 h (96-well plate)	[185]
TPP	67, 50-150 150-400	84 86	<20	HEK 293 GFP	50 nM siRNA overnight in serum-free medium	[195]
Thiamine pyrophosphate	20, 40 200, 460	85	70 50	HepG2 GFP	20 pmol/well siRNA for 24 h (96-well plate)	[189]

Efficiency enhancer						
Enhancer	**MW (kDa)**	**DD (%)**	**Protein /mRNA silencing (%)**	**Cell model**	**Transfection conditions**	**Ref**
PEI branched 25 kDa	100	87.7	55	A549 previously transfected with pGFP/Lipofectamine	50 pmol siRNA/well in serum-free medium for 12 h	[196]
PLR	50-150	87	Not quantified	Hepa 1-6, VK2, A549, 293 T-GFP	48h incubation (doses nc)	[197]
HA (+TPP)	HCl 57	93	20-30	HEK 293 GFP, HEK 293 GFP-Snail	100 nM in HBSS pH 6,4 for 3 h	[188]
	HCl 119	75-90	85	A549 luc	0.15 µg siRNA/well in medium for 4 h (24-well plate)	[198]
TAT (+TPP)	Low MW	80	> 80	Neuro2a transfected with Ataxin plasmid	40 nM/well siRNA in serum-free medium for 4 h	[199]
Psp	5	85	> 80	MDA-MB-231 luc	300 ng siRNA in serum-free medium for 4 h (24-well plate)	[182]
Peptide PGA	80	85	80	HT1080 luc	0.25 µg siRNA/well in serum-free medium pH 6 for 1 h (24-well plate)	[200]
PG	Glu 470	86	55-60	HEK 293, HeLa previously transfected with pLuc	50 pmol siRNA/well in serum-free medium for 24 h	[201]
			35 (30 mRNA)	Jurkat, A3.01 (expressing CD4 cells)	200 pmol siRNA/well in serum-free medium for 4 h	[202]
CD	150	83	60 (84 if PEG)	HEK 293, L929 previously transfected with pLuc	125 nM in complete medium	[203]
Guanidinylation	50	92	34.9	HEK 293 GFP	0.5 µg siRNA in complete medium for 4 h (24-well plate)	[184]
Targeting						
Targeting ligand	**MW (kDa)**	**DD (%)**	**Protein /mRNA silencing (%)**	**Cell model**	**Transfection conditions**	**Ref**
CD7 antibody (+PG)	Glu 470	86	65 (80 mRNA)	Jurkat, A3.01(expressing CD4 cells)	200 pmol siRNA/well in serum-free medium for 4 h	[202]
FA	25	96	42 in OV-3, 57 in HeLa (mRNA)	HeLa, OV-3, MG 63 FA(-) cells	5 µg siRNA/well in complete medium for 6 h (24-well plate)	[180]
	50	96	57 in both cell lines (mRNA) <1 in MG 63			
RGD	50-190	nc	NPs were not tested for *in vitro* silencing			[204]

CD : cyclodextrin, CD4 : human T cell receptor CD4, DPP-IV : dipeptidyl peptidase IV, FA folate, FA (-) : folate receptor negative, FHL-2 : 4-1/2 LIM protein 2, Glu: chitosan glutamate, HA: hyaluronic acid, HCl : chitosan hydrochloride, PG : polyguluronate, PGA : poly(8 pluronic acid) , PLR : poly-L-arginine, Psp: phosphorylatable peptide, RGD : Arg-Gly-Asp, SSB : Sjögren syndrome antigen, nc : not communicated

III.2.2. Improving siRNA chitosan-based NPs

Initial publications demonstrated the great potential of native chitosan for siRNA delivery, provided that the transfection protocol and/or cell models were optimal. However, when the studies were extended to other cell models or different transfection conditions (such as serum-containing medium), the reduced gene silencing efficiency of such NPs was noticed. For most applications, practical use of chitosan has been limited by its low water solubility at physiological pH and its poor buffering capacity. The limitations of native chitosan were then clearly identified, as was their impact on the NP *in vitro* efficiency [205] [206]. To overcome chitosan limitations and to improve or impart new properties to the polymer, further developments of chitosan-based delivery systems were developed by grafting or mixing additional materials to the formulation.

III.2.2.1.1 Chitosan derivatives

Chemical modifications of the chitosan chains generally either by grafting small molecules or polymer chains onto the chitosan backbone or by the quaternization of the amino groups were investigated. Chitosan chains possess three attractive reactive sites for chemical modification: two hydroxyl groups (primary or secondary) and one primary amine by glucosamine units (Fig 12). The site of modification is dictated by the desired application of the final chitosan derivative. Regarding nucleic acid binding, the preservation of the primary amine is required. Various chitosan derivatives have emerged for siRNA delivery. These strategies resulted in improved solubility, transfection efficiency and/or stability. A non-exhaustive list of these polymers is presented in Table VII.

Table VII: Chitosan derivatives for siRNA delivery

Derivatives	**Improvements**	**Ref**
PEGylated chitosan	Increased solubility and stability	[199,203,207,208]
Trimethyl chitosan (TMC)	Increased solubility; pH independence	[209,210]
Thiolated chitosan/TMC	Increased extracellular stability through the formation of intra- and intermolecular disulfide bonds Enhanced intracellular release	[211,212]
Glycol chitosan	Increased stability	[213,214]
Guanidinylated chitosan	Improved cellular uptake by mimicking the CPP trans-membrane activity	[184]

III.2.2.1.2 Addition of excipients to the formulation

If it is not possible to chemically modify chitosan, another possibility is to add to the formulation an excipient that has the wanted properties and that can impart it to the final delivery system. Numerous examples have been described in the literature, such as the inclusion of amine rich polymers, peptides, negatively-charged components or cyclodextrin.

III.2.2.1.2.1 *Amine rich polymers*

Amine-rich polymers are interesting endosome-disrupting agents: the protonation of their amino-groups at acidic pH provokes the rupture of the endosome and the release of siRNA in the cytoplasm. Of these polymers, PEI [56], poly-l-arginine (PLR) [215,216] have been used in combination to chitosan.

PEI has shown high transfection efficiency due to its numerous primary amines. However, this polymer often exhibits toxicity, and the lack of stability of siRNA-PEI or siRNA-PEG-PEI polyplexes in the blood has been demonstrated [217]. Therefore, PEI itself does not constitute an adequate candidate for siRNA delivery. However, its interesting buffering ability can be exploited in combination with other polymers as a strategy to increase their efficiency. Jere and colleagues grafted branched PEI onto chitosan using an imine reaction, thus increasing the water solubility of the co-polymer and the gene silencing efficiency: the GFP expression on A549 cells was reduced 2.5-fold compared with PEI-siRNA complexes, without any toxicity (90% cell viability for chitosan-g-PEI and only 50% for PEI) [196]. Another siRNA carrier made of glycol chitosan mixed with PEI achieved 80% of red fluorescent protein silencing on B16F10 cells. Moreover, these NPs protected siRNA against RNAse degradation for 2 h [213].

PLR and its derivatives offer promising approaches to enhance chitosan efficiency. In a recent study, chitosan was grafted with PLR and PEG. The cellular levels of GFP and survivin were highly reduced with the Cs-PEG-PLR conjugate in different cell lines compared to chitosan alone. Moreover, due to the presence of PEG, the NPs were stable in the presence of high serum content (10 to 50%), unlike the chitosan-PLR complexes. The coupling increased both the size and the zeta potential of the NPs compared with the chitosan/siRNA complexes: from 117 to 375 nm and from 16 to 24 mV, respectively [197].

III.2.2.1.2.2 *Peptides and their mimics*

Cell-penetrating peptides (CPPs) have recently attracted attention because of their membrane fusion properties that are used to increase NP uptake. CPPs are composed of positively charged amino acids

such as arginine or lysine. Therefore, due to their high primary amine content, they can also act as endosomal disruptors. In one study, the TAT peptide was covalently linked to the chitosan-PEG [199]. The characteristics of the particles were modified by grafting: chitosan-PEG-TAT NPs had diameters of 5 nm and were more spherical and monodisperse than those obtained using unmodified chitosan, which possessed a diameter of 50 nm. This size difference could be explained by a breaking of the chitosan chains due to the use of hydrazine monohydrate during the polymer synthesis. The chitosan-PEG-TAT NPs displayed low toxicity (< 10%). Finally, chitosan-PEG-TAT NPs showed successful ataxin silencing on Neuro2a cells. Another group developed guanidinylated-chitosan to mimic the CPP mechanism. The NPs made from this co-polymer exhibited no cytotoxicity, whereas chitosan NPs showed a slight decrease in cell viability at high ratios. Moreover, the GFP silencing on HEK293 GFP cells was increased: 34.9% and < 10% for guanidinylated-chitosan NPs and chitosan NPs, respectively [184].

Finally, a phosphorylatable short peptide (pSP) was conjugated to very low MW chitosan. The conjugation of pSP to chitosan did not alter the particle size or intracellular uptake of NPs. However, the luciferase silencing obtained with these NPs was greatly increased and comparable to Lipofectamine because of the enhanced buffering capacity of the pSP. Indeed, the authors demonstrated that once in the cell, the pSP was phosphorylated by cytoplasmic Jak2 kinase, leading to the unpacking of the NPs and consequently to siRNA release [182].

III.2.2.1.2.3 *Negatively charged components*

Some publications reported the use of negatively charged components to increase the performances of chitosan-based NPs for siRNA delivery *in vitro*. One example of such a component is hyaluronic acid (HA), which is known to be a biocompatibility enhancer. HA-PEG-chitosan NPs showed high cell viability (> 80%), even at elevated concentrations, whereas chitosan-PEG and chitosan NPs showed reduced viability [188,198]. Moreover, the HA-PEG-chitosan NPs showed good protection of the siRNA in 50% serum [188]. The gene silencing obtained with these NPs was relatively high, reaching 85% luciferase knockdown in A549 cells. It was hypothesized that the HA was able to decrease the binding of siRNA to chitosan due to competition, thus leading to a faster disassembly in cells [198].

Another approach for the uptake and gene silencing enhancement was to include the negatively charged peptide poly(γ-glutamic acid) (PGA) in the formulation. The cell uptake and luciferase silencing were increased with the inclusion of PGA (72% silencing compared with only 50% for NPs without PGA). The authors suggested that a PGA-specific receptor-mediated pathway should be involved, in an attempt to explain the higher cellular uptake. Furthermore, the inclusion of PGA leads

to a faster rupture of the NPs and release of siRNA in the cells compared to chitosan NPs, with which the release might occur via the enzymatic degradation of chitosan chains [200].

The inclusion of alginate into chitosan NPs has shown to enhance the efficiency of chitosan NPs loaded with DNA or drugs. However, with siRNA, the formulation of such NPs appears to be uncontrollable and leads to the formation of aggregates. Therefore, polyguluronate, a sodium alginate derivative with low MW, was used instead. The inclusion of this derivative enhanced the stability and the efficiency of the NPs *in vitro [201]* and showed good efficacy *in vivo* [202].

III.2.2.1.2.4 *Cyclodextrin*

Finally, chitosan-grafted-(PEI-β-cyclodextrin) was elaborated to combine the biocompatibility of cyclodextrin (CD) to the condensation and buffering capacities of chitosan and PEI. These NPs showed higher cell viability and higher luciferase knockdown than PEI-siRNA complexes. Moreover, the presence of β-CD can be exploited to achieve non-covalent PEGylation using adamantyl-polyethyleneglycol (Ad-PEG), where the Ad moieties are included into the hydrophobic β-CD units and the PEG chains coat the external hydrophilic surface. The PEGylated NPs demonstrated higher gene silencing (84%) than the non-PEGylated ones (60%). The authors suggested that PEG might mediate complex destabilization in the cells. However, the mechanism remains unclear [203].

III.2.3. Ligand grafting for active cell targeting

The specific delivery of siRNA to a particular cell type can be achieved by grafting a ligand onto the NP surface, which will then recognize a receptor expressed by the cell. The role of a targeting ligand is to increase the selective uptake by the target cells and to reduce accumulation in other cells or organs. While the conjugation of ligand to chitosan has been widely described for drug delivery [218], only a few publications report their use for siRNA delivery. The presence of ligand can modify the NP characteristics, such as their size or zeta potential, by hiding the surface charges, especially if PEG chains are grafted. Moreover, the hydrophilic or hydrophobic nature of the ligand can influence its availability at the NP surface and its binding to the receptor [219]. Furthermore, if the ligand is grafted on chitosan amino groups, a lower amount of available positive charges may be available for siRNA binding. Consequently, these parameters must be considered for efficient NP formulation. In some cases, the ligand is directly linked to the functional groups of chitosan. However, PEG usually plays the role of a linker between chitosan and ligand; PEGylation has also been shown to be highly advantageous *in vivo*.

$\alpha_v\beta_3$ integrins are attractive receptors for tumor targeting and are overexpressed in most solid tumors and in tumor vasculature. RGD peptide is the most popular ligand that targets $\alpha_v\beta_3$ integrins

[53]. RGD peptide was conjugated directly to chitosan via a thiolation reaction [204]. The inclusion of RGD did not modify the characteristics of the NPs (200 nm, 40 mV). *In vitro*, the NP-cell association increases in a RGD-concentration dependent manner, with a maximum at 1.45 µg RGD/mg chitosan.

Antibodies are another type of ligand through which active targeting can be achieved. To target the CD7 antigen on T cells, Lee and colleagues conjugated CD-7 single-chain antibody (scFvCD7) directly to the amino group of chitosan [202]. Various percentages of targeting ligand were investigated, and this parameter influenced both the particle characteristics and the biological activity. Indeed, at 30 mol% ligand grafting, NPs presented a significantly increased diameter (350 nm) in comparison with NPs without the ligand (approximately 300 nm). However, 5 to 20% ligand grafting did not affect the size of NPs. A high increase in cell association occurred at 10 mol% ligand (80% of cellular association) compared with 5 mol% ligand (only 50%). The targeted NPs showed a greater decrease in both CD4 protein and mRNA expression (65 and 80%, respectively) compared with non-targeted NPs (35 and 30%, respectively). However, increasing the percentage to 20 mol% did not result in an enhancement of cell association or in an increase of silencing, most likely because of the steric effect of the antibody [202].

Folate receptor targeting can be exploited for cancer or inflammatory diseases: these receptors are overexpressed in malignant cells as well as in activated macrophages, which are responsible for inflammation [220]. The grafting of folate onto chitosan (approximately 1 mol%) was achieved by using PEG as a spacer. Interestingly, the presence of the ligand decreased the mean diameter of the particles (120 nm) and the zeta potential compared with non-targeted NPs (210 nm). The gene silencing efficiency on HeLA and OV-1 cells was enhanced by the ligand. Moreover, a competition assay with free folic acid confirmed that the uptake of targeted NPs was mediated via the folate receptor [180].

To target the β2-adrenergic receptor (β2-AR) on lung cells, salbutamol, a β2-AR agonist, was coupled to guanidinylated chitosan at 3.5%. The grafting of salbutamol did not modify the physico-chemical characteristics of the NPs (a diameter of 150 nm and a zeta potential of approximately 4 mV). A dose of 5 µg siRNA per day for 3 days was administered to GFP-transgenic mice. The lung tissues were collected to measure GFP silencing. The GFP was 40% reduced with the targeted NPs, while it was only 20% reduced with the non-targeted NPs. The authors suggested that the benefit of targeted NPs was due more to their specificity to the β2-AR than to the bronchodilational effect of salbutamol, present in low concentrations [184].

III.2.4. In vivo therapeutic applications of siRNA chitosan-based delivery systems

As for any other siRNA delivery system, the transition to the *in vivo* administration of chitosan/siRNA NPs is highly challenging. Indeed, the *in vitro* optimization work does not guarantee suitable properties for *in vivo* delivery. Although the characteristics of the NPs are appropriate for the delivery of siRNA in culture medium, these systems would certainly be inappropriate to protect and transport siRNA in a more complex and aggressive context, such as the biological environment [34]. Moreover, the NP characteristics should be adapted depending on the administration route and should present a good safety profile. Furthermore, the stability in biological fluids is highly required [34].

Synthetic polymers such as PEI or PLL and natural polymers such as chitosan have both been investigated *in vivo*. They offer plenty of possibilities for chemical modification and surface functionalization. However, in comparison with chitosan, synthetic polymers possess higher charge density and are responsible for their important transfection efficiency on the one hand and their cellular toxicity on the other hand [29,221]. Moreover, polycation-based materials activate the complement system in a charge density-dependent manner [222]. Here, the chitosan/siRNA delivery systems that have been described for local and systemic delivery *in vivo* are reviewed.

III.2.4.1. Systemic delivery

Few studies have described the I.V. administration of chitosan/siRNA NPs, all of which have considered cancer treatment. NPs have to present good stability in the bloodstream to avoid dissociation or aggregation due to interactions with blood components [34]. Additionally, NPs should escape phagocytic capture and reach the target organ in sufficient concentrations [223].

To achieve *in vivo* tumor targeting, RGD-chitosan/siRNA NPs were injected intravenously at 150 µg siRNA/kg body weight in orthotopic ovarian cancer mice models. The siRNA used was targeted against periostin, which is involved in angiogenesis. At 24 h post-injection, the expression of the target protein in SKOV3 tumor tissues (human epithelial ovarian cancer, which expresses integrins) was reduced by 50% using RGD-NPs and by only 20% using non-targeted NPs. Moreover, the poor accumulation of RGD NPs was observed in other organs (e.g., kidneys, liver), suggesting the efficient targeting ability of these NPs. A tumor growth study was performed, and the RGD-NPs induced a significant decrease in tumor weight. Furthermore, using a docetaxel combination (100 µg injected intraperitoneally), the NP efficiency was even more increased [204].

In another study, thiolated glycol chitosan NPs were formulated to deliver polymerized siRNA (12 siRNA linked together). The particularities of this polymerized siRNA are its high MW and its

increased number of anionic charges, which helps enhance the NP stability *in vivo*. Biodistribution in SCC7 tumor-bearing mice showed a major accumulation of the NPs within the tumor, likely due to passive targeting via the enhanced permeability and retention (EPR) effect because these NPs did not present any targeting ligand. The fluorescence signal occurred at a maximum of 1 day post-injection and persisted until 3 days post-injection. A fraction of the NPs were found in the kidneys. In comparison, complexes made of PEI and polymerized siRNA were mostly located in the liver. First, the efficiency was evaluated using a siRNA against red fluorescent protein (RFP) in a RFP-positive B16F10 tumor model (17% RFP silencing). Then, a tumor growth study was performed using VEGF-siRNA. The NPs were injected every 3 days at a dose of 50 µg siRNA and significantly reduced tumor growth (by 80% compared with an untreated group) and microvessel formation, without triggering any immune response [202]. The same authors had already described efficient RFP silencing after the I.V. administration of PEI-glycol chitosan nanocarrier [213].

III.2.4.2. Local delivery

Due to the difficulties associated to systemic administration, alternative routes were examined. Local delivery offers the advantages of being readily accessible, thus avoiding the requirements for systemic administration and the ability to deliver NPs directly to the target site with maximum efficacy and minimum side-effects at lower doses.

Intratumoral delivery was investigated for cancer treatment. This localized gene therapy allows the delivery of therapeutic doses to the tumor site. Moreover, it should, in theory, maintain the continuous exposure of the tumor to the NPs. However, the major challenge is to obtain a complete diffusion of the NPs within the tumor. Chitosan/siRNA NPs were injected intratumorally at a siRNA dose of 25 µg in mice. The NPs were approximately 276 nm and contained a combination of 4 different siRNA that targeted VEGF and its receptors. In a slow-growing breast tumor rat model, the NPs induced a 94% reduction of tumor volume in comparison with an untreated group. No interferon γ-mediated immune response was detected [224]. Moreover, intratumoral injections of PLR-PEG-chitosan NPs (10 µg siRNA per mouse) in B16F10-RFP-bearing mice induced a significant reduction of RFP fluorescence [197].

The mucosal delivery of chitosan NPs is another interesting possibility because chitosan presents mucoadhesive and mucopermeable properties that can be exploited to cross the mucus layer [225]. To reach the epithelial cells, NPs in the range of 200 nm are optimal. Howard and colleagues investigated the nasal route to mediate RNAi at respiratory sites [183]. They obtained 37% GFP silencing within bronchiole epithelial cells in a transgenic GFP mice model. However, nasal administration leads to a hardly controllable deposition in the lung airways due to NP loss during the

nasal-to-lung transit (*i.e.* adherence in the nasal cavity and a possible gastrointestinal clearance). Therefore, chitosan/siRNA aerosols were investigated for the improved pulmonary delivery of siRNA. The GFP silencing was evaluated *in vivo* after non-invasive intratracheal administration using a nebulizing catheter in a GFP transgenic model and was compared to the intranasal route [226]. The siRNA distribution in the lungs was improved with the intratracheal route, and 37% GFP inhibition was obtained in alveoli and bronchiolar regions. The gene silencing results are similar to those obtained with intranasal administration in Howard's study. However, lower siRNA doses were used via the intratracheal route (0.26 µg siRNA per dose) compared with the intranasal route (30 µg). In conclusion, chitosan/siRNA NPs demonstrate good ability to mediate RNAi at respiratory sites and constitute a promising approach for the treatment of pulmonary diseases.

Finally, the intraperitoneal route was investigated to bypass the instability issue of NPs in the blood stream [227,228]. The aim of the study was to prevent radiation-induced fibrosis, which is a side-effect of radiation therapy and involves numerous cytokines, such as tumor necrosis factor α (TNFα), which is released by macrophages [228]. Chitosan/anti-TNFα siRNA NPs were formulated and injected in the peritoneal cavity to deliver the NPs directly to the peritoneal macrophages. However, this route can contribute to a systemic effect. The mice treated with the NPs for 22 days or longer did not develop any radiation-induced fibrosis up to 8 months after radiation. Furthermore, the NPs did not induce any cytotoxic side effects [227]. Howard and colleagues also investigated the intraperitoneal administration of chitosan/TNFα DsiRNA NPs but did so in a collagen type II DBA/I arthritis model. The arthritis score was significantly reduced after 5 injections of NPs (5 µg TNFα DsiRNA) in comparison with the control group. Moreover, 100% survival was obtained [193].

Recently, the oral administration of chitosan/siRNA polyplexes in C57BL/6J mice was investigated. The authors showed that siRNA was efficiently protected by the chitosan, resulting in a deposition in the gastro-intestinal tract and accumulation in other organs, suggesting a systemic translocation [229].

Relatively few polymeric nanocarriers have been evaluated in clinical trials for siRNA delivery. The aforementioned studies are highly promising: they found that chitosan-based delivery systems can be safely and successfully administered *in vivo* via different administration routes and can lead to efficient gene silencing. Thus, by combining chitosan potential to the versatility of siRNA, chitosan/siRNA NPs represent valuable candidates for future clinical studies that need to be tested in clinical trials.

IV. REFERENCES

[1] A. L. Jackson and P. S. Linsley, Recognizing and avoiding siRNA off-target effects for target identification and therapeutic application, Nat. Rev. Drug Discov., 9 (2010) 57-67.

[2] C. R. Sibley, Y. Seow, and M. J. Wood, Novel RNA-based strategies for therapeutic gene silencing, Mol. Ther., 18 (2010) 466-476.

[3] N. Bushati and S. M. Cohen, microRNA functions, Annu. Rev. Cell Dev. Biol., 23 (2007) 175-205.

[4] A. Schroeder, C. G. Levins, C. Cortez, R. Langer, and D. G. Anderson, Lipid-based nanotherapeutics for siRNA delivery, J. Intern. Med., 267 (2010) 9-21.

[5] V. N. Kim, J. Han, and M. C. Siomi, Biogenesis of small RNAs in animals, Nat. Rev. Mol. Cell Biol., 10 (2009) 126-139.

[6] Y. K. Kim, I. Heo, and V. N. Kim, Modifications of small RNAs and their associated proteins, Cell, 143 (2010) 703-709.

[7] D. E. Golden, V. R. Gerbasi, and E. J. Sontheimer, An inside job for siRNAs, Mol. Cell, 31 (2008) 309-312.

[8] S. M. Elbashir, J. Harborth, W. Lendeckel, A. Yalcin, K. Weber, and T. Tuschl, Duplexes of 21-nucleotide RNAs mediate RNA interference in cultured mammalian cells, Nature, 411 (2001) 494-498.

[9] K. Gavrilov and W. M. Saltzman, Therapeutic siRNA: principles, challenges, and strategies, Yale J. Biol. Med., 85 (2012) 187-200.

[10] S. D. Rose, D. H. Kim, M. Amarzguioui, J. D. Heidel, M. A. Collingwood, M. E. Davis, J. J. Rossi, and M. A. Behlke, Functional polarity is introduced by Dicer processing of short substrate RNAs, Nucleic Acids Res., 33 (2005) 4140-4156.

[11] E. Hefner, K. Clark, C. Whitman, M. A. Behlke, S. D. Rose, A. S. Peek, and T. Rubio, Increased potency and longevity of gene silencing using validated Dicer substrates, J. Biomol. Tech., 19 (2008) 231-237.

[12] D. H. Kim, M. A. Behlke, S. D. Rose, M. S. Chang, S. Choi, and J. J. Rossi, Synthetic dsRNA Dicer substrates enhance RNAi potency and efficacy, Nat. Biotechnol., 23 (2005) 222-226.

[13] M. A. Collingwood, S. D. Rose, L. Huang, C. Hillier, M. Amarzguioui, M. T. Wiiger, H. S. Soifer, J. J. Rossi, and M. A. Behlke, Chemical modification patterns compatible with high potency dicer-substrate small interfering RNAs, Oligonucleotides., 18 (2008) 187-200.

[14] G. R. Rettig and M. A. Behlke, Progress toward in vivo use of siRNAs-II, Mol. Ther., 20 (2012) 483-512.

[15] D. D. Rao, J. S. Vorhies, N. Senzer, and J. Nemunaitis, siRNA vs. shRNA: similarities and differences, Adv. Drug Deliv. Rev., 61 (2009) 746-759.

[16] D. Grimm, K. L. Streetz, C. L. Jopling, T. A. Storm, K. Pandey, C. R. Davis, P. Marion, F. Salazar, and M. A. Kay, Fatality in mice due to oversaturation of cellular microRNA/short hairpin RNA pathways, Nature, 441 (2006) 537-541.

[17] S. Barik, RNAi in moderation, Nat. Biotechnol., 24 (2006) 796-797.

[18] Z. Wang, D. D. Rao, N. Senzer, and J. Nemunaitis, RNA interference and cancer therapy, Pharm. Res., 28 (2011) 2983-2995.

[19] Y. Takahashi, K. Yamaoka, M. Nishikawa, and Y. Takakura, Quantitative and temporal analysis of gene silencing in tumor cells induced by small interfering RNA or short hairpin RNA expressed from plasmid vectors, J. Pharm. Sci., 98 (2009) 74-80.

[20] R. L. Kanasty, K. A. Whitehead, A. J. Vegas, and D. G. Anderson, Action and reaction: the biological response to siRNA and its delivery vehicles, Mol. Ther., 20 (2012) 513-524.

[21] J. W. Engels, Gene silencing by chemically modified siRNAs, N. Biotechnol., 30 (2012) 302-307.

[22] Y. Shao, C. Y. Chan, A. Maliyekkel, C. E. Lawrence, I. B. Roninson, and Y. Ding, Effect of target secondary structure on RNAi efficiency, RNA., 13 (2007) 1631-1640.

[23] E. M. Westerhout and B. Berkhout, A systematic analysis of the effect of target RNA structure on RNA interference, Nucleic Acids Res., 35 (2007) 4322-4330.

[24] M. Overhoff, M. Alken, R. K. Far, M. Lemaitre, B. Lebleu, G. Sczakiel, and I. Robbins, Local RNA target structure influences siRNA efficacy: a systematic global analysis, J. Mol. Biol., 348 (2005) 871-881.

[25] E. Larsson, C. Sander, and D. Marks, mRNA turnover rate limits siRNA and microRNA efficacy, Mol. Syst. Biol., 6 (2010) 433.

[26] S. Singh, A. S. Narang, and R. I. Mahato, Subcellular fate and off-target effects of siRNA, shRNA, and miRNA, Pharm. Res., 28 (2011) 2996-3015.

[27] F. Petrocca and J. Lieberman, Promise and challenge of RNA interference-based therapy for cancer, J. Clin. Oncol., 29 (2011) 747-754.

[28] D. Castanotto, K. Sakurai, R. Lingeman, H. Li, L. Shively, L. Aagaard, H. Soifer, A. Gatignol, A. Riggs, and J. J. Rossi, Combinatorial delivery of small interfering RNAs reduces RNAi efficacy by selective incorporation into RISC, Nucleic Acids Res., 35 (2007) 5154-5164.

[29] Y. K. Oh and T. G. Park, siRNA delivery systems for cancer treatment, Adv. Drug Deliv. Rev., 61 (2009) 850-862.

[30] R. Juliano, J. Bauman, H. Kang, and X. Ming, Biological barriers to therapy with antisense and siRNA oligonucleotides, Mol. Pharm., 6 (2009) 686-695.

[31] K. Raemdonck, T. F. Martens, K. Braeckmans, J. Demeester, and S. C. De Smedt, Polysaccharide-based nucleic acid nanoformulations, Adv. Drug Deliv. Rev., (2013).

[32] T. Miller, A. Hill, S. Uezguen, M. Weigandt, and A. Goepferich, Analysis of immediate stress mechanisms upon injection of polymeric micelles and related colloidal drug carriers: implications on drug targeting, Biomacromolecules., 13 (2012) 1707-1718.

[33] K. Buyens, B. Lucas, K. Raemdonck, K. Braeckmans, J. Vercammen, J. Hendrix, Y. Engelborghs, S. C. De Smedt, and N. N. Sanders, A fast and sensitive method for measuring the integrity of siRNA-carrier complexes in full human serum, J. Control Release, 126 (2008) 67-76.

[34] K. Buyens, M. Meyer, E. Wagner, J. Demeester, S. C. De Smedt, and N. N. Sanders, Monitoring the disassembly of siRNA polyplexes in serum is crucial for predicting their biological efficacy, J. Control Release, 141 (2010) 38-41.

[35] K. Braeckmans, K. Buyens, W. Bouquet, C. Vervaet, P. Joye, V. F. De, L. Plawinski, L. Doeuvre, E. Angles-Cano, N. N. Sanders, J. Demeester, and S. C. De Smedt, Sizing nanomatter in biological fluids by fluorescence single particle tracking, Nano. Lett., 10 (2010) 4435-4442.

[36] B. Naeye, H. Deschout, M. Roding, M. Rudemo, J. Delanghe, K. Devreese, J. Demeester, K. Braeckmans, S. C. De Smedt, and K. Raemdonck, Hemocompatibility of siRNA loaded dextran nanogels, Biomaterials, 32 (2011) 9120-9127.

[37] H. Hillaireau and P. Couvreur, Nanocarriers' entry into the cell: relevance to drug delivery, Cell Mol. Life Sci., 66 (2009) 2873-2896.

[38] T. Shehata, K. Ogawara, K. Higaki, and T. Kimura, Prolongation of residence time of liposome by surface-modification with mixture of hydrophilic polymers, Int. J. Pharm., 359 (2008) 272-279.

[39] B. Naeye, H. Deschout, V. Caveliers, B. Descamps, K. Braeckmans, C. Vanhove, J. Demeester, T. Lahoutte, S. C. De Smedt, and K. Raemdonck, In vivo disassembly of IV administered siRNA matrix nanoparticles at the renal filtration barrier, Biomaterials, 34 (2013) 2350-2358.

[40] W. A. Dufay, H. Hillaireau, T. L. Nascimento, S. Arpicco, M. Taverna, S. Ribes, M. Bourge, V. Nicolas, A. Bochot, C. Vauthier, N. Tsapis, and E. Fattal, Hyaluronic acid-bearing lipoplexes: physico-chemical characterization and in vitro targeting of the CD44 receptor, J. Control Release, 162 (2012) 545-552.

[41] D'Sa Raechelle A and R. J. P. B. K. a. M. B. J. Dickinson Peter J, Inhibition of lens epithelial cell growth via immobilisation of hyaluronic acid on atmospheric pressure plasma modified polystyrene, Soft Matter, 7 (2010) 608-617.

[42] J. E. Zuckerman, C. H. Choi, H. Han, and M. E. Davis, Polycation-siRNA nanoparticles can disassemble at the kidney glomerular basement membrane, Proc. Natl. Acad. Sci. U. S. A, 109 (2012) 3137-3142.

[43] R. Juliano, M. R. Alam, V. Dixit, and H. Kang, Mechanisms and strategies for effective delivery of antisense and siRNA oligonucleotides, Nucleic Acids Res., 36 (2008) 4158-4171.

[44] H. Maeda, T. Sawa, and T. Konno, Mechanism of tumor-targeted delivery of macromolecular drugs, including the EPR effect in solid tumor and clinical overview of the prototype polymeric drug SMANCS, J. Control Release, 74 (2001) 47-61.

[45] D. Vercauteren, J. Rejman, T. F. Martens, J. Demeester, S. C. De Smedt, and K. Braeckmans, On the cellular processing of non-viral nanomedicines for nucleic acid delivery: mechanisms and methods, J. Control Release, 161 (2012) 566-581.

[46] T. M. Allen, Ligand-targeted therapeutics in anticancer therapy, Nat. Rev. Cancer, 2 (2002) 750-763.

[47] J. D. Humphries, A. Byron, and M. J. Humphries, Integrin ligands at a glance, J. Cell Sci., 119 (2006) 3901-3903.

[48] V. Rerat, G. Dive, A. A. Cordi, G. C. Tucker, R. Bareille, J. Amedee, L. Bordenave, and J. Marchand-Brynaert, alphavbeta3 Integrin-targeting Arg-Gly-Asp (RGD) peptidomimetics containing oligoethylene glycol (OEG) spacers, J. Med. Chem., 52 (2009) 7029-7043.

[49] S. Biltresse, M. Attolini, G. Dive, A. Cordi, G. C. Tucker, and J. Marchand-Brynaert, Novel RGD-like molecules based on the tyrosine template: design, synthesis, and biological evaluation on isolated integrins alphaVbeta3/alphaIIbbeta3 and in cellular adhesion tests, Bioorg. Med. Chem., 12 (2004) 5379-5393.

[50] F. Danhier, V. Pourcelle, J. Marchand-Brynaert, C. Jerome, O. Feron, and V. Preat, Targeting of tumor endothelium by RGD-grafted PLGA-nanoparticles, Methods Enzymol., 508 (2012) 157-175.

[51] A. Abdollahi and J. Folkman, Evading tumor evasion: current concepts and perspectives of anti-angiogenic cancer therapy, Drug Resist. Updat., 13 (2010) 16-28.

[52] E. Kenjo, T. Asai, N. Yonenaga, H. Ando, T. Ishii, K. Hatanaka, K. Shimizu, Y. Urita, T. Dewa, M. Nango, H. Tsukada, and N. Oku, Systemic delivery of small interfering RNA by use of targeted polycation liposomes for cancer therapy, Biol. Pharm. Bull., 36 (2013) 287-291.

[53] F. Danhier, B. A. Le, and V. Preat, RGD-based strategies to target alpha(v) beta(3) integrin in cancer therapy and diagnosis, Mol. Pharm., 9 (2012) 2961-2973.

[54] K. L. Douglas, C. A. Piccirillo, and M. Tabrizian, Cell line-dependent internalization pathways and intracellular trafficking determine transfection efficiency of nanoparticle vectors, Eur. J Pharm Biopharm., 68 (2008) 676-687.

[55] J. Nguyen and F. C. Szoka, Nucleic acid delivery: the missing pieces of the puzzle?, Acc. Chem. Res., 45 (2012) 1153-1162.

[56] A. Akinc, M. Thomas, A. M. Klibanov, and R. Langer, Exploring polyethylenimine-mediated DNA transfection and the proton sponge hypothesis, J. Gene Med., 7 (2005) 657-663.

[57] R. V. Benjaminsen, M. A. Mattebjerg, J. R. Henriksen, S. M. Moghimi, and T. L. Andresen, The possible "proton sponge " effect of polyethylenimine (PEI) does not include change in lysosomal pH, Mol. Ther., 21 (2013) 149-157.

[58] C. Chen, D. A. Ridzon, A. J. Broomer, Z. Zhou, D. H. Lee, J. T. Nguyen, M. Barbisin, N. L. Xu, V. R. Mahuvakar, M. R. Andersen, K. Q. Lao, K. J. Livak, and K. J. Guegler, Real-time quantification of microRNAs by stem-loop RT-PCR, Nucleic Acids Res., 33 (2005) e179.

[59] C. Chen, R. Tan, L. Wong, R. Fekete, and J. Halsey, Quantitation of microRNAs by real-time RT-qPCR, Methods Mol. Biol., 687 (2011) 113-134.

[60] S. Colombo, H. M. Nielsen, and C. Foged, Evaluation of carrier-mediated siRNA delivery: lessons for the design of a stem-loop qPCR-based approach for quantification of intracellular full-length siRNA, J. Control Release, 166 (2013) 220-226.

[61] A. Cheng, A. V. Vlassov, and S. Magdaleno, Quantification of siRNAs in vitro and in vivo, Methods Mol. Biol., 764 (2011) 183-197.

[62] Y. Landesman, N. Svrzikapa, A. Cognetta, III, X. Zhang, B. R. Bettencourt, S. Kuchimanchi, K. Dufault, S. Shaikh, M. Gioia, A. Akinc, R. Hutabarat, and R. Meyers, In vivo quantification of formulated and chemically modified small interfering RNA by heating-in-Triton quantitative reverse transcription polymerase chain reaction (HIT qRT-PCR), Silence., 1 (2010) 16.

[63] E. Varkonyi-Gasic, R. Wu, M. Wood, E. F. Walton, and R. P. Hellens, Protocol: a highly sensitive RT-PCR method for detection and quantification of microRNAs, Plant Methods, 3 (2007) 12.

[64] P. Guo, O. Coban, N. M. Snead, J. Trebley, S. Hoeprich, S. Guo, and Y. Shu, Engineering RNA for targeted siRNA delivery and medical application, Adv. Drug Deliv. Rev., 62 (2010) 650-666.

[65] J. B. Bramsen, M. M. Pakula, T. B. Hansen, C. Bus, N. Langkjaer, D. Odadzic, R. Smicius, S. L. Wengel, J. Chattopadhyaya, J. W. Engels, P. Herdewijn, J. Wengel, and J. Kjems, A screen of chemical modifications identifies position-specific modification by UNA to most potently reduce siRNA off-target effects, Nucleic Acids Res., 38 (2010) 5761-5773.

[66] M. Aleku, P. Schulz, O. Keil, A. Santel, U. Schaeper, B. Dieckhoff, O. Janke, J. Endruschat, B. Durieux, N. Roder, K. Loffler, C. Lange, M. Fechtner, K. Mopert, G. Fisch, S. Dames, W. Arnold, K. Jochims, K. Giese,

B. Wiedenmann, A. Scholz, and J. Kaufmann, Atu027, a liposomal small interfering RNA formulation targeting protein kinase N3, inhibits cancer progression, Cancer Res., 68 (2008) 9788-9798.

[67] J. Elmen, H. Thonberg, K. Ljungberg, M. Frieden, M. Westergaard, Y. Xu, B. Wahren, Z. Liang, H. Orum, T. Koch, and C. Wahlestedt, Locked nucleic acid (LNA) mediated improvements in siRNA stability and functionality, Nucleic Acids Res., 33 (2005) 439-447.

[68] L. M. Greenberger, I. D. Horak, D. Filpula, P. Sapra, M. Westergaard, H. F. Frydenlund, C. Albaek, H. Schroder, and H. Orum, A RNA antagonist of hypoxia-inducible factor-1alpha, EZN-2968, inhibits tumor cell growth, Mol. Cancer Ther., 7 (2008) 3598-3608.

[69] M. Manoharan, RNA interference and chemically modified small interfering RNAs, Curr. Opin. Chem. Biol., 8 (2004) 570-579.

[70] O. Mook, J. Vreijling, S. L. Wengel, J. Wengel, C. Zhou, J. Chattopadhyaya, F. Baas, and K. Fluiter, In vivo efficacy and off-target effects of locked nucleic acid (LNA) and unlocked nucleic acid (UNA) modified siRNA and small internally segmented interfering RNA (sisiRNA) in mice bearing human tumor xenografts, Artif. DNA PNA. XNA., 1 (2010) 36-44.

[71] J. H. Jeong, H. Mok, Y. K. Oh, and T. G. Park, siRNA conjugate delivery systems, Bioconjug. Chem., 20 (2009) 5-14.

[72] J. Soutschek, A. Akinc, B. Bramlage, K. Charisse, R. Constien, M. Donoghue, S. Elbashir, A. Geick, P. Hadwiger, J. Harborth, M. John, V. Kesavan, G. Lavine, R. K. Pandey, T. Racie, K. G. Rajeev, I. Rohl, I. Toudjarska, G. Wang, S. Wuschko, D. Bumcrot, V. Koteliansky, S. Limmer, M. Manoharan, and H. P. Vornlocher, Therapeutic silencing of an endogenous gene by systemic administration of modified siRNAs, Nature, 432 (2004) 173-178.

[73] K. Nishina, T. Unno, Y. Uno, T. Kubodera, T. Kanouchi, H. Mizusawa, and T. Yokota, Efficient in vivo delivery of siRNA to the liver by conjugation of alpha-tocopherol, Mol. Ther., 16 (2008) 734-740.

[74] S. A. Moschos, A. E. Williams, and M. A. Lindsay, Cell-penetrating-peptide-mediated siRNA lung delivery, Biochem. Soc. Trans., 35 (2007) 807-810.

[75] S. A. Moschos, S. W. Jones, M. M. Perry, A. E. Williams, J. S. Erjefalt, J. J. Turner, P. J. Barnes, B. S. Sproat, M. J. Gait, and M. A. Lindsay, Lung delivery studies using siRNA conjugated to TAT(48-60) and penetratin reveal peptide induced reduction in gene expression and induction of innate immunity, Bioconjug. Chem., 18 (2007) 1450-1459.

[76] D. Guzman-Villanueva, I. M. El-Sherbiny, D. Herrera-Ruiz, A. V. Vlassov, and H. D. Smyth, Formulation approaches to short interfering RNA and MicroRNA: challenges and implications, J. Pharm. Sci., 101 (2012) 4046-4066.

[77] L. C. Gomes-da-Silva, N. A. Fonseca, V. Moura, M. C. Pedroso de Lima, S. Simoes, and J. N. Moreira, Lipid-based nanoparticles for siRNA delivery in cancer therapy: paradigms and challenges, Acc. Chem. Res., 45 (2012) 1163-1171.

[78] E. Miele, G. P. Spinelli, E. Miele, F. E. Di, E. Ferretti, S. Tomao, and A. Gulino, Nanoparticle-based delivery of small interfering RNA: challenges for cancer therapy, Int. J. Nanomedicine., 7 (2012) 3637-3657.

[79] S. Y. Wu and N. A. McMillan, Lipidic systems for in vivo siRNA delivery, AAPS. J., 11 (2009) 639-652.

[80] B. Ozpolat, A. K. Sood, and G. Lopez-Berestein, Nanomedicine based approaches for the delivery of siRNA in cancer, J. Intern. Med., 267 (2010) 44-53.

[81] E. Fattal and A. Bochot, State of the art and perspectives for the delivery of antisense oligonucleotides and siRNA by polymeric nanocarriers, Int. J. Pharm., 364 (2008) 237-248.

[82] M. E. Davis, J. E. Zuckerman, C. H. Choi, D. Seligson, A. Tolcher, C. A. Alabi, Y. Yen, J. D. Heidel, and A. Ribas, Evidence of RNAi in humans from systemically administered siRNA via targeted nanoparticles, Nature, 464 (2010) 1067-1070.

[83] C. Troiber and E. Wagner, Nucleic acid carriers based on precise polymer conjugates, Bioconjug. Chem., 22 (2011) 1737-1752.

[84] K. Singha, R. Namgung, and W. J. Kim, Polymers in small-interfering RNA delivery, Nucleic Acid Ther., 21 (2011) 133-147.

[85] M. E. Davis, The first targeted delivery of siRNA in humans via a self-assembling, cyclodextrin polymer-based nanoparticle: from concept to clinic, Mol. Pharm., 6 (2009) 659-668.

[86] J. Wang, Z. Lu, M. G. Wientjes, and J. L. Au, Delivery of siRNA therapeutics: barriers and carriers, AAPS. J., 12 (2010) 492-503.

[87] B. Naeye, K. Raemdonck, K. Remaut, B. Sproat, J. Demeester, and S. C. De Smedt, PEGylation of biodegradable dextran nanogels for siRNA delivery, Eur. J. Pharm. Sci., 40 (2010) 342-351.

[88] J. Weiler, J. Hunziker, and J. Hall, Anti-miRNA oligonucleotides (AMOs): ammunition to target miRNAs implicated in human disease?, Gene Ther., 13 (2006) 496-502.

[89] F. Takeshita and T. Ochiya, Therapeutic potential of RNA interference against cancer, Cancer Sci., 97 (2006) 689-696.

[90] S. I. Pai, Y. Y. Lin, B. Macaes, A. Meneshian, C. F. Hung, and T. C. Wu, Prospects of RNA interference therapy for cancer, Gene Ther., 13 (2006) 464-477.

[91] D. Hanahan and R. A. Weinberg, Hallmarks of cancer: the next generation, Cell, 144 (2011) 646-674.

[92] J. Yano, K. Hirabayashi, S. Nakagawa, T. Yamaguchi, M. Nogawa, I. Kashimori, H. Naito, H. Kitagawa, K. Ishiyama, T. Ohgi, and T. Irimura, Antitumor activity of small interfering RNA/cationic liposome complex in mouse models of cancer, Clin. Cancer Res., 10 (2004) 7721-7726.

[93] A. M. Chen, M. Zhang, D. Wei, D. Stueber, O. Taratula, T. Minko, and H. He, Co-delivery of doxorubicin and Bcl-2 siRNA by mesoporous silica nanoparticles enhances the efficacy of chemotherapy in multidrug-resistant cancer cells, Small, 5 (2009) 2673-2677.

[94] N. Draoui and O. Feron, Lactate shuttles at a glance: from physiological paradigms to anti-cancer treatments, Dis. Model. Mech., 4 (2011) 727-732.

[95] B. C. Fuchs and B. P. Bode, Amino acid transporters ASCT2 and LAT1 in cancer: partners in crime?, Semin. Cancer Biol., 15 (2005) 254-266.

[96] B. C. Fuchs, R. E. Finger, M. C. Onan, and B. P. Bode, ASCT2 silencing regulates mammalian target-of-rapamycin growth and survival signaling in human hepatoma cells, Am. J. Physiol Cell Physiol, 293 (2007) C55-C63.

[97] M. Hassanein, M. D. Hoeksema, M. Shiota, J. Qian, B. K. Harris, H. Chen, J. E. Clark, W. E. Alborn, R. Eisenberg, and P. P. Massion, SLC1A5 mediates glutamine transport required for lung cancer cell growth and survival, Clin. Cancer Res., 19 (2013) 560-570.

[98] C. Corbet, N. Draoui, and O. Feron, Acidic stress induces a glucose-independent glutamine metabolism for proliferation in tumor cells, in preparation, (2013).

[99] Y. Takei, K. Kadomatsu, Y. Yuzawa, S. Matsuo, and T. Muramatsu, A small interfering RNA targeting vascular endothelial growth factor as cancer therapeutics, Cancer Res., 64 (2004) 3365-3370.

[100] R. M. Schiffelers, A. Ansari, J. Xu, Q. Zhou, Q. Tang, G. Storm, G. Molema, P. Y. Lu, P. V. Scaria, and M. C. Woodle, Cancer siRNA therapy by tumor selective delivery with ligand-targeted sterically stabilized nanoparticle, Nucleic Acids Res., 32 (2004) e149.

[101] W. Yuan, Z. Chen, Z. Chen, S. Wu, J. Guo, J. Ge, P. Yang, and J. Huang, Silencing of EphA2 inhibits invasion of human gastric cancer SGC-7901 cells in vitro and in vivo, Neoplasma, 59 (2012) 105-113.

[102] C. N. Landen, Jr., A. Chavez-Reyes, C. Bucana, R. Schmandt, M. T. Deavers, G. Lopez-Berestein, and A. K. Sood, Therapeutic EphA2 gene targeting in vivo using neutral liposomal small interfering RNA delivery, Cancer Res., 65 (2005) 6910-6918.

[103] H. Wu, W. N. Hait, and J. M. Yang, Small interfering RNA-induced suppression of MDR1 (P-glycoprotein) restores sensitivity to multidrug-resistant cancer cells, Cancer Res., 63 (2003) 1515-1519.

[104] S. J. Collis, M. J. Swartz, W. G. Nelson, and T. L. DeWeese, Enhanced radiation and chemotherapy-mediated cell killing of human cancer cells by small inhibitory RNA silencing of DNA repair factors, Cancer Res., 63 (2003) 1550-1554.

[105] A. G. Bader, D. Brown, and M. Winkler, The promise of microRNA replacement therapy, Cancer Res., 70 (2010) 7027-7030.

[106] P. Trang, J. F. Wiggins, C. L. Daige, C. Cho, M. Omotola, D. Brown, J. B. Weidhaas, A. G. Bader, and F. J. Slack, Systemic delivery of tumor suppressor microRNA mimics using a neutral lipid emulsion inhibits lung tumors in mice, Mol. Ther., 19 (2011) 1116-1122.

[107] L. Ma, F. Reinhardt, E. Pan, J. Soutschek, B. Bhat, E. G. Marcusson, J. Teruya-Feldstein, G. W. Bell, and R. A. Weinberg, Therapeutic silencing of miR-10b inhibits metastasis in a mouse mammary tumor model, Nat. Biotechnol., 28 (2010) 341-347.

[108] M. Verreault, S. A. Weppler, A. Stegeman, C. Warburton, D. Strutt, D. Masin, and M. B. Bally, Combined RNAi-mediated suppression of Rictor and EGFR resulted in complete tumor regression in an orthotopic glioblastoma tumor model, PLoS. One., 8 (2013) e59597.

[109] H. Shen, C. Rodriguez-Aguayo, R. Xu, V. Gonzalez-Villasana, J. Mai, Y. Huang, G. Zhang, X. Guo, L. Bai, G. Qin, X. Deng, Q. Li, D. R. Erm, B. Aslan, X. Liu, J. Sakamoto, A. Chavez-Reyes, H. D. Han, A. K. Sood, M. Ferrari, and G. Lopez-Berestein, Enhancing chemotherapy response with sustained EphA2 silencing using multistage vector delivery, Clin. Cancer Res, 19 (2013) 1806-1815.

[110] D. Kunze, K. Kraemer, K. Erdmann, M. Froehner, M. P. Wirth, and S. Fuessel, Simultaneous siRNA-mediated knockdown of antiapoptotic BCL2, Bcl-xL, XIAP and survivin in bladder cancer cells, Int J Oncol., 41 (2012) 1271-1277.

[111] B. Cun, X. Song, R. Jia, H. Wang, X. Zhao, B. Liu, S. Ge, and X. Fan, Cell growth inhibition in HPV 18 positive uveal melanoma cells by E6/E7 siRNA, Tumour. Biol., 34 (2013) 1801-1806.

[112] P. Sonveaux, F. Vegran, T. Schroeder, M. C. Wergin, J. Verrax, Z. N. Rabbani, C. J. De Saedeleer, K. M. Kennedy, C. Diepart, B. F. Jordan, M. J. Kelley, B. Gallez, M. L. Wahl, O. Feron, and M. W. Dewhirst, Targeting lactate-fueled respiration selectively kills hypoxic tumor cells in mice, J Clin. Invest, 118 (2008) 3930-3942.

[113] W. Wei, P. P. Lv, X. M. Chen, Z. G. Yue, Q. Fu, S. Y. Liu, H. Yue, and G. H. Ma, Codelivery of mTERT siRNA and paclitaxel by chitosan-based nanoparticles promoted synergistic tumor suppression, Biomaterials, 34 (2013) 3912-3923.

[114] M. D. Tsai, P. R. Chen, L. T. Tien, Y. J. Cai, and Y. J. Lee, Nuclear condensation and cell cycle arrest induced by telomerase siRNA in neuroblastoma cells, J Neurooncol., 111 (2013) 265-272.

[115] X. Q. Liu, M. H. Xiong, X. T. Shu, R. Z. Tang, and J. Wang, Therapeutic delivery of siRNA silencing HIF-1 alpha with micellar nanoparticles inhibits hypoxic tumor growth, Mol. Pharm, 9 (2012) 2863-2874.

[116] W. A. Osta, Y. Chen, K. Mikhitarian, M. Mitas, M. Salem, Y. A. Hannun, D. J. Cole, and W. E. Gillanders, EpCAM is overexpressed in breast cancer and is a potential target for breast cancer gene therapy, Cancer Res., 64 (2004) 5818-5824.

[117] N. Liu, F. Bi, Y. Pan, L. Sun, Y. Xue, Y. Shi, X. Yao, Y. Zheng, and D. Fan, Reversal of the malignant phenotype of gastric cancer cells by inhibition of RhoA expression and activity, Clin. Cancer Res., 10 (2004) 6239-6247.

[118] N. Rubinstein, M. Alvarez, N. W. Zwirner, M. A. Toscano, J. M. Ilarregui, A. Bravo, J. Mordoh, L. Fainboim, O. L. Podhajcer, and G. A. Rabinovich, Targeted inhibition of galectin-1 gene expression in tumor cells results in heightened T cell-mediated rejection; A potential mechanism of tumor-immune privilege, Cancer Cell, 5 (2004) 241-251.

[119] M. Abbasi, H. M. Aliabadi, E. H. Moase, A. Lavasanifar, K. Kaur, R. Lai, C. Doillon, and H. Uludag, siRNA-mediated down-regulation of P-glycoprotein in a Xenograft tumor model in NOD-SCID mice, Pharm Res, 28 (2011) 2516-2529.

[120] J. D. Heidel, J. Y. Liu, Y. Yen, B. Zhou, B. S. Heale, J. J. Rossi, D. W. Bartlett, and M. E. Davis, Potent siRNA inhibitors of ribonucleotide reductase subunit RRM2 reduce cell proliferation in vitro and in vivo, Clin. Cancer Res, 13 (2007) 2207-2215.

[121] J. D. Heidel, Z. Yu, J. Y. Liu, S. M. Rele, Y. Liang, R. K. Zeidan, D. J. Kornbrust, and M. E. Davis, Administration in non-human primates of escalating intravenous doses of targeted nanoparticles containing ribonucleotide reductase subunit M2 siRNA, Proc. Natl. Acad. Sci U. S. A, 104 (2007) 5715-5721.

[122] M. A. Rahman, A. R. Amin, X. Wang, J. E. Zuckerman, C. H. Choi, B. Zhou, D. Wang, S. Nannapaneni, L. Koenig, Z. Chen, Z. G. Chen, Y. Yen, M. E. Davis, and D. M. Shin, Systemic delivery of siRNA nanoparticles targeting RRM2 suppresses head and neck tumor growth, J. Control Release, 159 (2012) 384-392.

[123] F. A. Barr, H. H. Sillje, and E. A. Nigg, Polo-like kinases and the orchestration of cell division, Nat. Rev. Mol. Cell Biol., 5 (2004) 429-440.

[124] http://tekmira.com. 2013.
Ref Type: Online Source

[125] Ramanathan R., Hamburg S.I., Borad M.J., Seetharam M., Kundranda M.N., Lee P., Fredlund P., Gilbert M., Mast C., Semple S.C., Judge A.D., Crowell B., Vocila L., MacLachlan I., and Northfelt D.W., A Phase 1 Dose Escalation Study of TKM-080301, a RNAi Therapeutic Directed Against PLK1, in Patients With Advanced Solid Tumors, 2013.

[126] J. Tabernero, G. I. Shapiro, P. M. Lorusso, A. Cervantes, G. K. Schwartz, G. J. Weiss, L. Paz-Ares, D. C. Cho, J. R. Infante, M. Alsina, M. M. Gounder, R. Falzone, J. Harrop, A. C. White, I. Toudjarska, D. Bumcrot, R. E. Meyers, G. Hinkle, N. Svrzikapa, R. M. Hutabarat, V. A. Clausen, J. Cehelsky, S. V. Nochur, C. Gamba-Vitalo, A. K. Vaishnaw, D. W. Sah, J. A. Gollob, and H. A. Burris, III, First-in-Humans Trial of an RNA Interference Therapeutic Targeting VEGF and KSP in Cancer Patients with Liver Involvement, Cancer Discov., 3 (2013) 406-417.

[127] Lewis N., Cohen R.B., Nishida Y, Hurwitz H.I., Arrowwood C., Uronis H.E., Gilles E., Longley C., Buchbinder A., and Figueroa J., Phase I, pharmacokinetic (PK), dose-escalation study of EZN-2968, a

novel hypoxia-inducible factor-1 alpha (HIF-1 alpha) RNA antagonist, administered weekly in patients (pts) with solid tumors, 2008.

[128] http:www.enzon.com. 2013.
Ref Type: Online Source

[129] Tolcher A.W., Patnaik A., Papadopoulos K.P., Agnew J., Lokiec F.M., Rezaï K., Kalambakas S., and Buchbinder A., Results of a Phase 1, open-label, dose-escalation study evaluating the safety and tolerability of EZN-3042, a survivin messenger ribonucleic acid (mRNA) antagonist, administered with or without docetaxel in adult patients with advanced solid tumors or lymphoma, 2011.

[130] P. Sapra, M. Wang, R. Bandaru, H. Zhao, L. M. Greenberger, and I. D. Horak, Down-modulation of survivin expression and inhibition of tumor growth in vivo by EZN-3042, a locked nucleic acid antisense oligonucleotide, Nucleosides Nucleotides Nucleic Acids, 29 (2010) 97-112.

[131] S. Rachagani, S. Senapati, S. Chakraborty, M. P. Ponnusamy, S. Kumar, L. M. Smith, M. Jain, and S. K. Batra, Activated KrasG(1)(2)D is associated with invasion and metastasis of pancreatic cancer cells through inhibition of E-cadherin, Br. J. Cancer, 104 (2011) 1038-1048.

[132] J. H. Park, G. Saravanakumar, K. Kim, and I. C. Kwon, Targeted delivery of low molecular drugs using chitosan and its derivatives, Adv. Drug Deliv. Rev., 62 (2010) 28-41.

[133] Rinaudo M and Auzely R. Specific interactions in modified chitosan systems. Biomacromolecules 6, 2396-2407. 2005.
Ref Type: Journal (Full)

[134] Versali M.F., Clerisse F., Bruyere J.M., S. Gauthier, and Kitozyme S.A., Cell wall derivatives from biomass and preparation thereof, *, WO2003EP01375 20030212 (2003).

[135] Rane KD and Hoover DG. Production of chitosan by funghi. Food Biotechnol , 11-33. 1993.
Ref Type: Generic

[136] Gautier S. Ultra-pure chitosan: insight on new non-animal sources for use in advanced drug delivery and cell therapy. Drug delivery today 9[8], 20-22. 2009.
Ref Type: Generic

[137] Bagheri-Khoulenjani S and Taghizadeh SM. An investigation on the short-term biodegradability of chitosan with various molecular weights and degrees of deacetylation. Carbohydr Polym 78, 773-778. 2009.
Ref Type: Generic

[138] Varum KM and Myhr MM. In vitro degradation rates of partially N-acetylated chitosans in human serum. Carbohydr Res 299, 99-101. 1997.
Ref Type: Generic

[139] Sashiwa H and Aiba SI. Chemically modified chitin and chitosan as biomaterials. ProgPolym Sci 29, 887-908. 2004.
Ref Type: Generic

[140] VandeVord PJ and Matthew HWT. Evaluation of the biocompatibility of a chitosan scaffold in mice. J Biomed Mater Res 59, 585-590. 2002.
Ref Type: Generic

[141] T. Kean and M. Thanou, Biodegradation, biodistribution and toxicity of chitosan, Adv. Drug Deliv. Rev., 62 (2010) 3-11.

[142] M. Garcia-Fuentes and M. J. Alonso, Chitosan-based drug nanocarriers: where do we stand?, J. Control Release, 161 (2012) 496-504.

[143] Hirano S. Chitin biotechnology applications. Biotechnol Annu Rev , 237-258. 1996.
Ref Type: Generic

[144] A. Chaudhury and S. Das, Recent advancement of chitosan-based nanoparticles for oral controlled delivery of insulin and other therapeutic agents, AAPS. PharmSciTech., 12 (2011) 10-20.

[145] N. S. Tapola, M. L. Lyyra, R. M. Kolehmainen, E. S. Sarkkinen, and A. G. Schauss, Safety aspects and cholesterol-lowering efficacy of chitosan tablets, J. Am. Coll. Nutr., 27 (2008) 22-30.

[146] P. Baldrick, The safety of chitosan as a pharmaceutical excipient, Regul. Toxicol. Pharmacol., 56 (2010) 290-299.

[147] Calvo P, Vila-Jato L. J Alonso M. Evaluation of cationic polymer-coated nanocapsules as ocular drug carriers. International Journal of Pharmaceutics 153, 41-50. 1997.
Ref Type: Generic

[148] B. C. Cho, E. H. Kim, H. J. Choi, J. H. Kim, J. K. Roh, H. C. Chung, J. B. Ahn, J. D. Lee, J. T. Lee, N. C. Yoo, and J. H. Sohn, A pilot study of trans-arterial injection of 166Holmium-Chitosan complex for treatment of small hepatocellular carcinoma, Yonsei Med. J., 46 (2005) 799-805.

[149] Minami, S., Oh-oka, M., Okamoto, Y., Miyatake, K., Matsuhashi, A., Shigemasa, Y., and Fukumoto, Y. Chitosan-inducing hemorrhagic pneumonia in dogs. Carbohydr.Polymers 28, 241-246. 1996.
Ref Type: Generic

[150] D. S. Jones and H. J. Mawhinney, Chitosan, Handbook of Pharmaceutical Excipients 5th, 2006, pp. 159-162.

[151] C. Qin, J. Gao, L. Wang, L. Zeng, and Y. Liu, Safety evaluation of short-term exposure to chitooligomers from enzymic preparation, Food Chem. Toxicol., 44 (2006) 855-861.

[152] K. Y. Lee, M. Shibutani, H. Takagi, T. Arimura, S. Takigami, C. Uneyama, N. Kato, and M. Hirose, Subchronic toxicity study of dietary N-acetylglucosamine in F344 rats, Food Chem. Toxicol., 42 (2004) 687-695.

[153] J. W. Anderson, R. J. Nicolosi, and J. F. Borzelleca, Glucosamine effects in humans: a review of effects on glucose metabolism, side effects, safety considerations and efficacy, Food Chem. Toxicol., 43 (2005) 187-201.

[154] S. K. Kim, P. J. Park, H. P. Yang, and S. S. Han, Subacute toxicity of chitosan oligosaccharide in Sprague-Dawley rats, Arzneimittelforschung., 51 (2001) 769-774.

[155] Y. Naito, K. Tago, T. Nagata, M. Furuya, T. Seki, H. Kato, T. Morimura, and N. Ohara, A 90-day ad libitum administration toxicity study of oligoglucosamine in F344 rats, Food Chem. Toxicol., 45 (2007) 1575-1587.

[156] K. Tago, Y. Naito, T. Nagata, T. Morimura, M. Furuya, T. Seki, H. Kato, and N. Ohara, A ninety-day feeding, subchronic toxicity study of oligo-N-acetylglucosamine in Fischer 344 rats, Food Chem. Toxicol., 45 (2007) 1186-1193.

[157] M. Takahashi, K. Inoue, M. Yoshida, T. Morikawa, M. Shibutani, and A. Nishikawa, Lack of chronic toxicity or carcinogenicity of dietary N-acetylglucosamine in F344 rats, Food Chem. Toxicol., 47 (2009) 462-471.

[158] Y. Tanaka, S. Tanioka, M. Tanaka, T. Tanigawa, Y. Kitamura, S. Minami, Y. Okamoto, M. Miyashita, and M. Nanno, Effects of chitin and chitosan particles on BALB/c mice by oral and parenteral administration, Biomaterials, 18 (1997) 591-595.

[159] L. Illum, Chitosan and its use as a pharmaceutical excipient, Pharm. Res., 15 (1998) 1326-1331.

[160] Carreno-Gomez, B. and Duncan, R. Evaluation of the biological properties of soluble chitosan and chitosan microspheres. Int J Pharm 148, 231-240. 1997.
Ref Type: Generic

[161] Hirano, S., Itakura, C, Seino, H., Akiyama, Y, Nonaka, I, Kanbara, N, and Kawakami, T. Chitosan as an ingredient for domestic animal feeds. J.Agric.Food Chem 38, 1214-1217. 1990.
Ref Type: Generic

[162] Kumar M and Muzzarelli RAA. Chitosan chemistry and pharmaceutical perspectives. Chem Rev 104, 6017-6084. 2004.
Ref Type: Generic

[163] Minagawa T and Okamura Y. Effects of molecular weight and deacetylation degree of chitin/chitosan on wound healing. Carbohydr Polym 67, 640-644. 2007.
Ref Type: Generic

[164] Yang J and Tian F. Effect of chitosan molecular weight and deacetylation degree on hemostasis. J Biomed Mater Res B Appl Biomater 84b, 131-137. 2008.
Ref Type: Generic

[165] Ong SY and Wu J. Development of a chitosan-based wound dressing with improved hemostatic and antimicrobial properties. Biomaterials 29, 4323-4332. 2008.
Ref Type: Generic

[166] Sudarshan NR and Hoover DG. Antibacterial action of chitosan. Food Biotechnol 6, 257-272. 1992.
Ref Type: Generic

[167] Rabea EI, Badawy ME, Stevens CV, Smagghe G, and Steurbaut W. Chitosan as antimicrobial agent: applications and mode of action. Biomacromolecules 4, 1457-1465. 2003.
Ref Type: Generic

[168] Lehr C-M and Bouwstra JA. In vitro evaluation of mucoadhesive properties of chitosan and some other natural polymers. Int J Pharm 78, 43-48. 1992.
Ref Type: Generic

[169] A. D. Sezer and E. Cevher, Topical drug delivery using chitosan nano- and microparticles, Expert. Opin. Drug Deliv., 9 (2012) 1129-1146.

[170] X. Zhang, H. Zhang, Z. Wu, Z. Wang, H. Niu, and C. Li, Nasal absorption enhancement of insulin using PEG-grafted chitosan nanoparticles, Eur. J Pharm Biopharm., 68 (2008) 526-534.

[171] L. Illum, I. Jabbal-Gill, M. Hinchcliffe, A. N. Fisher, and S. S. Davis, Chitosan as a novel nasal delivery system for vaccines, Adv. Drug Deliv. Rev., 51 (2001) 81-96.

[172] Y. K. Kim, A. Minai-Tehrani, J. H. Lee, C. S. Cho, M. H. Cho, and H. L. Jiang, Therapeutic efficiency of folated poly(ethylene glycol)-chitosan-graft-polyethylenimine-Pdcd4 complexes in H-ras12V mice with liver cancer, Int J Nanomedicine., 8 (2013) 1489-1498.

[173] L. Mai, A. Yao, J. Li, Q. Wei, M. Yuchi, X. He, M. Ding, and Q. Zhou, Cyanine 5.5 conjugated nanobubbles as a tumor selective contrast agent for dual ultrasound-fluorescence imaging in a mouse model, PLoS. One., 8 (2013) e61224.

[174] F. Wang, D. Zhang, Q. Zhang, S. Guo, D. Zheng, L. Hao, H. Guo, and C. Li, Tissue distribution and pharmacokinetics evaluation of DOMC-FA micelles for intravenous delivery of PTX, J. Drug Target, 21 (2013) 137-145.

[175] M. R. Cheng, Q. Li, T. Wan, B. He, J. Han, H. X. Chen, F. X. Yang, W. Wang, H. Z. Xu, T. Ye, and B. B. Zha, Galactosylated chitosan/5-fluorouracil nanoparticles inhibit mouse hepatic cancer growth and its side effects, World J. Gastroenterol., 18 (2012) 6076-6087.

[176] K. Nagpal, S. K. Singh, and D. N. Mishra, Formulation, optimization, in vivo pharmacokinetic, behavioral and biochemical estimations of minocycline loaded chitosan nanoparticles for enhanced brain uptake, Chem. Pharm. Bull. (Tokyo), 61 (2013) 258-272.

[177] X. K. He, Z. X. Yuan, X. J. Wu, C. Q. Xu, and W. Y. Li, Low molecular weight hydroxyethyl chitosan-prednisolone conjugate for renal targeting therapy: synthesis, characterization and in vivo studies, Theranostics., 2 (2012) 1054-1063.

[178] S. Mao, W. Sun, and T. Kissel, Chitosan-based formulations for delivery of DNA and siRNA, Adv. Drug Deliv. Rev., 62 (2010) 12-27.

[179] X. Liu, K. A. Howard, M. Dong, M. O. Andersen, U. L. Rahbek, M. G. Johnsen, O. C. Hansen, F. Besenbacher, and J. Kjems, The influence of polymeric properties on chitosan/siRNA nanoparticle formulation and gene silencing, Biomaterials, 28 (2007) 1280-1288.

[180] J. C. Fernandes, X. Qiu, F. M. Winnik, M. Benderdour, X. Zhang, K. Dai, and Q. Shi, Low molecular weight chitosan conjugated with folate for siRNA delivery in vitro: optimization studies, Int. J. Nanomedicine., 7 (2012) 5833-5845.

[181] M. Alameh, D. Dejesus, M. Jean, V. Darras, M. Thibault, M. Lavertu, M. D. Buschmann, and A. Merzouki, Low molecular weight chitosan nanoparticulate system at low N:P ratio for nontoxic polynucleotide delivery, Int. J. Nanomedicine., 7 (2012) 1399-1414.

[182] F. Kong, G. Liu, B. Sun, S. Zhou, A. Zuo, R. Zhao, and D. Liang, Phosphorylatable short peptide conjugated low molecular weight chitosan for efficient siRNA delivery and target gene silencing, Int. J. Pharm., 422 (2012) 445-453.

[183] K. A. Howard, U. L. Rahbek, X. Liu, C. K. Damgaard, S. Z. Glud, M. O. Andersen, M. B. Hovgaard, A. Schmitz, J. R. Nyengaard, F. Besenbacher, and J. Kjems, RNA interference in vitro and in vivo using a novel chitosan/siRNA nanoparticle system, Mol. Ther., 14 (2006) 476-484.

[184] Y. Luo, X. Zhai, C. Ma, P. Sun, Z. Fu, W. Liu, and J. Xu, An inhalable beta(2)-adrenoceptor ligand-directed guanidinylated chitosan carrier for targeted delivery of siRNA to lung, J. Control Release, 162 (2012) 28-36.

[185] H. Katas and H. O. Alpar, Development and characterisation of chitosan nanoparticles for siRNA delivery, J. Control Release, 115 (2006) 216-225.

[186] P. Holzerny, B. Ajdini, W. Heusermann, K. Bruno, M. Schuleit, L. Meinel, and M. Keller, Biophysical properties of chitosan/siRNA polyplexes: profiling the polymer/siRNA interactions and bioactivity, J. Control Release, 157 (2012) 297-304.

[187] J. Malmo, H. Sorgard, K. M. Varum, and S. P. Strand, siRNA delivery with chitosan nanoparticles: Molecular properties favoring efficient gene silencing, J. Control Release, 158 (2012) 261-268.

[188] M. Ravina, E. Cubillo, D. Olmeda, R. Novoa-Carballal, E. Fernandez-Megia, R. Riguera, A. Sanchez, A. Cano, and M. J. Alonso, Hyaluronic acid/chitosan-g-poly(ethylene glycol) nanoparticles for gene therapy: an application for pDNA and siRNA delivery, Pharm. Res., 27 (2010) 2544-2555.

[189] T. Rojanarata, P. Opanasopit, S. Techaarpornkul, T. Ngawhirunpat, and U. Ruktanonchai, Chitosan-thiamine pyrophosphate as a novel carrier for siRNA delivery, Pharm. Res., 25 (2008) 2807-2814.

[190] S. Techaarpornkul, S. Wongkupasert, P. Opanasopit, A. Apirakaramwong, J. Nunthanid, and U. Ruktanonchai, Chitosan-mediated siRNA delivery in vitro: effect of polymer molecular weight, concentration and salt forms, AAPS. PharmSciTech., 11 (2010) 64-72.

[191] J. Malmo, K. M. Varum, and S. P. Strand, Effect of chitosan chain architecture on gene delivery: comparison of self-branched and linear chitosans, Biomacromolecules., 12 (2011) 721-729.

[192] M. Jean, M. Alameh, J. D. De, M. Thibault, M. Lavertu, V. Darras, M. Nelea, M. D. Buschmann, and A. Merzouki, Chitosan-based therapeutic nanoparticles for combination gene therapy and gene silencing of in vitro cell lines relevant to type 2 diabetes, Eur. J. Pharm. Sci., 45 (2012) 138-149.

[193] K. A. Howard, S. R. Paludan, M. A. Behlke, F. Besenbacher, B. Deleuran, and J. Kjems, Chitosan/siRNA nanoparticle-mediated TNF-alpha knockdown in peritoneal macrophages for anti-inflammatory treatment in a murine arthritis model, Mol. Ther., 17 (2009) 162-168.

[194] A. M. Ji, D. Su, O. Che, W. S. Li, L. Sun, Z. Y. Zhang, B. Yang, and F. Xu, Functional gene silencing mediated by chitosan/siRNA nanocomplexes, Nanotechnology., 20 (2009) 405103.

[195] V. Dehousse, N. Garbacki, S. Jaspart, D. Castagne, G. Piel, A. Colige, and B. Evrard, Comparison of chitosan/siRNA and trimethylchitosan/siRNA complexes behaviour in vitro, Int. J. Biol. Macromol., 46 (2010) 342-349.

[196] D. Jere, H. L. Jiang, Y. K. Kim, R. Arote, Y. J. Choi, C. H. Yun, M. H. Cho, and C. S. Cho, Chitosan-graft-polyethylenimine for Akt1 siRNA delivery to lung cancer cells, Int. J. Pharm., 378 (2009) 194-200.

[197] S. M. Noh, M. O. Park, G. Shim, S. E. Han, H. Y. Lee, J. H. Huh, M. S. Kim, J. J. Choi, K. Kim, I. C. Kwon, J. S. Kim, K. H. Baek, and Y. K. Oh, Pegylated poly-l-arginine derivatives of chitosan for effective delivery of siRNA, J. Control Release, 145 (2010) 159-164.

[198] S. Al-Qadi, M. Alatorre-Meda, E. M. Zaghloul, P. Taboada, and C. Remunan-Lopez, Chitosan-hyaluronic acid nanoparticles for gene silencing: The role of hyaluronic acid on the nanoparticles' formation and activity, Colloids Surf. B Biointerfaces., 103C (2012) 615-623.

[199] M. Malhotra, C. Tomaro-Duchesneau, and S. Prakash, Synthesis of TAT peptide-tagged PEGylated chitosan nanoparticles for siRNA delivery targeting neurodegenerative diseases, Biomaterials, 34 (2013) 1270-1280.

[200] Z. X. Liao, Y. C. Ho, H. L. Chen, S. F. Peng, C. W. Hsiao, and H. W. Sung, Enhancement of efficiencies of the cellular uptake and gene silencing of chitosan/siRNA complexes via the inclusion of a negatively charged poly(gamma-glutamic acid), Biomaterials, 31 (2010) 8780-8788.

[201] D. W. Lee, K. S. Yun, H. S. Ban, W. Choe, S. K. Lee, and K. Y. Lee, Preparation and characterization of chitosan/polyguluronate nanoparticles for siRNA delivery, J. Control Release, 139 (2009) 146-152.

[202] J. Lee, K. S. Yun, C. S. Choi, S. H. Shin, H. S. Ban, T. Rhim, S. K. Lee, and K. Y. Lee, T Cell-Specific siRNA Delivery Using Antibody-Conjugated Chitosan Nanoparticles, Bioconjug. Chem., 30 (2012) 1174-1180.

[203] Y. Ping, C. Liu, Z. Zhang, K. L. Liu, J. Chen, and J. Li, Chitosan-graft-(PEI-beta-cyclodextrin) copolymers and their supramolecular PEGylation for DNA and siRNA delivery, Biomaterials, 32 (2011) 8328-8341.

[204] H. D. Han, L. S. Mangala, J. W. Lee, M. M. Shahzad, H. S. Kim, D. Shen, E. J. Nam, E. M. Mora, R. L. Stone, C. Lu, S. J. Lee, J. W. Roh, A. M. Nick, G. Lopez-Berestein, and A. K. Sood, Targeted gene silencing using RGD-labeled chitosan nanoparticles, Clin. Cancer Res., 16 (2010) 3910-3922.

[205] T. H. Kim, S. I. Kim, T. Akaike, and C. S. Cho, Synergistic effect of poly(ethylenimine) on the transfection efficiency of galactosylated chitosan/DNA complexes, J. Control Release, 105 (2005) 354-366.

[206] W. F. Lai and M. C. Lin, Nucleic acid delivery with chitosan and its derivatives, J. Control Release, 134 (2009) 158-168.

[207] L. Casettari, D. Vllasaliu, G. Mantovani, S. M. Howdle, S. Stolnik, and L. Illum, Effect of PEGylation on the Toxicity and Permeability Enhancement of Chitosan, Biomacromolecules., (2010).

[208] M. Malhotra, C. Lane, C. Tomaro-Duchesneau, S. Saha, and S. Prakash, A novel method for synthesizing PEGylated chitosan nanoparticles: strategy, preparation, and in vitro analysis, Int. J. Nanomedicine., 6 (2011) 485-494.

[209] V. Dehousse, N. Garbacki, A. Colige, and B. Evrard, Development of pH-responsive nanocarriers using trimethylchitosans and methacrylic acid copolymer for siRNA delivery, Biomaterials, 31 (2010) 1839-1849.

[210] J. Zhang, C. He, C. Tang, and C. Yin, Ternary polymeric nanoparticles for oral siRNA delivery, Pharm. Res., 30 (2013) 1228-1239.

[211] M. Werle and A. Bernkop-Schnurch, Thiolated chitosans: useful excipients for oral drug delivery, J. Pharm. Pharmacol., 60 (2008) 273-281.

[212] A. K. Varkouhi, R. J. Verheul, R. M. Schiffelers, T. Lammers, G. Storm, and W. E. Hennink, Gene silencing activity of siRNA polyplexes based on thiolated N,N,N-trimethylated chitosan, Bioconjug. Chem., 21 (2010) 2339-2346.

[213] M. S. Huh, S. Y. Lee, S. Park, S. Lee, H. Chung, S. Lee, Y. Choi, Y. K. Oh, J. H. Park, S. Y. Jeong, K. Choi, K. Kim, and I. C. Kwon, Tumor-homing glycol chitosan/polyethylenimine nanoparticles for the systemic delivery of siRNA in tumor-bearing mice, J. Control Release, 144 (2010) 134-143.

[214] S. J. Lee, M. S. Huh, S. Y. Lee, S. Min, S. Lee, H. Koo, J. U. Chu, K. E. Lee, H. Jeon, Y. Choi, K. Choi, Y. Byun, S. Y. Jeong, K. Park, K. Kim, and I. C. Kwon, Tumor-homing poly-siRNA/glycol chitosan self-cross-linked nanoparticles for systemic siRNA delivery in cancer treatment, Angew. Chem. Int. Ed Engl., 51 (2012) 7203-7207.

[215] E. J. Kim, G. Shim, K. Kim, I. C. Kwon, Y. K. Oh, and C. K. Shim, Hyaluronic acid complexed to biodegradable poly L-arginine for targeted delivery of siRNAs, J. Gene Med., 11 (2009) 791-803.

[216] O. Veiseh, F. M. Kievit, H. Mok, J. Ayesh, C. Clark, C. Fang, M. Leung, H. Arami, J. O. Park, and M. Zhang, Cell transcytosing poly-arginine coated magnetic nanovector for safe and effective siRNA delivery, Biomaterials, 32 (2011) 5717-5725.

[217] O. M. Merkel, D. Librizzi, A. Pfestroff, T. Schurrat, K. Buyens, N. N. Sanders, S. C. De Smedt, M. Behe, and T. Kissel, Stability of siRNA polyplexes from poly(ethylenimine) and poly(ethylenimine)-g-poly(ethylene glycol) under in vivo conditions: effects on pharmacokinetics and biodistribution measured by Fluorescence Fluctuation Spectroscopy and Single Photon Emission Computed Tomography (SPECT) imaging, J. Control Release, 138 (2009) 148-159.

[218] M. P. Patel, R. R. Patel, and J. K. Patel, Chitosan mediated targeted drug delivery system: a review, J. Pharm. Pharm. Sci., 13 (2010) 536-557.

[219] P. M. Valencia, M. H. Hanewich-Hollatz, W. Gao, F. Karim, R. Langer, R. Karnik, and O. C. Farokhzad, Effects of ligands with different water solubilities on self-assembly and properties of targeted nanoparticles, Biomaterials, 32 (2011) 6226-6233.

[220] X. Zhao, H. Li, and R. J. Lee, Targeted drug delivery via folate receptors, Expert. Opin. Drug Deliv., 5 (2008) 309-319.

[221] D. Fischer, Y. Li, B. Ahlemeyer, J. Krieglstein, and T. Kissel, In vitro cytotoxicity testing of polycations: influence of polymer structure on cell viability and hemolysis, Biomaterials, 24 (2003) 1121-1131.

[222] B. Ballarin-Gonzalez and K. A. Howard, Polycation-based nanoparticle delivery of RNAi therapeutics: adverse effects and solutions, Adv. Drug Deliv. Rev., 64 (2012) 1717-1729.

[223] D. E. Owens, III and N. A. Peppas, Opsonization, biodistribution, and pharmacokinetics of polymeric nanoparticles, Int. J. Pharm., 307 (2006) 93-102.

[224] E. Salva, L. Kabasakal, F. Eren, N. Ozkan, F. Cakalagaoglu, and J. Akbuga, Local delivery of chitosan/VEGF siRNA nanoplexes reduces angiogenesis and growth of breast cancer in vivo, Nucleic Acid Ther., 22 (2012) 40-48.

[225] A. Bernkop-Schnurch and S. Dunnhaupt, Chitosan-based drug delivery systems, Eur. J. Pharm. Biopharm., 81 (2012) 463-469.

[226] E. J. Nielsen, J. M. Nielsen, D. Becker, A. Karlas, H. Prakash, S. Z. Glud, J. Merrison, F. Besenbacher, T. F. Meyer, J. Kjems, and K. A. Howard, Pulmonary gene silencing in transgenic EGFP mice using aerosolised chitosan/siRNA nanoparticles, Pharm. Res., 27 (2010) 2520-2527.

[227] I. Nawroth, J. Alsner, M. A. Behlke, F. Besenbacher, J. Overgaard, K. A. Howard, and J. Kjems, Intraperitoneal administration of chitosan/DsiRNA nanoparticles targeting TNFalpha prevents radiation-induced fibrosis, Radiother. Oncol., 97 (2010) 143-148.

[228] I. Nawroth, J. Alsner, B. W. Deleuran, F. Dagnaes-Hansen, C. Yang, M. R. Horsman, J. Overgaard, K. A. Howard, J. Kjems, and S. Gao, Peritoneal macrophages mediated delivery of chitosan/siRNA nanoparticle to the lesion site in a murine radiation-induced fibrosis model, Acta Oncol., (2012).

[229] B. Ballarin-Gonzalez, F. Dagnaes-Hansen, R. A. Fenton, S. Gao, S. Hein, M. Dong, J. Kjems, and K. A. Howard, Protection and Systemic Translocation of siRNA Following Oral Administration of Chitosan/siRNA Nanoparticles, Mol. Ther. Nucleic Acids, 2 (2013) e76.

CHAPTER II.
AIM OF THE THESIS

The aim of the present project was to elaborate an efficient siRNA delivery system for cancer treatment. We hypothesized that chitosan NPs decorated with a specific ligand that targets receptors that are overexpressed in tumor cells would be a promising strategy for siRNA delivery. First, chitosan exhibits attractive properties, such as its biocompatibility, cationic nature and chemical versatility that make it an ideal basis for NP construction. Numerous examples in the literature have demonstrated the formulation of chitosan/siRNA NPs. Second, the choice of RGD and RGD peptidomimetics as ligands to target the $\alpha_v\beta_3$ integrins was based on previous work on RGD-grafted PLGA NPs for paclitaxel delivery [1]. The NPs equipped with these ligands demonstrated an enhanced ability to target and deliver the chemotherapeutic agent to tumors, resulting in an increased anti-tumoral efficiency. Finally, depriving the tumor cells of their energetic fuel has been proven to be a powerful strategy to induce tumor death [2,3]. Thus, transporters involved in tumor metabolism have been chosen as the siRNA therapeutic targets in collaboration with the laboratory of Professor Feron (FATH, UCL).

This collaborative project also involves the laboratory of Professor Jérôme (CERM, Université de Liège) for the PEGylation of chitosan and the laboratory of Professor Marchand-Brynaert (INMC, UCL), in which the RGDp ligands were synthesized. The NPs were designed, evaluated and selected with respect to their physico-chemical characteristics, *in vitro* activity, lack of cytotoxicity and ability to target cancer cells. Because the NPs are intended for I.V. administration, their stability in plasma was also considered.

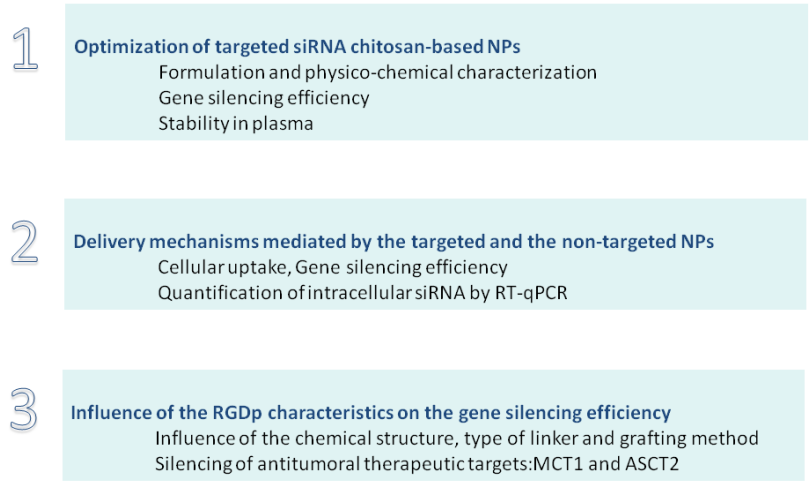

Figure 1: Aim of the thesis, conducted in three steps

The work was conducted in three steps. The aim of the first part *(Chapter III)* was to establish the formulation parameters for the design of optimal siRNA NPs using chitosan. The principle requirements for ideal NPs were suitable physico-chemical characteristics, especially size and polydispersity, high gene silencing activity without cytotoxicity and stability in plasma. This chapter provided the basis for the further design of ligand-grafted NPs.

The second part *(Chapter IV)* focused on the *in vitro* evaluation of $\alpha_v\beta_3$ targeted nanoparticles and, more precisely, on the investigation of their intracellular delivery mechanisms using a new method of stem-loop RT-qPCR. This phase of the project provided a proof of principle of the cancer-cell targeting ability of our delivery system.

Finally, different RGDp structures, grafting strategies (clip *versus* chain-end coupling) and linker properties (hydrophilic *versus* lipophilic) were investigated to determine whether these parameters influence NP efficacy. Moreover, with the prospect of future *in vivo* testing, the NPs were evaluated *in vitro* for their ability to silence the therapeutic targets implicated in cancer metabolism *(Chapter V)*.

REFERENCES

[1] F. Danhier, B. Vroman, N. Lecouturier, N. Crokart, V. Pourcelle, H. Freichels, C. Jerome, J. Marchand-Brynaert, O. Feron, and V. Preat, Targeting of tumor endothelium by RGD-grafted PLGA-nanoparticles loaded with paclitaxel, J Control Release 140(2) (2009) 166-173.

[2] C. Corbet, N. Draoui and O. Feron, Acidic stress induces a glucose-independent glutamine metabolism for proliferation in tumor cells, in preparation

[3] P. Sonveaux, F. Vegran, T. Schroeder, M.C. Wergin, J. Verrax, Z.N. Rabbani, et al. Targeting lactate-fueled respiration selectively kills hypoxic tumor cells in mice. J Clin Invest 118 (2008) 3930–3942.

CHAPTER III.
CHITOSAN NANOPARTICLES FOR SIRNA DELIVERY: OPTIMIZING FORMULATION TO INCREASE STABILITY AND EFFICIENCY

Chitosan nanoparticles for siRNA delivery: optimizing formulation to increase stability and efficiency

Ragelle H., Riva R., Vandermeulen G., Naeye B., Pourcelle V., Le Duff C.S., D'Haese C., Nysten B., Braeckmans K., de Smedt S., Jérôme C., Préat V.

ABSTRACT

Although most of the chitosan/siRNA delivery systems are intended for intravenous injection, none evaluated their stability in biological fluids like plasma. This study aims at developing chitosan-based nanoparticles suitable for an intravenous administration of siRNA able to achieve (i) high gene silencing without cytotoxicity, (ii) stability in biological media including blood. Therefore, the influence of chitosan/TPP ratio, chitosan physicochemical properties, PEGylation of chitosan as well as of the addition of an endosomal disrupting agent and a negatively charged polymer were assessed. The gene silencing activity and cytotoxicity were evaluated on B16 melanoma cells expressing luciferase. We monitored the integrity and the size behaviour of siRNA nanoparticles in human plasma using fluorescence fluctuation spectroscopy and single particle tracking respectively. The presence of PEGylated chitosan and PEI was essential for high levels of gene silencing *in vitro*. Chitosan nanoparticles immediately released siRNA in plasma while the inclusion of hyaluronic acid and high amount of PEG in the formulation improved the stability of the particles. The developed formulations of PEGylated chitosan-based nanoparticles that achieve high gene silencing in vitro, low cytotoxicity and high stability in plasma could be promising for intravenous delivery of siRNA.

Keywords: siRNA delivery, chitosan, nanoparticles, stability in plasma

TABLE OF CONTENTS

I. INTRODUCTION

Over the past few decades, RNA interference (RNAi) has emerged as a promising strategy for the treatment of a wide range of diseases by silencing a gene and therefore by hindering the corresponding protein expression [1]. This mechanism constitutes a highly precise tool due to sequence specificity of the siRNA and the use of this nucleic acid in cancer therapy has promising potential as several oncologic targets have already been identified [2]. Clinical trials are currently being conducted on patients with solid tumors [3,4].

Since the instability and the lack of efficiency of naked siRNA have been demonstrated, many types of nanovectors have been investigated and some of them showed very good activity *in vitro* [5,6]. Nevertheless, the fact that a vector is efficient *in vitro* does not necessarily mean that it will be effective *in vivo*. Indeed, siRNA carriers are confronted with several barriers from their administration to their target site, *i.e.* the cell cytoplasm where the RNAi mechanism is located. If we consider the intravenous route which is one of the more direct ways to reach drug target (tumor tissues, endothelial tumor blood vessels), an ideal vector should gather the following characteristics: (i) its size must be below 200 nm, (ii) all the components have to be biocompatible, (iii) it must be stable enough in blood to protect the nucleic acid, (iv) opsonisation and uptake by macrophages have to be avoided, and (v) after reaching the target site, (vi) endocytosis should occur in the cell but the nucleic acid must be able to further escape the endosome and be released in the cell cytoplasm [7]. All of these barriers need to be taken into account to develop powerful siRNA delivery systems.

Chitosan is one of the most commonly studied polymers in non-viral gene therapy. Its positive charges under slightly acidic conditions allow its interaction with the siRNA and the formation of complexes or nanoparticles [8-13]. In addition, chitosan is biocompatible and biodegradable making it enable for *in vivo* use through intraperitoneal [14,15] or intravenous administration [16,17]. This polymer provides a good basis for nanoparticle construction but needs further developments in order to mediate high gene silencing, in particular after intravenous injection. One of the major limitations of this polymer is its low water solubility at physiological pH because of the partial protonation of the amino groups. This pH-dependence influences nucleic acid binding capability [18] and therefore can affect the stability of the nanoparticles in the blood stream and thus their biological activity. Thus, poly(ethylene glycol) (PEG) grafting onto chitosan has been described [19-21].

The gene silencing efficiency is also dependent on the ability of the nanocarrier to escape the endosome and release siRNA in the cell cytoplasm. The endosomal rupture occurs thanks to the so

called proton sponge effect: the acidification of the endosomes provokes an inlet of water and ions resulting in osmotic swelling and physical rupture of the endosomal vesicles [22]. However, native chitosan has demonstrated less efficient to promote endosomal disruption in comparison to others cationic polymers like poly(ethylene imine) (PEI), resulting in low efficiency *in vitro* [23]. Based on these findings, publications have reported the design of improved chitosan-based delivery system to bypass the polymer limitations and therefore to increase the efficiency of the carrier [24-28].

In this study, we aimed at developing chitosan-based nanoparticles suitable for an intravenous administration of siRNA. The formulations had to achieve (i) high gene silencing without cytotoxicity and (ii) stability in biological media including blood. Therefore, the influence of chitosan physicochemical properties, PEGylation of chitosan as well as the addition of an endosomal disrupting agent and a negatively charged polymer were assessed.

II. MATERIAL AND METHODS

II.1 MATERIALS

Several types of chitosan provided by Sigma-Aldrich (Belgium) and Kitozyme (Belgium) were tested. Their characteristics are summarized in Table I. Branched poly(ethylene imine) (PEI, 25 kDa), sodium tripolyphosphate (TPP) and poly(L-arginine) (PLR) were purchased by Sigma-Aldrich. The methacrylic acid copolymer Eudragit S 100 ® was purchased from Evonik (Germany). Hyaluronic acid (234,400 Da) was purchased by Lifecore Biomedical (USA).

Table I: characteristics of the different chitosans used

	Molecular weight (kDa)	Deacetylation degree DD (mol%)	Origin	Supplier
C_1	90[a]	79.7	Fungi (*Agaricus bisporus*)	Kitozyme
C_2	50- 190[a]	75-85	Animal (shrimp and crab shells)	Sigma-Aldrich
C_3	190-310[a] / 250[b]	75-85	Animal (shrimp and crab shells)	Sigma-Aldrich
C_4	173[a]	65.0	Fungi (*Agaricus bisporus*)	Kitozyme
C_{36}	36[a]	83.0	Fungi (*Agaricus bisporus*)	Kitozyme
C_{82}	82[a]	77.6	Fungi (*Agaricus bisporus*)	Kitozyme
C_{120}	120[a]	80.7	Fungi (*Agaricus bisporus*)	Kitozyme

[a] based on intrinsic viscosity and [b] determined by Gel Permeation Chromatography

Luc siRNA (sense 5'- CUUACGCUGAGUACUUCGATT-3') [29] or control siRNA duplex (sense 5'-AUAGUGCAACGAUGAGCUCTT-3') were bought from Eurogentec (Belgium). SiRNA labelled with Alexa488 (λ_{exc} = 495 nm and λ_{em} = 519 nm) at the 3'end of the sense strand (A488-siRNA) was purchased from Qiagen (Venlo, Netherlands). EGFP22 siRNA duplex (sense 5'-GCAAGCUGACCCUGAAGUUCAU-3', [30], was supplied from Eurogentec.

II.2 SYNTHESIS AND CHARACTERIZATION OF PEGYLATED CHITOSAN

1 g of chitosan C_1 was transferred into a glass tube containing 5 mL of anhydrous DMF. 2.4 g of phtalic anhydride (Aldrich, Belgium) were then added to the solution. The solution was then stirred at 130°C for 7 h. The homogeneous solution was rapidly poured in a water/ice mixture under vigorous stirring. After filtration, chitosan-phtalimid was lyophilized and kept under N_2 at 6°C. 500 mg of phtalimid-chitosan were dried under vacuum overnight. After solubilization in 25 mL of anhydrous

DMF, 0.48 g isocyanate terminated methoxy-PEG (M_n = 1,000 g/mol) were added into the reactor. After one night of reaction at room temperature, 0.8 mL of hydrazine (Aldrich, Belgium) was added to the solution and the temperature was increased to 110°C. After 3 h of reaction, the C_{PEG} solution was dried under vacuum. After solubilization of the collected residues into HAc/NaAc buffer, the solution was filtered off in order to remove phtalimide derivatives. The pH of the solution was increased to 10 by addition of a NaOH solution. The solution was then dialyzed against water until neutral pH before to be lyophilized. ^{1}H NMR spectra were recorded in D_2O/DCl at 400 MHz in the FT mode with a Bruker AN 400 apparatus at 25°C.

II.3 PREPARATION OF CHITOSAN-SIRNA NANOPARTICLES

To avoid RNAse contamination, chitosan and PEI solutions were treated with the reagent RNAsecure (Ambion, Belgium) as described by the manufacturer, except for the chitosan-PEG solution. If not mentioned, the solutions were made in RNAse-free water (Gibco, Belgium) and filtered through 0.22 µm filters (VWR, Belgium). Throughout all experiments, RNase free materials and conditions were carefully applied.

The method used to formulate the nanoparticles is the ionic gelation [9]. The negatively charged components *i.e.* siRNA (50 µM), tripolyphosphate (1 mg/mL) and when stated hyaluronic acid (1 mg/mL) were added to the positively charged components *i.e.* chitosan (1 mg/mL in sodium acetate buffer 0.2 M pH 5.5), PEGylated chitosan (1 mg/mL) and/or PEI (1 mg/mL) and then vortexed 30 s. The mix was left 1 h and centrifugated 30 min at 17,860 xg (15,000 rpm Biofuge 15R, Heraeus Sepatech). The amount of the different components was modified in order to modulate the chitosan/TPP weight ratio and/or the loading rate of siRNA.

II.4 CHARACTERIZATION OF THE NANOPARTICLES

II.4.1 Size and zeta potential

The size and the zeta potential of the nanoparticles were determined using the Nanosizer NanoZS (Malvern Instruments Ltd., Malvern, UK) by photon correlation spectroscopy and electrophoretic mobility respectively. All samples were measured in triplicate in RNAse-free water.

II.4.2 Encapsulation efficiency

The percentage of encapsulation was calculated using Oligreen® reagent (InVitrogen, Belgium) according to the manufacturer guidelines: 100 µL of each samples were transferred in a 96-well plate and mixed with 100 µL of a diluted solution of Oligreen® (1:200 in buffer TE 1x). The plate was incubated at room temperature covered from light for 5 min. The fluorescence measured corresponds to the free (*i.e.* non-encapsulated) siRNA. The wavelengths of excitation and emission were 480 and 520 nm respectively (Victor Perkin Elmer, Belgium).

II.4.3 ^{1}H NMR Spectroscopy of nanoparticles

NMR spectroscopy (NMR) data were recorded on a Bruker Avance spectrometer operating at 500 MHz and 202 MHz for ^{1}H and ^{31}P, respectively. A nanoparticle solution was prepared as described above (II.3) but using deuterated solvents and reagents, *i.e.* acetic acid-d_4 (99.5 atom%D, Aldrich, Belgium), trimethyl silyl-3-propionic acid-d_4 sodium salt (TMSP, 98 atom%D, Euriso-Top, Belgium) and D_2O (99.9 atom%D, Euriso-Top, Belgium). 12 µg siRNA (81 µM), 99.6 µg tripolyphosphate (1 mg/mL in D_2O) were added to 300 µg PEGylated chitosan (1 mg/mL in D_2O) and 60 µg PEI (1 mg/mL in D_2O adjusted to pD 6.5-7 with acetic acid-d_4). The mixture was left to rest for 1 h and then centrifuged for 30 min at 17,860 xg (15,000 rpm). Given the small amount of material available, a Shigemi tube was used, which, by requiring only a volume of about 250 µL, lead a higher concentration sample, which in turns gave a better signal to noise ratio. The glass bottom of the Shigemi was matched to the magnetic susceptibility of D_2O, the solvent in which the samples of C_{PEG} PEI nanoparticles were prepared. Thus, the residue was suspended in 250 µL of a 1 mM solution of TMSP in D_2O and introduced in a 5 mm Shigemi microtube. The ^{1}H-NMR analyses were acquired at 20 °C with the following experimental settings: delay between scans (D1) of 20 s, number of scans (ns) between 3,000 (17 h) and 17,000 (4 days). The HDO signal was suppressed using presaturation prior to acquisition of the ^{1}H signal. The TMSP signal was used as reference (0 ppm).

II.4.4 Determination of nanoparticle morphology using Atomic Force Microscopy

Nanoparticles were diluted 1/10 in RNAse-free water. A sample of 10 µL was deposed onto freshly cleaved mica. The samples were purged with Argon and imaged in tapping mode using Nanoscope IIIa (Veeco Brucker).

II.5 EVALUATION OF NANOPARTICLE STABILITY

II.5.1 siRNA release assay by Fluorescence Fluctuation Spectroscopy

The amount of siRNA released from the nanoparticles incubated at 37°C in either RNAse-free water or 80% plasma as a function of time was determined using Fluorescence Fluctuation Spectroscopy (FFS) following a previously established protocol [31]. Briefly, the fluorescence fluctuations of naked Alexa488-siRNA (λ_{exc} = 495 nm and λ_{em} = 519 nm) and encapsulated Alexa488-siRNA (0.1 µM for all samples) in the excitation volume of a confocal microscope (MRC1024 Bio-Rad) were recorded at several time points in triplicate. As the fluorescence intensity of the baseline is proportional to the siRNA concentration in the solution, it is then possible to determine the amount of siRNA released from the particles and therefore the percentage of complexation over time.

II.5.2 Sizing using Single particle tracking

Single Particle Tracking (SPT) assays were carried out to measure the aggregation of the nanoparticles, using a custom-built laser widefield epi-fluoresence microscope set up, described by Braeckmans et al [32]. A volume of 5 µL of sample containing fluorescently labelled nanoparticles (Alexa488-siRNA) in medium (either RNAse free water or fresh plasma) was applied between a microscope slide and cover glass with double-sided adhesive sticker. The samples were excited using widefield laser illumination and movies of individual nanoparticles diffusing in the medium were recorded and analyzed. From the motion trajectories of all individual particles, the distribution of diffusion coefficients was obtained and was converted to a size distribution using the Stokes-Einstein equation. According to Braeckmans et al [32], the viscosity of human plasma was set to 1.35 cP at 37°C for the calculations.

II.6 IN VITRO STUDIES

The murine melanoma cell line B16F10 which stably expresses firefly luciferase (B16F10 luc, Caliper Life sciences, Belgium) was used for the *in vitro* experiments. Cells were cultivated in Minimum essential medium with Glutamax (MEM alpha with Glutamax, Gibco, Belgium) supplemented with 10% fetal bovine serum (FBS), 100 U/mL penicillin and 100 µg/mL streptomycin (Gibco, Belgium) at 37°C and 5% CO_2 atmosphere.

II.6.1 2.6.1. Cytotoxicity

B16F10 luc cells were seeded (8,000 cells/well) onto 96-well plates. After 24 h, cells were incubated 4 h with the nanoparticles up to 400 nM siRNA/well. Triton 1% was used as positive control and untreated cells were used as a normal cell control.

LDH Cytotoxicity Detection Kit (Roche, France) was used to measure the LDH release of B16F10 luc cells after 4 h incubation with nanoparticles. The LDH activity was measured using the supernatant of the cell culture media (diluted 1/5 in PBS after centrifugation 5 min at 250xg, Eppendorf Centrifuge 5804R) according to manufacturer's instructions. The absorbance was read at 492 nm using a microplate photometer (Thermo Scientific, Belgium).

MTT test was performed to quantify the cell viability after incubation with the several formulations. 48 h after the initiation of *in vitro* transfection, 10 µL of MTT (Sigma, Belgium) (5 mg/mL filtered solution in medium) was added to the cells and incubated for 3 h at 37°C. After incubation, the medium was removed, and 100 µL of dimethylsulfoxide were added to each well. The absorbance was read at 560 nm using a microplate photometer (Thermo Scientific, Belgium).

II.6.2 Transfection efficiency

B16F10 luc cells were plated on 96-well plates (8,000 cells/well) in 100 µL of medium containing 10% FBS 24 h prior to the transfection. Cells were incubated with the nanoparticles or the positive control INTERFERin® (Polyplus Transfection, France), containing luc siRNA or control siRNA duplex at 100 or 200 nM siRNA/well (*i.e.* 10 or 20 pmol/well). After 4 h incubation, the medium was replaced with fresh medium. At 48 h, 100 µL ONE-Glo™ reagent (Promega, Netherlands) was added to the cells grown in 100 µL of medium. The luminescence (Relative Light Units, RLU) was measured within 30 min using Victor Perkin Elmer luminometer. The percentage of luciferase inhibition is expressed by the equation : %inhibition = 100 – ((100 x RLU_{luc}) / RLU_{ctl}) where RLU_{luc} is the mean of RLU for luc siRNA and RLU_{ctl} is the mean of RLU for control siRNA.

Using the same protocol, the transfection efficiency was assessed SiHa cells (human cervical tumor cells) expressing green fluorescence protein (GFP) using EGFP22 siRNA duplex (sense 5'-GCAAGCUGACCCUGAAGUUCAU-3', [30]) supplied from Eurogentec. The GFP SiHa cells were observed using an inverted fluorescent microscope (Axiovert S100, Zeiss) equipped with a objective 20x LD Plan-Neofluar.

II.6.3 Confocal microscopy

B16F10 luc cells were seeded in 2 chamber Labtek® ($1.5x10^5$ cells/chamber) and transfected with nanoparticles for 4 h at a concentration of 200 nM Alexa488-siRNA. Following transfection, cells were subjected to Hoechst 342 and Lysotracker Red DND 99 staining (Invitrogen, Belgium) to visualize nuclei and acidic endosomal vesicles respectively. Uptake of duplex siRNA was monitored by a Zeiss confocal microscope Cell Observer Spinning Disk equipped with a 100x oil objective.

II.6.4 Flow cytometry

Cellular uptake of nanoparticles was quantified by flow cytometry instrument. B16F10 luc cells were seeded in 12-well plates ($2x10^5$ cells/well) 24 h before experiment. Cells were incubated with nanoparticles for 4 h at a concentration of 100 nM Alexa488-siRNA. To quench extracellular fluorophores, cells were incubated with trypan blue (0.2% v/v) for 7 min. Cells were rinsed 2 times with PBS, trypsinized (0.25% trypsin) and diluted with medium. After centrifugation (250xg, 5 min, 4°C), the cell pellet was resuspended in 200 µL PBS. The measurements were done on a FACSscan cytometer and the data were analyzed using FlowJo software. 10^4 cells were analyzed in each measurement.

II.7 STATISTICS

The experiments were performed in triplicate, unless otherwise stated. Values are given as means ± standard deviations (SD). For the statistics and plotting, PRISM (GraphPad, USA) was used. Statistically significant differences were assessed by an analysis of variance (ANOVA) at a 0.05 significance level and followed by Tukey´s post test.

III. RESULTS

III.1 SYNTHESIS OF PEGYLATED CHITOSAN C_{PEG}

In order to increase the solubility of chitosan into water and provide stealth properties to the nanoparticles, PEG chains were selectively grafted onto the hydroxyl groups of chitosan. For this purpose, the coupling of PEG chains functionalized at one chain-end by an isocyanate group with a chitosan chain, whose primary amines were protected by phthalimid groups was investigated. A percentage of grafting of 35 mol% was targeted, in order to achieve a complete solubility of the polymer C_{PEG} in water [33].

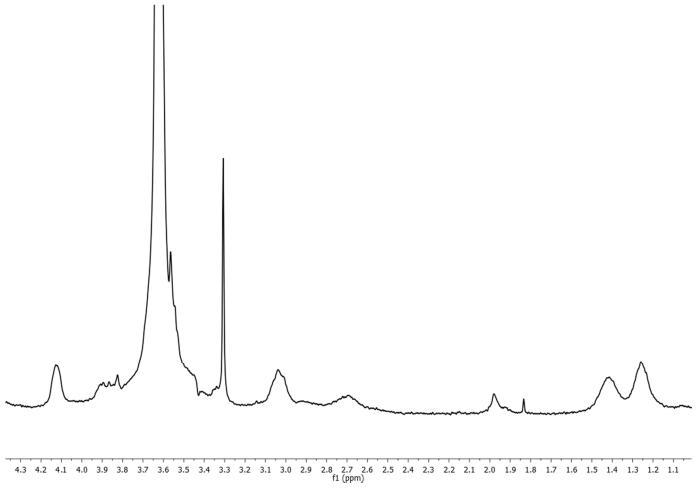

Figure 1 : ^{1}H RMN spectrum of C_{PEG}. The pics at 3.6, 3.3 and 3.0 ppm correspond to the signals of the CH_2 of PEG, CH_3 of PEG and CH of chitosan respectively.

The ^{1}H NMR analysis of the purified C_{PEG} allowed the determination of the number of PEG graft by chitosan chain by comparison of the intensity of the integrals of the signal of the two CH_2 of PEG (3.6 ppm) with the signal of the CH of chitosan (3.0 ppm). The molecular weight of the PEG graft was also calculated by comparison of the signal of the two CH_2 of PEG (3.6 ppm) with the signal of the terminal CH_3 of PEG (3.3 ppm). The percentage of grafting measured by NMR was equal to 30 mol%, which was lower than the expected value of 35 mol%. This observation could be explained by a partial deactivation of the terminal isocyanate of PEG, highly sensitive to hydrolysis. As expected, C_{PEG} was soluble into water at neutral pH. After the synthesis, the characteristics of C_{PEG} were measured: the deacetylation degree was found to be 84% and the Mw 37 kDa due to a supposed degradation during the deprotection step. $C_{PEG'}$ (12 mol% grafting, Mw 20 kDa, DD 84%) was synthesized and characterized using the same methods.

III.2 FORMULATION AND CHARACTERIZATION OF SIRNA LOADED CHITOSAN-BASED NANOPARTICLES

III.2.1 Formulation of the nanoparticles

The rationale for the selection of the excipients to formulate chitosan-based nanoparticles loaded with siRNA was the following. First, as the optimal properties of chitosan are still controversial, chitosan of different origin and molecular weight were tested [34]. Secondly, TPP was used for ionic gelation method, which ensured a good entrapment of the nucleic acid. In preliminary experiments, the optimum C/TPP weight ratio for nanoparticle formation was determined. Depending on the composition of the particles, this ratio was ranged between 4/1 and 2/1. Third, PEGylated chitosan was used to enhance chitosan solubility at physiological pH and to provide stealth properties in blood and PEI, PLR or the metacrylic acid copolymer Eudragit® were added as endosomal disrupting agents [35]. Finally, hyaluronic acid was tested to strengthen nanoparticle stability [36]. The amount of siRNA was fixed at 4 % of chitosan weight.

The Fig. 2 shows the composition of several formulations that were tested.

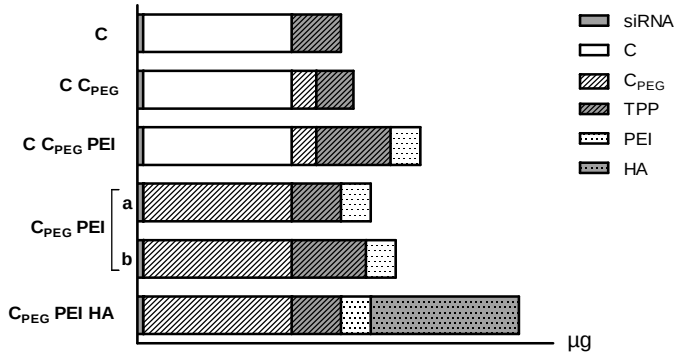

Figure 2: Composition of the formulations. Grey bars represent negatively charged components, white bars represent positively charged components.

III.2.2 Physicochemical characteristics of the nanoparticles

Table II: Characteristics of the formulations (N≥3)

Type of NP	Type of chitosan(s)	Size in buffer DLS (nm)	Polydispersity index	Zeta Potential (mV)	Encapsulation efficiency (%) in buffer	
					Oligreen	FFS
C	C_1	294 ± 131	0.29 ± 0.17	27.8 ± 1.2	99.8 ± 0.1	–
	C_2	180 ± 36	0.23 ± 0.06	26.0 ± 1.3	99.8 ± 0.1	–
	C_3	178 ± 29	0.23 ± 0.07	25.4 ± 2.9	99.7 ± 0.2	94.6 ± 0.9
	C_4	135 ± 11	0.27 ± 0.01	20.4 ± 1.4	99.0 ± 0.2	–
C C_{PEG}	C_3, C_{PEG}	124 ± 2	0.18 ± 0.01	21.7 ± 0.4	99.9 ± 0.1	–
C C_{PEG} PEI	C_2, C_{PEG}	181 ± 22	0.20 ± 0.02	28.8 ± 1.1	99.8 ± 0.1	–
	C_3, C_{PEG}	191 ± 29	0.25 ± 0.04	31.7 ± 5.5	99.8 ± 0.1	98.8 ± 0.2
	C_4, C_{PEG}	188 ± 18	0.28 ± 0.04	25.3 ± 1.8	99.2 ± 0.1	98.5 ± 0.2
C_{PEG} PEI a	C_{PEG}	229 ± 30	0.25 ± 0.07	5.8 ± 8.0	90.9 ± 2.8	99.8 ± 0.1
C_{PEG} PEI b		242 ± 20	0.28 ± 0.07	- 1.0 ± 7.6	89.3 ± 3.8	99.7 ± 0.2
C_{PEG} PEI HA	C_{PEG}	181 ± 35	0.19 ± 0.01	- 15.6 ± 2.5	96.7 ± 1.5	–

The characteristics of the siRNA loaded chitosan-based nanoparticles are summarized in Table II. The nanoparticles had homogenous sizes, using dynamic light scattering (DLS). Indeed, the mean diameter was between 120 and 290 nm and the size distribution was relatively narrow, as shown by the polydispersity index (from 0.18 to 0.29) irrespective of the formulation composition. The molecular weight and the origin of chitosans did not influence the mean diameter or the PDI of the particles ($p<0.05$). However, based on the zeta potential, 3 types of nanoparticles were distinguished. The nanoparticles containing a majority of non-PEGylated chitosan (nanoparticles C, C C_{PEG}, and C C_{PEG} PEI) were positively charged. The C_{PEG} PEI a and C_{PEG} PEI b nanoparticles showed a zeta potential close to neutrality. Finally, the inclusion of the negatively charged polymer hyaluronic acid (HA) led to the formation of negatively charged nanoparticles. The encapsulation efficiency was higher than 90% for all formulations using Oligreen assay. These results were correlated with those obtained with the FFS technique.

To confirm the structure of the nanoparticles, C_{PEG} PEI nanoparticles were investigated by NMR spectroscopy. Very long accumulations were required in order to obtain the spectra shown on figure

3C. This characterisation gives information on the soluble parts of the nanoparticles, *i.e* the surface or the surrounding solution. On figure 3C it can be seen that the CH_2 of PEG (3.7 ppm) gave a narrow signal which demonstrated the presence of PEG as a stabilizing corona. On the contrary, chitosan protons gave a broad peak centred at 3.5 ppm which means that they were in blocked conformations and were very poorly soluble. This signifies that chitosan was organised in a rigid structure forming a solid core and that only a small part of it was in contact with water. Surprisingly three groups of proton situated at 2.6, 2.8, 3.1 ppm and corresponding to CH_2 of PEI appeared clearly after long measuring times and a sojourn of several days in water (Fig. 3C). These peaks were well defined and so could correspond to small amounts of free PEI. With a freshly prepared solution and reasonable accumulation times, those protons were also visible but emerged from a broad peak (see Fig. 3B) corresponding to poorly soluble rigid PEI. One interpretation of these facts could be that nanoparticles suffered self-reorganisation as part of the PEI migrated inside of the solid core whereas some of it ended up close to the surface or in the surrounding media. Nanoparticles were also submitted to ^{31}P NMR but no peak was detected. Both TPP and siRNA presented phosphorus atoms consequently, since they were not detected by NMR, it could be supposed that they were situated inside of the nanoparticles and that only small amounts (under the detection limit of NMR) were present outside. It is worth noticing that, at these concentrations and with the same NMR protocol, TPP in D_2O gave three signals in ^{31}P NMR at -5.9, -7.1, -21.2 ppm. So NMR findings showed nanoparticles with a PEG corona, a solid chitosan core collapsed around TPP and siRNA and PEI segments that seemed to be situated both inside and outside of the nanoparticles. This is coherent with the zeta potentials exhibiting a slightly positive charge certainly due to the shielding effect of PEG and a partial contact of water with chitosan and PEI.

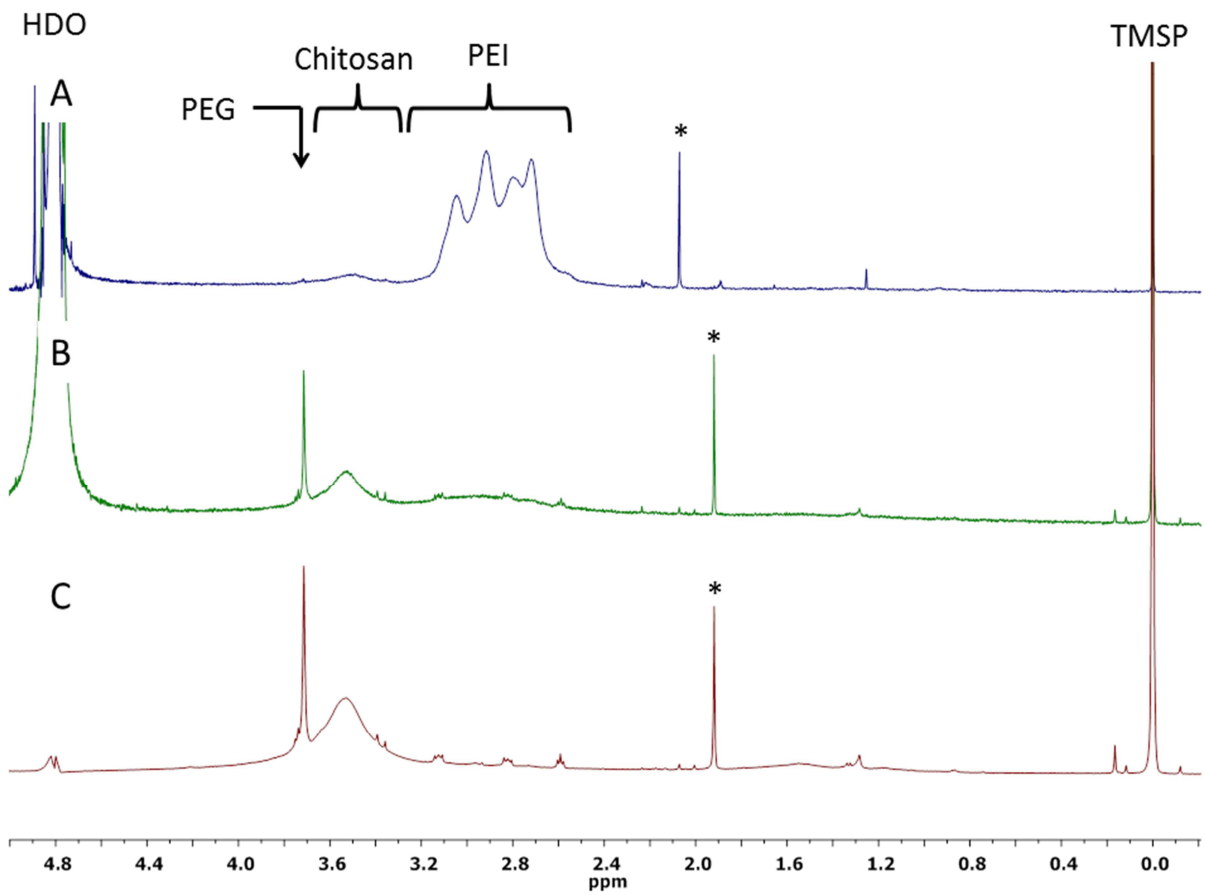

Figure 3: ^{1}H NMR spectra of: A) PEI and TPP (1:1, w:w) in D_2O adjusted at pD 6.5-7; B) C_{PEG} PEI a type of nanoparticles in D_2O with number of scans ns = 3000 (17 h) ; C) C_{PEG} PEI a type of nanoparticles in D_2O with ns = 17000 (4 days); * non deuterated CH_3COOH residual peak.

To further characterize the formulations, C_{PEG} PEI a nanoparticles were analyzed using atomic force microscopy (AFM). In Fig. 4, it can be observed that the particles have a spherical shape. Furthermore, we noticed the coexistence of very small particles with larger particles of around 200 nm diameter, which might be aggregates of the smaller ones. The nanoparticles presented smaller size when using AFM than when measured by DLS. This can be explained by the fact that the PEG chains were not in a hydrated state, hence were not extended, as they are during the DLS measurements.

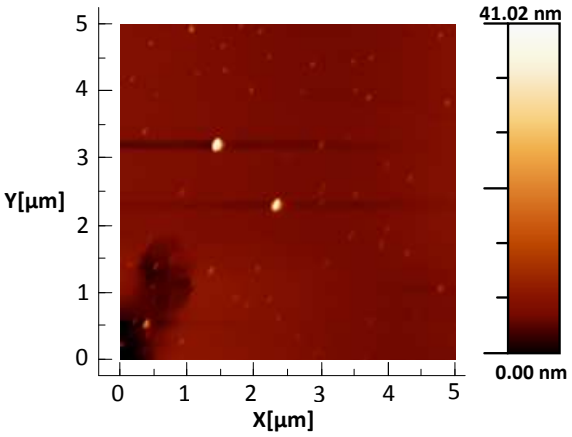

Figure 4: Atomic force microscopy images of nanoparticles CPEG PEI a (scale 5 x 5 µm).

III.3 TRANSFECTION EFFICIENCY OF THE NANOPARTICLES

To evaluate the gene knockdown efficiency of the formulations, B16F10 luc cells were incubated with the different formulations loaded with luc siRNA. The specificity of knockdown was confirmed using scramble siRNA formulations.

III.3.1 Determination of the optimal dose of siRNA

To determine the optimal siRNA concentration for the transfection efficiency, several siRNA doses ranging from 1 nM to 400 nM siRNA/well were investigated, using C_{PEG} PEI a nanoparticles (Fig. 5). No effect was noticed at the lower concentrations (1 and 10 nM siRNA/well). At a dose of 400 nM, RLU signal of nanoparticles loaded with scramble siRNA decreased, suggesting toxicity of the nanoparticles or an off-target effect. Therefore, the gene silencing experiments were performed at 100 and 200 nM.

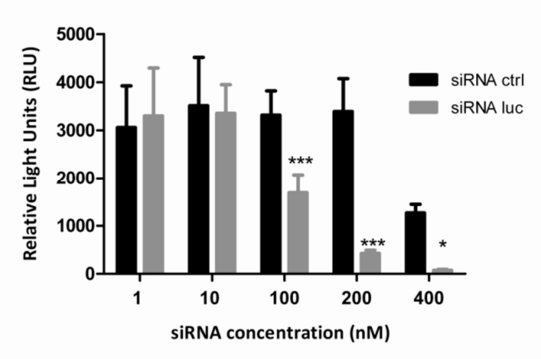

Figure 5: Effect of the concentration of siRNA on the luciferase inhibition for the formulation C_{PEG} PEI a. Cells were incubated for 4 h with the nanoparticles and the luciferase expression was measured 48 h after. Nanoparticles encapsulating control siRNA (black bars) where compared to nanoparticles containing luc siRNA (grey bars): * p< 0.05, ** p< 0.01, *** p< 0.001. Data represent mean ± SD (N= 3, n= 8).

III.3.2 Gene silencing mediated by siRNA loaded chitosan-based nanoparticles

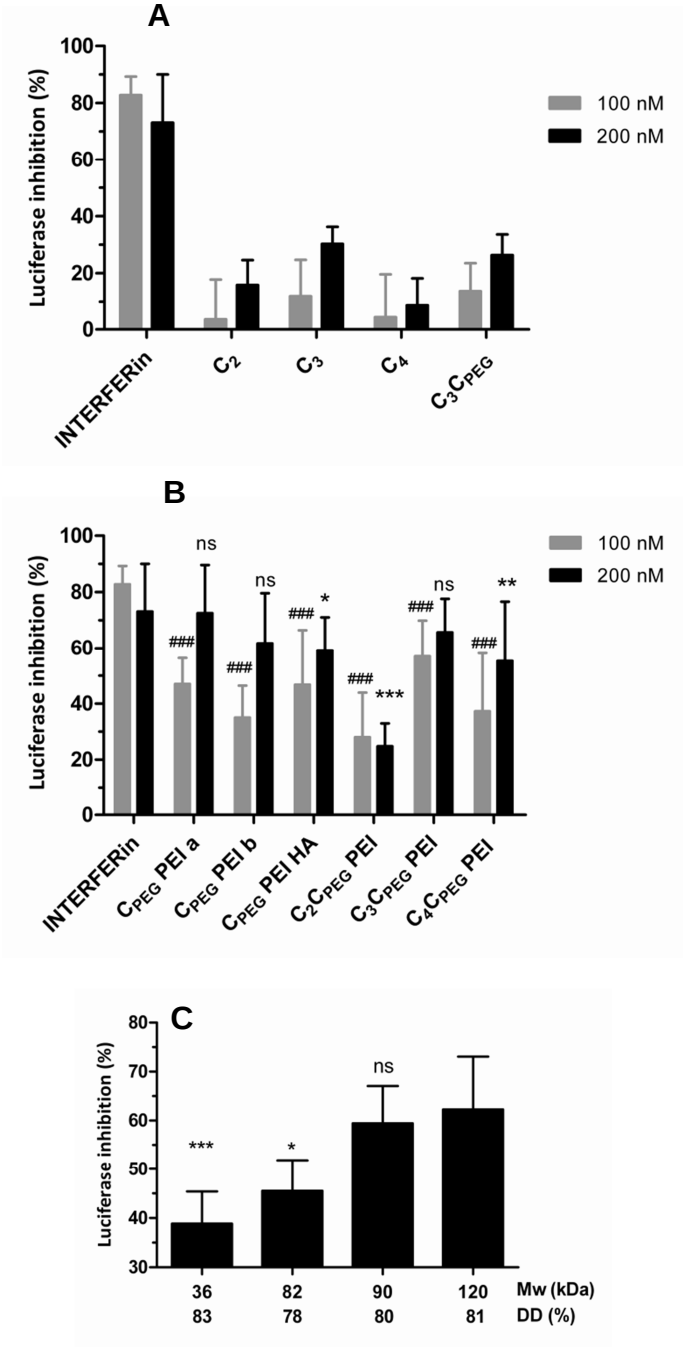

Figure 6: Percentage of luciferase inhibition with different types of nanoparticles. Luminescence was measured 48h after an incubation time of 4h with the nanoparticles. Data represent mean ± SD. A: Chitosan-based nanoparticles. B: Chitosan and PEI PEGylated nanoparticles. The nanoparticles were compared to the positive control INTERFERin at 100 nM (#) or 200 nM (*). C: Influence of the chitosan molecular weight on the luciferase inhibition by CC_{PEG} PEI nanoparticles at 200 nM siRNA/well. The nanoparticles were compared to those made with chitosan of 120 kDa (* p< 0.05, ** p< 0.01, *** p< 0.001) (N=2-4, n=8).

The basic formulations containing chitosan and TPP only demonstrated poor transfection efficacy regardless of the type of chitosan employed (Fig. 6A, p<0.05). Based on the literature, we

hypothesised that this low efficiency could be due to the poor buffering capacity of chitosan [37]. Consequently, nanoparticles with endosomal disruption properties were formulated. To promote endosomal escape, the amine rich polymers polyethyleneimine (PEI) or poly-L-arginine (PLR) were included in the formulations (data not shown). A third formulation was prepared, loading the nanoparticles with methacrylic acid copolymer Eudragit® which also demonstrated good buffering capacities [38]. The nanoparticles possessed suitable physico-chemical characteristics (data not shown). Among these approaches, better luciferase inhibition was obtained with the addition of PEI, therefore this polymer was chosen as additional component for the rest of the study.

Regardless of the formulation, higher level of luciferase inhibition was observed at 200 nM (54% to 71%) than at 100 nM (35% to 56%). Moreover, no significant difference was noticed between the positive control INTERFERin (78% luciferase inhibition) and three of the formulations, *i.e.* C_{PEG} PEI a (71%), C_{PEG} PEI b (62%) and C_3C_{PEG} PEI (66%), on B16F10 luc cells.

Regarding CC_{PEG} PEI nanoparticles, an influence of the chitosan molecular weight on the transfection efficiency was observed. Indeed, nanoparticles made of low molecular weight chitosan (C_2) seemed to be less efficient than the same formulation composed of high molecular weight chitosan (C_3 and C_4). To fortify these results, a second assay was performed with several fungal chitosans of molecular weight ranging from 36 to 120 kDa and 12%mol pegylated chitosan $C_{PEG'}$. As shown in Fig. 6C, a strong correlation between molecular weight and luciferase inhibition was observed.

To confirm the gene silencing observed on B16F10 luc cells, the biological activity of three of our formulations (C_{PEG}PEI HA, C_{PEG}PEI a, C_3C_{PEG} PEI) was tested on a different cell model, using another protein reporter. SiHa cells expressing the green fluorescence protein (GFP) were transfected with nanoparticles loaded with EGFP siRNA. As shown in Fig. 7, C_{PEG}PEI HA nanoparticles were able to decrease the GFP signal. The same effect was observed for C_{PEG}PEI a and C_3C_{PEG} PEI nanoparticles (data not shown). This suggested the high potential of these nanoparticles in different cell models.

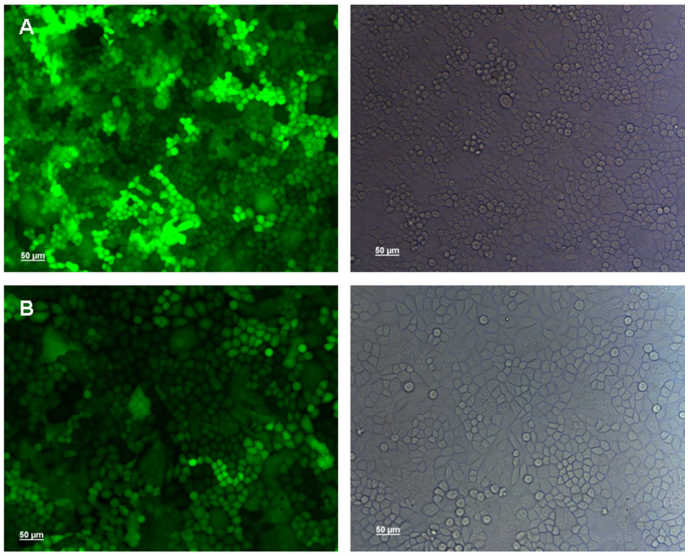

Figure 7: SiHa GFP cells A: medium, B: cells transfected with C_{PEG} PEI HA at 200 nM. Observation of the cells 48 h after the initiation of transfection.

III.4 UPTAKE PROFILES OF THE NANOPARTICLES: CONFOCAL MICROSCOPY AND FLOW CYTOMETRY STUDIES

To better understand the mechanisms of intracellular trafficking of siRNA depending on the characteristics of its carrier, confocal microscopy studies were performed. SiRNA molecules were labelled in green and acidic endosomal vesicles were stained in red. B16F10 luc cells did not present any intracellular siRNA signal after incubation with C_2C_{PEG} PEI nanoparticles (Fig. 8D) or C_2 nanoparticles (data not shown). On the contrary, regarding C_{PEG} PEI, C_3C_{PEG} PEI or C_{PEG} PEI HA particles, siRNA molecules were present in the acidic endosomes as revealed by the yellow dots. Moreover, the green dots suggested that a fraction of siRNA were localized in non-acidic vesicles or were released into the cytoplasm (Fig. 8A-C). Flow cytometry experiments confirmed the results that have been observed in the confocal microscopy study. Indeed, only few amount of C_2C_{PEG} PEI nanoparticles was taken up by the cells (58% uptake Fig. 9) contrary to the other types of particles (100 % of the cells have taken up the particles).

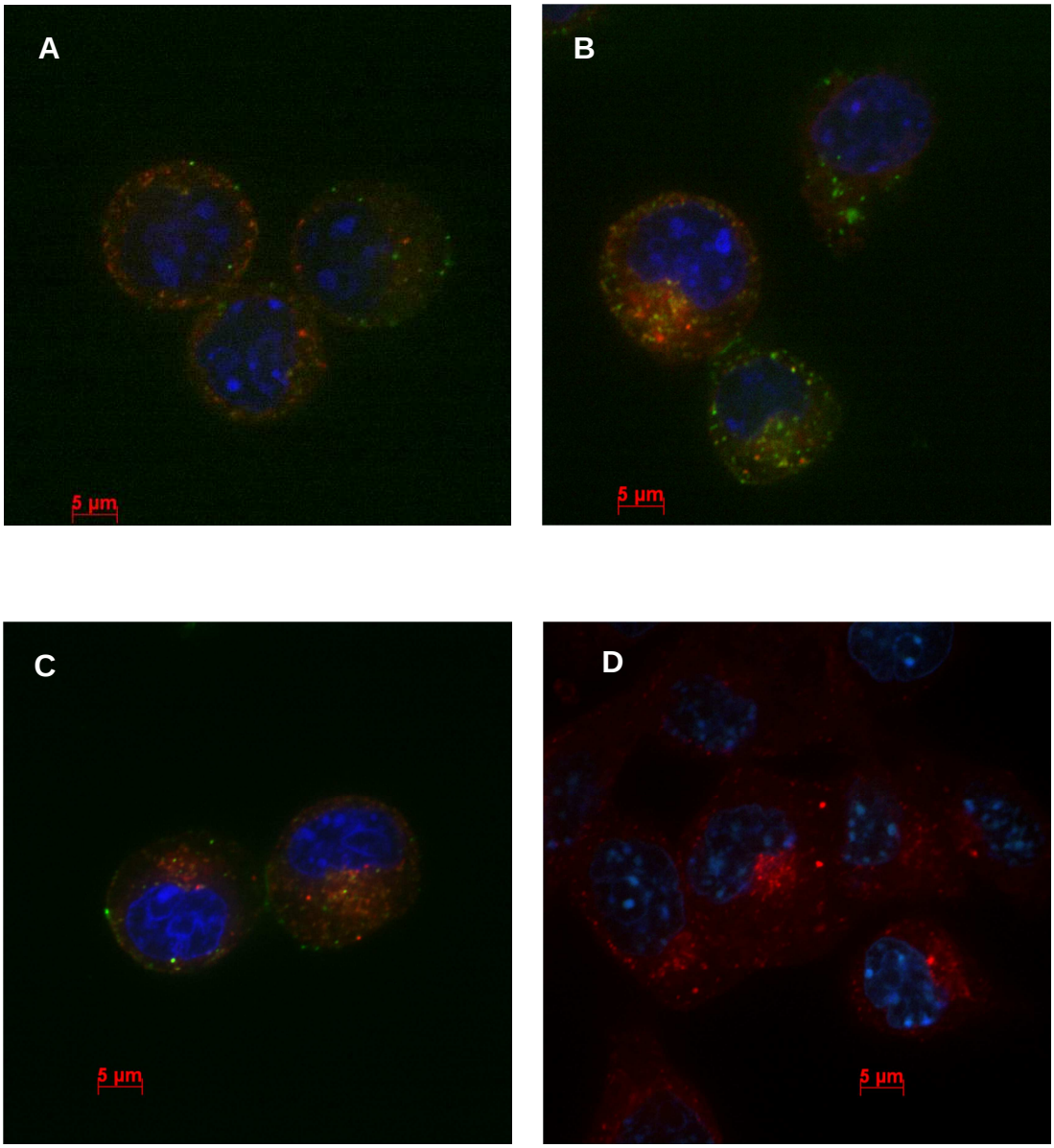

Figure 8 : confocal microscopy images of B16F10 luc cells treated with C_{PEG} PEI (A), C_3C_{PEG} PEI (B), C_{PEG} PEI HA (C), C_2C_{PEG} PEI (D) for 4 h at 200 nM A488-siRNA.

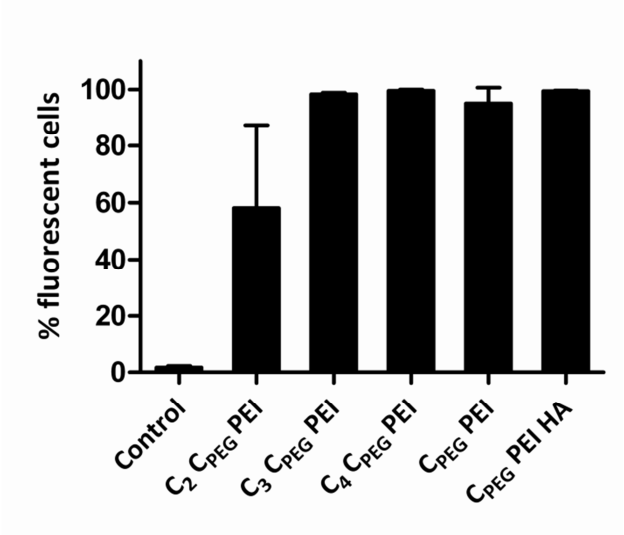

Figure 9: Percentage of fluorescent B16F10 luc cells after 4 h incubation with the several formulations at 100 nM A488-siRNA. Data represent mean values ± SD (N=2-3, n=3).

III.5 CYTOTOXICITY

Toxicity of the formulations was assessed on B16F10 luc cells, at 200 nM siRNA, using MTT and LDH tests to quantify cell viability and cell mortality respectively (Fig. 10). The formulations were compared to siRNA-PEI complexes, containing the same amount of PEI. These complexes induced a toxic effect with more than 40% cell mortality. On the other hand, the nanoparticles did not exhibit any severe toxicity (10 to 20% cell mortality with LDH test). This suggested that the presence of chitosan and PEGylated chitosan enhanced the toxicity profile of the formulations. However, regarding more precisely MTT test results, C_{PEG}PEI and C_{PEG}PEI HA nanoparticles showed higher cell viability (82% and 72 % respectively) than type CC_{PEG}PEI (60% viability). Moreover, no significant difference was noticed between C_{PEG}PEI nanoparticles and cells growing in medium.

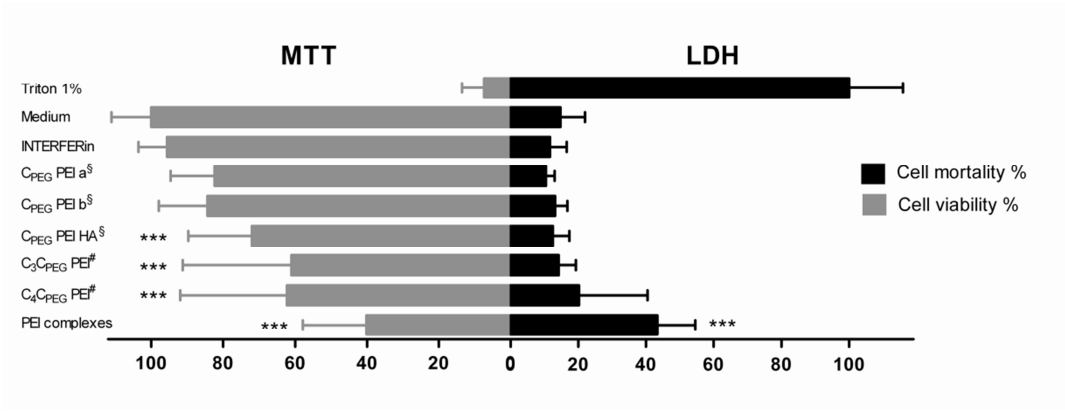

Figure 10: B16F10 luc cell viability (MTT) and mortality (LDH) after treatment with the same formulations used in transfection study, in the same conditions (incubation at 200 nM siRNA/well for 4 h). §concentration of C_{PEG} 68.5 µg/mL; #concentration of C_3 or C_4: 68.5 µg/mL and concentration of C_{PEG} 11.4 µg/mL). Data represent mean values ± SD (N = 3; n= 8). Results significantly different from medium are indicated: ***$p < 0.001$.

III.6 NANOPARTICLE STABILITY IN PLASMA

Little knowledge is available about the stability of chitosan-based particles in plasma although most of them are designated to I.V. administration. Assisted by two innovative technologies *i.e.* fluorescence fluctuation spectroscopy and single particle tracking, we were able, both to determine the ability of our formulations to protect siRNA in plasma and to measure the size of our particles in plasma.

III.6.1 SiRNA release in plasma using Fluorescence Fluctuation Spectroscopy (FFS)

The first consideration is an effective protection of the siRNA molecules in blood. Using FFS it is possible to quantify the siRNA release and therefore to determine the integrity of the formulations in plasma. The complexation efficiency of the formulations was monitored in 80 % plasma as a function of time (Fig. 11). After 2h incubation, approximately 100 % complexation efficiency was maintained for the majority of the nanoparticles, suggesting that they did not dissociate in plasma. However, regarding the C_{PEG} free formulation (C_3 nanoparticles), a very fast release of siRNA occurred.

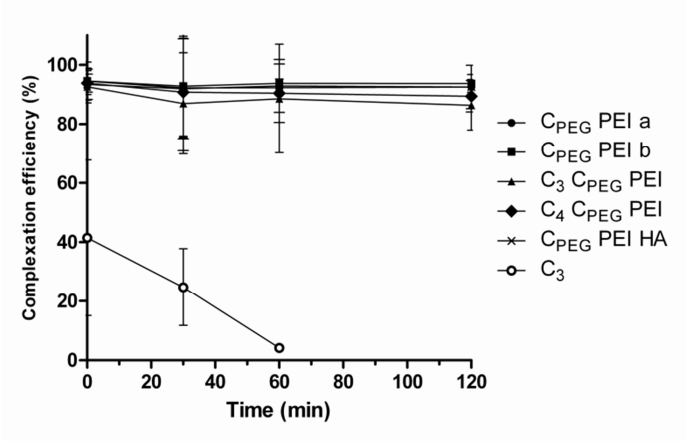

Figure 11: SiRNA complexation efficiency of the formulations in 80 % plasma as a function of time (n=3).

III.6.2 Sizing using Single Particle Tracking (SPT)

Another crucial parameter of stability is size, since it affects the nanoparticle biodistribution in blood and the potential *in vivo* toxicity. Unlike Dynamic Light Scattering (DLS), SPT allows the study of nanoparticle aggregation in real time in biological fluids such as plasma.

Initially, the measurements were performed in RNAse-free water at 37°C. The size distributions are shown in Fig. 12A. At this temperature, the aggregation process is speeded up. Indeed, we noticed an instable behaviour for some of the formulations (C_3C_{PEG} PEI, C_4C_{PEG} PEI and C_3) which was expressed by an increase in their mean diameter. These formulations did not contain C_{PEG} (C_3) but only a low amount of C_{PEG} (C_3C_{PEG} PEI or C_4C_{PEG} PEI), which may not have been sufficient to prevent aggregation. On the other hand, C_{PEG} PEI a, C_{PEG} PEI b and C_{PEG} PEI HA nanoparticles, containing a high amount of C_{PEG}, remained stable at 37°C. Indeed, their size distributions at 37°C were similar to those measured at 25°C with DLS.

Afterwards, the experiments were carried in plasma at 37°C: the formulations were incubated in 80 % plasma and the measurements were done immediately after the incubation. As seen with FFS, C_3 particles fell apart and released the majority of siRNA. C_3C_{PEG} PEI and C_4C_{PEG} PEI nanoparticles aggregated immediately after incubation in plasma. In the case of C_{PEG} PEI particles, the aggregation process occurred as well, even though it was more delayed. Compared to buffer, their size distribution was broadened and the mean diameter was increased (Fig. 12B). On the other hand, the size profile of C_{PEG} PEI HA nanoparticles did not change in plasma (Fig. 12B).

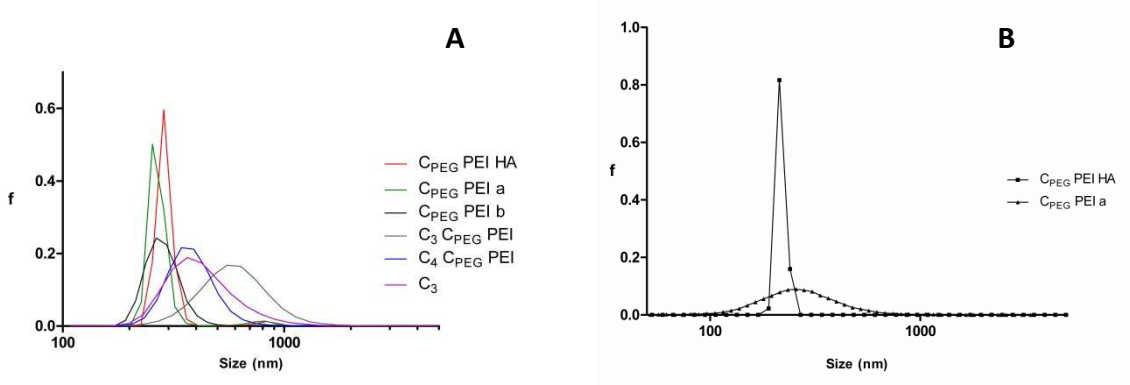

Figure 12: Size distribution of the formulations obtained by SPT at 37°C. A: Size distribution in buffer. B: Size distribution in plasma.

IV. DISCUSSION

Numerous barriers have to be faced in order to deliver the siRNA molecules in the cell cytoplasm. First, the nanoparticles have to remain stable in the biological fluid (blood when I.V. is required), to be taken up by the cells and finally to escape the endosomes in order to deliver the siRNA in the cell cytoplasm, where the RNAi machinery is located. Chitosan possess attractive properties, especially its biodegradability, biocompatibility and easy formulation into NPs. However, the major limitations of this polymer are first its low water solubility at physiological pH that can result in a lack of stability, and secondly its poor endosomal disrupting properties [39]. In this work, we aimed at elucidating the parameters influencing the formulation of efficient chitosan-based systems for I.V. siRNA delivery.

The first method of nanoparticle formulation described in the literature was the simple complexation, where the chitosan and the siRNA were simply mixed [40]. In our hands, this method did not lead to the formation of nanoparticles, probably because of the electrostatic interactions between siRNA and chitosan that were too weak. Another approach, called the ionic gelation, consisted in the addition of a cross-linker agent, mostly TPP to strengthen the interactions between siRNA and chitosan [41]. By using this method of formulation, nanoparticles with suitable physico-chemical characteristics were obtained (mean diameter <300 nm, PDI <0.29). However, these nanoparticles were not efficient to silence the luciferase gene in a murine B16F10 melanoma cell model stably expressing luciferase, regardless of the type of chitosan employed (Fig. 6A). It has been described that chitosan possesses inferior endosomal disrupting properties than the other cationic polymers such as PEI or PLR [23]. Recently, some authors hypothesized that a threshold concentration of chitosan in the complex and/or in the free form could be required to mediate an efficient endosomal escape. Moreover, free PEI seemed to be more efficient than free chitosan at disrupting the endosomal membrane, because of its higher charge density and lower intercharge spacing [42]. Thus, to promote the siRNA release from the endosomes, three types of nanoparticles, all of them containing a low fraction of PEI (1/5 w/w of the amount of chitosan) were formulated. The first kind of nanoparticles (CC_{PEG} PEI) was prepared by mixing non-PEGylated chitosan and C_{PEG}. The nanoparticles thus obtained were positively charged. The second type of nanoparticles contained C_{PEG} only and presented a zeta potential close to the neutrality. In this case, the PEG chains of chitosan may hide the positive charges on the surface of the nanoparticles. Finally, with the inclusion of the anionic polymer hyaluronic acid, negatively charged nanoparticles were obtained (C_{PEG} PEI HA). Three of these formulations (C_{PEG} PEI a, C_3C_{PEG} PEI and C_{PEG} PEI HA) were found to be as efficient as the positive control INTERFERin and mediated up to 70% luciferase inhibition. Interestingly, the C_2C_{PEG} PEI nanoparticles exhibited a lower gene silencing efficiency (30%) than the

same formulation made with a chitosan of higher MW (C_3C_{PEG} PEI or C_4C_{PEG} PEI) (66% and 60% luciferase silencing respectively, Fig. 6B). Furthermore, confocal microscopy and flow cytometry experiments revealed that the C_2C_{PEG} PEI nanoparticles were poorly taken up by the cells (Fig. 8D and 9), compared with the other formulations. Therefore, the poor luciferase inhibition obtained with C_2C_{PEG} PEI particles may have resulted from their instability in serum containing medium. Thus, CC_{PEG} PEI particles made of low molecular chitosans were probably not densely packaged enough to protect siRNA efficiently and released a large amount of siRNA before being endocytosed by the cells. As demonstrated for other cationic polymers [43], these results confirmed the importance of the chemical composition as well as the physical structure of the nanoparticles in their biological activity. Despite the low molecular weight of C_{PEG} (35 kDa, due to a degradation of the chitosan chains during the synthesis), the C_{PEG} PEI and C_{PEG} PEI HA nanoparticles were efficiently taken up by the cells and mediated high gene silencing. In this case, the presence of PEG may compensate for the low molecular weight of the chitosan.

One of the major concerns when designing a delivery system intended for I.V. administration is to maintain a good stability in blood. On one hand, the nanoparticles can be destabilized by interactions with the blood components, resulting in the dissociation of the nanoparticles and thus in the release of siRNA [44]. On the other hand, the binding of blood components on the surface of nanoparticles can lead to the formation of aggregates, affecting the biodistribution of the delivery system and potentially causing toxicity [45]. Assisted by two innovative techniques, namely the Fluorescence Fluctuation Spectroscopy (FFS) and the Single Particle Tracking (SPT), the stability of the formulations was evaluated in human plasma. FFS is a microscopy-based technique that can monitor the integrity of the delivery system, while SPT allows the determination of the size distribution of the nanoparticles in human plasma [46,47]. First, the complexation efficiency of the nanoparticles was monitored by FFS. A rapid disassembly of the C_{PEG}-free nanoparticles (C_3) was observed (Fig. 11). Indeed, 70 % of the initial amount of siRNA was released in 30 minutes, indicating that these nanoparticles may have fallen apart right after the incubation in plasma, rendering them insufficiently stable to deliver siRNA *in vivo*. These results were also confirmed by the SPT measurements, where no remaining C_{PEG}-free nanoparticles were visible after incubation in plasma (data not shown). This instability might be explained by the deprotonation of some of the chitosan amino groups at physiological pH, rendering the binding to siRNA less effective. Moreover, competition between siRNA and anionic plasma proteins for chitosan binding might play a part in the dissociation of these nanoparticles. Therefore, nanoparticles made of TPP and chitosan are not suitable for I.V. administration of siRNA.

On the other hand, the PEGylated nanoparticles did not dissociate in human plasma: approximately 100% complexation efficiency was maintained after 2 h incubation, showing that the PEGylation of the nanoparticles contributes to their stabilisation in plasma. The ^{1}H NMR analysis of the surface of the C_{PEG} PEI a particles confirmed that the nanoparticles displayed a PEG corona (Fig. 3).

By using SPT, C_{PEG} PEI particles appeared to be more stable than the nanoparticles containing a lower amount of PEG (C_3C_{PEG} PEI and C_4C_{PEG} PEI). Indeed, C_3C_{PEG} PEI and C_4C_{PEG} PEI particles aggregated rapidly in plasma. Plasma proteins, such as fibrinogen, may adsorb on these cationic particles creating a linkage between them and leading to aggregation. According to the previous FFS results, the complexation efficiency of these formulations was around 100 %, indicating that the siRNA molecules may be encapsulated in the aggregates. The amount of PEG seemed thus to be an important factor of stability by reducing interparticular aggregation. Indeed, it has been demonstrated that the aggregation of liposomes in blood became more significant as the PEGylation decreased [32]. Moreover, by enhancing the proportion of C_{PEG} into the nanoparticles, the cell viability was improved (Fig. 10). The PEG chains may hide the cationic charges of chitosan, responsible for interactions with cell membrane and thus toxicity [33]. Finally, the inclusion of hyaluronic acid seemed to increase the stability of the particles in plasma, as the size distribution of the C_{PEG} PEI HA nanoparticles did not change upon incubation in plasma (Fig. 12B). This could be attributed to the negative zeta potential of these nanoparticles, leading to repulsive forces between particles and anionic plasma components. Moreover, hyaluronic acid possesses a shielding effect that might have reinforced the stability of the nanoparticles [48,49].

V. CONCLUSION

We aimed at developing siRNA loaded chitosan-based nanoparticles suitable for I.V. administration and thereby to better understand the parameters governing the ability of a carrier to deliver siRNA efficiently. We showed that the inclusion in the formulations of the amine-rich polymer PEI led to high gene silencing. Moreover, we demonstrated that the stability of the nanocarrier is a crucial parameter for reaching its final goal. Combining TPP to chitosan, as described frequently in the literature, would not be a relevant strategy when I.V. route is required. The addition of PEG as well as the use of high molecular weight chitosan, strengthened the structure of the nanoparticles, providing stability and subsequently great levels of *in vitro* gene silencing. Nevertheless, if I.V. administration is required, stability in plasma and in blood is crucial. We demonstrated that by increasing the amount of PEG and by including an anionic polymer (HA), it was possible to generate nanocarriers which were stable in plasma without altering their biological activity. These novel nanoparticles are promising for *in vivo* systemic delivery and will create new perspectives for future gene silencing treatments.

Acknowledgements

This work was supported by the Region Wallonne (BioWin project). The authors thank Dr Paolo Porporato who kindly provided SiHa cells, Dr Patrick Van der Smissen for the help with the confocal microscopy and Min Suk Schauder.

VI.REFERENCES

[1] A. Fire, S. Xu, M. K. Montgomery, S. A. Kostas, S. E. Driver, and C. C. Mello, Potent and specific genetic interference by double-stranded RNA in Caenorhabditis elegans, Nature, 391 (1998) 806-811.

[2] F. Petrocca and J. Lieberman, Promise and challenge of RNA interference-based therapy for cancer, J. Clin. Oncol., 29 (2011) 747-754.

[3] J. Tabernero, G. I. Shapiro, P. M. Lorusso, A. Cervantes, G. K. Schwartz, G. J. Weiss, L. Paz-Ares, D. C. Cho, J. R. Infante, M. Alsina, M. M. Gounder, R. Falzone, J. Harrop, A. C. White, I. Toudjarska, D. Bumcrot, R. E. Meyers, G. Hinkle, N. Svrzikapa, R. M. Hutabarat, V. A. Clausen, J. Cehelsky, S. V. Nochur, C. Gamba-Vitalo, A. K. Vaishnaw, D. W. Sah, J. A. Gollob, and H. A. Burris, III, First-in-Humans Trial of an RNA Interference Therapeutic Targeting VEGF and KSP in Cancer Patients with Liver Involvement, Cancer Discov., 3 (2013) 406-417.

[4] M. A. Rahman, A. R. Amin, X. Wang, J. E. Zuckerman, C. H. Choi, B. Zhou, D. Wang, S. Nannapaneni, L. Koenig, Z. Chen, Z. G. Chen, Y. Yen, M. E. Davis, and D. M. Shin, Systemic delivery of siRNA nanoparticles targeting RRM2 suppresses head and neck tumor growth, J. Control Release, 159 (2012) 384-392.

[5] K. Raemdonck, T. F. Martens, K. Braeckmans, J. Demeester, and S. C. De Smedt, Polysaccharide-based nucleic acid nanoformulations, Adv. Drug Deliv. Rev., (2013).

[6] B. Ballarin-Gonzalez and K. A. Howard, Polycation-based nanoparticle delivery of RNAi therapeutics: adverse effects and solutions, Adv. Drug Deliv. Rev., 64 (2012) 1717-1729.

[7] J. Nguyen and F. C. Szoka, Nucleic acid delivery: the missing pieces of the puzzle?, Acc. Chem. Res., 45 (2012) 1153-1162.

[8] K. A. Howard, U. L. Rahbek, X. Liu, C. K. Damgaard, S. Z. Glud, M. O. Andersen, M. B. Hovgaard, A. Schmitz, J. R. Nyengaard, F. Besenbacher, and J. Kjems, RNA interference in vitro and in vivo using a novel chitosan/siRNA nanoparticle system, Mol. Ther., 14 (2006) 476-484.

[9] H. Katas and H. O. Alpar, Development and characterisation of chitosan nanoparticles for siRNA delivery, J. Control Release, 115 (2006) 216-225.

[10] J. Malmo, H. Sorgard, K. M. Varum, and S. P. Strand, siRNA delivery with chitosan nanoparticles: Molecular properties favoring efficient gene silencing, J. Control Release, 158 (2012) 261-268.

[11] J. C. Fernandes, X. Qiu, F. M. Winnik, M. Benderdour, X. Zhang, K. Dai, and Q. Shi, Low molecular weight chitosan conjugated with folate for siRNA delivery in vitro: optimization studies, Int. J. Nanomedicine., 7 (2012) 5833-5845.

[12] P. Holzerny, B. Ajdini, W. Heusermann, K. Bruno, M. Schuleit, L. Meinel, and M. Keller, Biophysical properties of chitosan/siRNA polyplexes: profiling the polymer/siRNA interactions and bioactivity, J. Control Release, 157 (2012) 297-304.

[13] M. Jean, M. Alameh, J. D. De, M. Thibault, M. Lavertu, V. Darras, M. Nelea, M. D. Buschmann, and A. Merzouki, Chitosan-based therapeutic nanoparticles for combination gene therapy and gene silencing of in vitro cell lines relevant to type 2 diabetes, Eur. J. Pharm. Sci., 45 (2012) 138-149.

[14] K. A. Howard, Delivery of RNA interference therapeutics using polycation-based nanoparticles, Adv. Drug Deliv. Rev., 61 (2009) 710-720.

[15] I. Nawroth, J. Alsner, B. W. Deleuran, F. Dagnaes-Hansen, C. Yang, M. R. Horsman, J. Overgaard, K. A. Howard, J. Kjems, and S. Gao, Peritoneal macrophages mediated delivery of chitosan/siRNA nanoparticle to the lesion site in a murine radiation-induced fibrosis model, Acta Oncol., (2012).

[16] H. D. Han, L. S. Mangala, J. W. Lee, M. M. Shahzad, H. S. Kim, D. Shen, E. J. Nam, E. M. Mora, R. L. Stone, C. Lu, S. J. Lee, J. W. Roh, A. M. Nick, G. Lopez-Berestein, and A. K. Sood, Targeted gene silencing using RGD-labeled chitosan nanoparticles, Clin. Cancer Res., 16 (2010) 3910-3922.

[17] Y. K. Kim, A. Minai-Tehrani, J. H. Lee, C. S. Cho, M. H. Cho, and H. L. Jiang, Therapeutic efficiency of folated poly(ethylene glycol)-chitosan-graft-polyethylenimine-Pdcd4 complexes in H-ras12V mice with liver cancer, Int. J. Nanomedicine., 8 (2013) 1489-1498.

[18] V. Dehousse, N. Garbacki, S. Jaspart, D. Castagne, G. Piel, A. Colige, and B. Evrard, Comparison of chitosan/siRNA and trimethylchitosan/siRNA complexes behaviour in vitro, Int. J. Biol. Macromol., 46 (2010) 342-349.

[19] Casettari L., Vllasaliu D., Mantovani G., Howdle S.M., Stolnik S., and Illum L, Effect of PEGylation on the Toxicity and Permeability Enhancement of Chitosan, Biomacromolecules, 11 (2010) 2825-3218.

[20] Y. K. Kim, A. Minai-Tehrani, J. H. Lee, C. S. Cho, M. H. Cho, and H. L. Jiang, Therapeutic efficiency of folated poly(ethylene glycol)-chitosan-graft-polyethylenimine-Pdcd4 complexes in H-ras12V mice with liver cancer, Int. J. Nanomedicine., 8 (2013) 1489-1498.

[21] M. Malhotra, C. Lane, C. Tomaro-Duchesneau, S. Saha, and S. Prakash, A novel method for synthesizing PEGylated chitosan nanoparticles: strategy, preparation, and in vitro analysis, Int. J. Nanomedicine., 6 (2011) 485-494.

[22] A. Akinc, M. Thomas, A. M. Klibanov, and R. Langer, Exploring polyethylenimine-mediated DNA transfection and the proton sponge hypothesis, J. Gene Med., 7 (2005) 657-663.

[23] H. Q. Mao, K. Roy, V. L. Troung-Le, K. A. Janes, K. Y. Lin, Y. Wang, J. T. August, and K. W. Leong, Chitosan-DNA nanoparticles as gene carriers: synthesis, characterization and transfection efficiency, J. Control Release, 70 (2001) 399-421.

[24] A. K. Varkouhi, R. J. Verheul, R. M. Schiffelers, T. Lammers, G. Storm, and W. E. Hennink, Gene silencing activity of siRNA polyplexes based on thiolated N,N,N-trimethylated chitosan, Bioconjug. Chem., 21 (2010) 2339-2346.

[25] Y. Luo, X. Zhai, C. Ma, P. Sun, Z. Fu, W. Liu, and J. Xu, An inhalable beta(2)-adrenoceptor ligand-directed guanidinylated chitosan carrier for targeted delivery of siRNA to lung, J. Control Release, 162 (2012) 28-36.

[26] D. Jere, H. L. Jiang, Y. K. Kim, R. Arote, Y. J. Choi, C. H. Yun, M. H. Cho, and C. S. Cho, Chitosan-graft-polyethylenimine for Akt1 siRNA delivery to lung cancer cells, Int. J. Pharm., 378 (2009) 194-200.

[27] F. Kong, G. Liu, B. Sun, S. Zhou, A. Zuo, R. Zhao, and D. Liang, Phosphorylatable short peptide conjugated low molecular weight chitosan for efficient siRNA delivery and target gene silencing, Int. J. Pharm., 422 (2012) 445-453.

[28] S. Al-Qadi, M. Alatorre-Meda, E. M. Zaghloul, P. Taboada, and C. Remunan-Lopez, Chitosan-hyaluronic acid nanoparticles for gene silencing: The role of hyaluronic acid on the nanoparticles' formation and activity, Colloids Surf. B Biointerfaces., 103C (2012) 615-623.

[29] D. P. Cioca, Y. Aoki, and K. Kiyosawa, RNA interference is a functional pathway with therapeutic potential in human myeloid leukemia cell lines, Cancer Gene Ther., 10 (2003) 125-133.

[30] N. J. Caplen, S. Parrish, F. Imani, A. Fire, and R. A. Morgan, Specific inhibition of gene expression by small double-stranded RNAs in invertebrate and vertebrate systems, Proc. Natl. Acad. Sci. U. S. A, 98 (2001) 9742-9747.

[31] K. Buyens, B. Lucas, K. Raemdonck, K. Braeckmans, J. Vercammen, J. Hendrix, Y. Engelborghs, S. C. De Smedt, and N. N. Sanders, A fast and sensitive method for measuring the integrity of siRNA-carrier complexes in full human serum, J. Control Release, 126 (2008) 67-76.

[32] K. Braeckmans, K. Buyens, W. Bouquet, C. Vervaet, P. Joye, V. F. De, L. Plawinski, L. Doeuvre, E. ngles-Cano, N. N. Sanders, J. Demeester, and S. C. De Smedt, Sizing nanomatter in biological fluids by fluorescence single particle tracking, Nano. Lett., 10 (2010) 4435-4442.

[33] L. Casettari, D. Vllasaliu, G. Mantovani, S. M. Howdle, S. Stolnik, and L. Illum, Effect of PEGylation on the Toxicity and Permeability Enhancement of Chitosan, Biomacromolecules., (2010).

[34] P. Holzerny, B. Ajdini, W. Heusermann, K. Bruno, M. Schuleit, L. Meinel, and M. Keller, Biophysical properties of chitosan/siRNA polyplexes: Profiling the polymer/siRNA interactions and bioactivity, J. Control Release, (2011).

[35] S. K. Tripathi, R. Goyal, P. Kumar, and K. C. Gupta, Linear polyethylenimine-graft-chitosan copolymers as efficient DNA/siRNA delivery vectors in vitro and in vivo, Nanomedicine., (2011).

[36] M. Ravina, E. Cubillo, D. Olmeda, R. Novoa-Carballal, E. Fernandez-Megia, R. Riguera, A. Sanchez, A. Cano, and M. J. Alonso, Hyaluronic acid/chitosan-g-poly(ethylene glycol) nanoparticles for gene therapy: an application for pDNA and siRNA delivery, Pharm. Res., 27 (2010) 2544-2555.

[37] S. Mao, W. Sun, and T. Kissel, Chitosan-based formulations for delivery of DNA and siRNA, Adv. Drug Deliv. Rev., 62 (2010) 12-27.

[38] V. Dehousse, N. Garbacki, A. Colige, and B. Evrard, Development of pH-responsive nanocarriers using trimethylchitosans and methacrylic acid copolymer for siRNA delivery, Biomaterials, 31 (2010) 1839-1849.

[39] H. Ragelle, G. Vandermeulen, and V. Preat, Chitosan-based siRNA delivery systems, J. Control Release, (2013).

[40] K. A. Howard, U. L. Rahbek, X. Liu, C. K. Damgaard, S. Z. Glud, M. O. Andersen, M. B. Hovgaard, A. Schmitz, J. R. Nyengaard, F. Besenbacher, and J. Kjems, RNA interference in vitro and in vivo using a novel chitosan/siRNA nanoparticle system, Mol. Ther., 14 (2006) 476-484.

[41] H. Katas and H. O. Alpar, Development and characterisation of chitosan nanoparticles for siRNA delivery, J. Control Release, 115 (2006) 216-225.

[42] I. Richard, M. Thibault, C. G. De, M. D. Buschmann, and M. Lavertu, Ionization behavior of chitosan and chitosan-DNA polyplexes indicate that chitosan has a similar capability to induce a proton-sponge effect as PEI, Biomacromolecules., 14 (2013) 1732-1740.

[43] A. M. Portis, G. Carballo, G. L. Baker, C. Chan, and S. P. Walton, Confocal microscopy for the analysis of siRNA delivery by polymeric nanoparticles, Microsc. Res. Tech., 73 (2010) 878-885.

[44] T. Miller, A. Hill, S. Uezguen, M. Weigandt, and A. Goepferich, Analysis of immediate stress mechanisms upon injection of polymeric micelles and related colloidal drug carriers: implications on drug targeting, Biomacromolecules., 13 (2012) 1707-1718.

[45] K. Buyens, B. Lucas, K. Raemdonck, K. Braeckmans, J. Vercammen, J. Hendrix, Y. Engelborghs, S. C. De Smedt, and N. N. Sanders, A fast and sensitive method for measuring the integrity of siRNA-carrier complexes in full human serum, J. Control Release, 126 (2008) 67-76.

[46] K. Buyens, M. Meyer, E. Wagner, J. Demeester, S. C. De Smedt, and N. N. Sanders, Monitoring the disassembly of siRNA polyplexes in serum is crucial for predicting their biological efficacy, J. Control Release, 141 (2010) 38-41.

[47] K. Braeckmans, K. Buyens, W. Bouquet, C. Vervaet, P. Joye, V. F. De, L. Plawinski, L. Doeuvre, E. Angles-Cano, N. N. Sanders, J. Demeester, and S. C. De Smedt, Sizing nanomatter in biological fluids by fluorescence single particle tracking, Nano. Lett., 10 (2010) 4435-4442.

[48] W. A. Dufay, H. Hillaireau, T. L. Nascimento, S. Arpicco, M. Taverna, S. Ribes, M. Bourge, V. Nicolas, A. Bochot, C. Vauthier, N. Tsapis, and E. Fattal, Hyaluronic acid-bearing lipoplexes: physico-chemical characterization and in vitro targeting of the CD44 receptor, J. Control Release, 162 (2012) 545-552.

[49] D'Sa Raechelle A and R. J. P. B. K. a. M. B. J. Dickinson Peter J, Inhibition of lens epithelial cell growth via immobilisation of hyaluronic acid on atmospheric pressure plasma modified polystyrene, Soft Matter, 7 (2010) 608-617.

CHAPTER IV.
DESIGN OF A MULTIFUNCTIONAL CHITOSAN-BASED SIRNA DELIVERY SYSTEM FOR ACTIVE TUMOR TARGETING: A MECHANISTIC APPROACH

DESIGN OF A MULTIFUNCTIONAL CHITOSAN-BASED SIRNA DELIVERY SYSTEM FOR ACTIVE TUMOR TARGETING: A MECHANISTIC APPROACH

Ragelle H., Colombo S., Pourcelle V., Vanvarenberg K., Vandermeulen G., Bouzin C., Marchand-Brynaert J., Mørck Nielsen H., Feron O., Foged C*., Préat V*.

* Corresponding co-authors

ABSTRACT

Specific delivery of small interfering RNA (siRNA) to tumors by exploiting the endocytosis mediated by receptors overexpressed on tumor cells is a promising strategy for cancer therapy. However, little is known about the quantitative aspect of the carrier-mediated intracellular delivery. We designed actively targeted, PEGylated chitosan-based multifunctional nanoparticles for siRNA delivery to tumor cells *via* $\alpha_v\beta_3$ integrin-mediated endocytosis by grafting of the arginine-glycine-aspartate (RGD) or RGD peptidomimetic (RGDp) ligands on the surface of the nanoparticles. Using an innovative method based on stem-loop reverse transcription quantitative polymerase chain reaction (RT-qPCR), the amount of the intracellular full-length dicer substrate siRNA (DsiRNA) delivered by using non-targeted and $\alpha_v\beta_3$-targeted nanoparticles were compared in H1299 cells expressing enhanced green fluorescent protein (EGFP). Moreover, the quantitative amount of siRNA delivered to the cytoplasm was correlated to the EGFP silencing efficiency determined by using flow cytometry. Grafting of the RGD or RGDp ligands triggered accelerated endocytosis and enhanced nanoparticles uptake, as compared to the non-targeted nanoparticles. Moreover, the $\alpha_v\beta_3$-targeted nanoparticles released the siRNA in the cell cytoplasm leading to approximately 90% of EGFP silencing, contrary to the non-targeted nanoparticles that did not mediate EGFP silencing probably because they remained entrapped in endocytic vesicles. Furthermore, the $\alpha_v\beta_3$ integrin-mediated endocytosis appeared to be strongly dependent on the local ligand concentration. Chitosan nanoparticles actively targeted against $\alpha_v\beta_3$ integrin are thus interesting systems for siRNA delivery to cancer cells, combining high gene silencing efficiency and tumor targeting properties in one single, multifunctional carrier system.

KEYWORDS $\alpha_v\beta_3$ integrin, nanoparticles, siRNA, RT-qPCR, delivery, intracellular concentration quantification

TABLE OF CONTENTS

I. INTRODUCTION

RNA interference (RNAi) has become an increasingly promising approach for the treatment of a wide range of diseases, and its discovery has dramatically broadened the number of therapeutic targets to encompass the entire genome [1]. However, the therapeutic exploitation of the potential of RNAi-based drugs has appeared to be fully dependent on the development of delivery systems that can efficiently help overcoming the numerous barriers existing for the intracellular delivery of the mediators of the RNAi process, *e.g.* the small interfering RNAs (siRNAs).

Among the polymers described in the literature for siRNA delivery, chitosan offers many advantages. First, its polycationic nature allows for the complexation and condensation of siRNA into nanoparticle *via* a fast, easy and gentle process [2,3]. Moreover, chitosan is biodegradable and biocompatible, which is a crucial factor with regards to *in vivo* administration [4,5]. Finally, the versatility chemical structure of chitosan enables numerous chemical modifications in order to impart new properties and improve the performances of the polymer [6]. As a carrier for intracellular delivery of RNA, chitosan suffers from low water solubility at pH values higher than 6.5 [6]. Moreover, the transfection efficiency mediated by chitosan is limited due to its poor buffering capacity and inability to mediate endosomal escape [7,8]. Therefore, a number of chitosan derivatives as well as formulation improvements have been described [9]. In this work, we used poly(ethylene glycol) (PEG) grafted chitosan (PEG-chitosan) to enhance the polymer solubility as well as the nanoparticle colloidal stability. Moreover, poly(ethylene imine) (PEI) was included in the formulation in order to improve the transfection efficiency of the nanoparticles, as described previously [10]. Lastly, arginine-glycine-aspartate peptide (RGD) or small protein-like chains that mimic the RGD motif, called RGD peptidomimetic (RGDp), were conjugated to the PEG chains in order to provide the nanoparticles with the ability to target the $\alpha_v\beta_3$ integrin receptors. The $\alpha_v\beta_3$ integrins are upregulated both in tumor cells and in angiogenic endothelial cells as compared to healthy cells [11], and they therefore represent interesting targets for the delivery of siRNA in cancer therapy. Delivery systems grafted with RGD or RGDp have been shown to increase the treatment efficacy due to the tumor targeting properties of the ligands, as compared to their non-targeted counterparts [12,13]. Moreover, RGDp-grafted systems have a longer half-life and a higher bioavailability than RGD-grafted systems because of the absence of a peptide bond in their structure [14].

The efficacy of nucleic acid-based therapies significantly depends on the ability of the delivery systems to carry the active compounds to their site of action, *i.e.* the cell cytoplasm. Little knowledge is available about the intracellular delivery mechanisms of nucleic acid delivery systems. Generally, the cellular uptake process is assessed by applying nucleic acids labelled with fluorophores in

combination with fluorescence microscopy or flow cytometry. An estimation of the siRNA delivery efficiency of the particles is thus obtained. However, these techniques are not fully quantitative for the delivery of the active compound, as they detect the fluorophore and not the siRNA itself. Therefore, the development of sensitive and robust analytical quantification techniques for small RNAs is needed in order to i) obtain a better understanding of the cellular delivery processes, ii) estimate the nucleic acid-based drug bioavailability and iii) select the optimal dose for subsequent *in vivo* experiments. The stem-loop reverse transcription quantitative polymerase chain reaction (RT-qPCR) approach has been developed to quantify the amount of the full-length active small RNAs delivered and maintained in the cells [15,16]. The major advantage of this method is its simplicity and convenience. In this work, a novel stem-loop primer set optimized for the detection of a dicer substrate siRNA (DsiRNA) targeting the enhanced green fluorescent protein (EGFP) was used, allowing for a highly accurate quantification of the amount of intracellular active DsiRNA molecules. Three different types of nanoparticles were investigated and compared with regards to their delivery efficiency using the H1299 EGFP cell model expressing the $\alpha_v\beta_3$ integrins [17]: non-targeted, RGD-grafted and RGDp-grafted nanoparticles. Furthermore, the parallel evaluation of EGFP knockdown allowed for a direct correlation between the dose and the effect.

Finally, two different types of small nucleic acids were studied: conventional siRNA, which are 19-21 nucleotides in length, and DsiRNA, which are 25-27 nucleotides in length. The latter are thought to be more efficient given that they are first processed by the Dicer enzyme, which may facilitate their further incorporation into the RNAi-induced silencing complex (RISC) and thus enhance gene silencing efficiency [7,18]

These results thus provided new insights into the uptake and intracellular trafficking processes of the $\alpha_v\beta_3$-integrin targeted nanoparticles. By applying the RT-qPCR approach, it was possible to quantify precisely the amount of DsiRNA in the cells and to improve the understanding of the intracellular behaviour of the different types of nanoparticles. Furthermore, these results demonstrate that $\alpha_v\beta_3$ targeted chitosan nanoparticles are interesting systems for siRNA and DsiRNA delivery to cancer cells, combining high gene silencing efficiency, tumor targeting properties and low cytotoxicity.

II. METHODS

II.1. MATERIALS

Branched poly(ethylene imine) (PEI, 25 kDa) and sodium tripolyphosphate (TPP) were purchased from Sigma-Aldrich (Diegem, Belgium).

GRGDS (named RGD) was purchased from NeoMPS. HO-PEG-OMe 5,000g/mol was purchased from Aldrich. RGD peptidomimetic (RGDp, Fig. 1) named (2S)-3-[3-{6-aminohexanamido}-4-{3-(5,6,7,8-tetrahydro-[1,8]-naphthyridin-2-yl)propoxy}phenyl]-2-[3-(trifluoromethyl)phenylsulfonamido] propanoïc acid, was synthesized following procedures described in [19] [20].

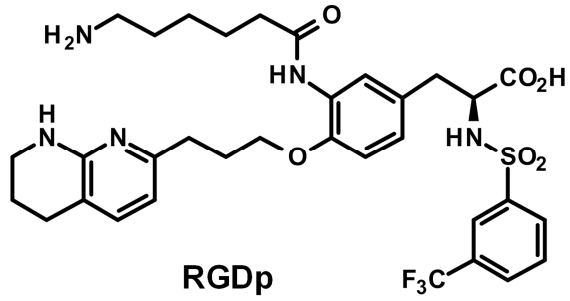

Figure 1: Structure of the RGD peptidomimetic based on a tyrosine scaffold

O-succinimidyl-4-(1-azi-2,2,2-trifluoroethyl)benzoate (NHS-TPD clip) was prepared as described in [21].

The siRNA duplex directed against green fluorescent protein (GFP) and a control (CTRL) siRNA duplex, as well as the Dicer substrate 25/27-mer siRNA targeting GFP (DsiRNA GFP) were supplied by Eurogentec (Seraing, Belgium). The siRNAs had the following sequences and modification patterns: GFP sense 5'-pACCCUGAAGUUCAUCUGCAcc-3', antisense 5'-pUGCAGAUGAACUUCAGGGUca-3', CTRL sense 5'- GAGCUCAUCGUUGCACUAUtt-3', antisense 5'-AUAGUGCAACGAUGAGCUCtt-3' , and DsiRNA GFP sense 5'-pACCCUGAAGUUCAUCUGCACCACcg-3' and antisense 5'-CGGUGGUGCAGAUGAACUUCAGGGUCA-3', where lower case letters represent deoxyribonucleotides, underlined capitals represent 2'-O-methylribonucleotides and p the phosphate residues [18].

SiRNA labelled with Alexa647 (λ_{exc} = 650 nm and λ_{em} = 668 nm) at the 3'end of the sense strand was purchased from Qiagen (Venlo, the Netherlands). DsiRNA GFP labelled with Alexa647 at the 5' end of the antisense strand was purchased from Eurogentec (Seraing, Belgium). INTERFERin® was purchased from Polyplus transfection (Illkirch, France). Unless otherwise stated, the solutions were prepared using RNAse-free water (Gibco, Invitrogen, Marelbeke, Belgium) and filtered through 0.22 µm filters

(VWR, Belgium). Throughout all experiments, RNase free materials and conditions were carefully applied.

II.2. SYNTHESIS AND CHARACTERIZATION OF PEG-RGD AND PEG-RGDP

PEG-RGD and PEG-RGDp were synthesized by the "clip photochemistry" methodology as described in [21] with slight modifications. Briefly, 500 mg of PEG was solubilized in 5 ml of dichloromethane with 16 mg of NHS-TPD clip in a 10 ml glass flask. After solvent evaporation the mixture was dried under vacuum and irradiated (3 x 8 W BLB lamps, 360 nm, placed at a distance of 4.5 cm) in a home-made rotating reactor under argon atmosphere for 60 min. The solid was solubilized in methanol (1 ml) and precipitated in 20 ml of diethylether at 4°C. After recovering of the solid and drying under vaccum, 435 mg of "NHS activated PEG" were obtained. Then 170 mg of this activated PEG were incubated in a solution of the desired compound (RGD or RGDp 10 mM) in 0.1 M phosphate buffer (PB):CH_3CN (1:1, v/v) at pH 8.0 and shaken for 48 h at 20°C. The solution was dialyzed for 100–130 h against water and then lyophilized. The solid obtained was solubilized in CH_2Cl_2, filtered on PTFE Acrodisc filters (0.2 mm) and the solvent was removed under vacuum. Then the solid was solubilized at room temperature in 0.1 ml of MeOH and precipitated in 3 ml of diisopropyl ether. The sample was then dried by azeotropic distillation of dry CH_3CN before being submitted to quantification by ^{19}F NMR.

Quantitative Fluorine NMR (^{19}F qNMR) was performed as described in [21] to quantify the amount of RGDp grafted on PEG. Briefly, aliquots of 20-30 mg of the sample were carefully weighted and solubilized in 0.6 ml of a 1 mM solution of trifluoroethanol in $CDCl_3$. Samples were submitted to a special quantification sequence programmed on a Brucker Avance II spectrometer at 282.09 MHz for fluor detection. Comparison of integrals of trifluoroethanol and of the CF_3 tag on the RGDp (see Fig. 1), gave an amount of 42 µmol of RGDp per gram of PEG, which corresponds to a functionalization of 21% of the PEG chains.

II.3. SYNTHESIS AND CHARACTERIZATION OF THE C_{PEG} CONJUGATES

The chitosan (Kitozyme, Herstal, Belgium) used for the synthesis of the C_{PEG} conjugates (*i.e.* C_{PEG}, $C_{PEG\ RGD}$ and $C_{PEG\ RGDp}$ copolymers) described in Table I had a molecular weight of 90 kDa, based on intrinsic viscosity measurements, and a deacetylation degree of 79.7%. The chitosan was grafted with 5 kDa PEG at a theoretical grafting of 20 mol%.

For the activation of the PEG chain-end, 1 g of PEG (0.2 mmol, M_n = 5,000 g/mol, Aldrich) was transferred into a clean and dried glass reactor. After three azeotropic distillations with anhydrous toluene (3 x 10 ml), PEG was dissolved into 10 ml of anhydrous toluene. 0.036 g *N,N'*-carbonyldiimidazole (CDI, 0.22 mmol, Aldrich) and 0.025 g dimetylaminopyridine (DMAP, 0.2 mmol, Aldrich) were transferred in the PEG solution and let react overnight at 25 °C. The carboylimidazole end-capped PEG was then purified by precipitation in cold diethylether and collected by centrifugation before being dried under vacuum. For the grafting of PEG onto chitosan, 0.230 g of chitosan (M_n = 90 KDa, DA = 20%, batch CSU09125) were dissolved into 20 ml of HAc/NaAc buffer (pH = 4.6). After the complete solubilization of chitosan, a fresh solution of carboylimidazole end-capped PEG in HAc/NaAc buffer (1 g of PEG in 10 ml of buffer) was prepared in a second glass tube. 0.009 g of DMAP was added to the PEG solution before to mix it with the chitosan solution. The solution was stirred at room temperature during 48 hours. The pH of the solution was increased to 10 by the addition of diluted NaOH (0.1M) in order to deprotonate the residual primary amino groups of the chitosan backbone. The C_{PEG} $C_{PEG\ RGD}$ and/or $C_{PEG\ RGDp}$ were finally purified by dialysis against MilliQ water (porosity = 8 KDa) during 2 days and were recovered by lyophilization.

Grafting rates of PEG on chitosan were determined by ^{1}H NMR. ^{1}H NMR spectra were recorded on a Bruker Avance 500 spectrometer operating at 500 MHz for ^{1}H. NMR samples were prepared by dissolving, under sonication, 10-15 mg of C_{PEG} in 1 ml of D_2O with 10 µl of DCl (20% in D_2O). The PEG grafting amounts were determined by comparison of integrals of chitosan and PEG protons as described in supporting information. It was found that 70 PEG 5k were grafted per chain of chitosan which correspond to the fonctionalization of 16% of the free deacetylated amines of chitosan.
The amount of RGDp on $C_{PEG\ RGDp}$ was determined by ^{19}F qNMR and found to be 29 µmol per gram of polymer, which corresponds to a 3 % molar ratio of the free deacetylated amines grafted with a PEG chain bearing a RGDp.

Table I: Characteristics of the copolymers

Polymer	PEG-ligand conjugate	Ligand/PEG chain (mol%)	PEG/Chitosan (mol%)[c]	Ligand/C_{PEG} (mol%)[d]
C_{PEG}	/	/	20%	/
$C_{PEG\ RGD\ 2\%}$	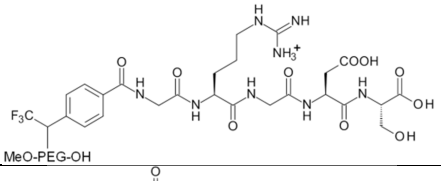	10% [a]	20%	2%
$C_{PEG\ RGDp\ 2\%}$	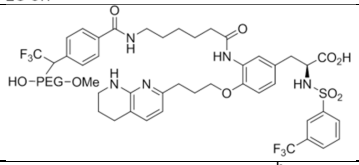	8% [b]	20%	1.6%
$C_{PEG\ RGDp\ 4\%}$		21% [b]	16%	3.4%

[a] estimated from ratios of reagents used, [b] calculated by ^{19}F qNMR, [c] molar ratio of the free deacetylated amines grafted with a PEG chain as estimated by ^{1}H NMR, [d] molar ratio of the free deacetylated amines grafted with a PEG chain bearing a ligand

II.4. FORMULATION OF SIRNA-LOADED NANOPARTICLES

The nanoparticles were prepared by using the ionic gelation method [22]. In brief, the negatively charged components, *i.e.* the DsiRNA or siRNA (50 µM), and TPP (1 mg/ml) were added to the positively charged components, *i.e.* C_{PEG}, $C_{PEG\ RGD}$ or $C_{PEG\ RGDp}$ (1 mg/ml in 0.2 M sodium acetate buffer, pH 5.7) or PEI (1 mg/ml in RNAse-free water, pH 7.4) and vortexed for 30 s. The mixtures were incubated for 1 h at room temperature. The type of formulation used was the C_{PEG} PEI a described in the *Chapter III*. The ratio between C_{PEG}, $C_{PEG\ RGD}$ or $C_{PEG\ RGDp}$ and PEI was 5/1 (w/w) for all formulations. The amount of siRNA or DsiRNA in the formulations was kept constant and was 11.35 µg/ml. The amount of TPP was optimized in order to obtain a monodisperse distribution of the nanoparticles. The copolymer/TPP ratio was between 2.7/1 and 3.3/1 (w/w).

The size and the zeta potential of the nanoparticles were determined using a Nanosizer NanoZS (Malvern Instruments, Malvern, UK) by photon correlation spectroscopy and electrophoretic mobility, respectively. All samples were measured in triplicate in RNAse-free water.

II.5. H1299 EGFP CELL CULTURE

The human non-small cell lung carcinoma cell line H1299 expressing the destabilized enhanced GFP (H1299 EGFP) was used for the *in vitro* tests as reported previously [23]. The H1299 EGFP cells were grown in RPMI 1640 medium (Gibco, Belgium) supplemented with 10% (v/v) fetal bovine serum (FBS, Gibco). The cells were grown in an atmosphere of 5% CO_2/95% O_2 at 37 °C changing the growth

medium three times a week and sub-cultured approximately 1:10 twice a week using trypsine (Gibco) for 5 min at 37 °C to detach the cells.

To detect the presence of $\alpha_v\beta_3$ integrins on H1299 EGFP cells, 10^6 cells were incubated with 10 µg of anti-$\alpha_v\beta_3$ antibody (mouse monoclonal BV3 against Integrin $\alpha_v\beta_3$, 0.1 mg/mL, GeneTex, Bio-Connect, Huissen, The Netherlands) or with 10 µg of isotype control FC antibody (APC Mouse IgG1, κ Isotype Ctrl (FC) Antibody, BioLegend, Imtec, Belgium) at 4 °C for 30 min. The cells were rinsed twice with phosphate-buffered saline (PBS) and incubated with 2 µg of a secondary antibody (Alexa647 goat–anti-mouse IgG1, 2 mg/mL, Molecular Probes, Belgium) at 4 °C for 30 min. As control, 10^6 cells were incubated with 2 µg of the secondary antibody. The measurements were done on a FACS Calibur cytometer (BD Biosciences, Belgium) in triplicate and the data were analyzed using the FlowJo software. A total number of 20,000 cells were analysed per sample.

II.6. EGFP SILENCING OF H1299 EGFP CELLS

The H1299 EGFP cells were seeded in 12-well plates at a density of 10^5 cells per well 24 h prior to the experiment. On the following day, the cells were transfected with the nanoparticles loaded with DsiRNA GFP, siRNA GFP or siRNA CTRL respectively in RPMI medium containing 10% FBS for 4 h. After 24 or 48 h, the cells were washed with PBS, trypsinized and resuspended in 300 µL PBS prior to the flow cytometric analysis. The percentage of gene silencing was calculated by using the FL-1 median (median of the GFP fluorescence histogram). The cells transfected with nanoparticles loaded with the siRNA CTRL were used as negative control. For each condition, three separate samples were analysed. A total number of 20,000 cells were analysed per sample.

II.7. RNA ISOLATION AND PURIFICATION

At 24 or 48 h post transfection, the cells were washed with PBS and trypsinized with TrypLE™ Express (Invitrogen, UK). Subsequently, the detached cells were pelleted by centrifugation for 10 min at 1,760 xg and washed twice with 1 ml PBS. Total RNA was isolated and purified using 800 µl of the RNAstat 60 reagent (AMS Biotechnology, UK). The RNA isolated was was precipitated overnight at 4°C from the water phase in one volume of isopropanol (Sigma) and collected by centrifugation for 20 min at 12,000 xg at 4°C. The concentration and the purity of the samples were verified by absorbance measurements using the Nanodrop 2000c Spectrophotometer (Thermo Scientific, USA). If the RNA quality was not acceptable ($A_{260}/A_{280} < 1.80$ and $A_{260}/A_{230} < 1.75$), the samples were diluted to a final volume of 200 µl and re-precipitated in 400 µl of ethanol and 60 µl of 3M sodium acetate (Sigma).

II.8. STEM-LOOP RT QPCR

The sequences of the stem-loop reverse transcription primers and of the PCR primers are described in [17]. Briefly, an purified RNA amount of 700 ng was reverse transcribed in a total reaction volume of 20 µl that also included 500 µM deoxynucleotide mix, 20 U Protector RNase Inhibitor, 10 U Transcriptor Reverse Transcriptase, 1x Transcriptor Reverse Transcriptase buffer, all from Roche, Basel, Switzerland. The RNA template was first denatured at 75 °C for 10 min immediately cooled on ice for 2 min. The reaction mix and the stem-loop primers (11 nM of each, final concentration) were then added during the cooling phase. The pulsed RT program consisted of 15 min at 14 °C, 10 min at 42 °C, followed by 25 cycles (15 s at 14 °C, 10 s at 42 °C and 15 s at 65 °C). Subsequently, the mixture was incubated for 5 min at 85 °C for transcriptase inactivation and cooled at 4 °C. The qPCR was performed with a LightCycler 480® (Roche) using the SYBR Green Master mix according to the manufacturer's instructions. An amount of 5 ng DNA was analyzed. The housekeeping gene snoRNA U109 (GenBank ID: AM055742.1) was used for normalization. The PCR program was 95 °C for 5 min, 37 cycles (95 °C for 15 s, 62 °C for 15 s, 72 °C for 1 s) followed by cooling at 4 °C. The PCR data analyses were performed essentially as described previously in [17].

II.9. UPTAKE OF THE SIRNA-LOADED NANOPARTICLES BY H1299 EGFP CELLS

The H1299 EGFP cells were seeded in 12-well plates (10^5 cells/well) containing a cover slip. After 24 h, the cells were incubated for 1 h with the nanoparticles loaded with Alexa647-labelled siRNA (at 100 nM), then fixed with fresh paraformaldehyde [2% (w/v) in PBS] and rinsed three times with PBS. In order to stain the nuclei, the cells were incubated with 4',6-diamidino-2-phenylindole DAPI (0.1 µg/ml) for 5 min and rinsed three times with PBS. The cells were incubated for 1h with AlexaFluor488-conjugated Concanavalin A (5 µg/ml in PBS, Molecular Probes) to stain the cell membranes. After washing, the cover slips were placed on a slide using the Vectashield® mounting medium. The slides were imaged using a structured illumination AxioImager microscope equipped by an Apotome module (Zeiss, Germany, magnification 40x).

Cellular uptake of nanoparticles was quantified by using flow cytometry. The H1299 EGFP cells were seeded in 12-well plates ($1.5x10^5$ cells/well) 24 h before the experiment, which was initiated by incubating the cells with nanoparticles for 1 h at a concentration of 100 nM Alexa 647-labelled siRNA in medium containing 10% FBS. Cells were rinsed 2 times with PBS, trypsinized (0.25% trypsin) and diluted with medium. After centrifugation (250 xg, 5 min, 4°C), the cell pellet was resuspended in 200 µl PBS. The measurements were performed by using a FACS Calibur flow cytometer (BD Biosciences, Belgium) and the data were analyzed using the FlowJo software (Tree Star Inc., USA). For each

condition, three separate samples were analysed. A total number of 20,000 cells were analyzed in each measurement.

II.10. EFFECT OF SIRNA-LOADED NANOPARTICLES ON CELL VIABILITY

The H1299 EGFP cells were seeded (8,000 cells/well) in 96-well plates. After 24 h, the cells were incubated for 4 h with the nanoparticles at siRNA concentrations ranging from 100 to 200 nM per well. The lactate deshydrogenase LDH Cytotoxicity Detection Kit (Roche, France) was used to measure the LDH release from the H1299 EGFP cells after 4 h of incubation with the nanoparticles. Cells incubated with Triton X-100 (1%, v/v) were used as a positive control, and untreated cells were used a negative control, respectively. The LDH activity was measured in the supernatant (diluted 1/5 in PBS after centrifugation for 5 min at 250 xg, Eppendorf Centrifuge 5804R) according to manufacturer's instructions. The absorbance was read at 492 nm using a microplate photometer (Multiskan Ex, Thermo Scientific, Belgium).

II.11. STATISTICS

The experiments were performed in triplicate, unless otherwise stated. Values are given as means ± standard deviations (SD). For the statistics and plotting, PRISM (GraphPad, La Jolla, CA, USA) was used. Statistically significant differences were assessed by an analysis of variance (ANOVA) at a 0.05 significance level and followed by the Tukey´s post test or by a 2-way analysis of variance followed by a Bonferoni's post test.

III. RESULTS

III.1. PREPARATION OF THE C_{PEG} CONJUGATES

In order to obtain C_{PEG} conjugated with PEG chains bearing RGD and RGDp we followed a modular approach, *i.e.* the PEG chains were coupled with the ligands prior to their grafting on the chitosan. We used the "clip photochemistry" methodology [21,24], to anchor the ligands randomly along the PEG chain. This technique allowed the use of a commercially available α-hydroxy-ω-methoxy-PEG (OH-PEG-OMe) of 5 kDa with an alcohol function that would be useful for the anchoring on the chitosan chain. Moreover, we were able to control the amount of ligand grafted simply by adjusting the initial quantity of the photo reactive NHS-TDP clip. Thus, we planned to prepare two batches of PEG with 10 and 20 %mol of ligand, respectively. After treatment, this amount was checked by fluorine quantitative NMR (^{19}F qNMR). As indicated in table I, the amounts calculated were closed to those expected (*i.e.* 8% instead of 10% and 21% instead of 20%). As the ligands were fixed along the polymer backbone, the chain end functions are still usable. Consequently, the alcohol function of the PEG-RGD(p) was derivatized into an imidazole carbonate by action carbonyldiimidazole (CDI), resulting in the formation of PEGs bearing on one end an activated carbonate, which is known to react very easily with amino groups. Approximately 20% of the free deacetylated amines of the chitosan were planned to be functionalized since this rate has shown to be a good balance between the solubility at neutral pH and the conservation of the complexation ability of chitosan *(see Chapter III)*. Four batches of chitosan-PEG were prepared: chitosan grafted with native PEG (C_{PEG}), chitosan grafted with a PEG conjugated with RGD at 10%mol ($C_{PEG\ RGD\ 2\%}$), chitosan grafted with a PEG conjugated with RGDp at 10%mol ($C_{PEG\ RGDp\ 2\%}$) and finally, chitosan grafted with a PEG conjugated with RGDp at 20%mol ($C_{PEG\ RGD\ 4\%}$). The CDI activated PEGs were simply reacted with chitosan in acetate buffer and, after treatments and washings, the PEG grafting rates were determined by ^{1}H NMR (see calculation in supporting information). We found values closed to thoses expected (Table I) and, as shown in Fig. 2, all the protons of PEG and chitosan were clearly seen with exception of the anomeric proton a, which is overlapped by water. The final amounts of ligands indicated in Table I were obtained by the combination of the grafting rates obtained on PEG and C_{PEG} (*i.e.* for $C_{PEG\ RGD\ 4\%}$ we calculated an amount of 3.4% which corresponds to a PEG conjugated with RGDp at 20%mol grafted at 16% molar ratio on chitosan). The RGDp amounts were checked by ^{19}F qNMR and were found to be the awaited values (*i.e.* a 3.0%mol amount of RGDp was calculated by ^{19}F qNMR for $C_{PEG\ RGD\ 4\%}$, see experimental section).

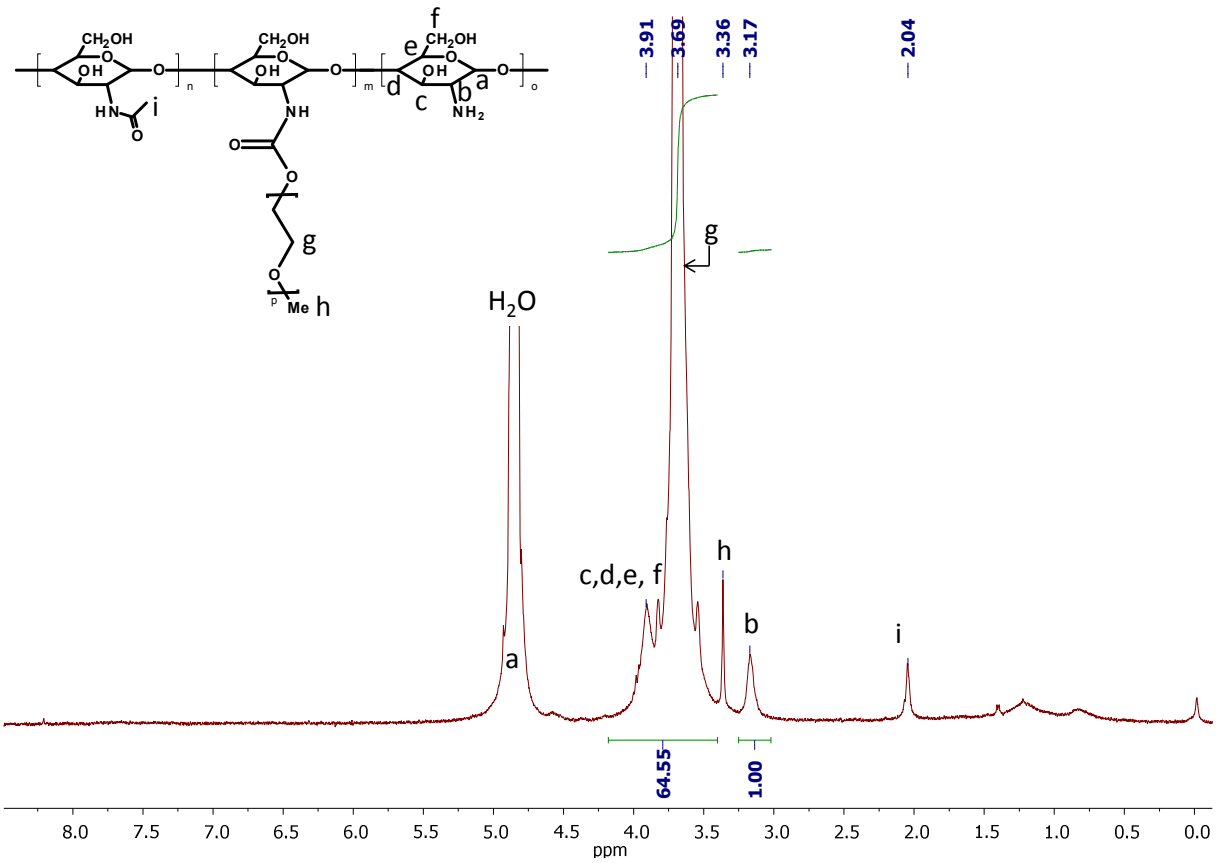

Figure 2: ^{1}H NMR spectrum of $C_{PEG\ RGDp\ 4\%}$ in D_2O/DCl

III.2. PHYSICOCHEMICAL CHARACTERISTICS OF THE NANOPARTICLES

The physicochemical characteristics of the nanoparticles are summarized in Table II. The particles had a mean diameter between 165 and 207 nm, regardless of their composition. The polydispersity index (PDI) was below 0.20, suggesting that the nanoparticle populations were monodisperse. Finally, all types of nanoparticles presented a positive zeta potential comprised between 5.6 and 11.0 mV (data not shown). There were no statistically significant differences between mean size and PDI of the different nanoparticle formulations.

The NP were loaded either with siRNA or the Dicer substrated siRNA (DsiRNA). The siRNA and DsiRNA differ by their number of nucleotides (21 and 25-27 per strand, respectively). In this project, this difference in length did not influence the physicochemical characteristics of the resulting nanoparticles (Table II). However there was a slight increase in the size when the siRNA was encapsulated as compared to the DsiRNA, but this difference was not statistically significant. In addition, the presence of the ligand and the ligand grafting ratio did not significantly influence the particle characteristics either.

Table II: Characteristics of the nanoparticles. Values represent mean ± SD (n =3-6)

Type of siRNA	Formulation	Copolymer	Size (nm)	PDI
DsiRNA	Non targeted nanoparticles NP	C_{PEG}	164 ± 15	0.10 ± 0.03
	RGDp NP 2%	$C_{PEG\ RGDp\ 2\%}$	166 ± 16	0.12 ± 0.04
	RGD NP 2%	$C_{PEG\ RGD\ 2\%}$	177 ± 30	0.15 ± 0.02
siRNA	NP	C_{PEG}	207 ± 36	0.11 ± 0,06
	RGDp NP 2%	$C_{PEG\ RGDp\ 2\%}$	191 ± 32	0.10 ± 0,04
	RGDp NP 4%	$C_{PEG\ RGDp\ 4\%}$	211 ± 18	0.16 ± 0,02

III.3. TARGETING NANOPARTICLES TO THE A_VB_3 INTEGRINS ENHANCES THEIR TRANSFECTION EFFICIENCY ON H1299 EGFP CELLS WITHOUT CAUSING TOXICITY

First, non-targeted nanoparticles, RGDp-grafted nanoparticles (RGDp NP 2%) and the RGD-grafted nanoparticles (RGD NP 2%) and loaded with DsiRNA were compared in terms of their ability to silence EGFP protein expression after 48 h of transfection of H1299 EGFP cells (Fig 3A). At low DsiRNA concentrations, ranging from 12.5 to 50 nM, no statistically significant differences were observed between the different types of nanoparticles. However, at an DsiRNA concentration of 100 nM and above, the percentage of gene silencing increased dramatically after transfection with the targeted nanoparticles, as compared to the non-targeted nanoparticles: as much as approximately 90% EGFP inhibition was achieved at 150 nM with both the RGDp NP 2% and the RGD NP 2%. On the other hand, increasing the initial DsiRNA concentration did not enhance the gene silencing efficiency of the non-targeted nanoparticles, irrespectively of the concentration used. Similar results were obtained 24 h after transfection (data not shown). The same experiments were performed with the nanoparticles loaded with siRNA, and similar tendencies were observed (Fig. 3B).

Subsequently, the effect of ligand density on the EGFP silencing was investigated (Fig. 3B): the RGDp nanoparticles with a ligand grafting density of 4 mol% were compared to similar formulations having a 2 mol% ligand grafting density. At 50 nM, 76 % EGFP silencing was obtained with the RGDp NP 4%. In comparison, only 35% knockdown was achieved with the nanoparticles, which had a grafting density of 2%. At higher DsiRNA concentrations (100 to 200 nM), no difference was noticed.

The gene silencing efficiencies of the Dicer substrate i.e. the DsiRNA and the corresponding Dicer product *i.e.* siRNA were compared by using RGDp NP: at a concentration of 100 nM, the EGFP silencing was slightly higher by using the DsiRNA compared to the siRNA ($p < 0.05$) but no statistically significant difference between the potency of the two types of nucleic acids was observed at 150 nM.

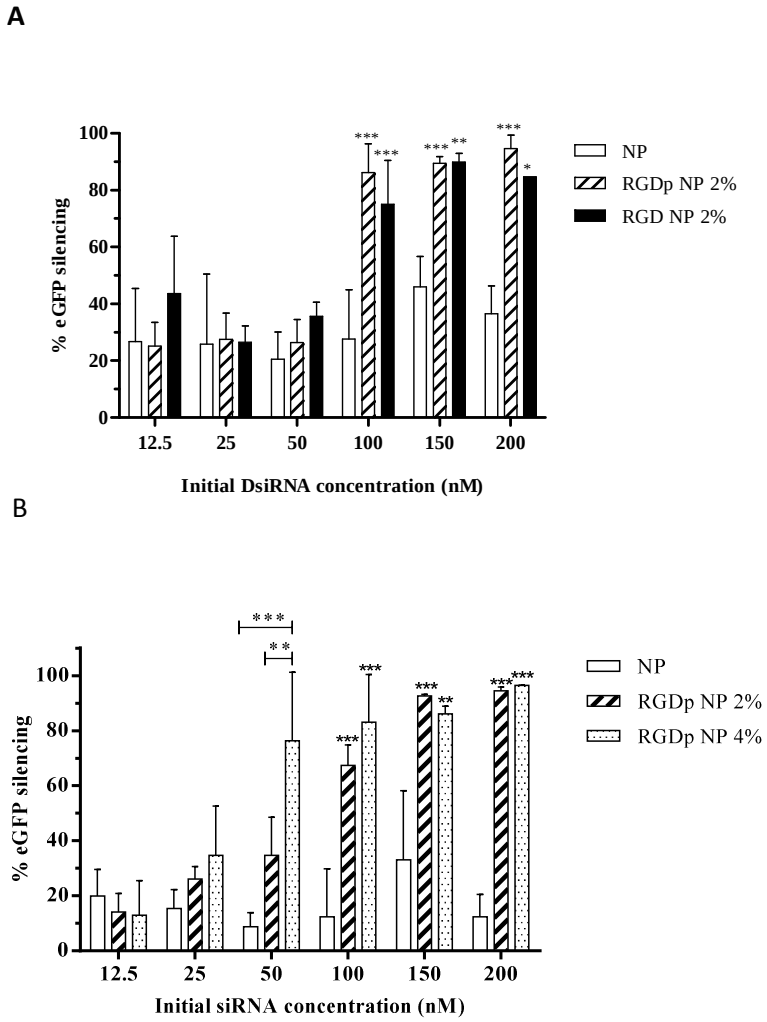

Figure 3: Percentage of EGFP silencing in H1299 EGFP cells 48 h after transfection with (A) NP, RGD NP 2% and RGDp NP 2% loaded with DsiRNA and (B) NP or RGDp NP presenting different ligand grafting densities (2% and 4%) loaded with siRNA. Data represent mean values ± SD (n=3). Results significantly different from NP are indicated: * $p < 0.5$, ** $p < 0.01$, *** $p < 0.001$.

Finally, the cytotoxicity of the nanoparticles was evaluated using the LDH assay (Fig. 4). No significant difference was observed between the values of cell death obtained for the nanoparticles at the three dose levels tested. This suggests that the nanoparticles are well tolerated by the cells, irrespectively of the surface grafting, and that reduction in EGFP expression observed above is in fact a result of

gene silencing and not a consequence of cell death. However, at 200 nM, we noticed a small but not statistically significant increase in the percentage of cell mortality, which might suggest a slight toxicity at such high siRNA concentrations. Similar results were obtained for nanoparticles loaded with DsiRNA using propidium iodide staining (data not shown).

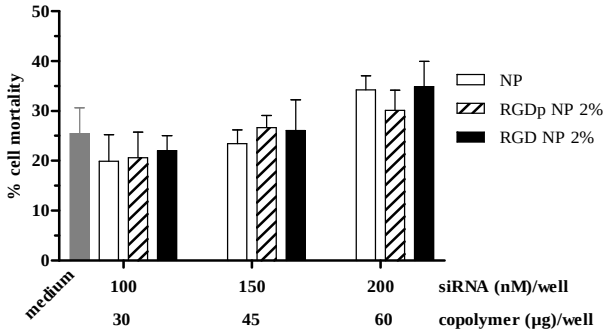

Figure 4: Percentage of cell mortality after 4 h transfection with the three different types of nanoparticles loaded with siRNA using the LDH release assay (N=3, n=8). Results denote mean values ± SD (n=3). Results were compared to cells exposed to the medium.

III.4. EVALUATION OF THE EFFECT OF A_VB_3 TARGETING ON INTRACELLULAR DSIRNA DELIVERY BY USING RT-QPCR

The amount of DsiRNA delivered intracellularly after transfection with the nanoparticles and maintained as full-length active sequence was quantified by using the RT-qPCR method recently described by Colombo *et al* [17]. Therefore, it was possible to compare the carrier-mediated DsiRNA delivery processes. Moreover, given that the stem-loop RT-qPCR method quantified the full-length active sequence of DsiRNA, *i.e.* the biologically active molecules, it was possible to correlate the quantitative results to the EGFP expression, in order to clarify the relationship between the intracellular DsiRNA dose and the effect on gene silencing.

By using a calibration curve, absolute quantitative RT-PCR was performed and the copy numbers of DsiRNA molecules per cell were estimated (Fig. 5A). With the relative quantification approach, the amount of DsiRNA is normalized using a housekeeping gene (snoRNA U109), and the results are thus expressed in arbitrary units. Similar trends in the results were obtained by using both quantification methods, which demonstrated their robustness. At low concentrations (from 12.5 to 50 nM of DsiRNA), the intracellular amount of DsiRNA was similar for all formulations, regardless of the type of surface modification ($p > 0.05$). However, at a concentration of 100 nM and above, the targeted nanoparticles were able to deliver a significantly higher amount of DsiRNA to the cells than the non-targeted nanoparticles ($p < 0.001$). The relative quantities delivered by RGDp NP 2% and RGD NP 2%

were respectively 1.4 and 2 higher, respectively, than the ones delivered by the non-targeted nanoparticles (Fig. 5B), which is in accordance with the 2-fold increase in the copies/cell (Fig. 5A). A number of approximately 2.7×10^5 DsiRNA copies/cell resulted in approximately 85% EGFP silencing for the targeted nanoparticles.

A

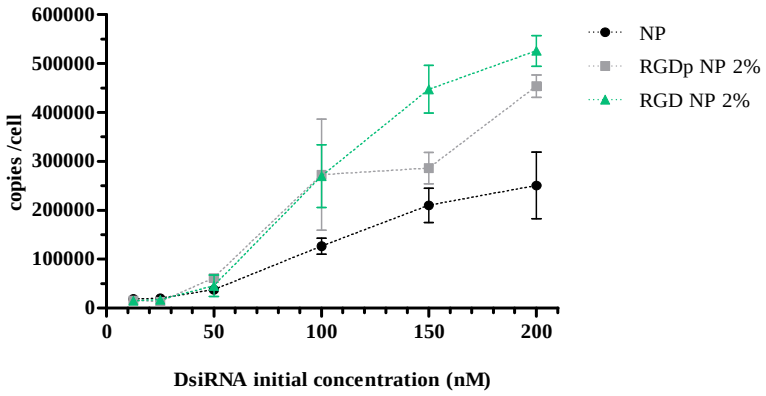

B

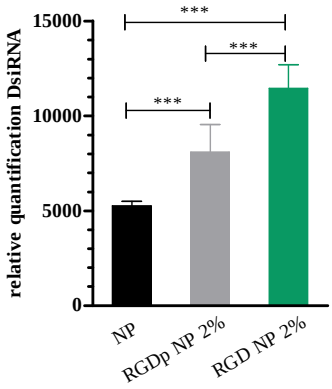

Figure 5: (A) Absolute quantification of intracellular DsiRNA 24 h after transfection with NP, RGDp NP 2% and RGD NP 2%. (B) Relative quantification of DsiRNA 24 h after transfection with NP, RGDp NP 2% or RGD NP 2% at 150 nM DsiRNA. Results denote mean values ± SD (n=3). Results significantly different are indicated: *** $p < 0.001$.

Figures 6A-E depict the correlation between the EGFP expression and the siRNA quantification at 24 h (Fig. 6A and C) and 48 h (Fig. 6B, D, E) post transfection. Similar profiles were observed for both types of targeted nanoparticles: the EGFP expression was reduced when the amount of DsiRNA in the cells was increased. For the non-targeted nanoparticles, little EGFP silencing was observed, despite relatively high levels of DsiRNA in the cells (Fig. 6A and B). Indeed, the number of DsiRNA copies/cell delivered by using the non-targeted nanoparticles at an initial concentration of 150 and 200 nM was in the same range (approximately 2.5×10^5) than what was estimated for the targeted nanoparticles to mediate EGFP silencing (Fig. 5A).

A

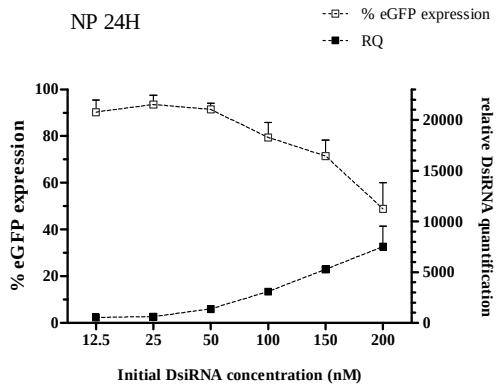

B

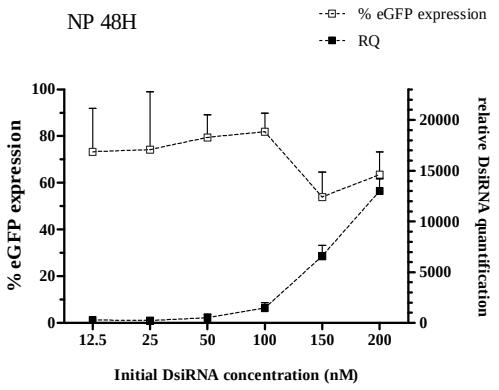

C

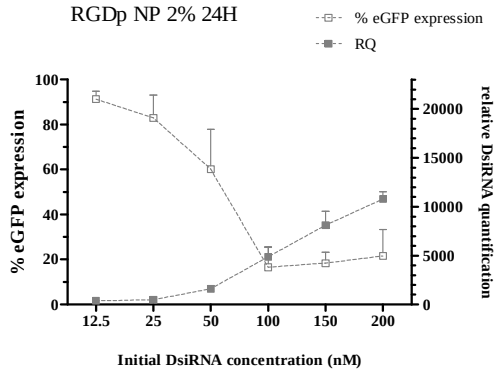

D

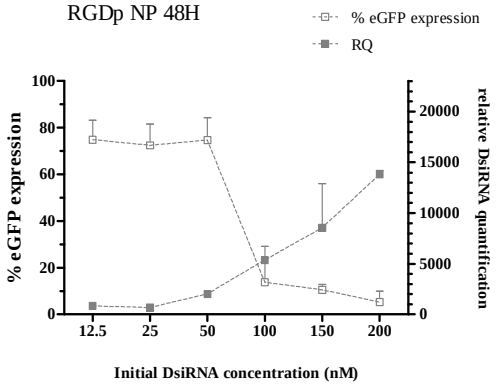

E

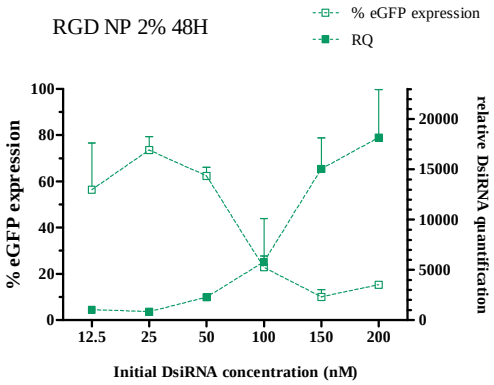

Figure 6: Correlation between the EGFP expression 24 h and 48h after transfection of H1299 EGFP cells with NP, RGD NP 2% and RGDp NP 2%. Results denote mean values ± SD (n=3).

III.5. THE RGD AND RGDP LIGANDS TRIGGER ENHANCED NANOPARTICLE ENDOCYTOSIS

To investigate the uptake mechanism of the nanoparticles further, microscopy experiments and flow cytometric analysis were carried out at different time points using H1299 EGFP cells, which expressed the $\alpha_v\beta_3$ integrins as demonstrated by Fig. 7.

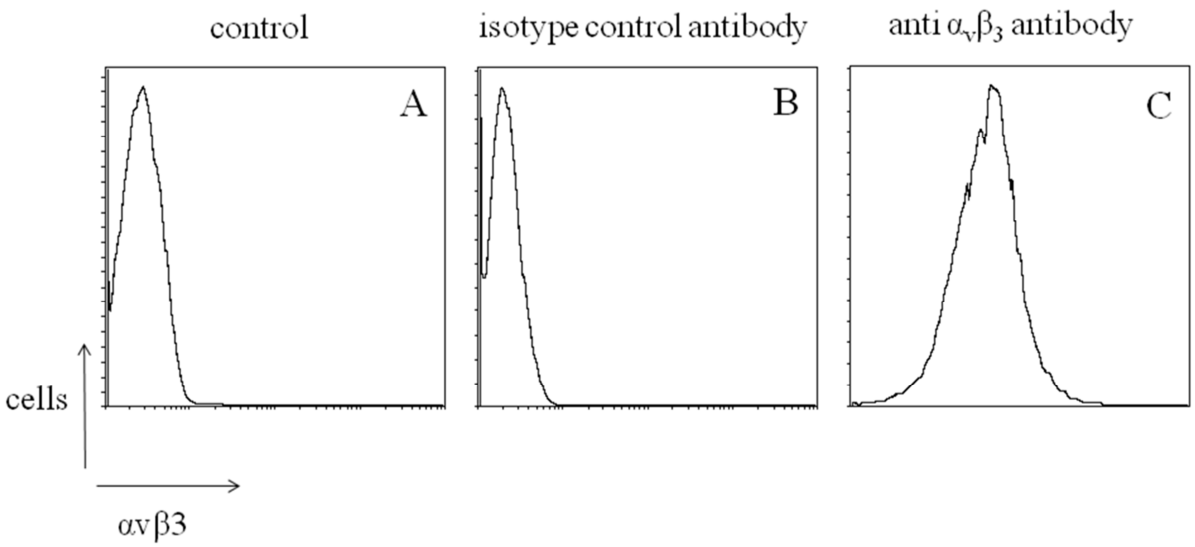

Figure 7: Detection of $\alpha_v\beta_3$ integrins on H1299 EGFP cells using an Alexa 647 secondary antibody. Fluorescence histograms of flow cytometric analyses (A): control, (B): incubation with isotype control FC antibody (C): incubation with anti-$\alpha_v\beta_3$ antibody.

The cells were visualized after 1 and 2 h incubation with the nanoparticles at 100 nM siRNA. After 1 h incubation, a very low uptake was observed for the non-targeted nanoparticles (Fig. 8A and E) while siRNA contained in the targeted RGDp NP was readily detectable in the cells (Fig. 8B and E). After 2 h incubation, larger numbers of fluorescent dots were observed in the cells for both types of formulation (Fig. 8C and D).

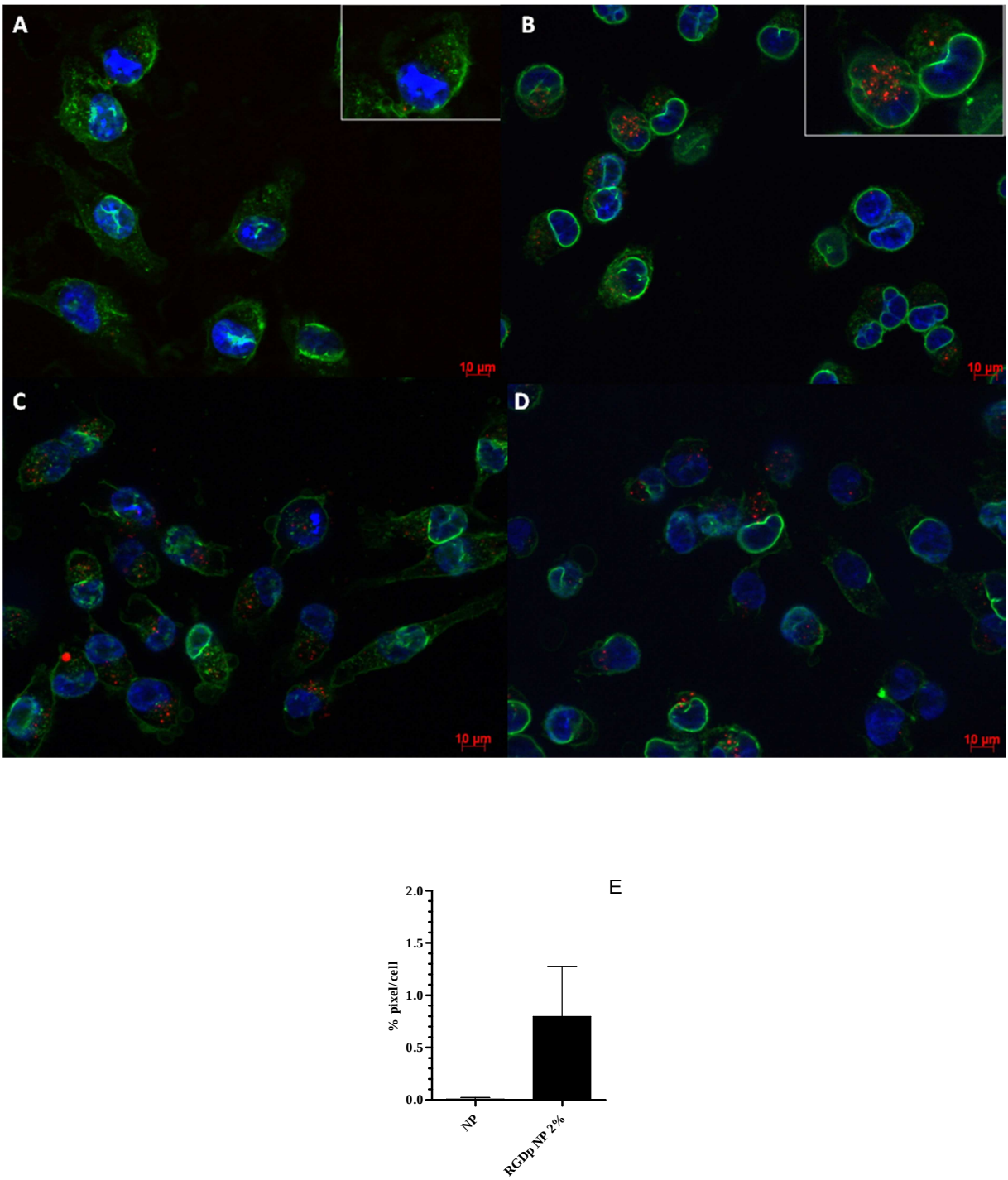

Figure 8: H1299 EGFP cells (blue: nuclei, green: membrane) transfected with nanoparticles loaded with 100 nM Alexa647-siRNA (red). A: 1 h incubation with NP, B: 1 h incubation with RGDp NP 2%, C: 2 h incubation with NP and D: 2 h incubation with RGDp NP 2%. E: red pixel quantification after 1 h of incubation.

The uptake process was then evaluated more quantitatively using flow cytometry. After 1 h of incubation of the cells with the RGDp NP and RGD NP, the fluorescence peaks presented a shoulder, corresponding to a fraction of cells, which internalized a higher amount of siRNA (Fig. 9, upper panel). This was not observed for the non-targeted nanoparticles, suggesting a slower uptake of these nanoparticles. After 4 h of incubation, the fluorescence peaks shifted to the right (Fig. 9, lower panel), indicating similar internalization of the siRNA for all the formulations.

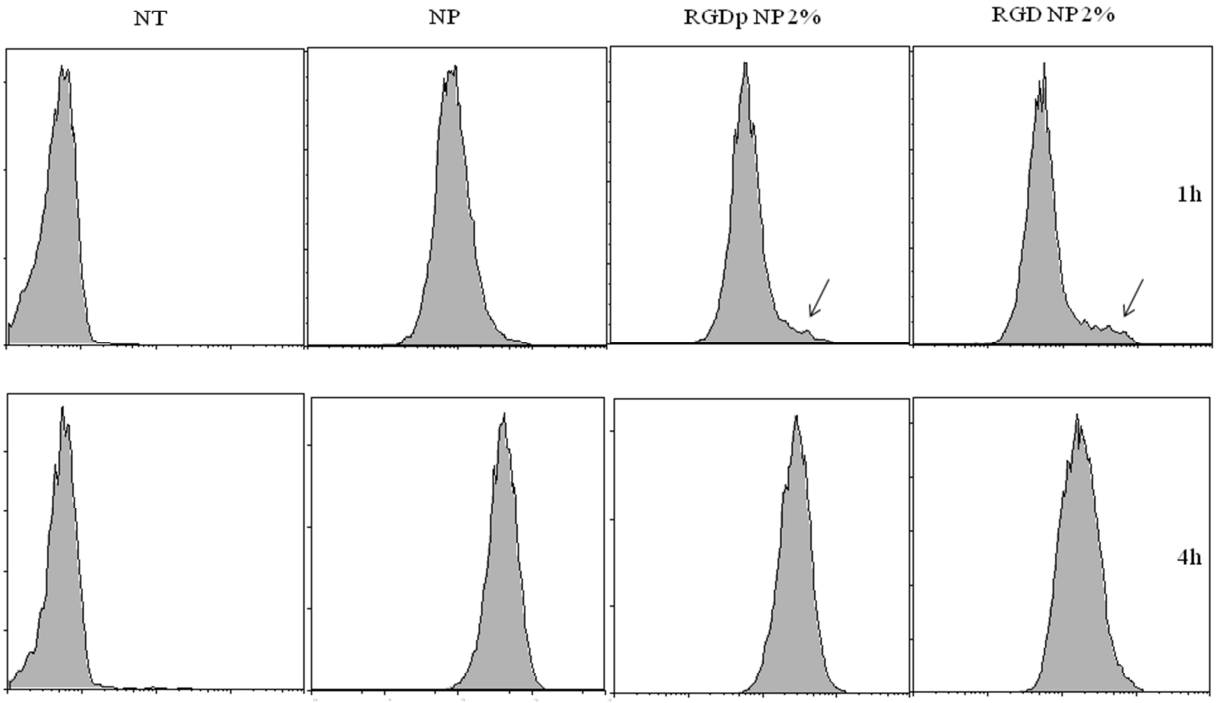

Figure 9: Fluorescence histograms in the FL4 channel of flow cytometric analysis after 1 and 4 h incubation of H1299 EGFP cells with NP, RGDp NP 2% and RGD NP 2% loaded with Alexa647-siRNA at a concentration of 100 nM.

To evaluate further the specificity of the uptake, the nanoparticle uptake was compared between H1299 EGFP cells, which are $\alpha_v\beta_3$ positive, and HeLa cells, which are $\alpha_v\beta_3$ negative (results not shown). The cellular internalization of the targeted nanoparticles was increased in the $\alpha_v\beta_3^+$ H1299 EGFP cells, as compared to $\alpha_v\beta_3^-$ HeLa cells (Fig. 10). For the non-targeted nanoparticles, similar uptake was observed in both cell lines. This suggests that the presence of RGD and RGDp on the nanoparticles surface increased the nanoparticle uptake *via* the $\alpha_v\beta_3$ integrin receptors. Moreover,

both non-specific endocytosis and $\alpha_v\beta_3$ -mediated endocytosis may be implicated in the cellular internalization of the targeted nanoparticles.

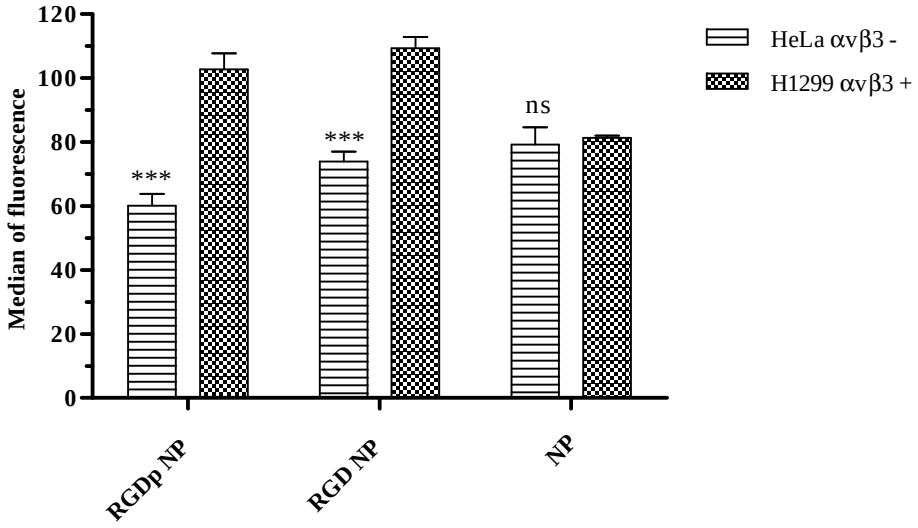

Figure 10: Uptake of NP, RGDp NP (1 h at 100 nM Alexa647-siRNA) in H1299 EGFP ($\alpha_v\beta_3$ $^+$) and HeLa ($\alpha_v\beta_3$ $^-$) cells. Results denote mean values ± SD (n=3). Results of H1299 EGFP cell uptake significantly different from the results of HeLa cell uptake are indicated: *** $p < 0.001$.

IV.DISCUSSION

Despite the fact the formulation and optimization of siRNA delivery systems have been described, little is generally known about the mechanisms of intracellular siRNA delivery using nanocarriers. Although analytical techniques such as stem-loop RT-qPCR, have been described for the quantification of small RNAs, these techniques have mainly been employed to quantify endogenous microRNA [25]. Only few studies have reported the use of RT-qPCR for the quantification of exogenous siRNA after delivery by using nanocarriers and to date, the only vehicles tested have been commercial transfection reagents and lipid nanoparticles [16,25-27]. Here, we report for the first time the use of stem-loop RT-qPCR to quantify the amount of siRNA delivered by using $\alpha_v\beta_3$-targeted chitosan-based nanoparticles. Moreover, the effect of active targeting of the nanoparticles to $\alpha_v\beta_3$ integrin via surface grafting of the RGD and RGDp was compared to non-targeted nanoparticles. The stem-loop RT-qPCR method has been designed and optimized for the quantification of a DsiRNA silencing EGFP, thereby rendering possible a direct correlation between the amount of active DsiRNA molecules delivered intracellularly and the gene silencing efficiency, as measured by using flow cytometry [17].

Interestingly, the selectivity of the $\alpha_v\beta_3$ targeting appeared to be dependent on the initial applied dose of nanoparticles (Fig. 5A). At low DsiRNA concentrations (between 12.5 and 50 nM), the rather low amount of DsiRNA delivered by using the $\alpha_v\beta_3$-targeted nanoparticles was similar to what was delivered by using non-targeted nanoparticles. At 100 nM and above, the amount of intracellular DsiRNA delivered by using $\alpha_v\beta_3$-targeted nanoparticles increased dramatically. The absolute quantity delivered at an initial applied concentration of 100 nM, was 5.9-fold and 4.4-fold increased for RGD NP and RGDp NP respectively, as compared to the quantity at 50 nM (Fig. 5A). Moreover, RGD NP delivered a significantly higher quantity than RGDp at the applied doses of 150 and 200 nM. For the non-targeted nanoparticles, the level of intracellular DsiRNA increased as well, but to a lower extent. The higher amount of DsiRNA delivered by the targeted nanoparticles can be explained by the very quick recycling within minutes of the integrins to the cell surface which provides the cells with a high endocytic capacity upon integrin receptor targeting [28]. In comparison, the non-specific uptake seemed to be less efficient, probably because of the saturation of non-specific binding sites.

The values obtained by relative quantification using RT-qPCR were correlated to the EGFP silencing at 24 h and 48 h, and similar profiles were overall observed at these two time points. At low concentrations, poor EGFP silencing (< 40%) was generally observed for the H1299 EGFP cells, regardless of the type of nanoparticles. These results are in accordance with the low values of relative quantification obtained by RT-qPCR. At 100 nM and above, the EGFP inhibition increased

dramatically after transfection with the $\alpha_v\beta_3$-targeted nanoparticles, reaching up to 90% gene silencing. This increased EGFP silencing efficiency is in agreement with the enhancement of the number of active DsiRNA molecules in the cells. Although RGD NP delivered a significantly higher amount than RGDp NP ($p < 0.001$), they did not mediate improved EGFP silencing, probably due to the saturation of the RISC machinery.

On the other hand, the EGFP inhibition mediated by the non-targeted nanoparticles remained low, irrespectively of the applied initial dose. Yet, according to the RT-qPCR results, the amount of DsiRNA delivered by using the non-targeted NP at 150 or 200 nM should be sufficient to induce EGFP silencing (Fig. 5A and Fig. 6A-B). Indeed, $2.5x10^5$ copies were delivered per cell, and this amount mediated 80% EGFP silencing in the case of the $\alpha_v\beta_3$-targeted NP. Given that the quantification values correspond to the total amount of full-length antisense strand DsiRNA present intracellularly *i.e.* in the endocytic vesicles and in the cytoplasm, it is likely that the non-targeted nanoparticles are taken up by the cells, but do not escape from the endosomes and/or release their DsiRNA cargo in the cytoplasm.

To further investigate the uptake mechanism (integrin-mediated or non-specific endocytosis), we performed microscopy and flow cytometry analysis. The cells were visualized after 1 h and 2 h of incubation with the non-targeted and RGDp NP containing fluorescently-labelled siRNA at a concentration of 100 nM. Contrary to the RGDp NP, which could readily be detected in the cells after 1 h of incubation, the non-targeted nanoparticles were visible in the cells only after 2 h, suggesting a delayed uptake in comparison to the $\alpha_v\beta_3$-targeted nanoparticles (Fig. 8). The flow cytometry experiments confirmed the slower uptake kinetics of the non-targeted nanoparticles in the H1299 EGFP cells. The peak shoulder observed after 1 h on the fluorescence histograms of RGD NP and RGDp NP which was absent for the non-targeted NP confirmed the delayed uptake observed by using microscopy. These findings are in line with previous reports, stating that the internalization rate of RGD-grafted micelles was higher than the rate for the non-targeted micelles [29]. This was also described for RGD-grafted nanoemulsions [30].

It appeared that the local ligand concentration should be sufficiently high to activate integrin-mediated endocytosis (Fig. 5A). Below a minimum threshold concentration of targeting ligand, non-specific interactions between the $\alpha_v\beta_3$-targeted NP and the cells occurred, resulting in non-specific endocytosis. Mickler *et al* demonstrated that the local RGD concentration had an influence on the internalization of RGD-grafted micelles [29]. However, this was solely observed when the targeted micelles were grafted with an incomplete PEG shielding as opposed to micelles with complete shielding. Indeed, the authors explained that the insufficient PEG shielding induced non-specific

interactions of the nanoparticles with the cell membranes, hindering the binding of the RGD peptide to integrins at low doses. These findings are in accordance with our results, as the PEG shielding of our nanoparticles is not complete, as shown by the positive zeta potential. The hypothesis of the requirement of a minimal ligand concentration to trigger integrin-mediated endocytosis was confirmed by the EGFP silencing results obtained with RGDp NP grafted with 4 mol% (Fig. 3B). At 50 nM, these nanoparticles mediated a 2-fold higher EGFP inhibition than the same formulation containing 2 mol% RGDp. At 100 nM however, this difference was no longer observed.

The specific internalization pathway used to engulf the delivery system has been shown to strongly influence the final efficiency of the delivery systems [31]. It was observed that chitosan-alginate DNA complexes taken up via the caveloae pathway remained entrapped in the caveosomes, whereas complexes taken up via the clathrin-mediated pathway in another cell line, mediated endosomal escape eventually resulting in high transfection efficiency. However, this cannot explain the discrepancy observed in our study between the non-targeted and the $\alpha_v\beta_3$ targeted nanoparticles. Indeed, $\alpha_v\beta_3$ integrin-mediated endocytosis has been described to be mainly clathrin-dependent and this was indeed verified for the three types of nanoparticles investigated in the current study (data not shown). For clathrin-mediated uptake, there are some indications in the literature towards the existence of two distinct populations of early endosomes, depending on the nature and destiny of their cargos [32]. Cargos destined for the degradation pathway are predominantly transported in highly mobile endosomes, which mature rapidly into late endosomes. On the other hand, cargos destined for recycling such as the recycling ligand transferrin have been shown to be sorted in both types of endosome populations, the second population being largely static and maturing more slowly. Given that the static endosomes are more important than the rapidly maturing endosomes, the transferrin ligand was found in the second population in a larger extent [30]. If we hypothesized that this model is applicable to $\alpha_v\beta_3$ integrins, a part of the targeted nanoparticles might thus be hypothesized to be taken up in the static endosomes and manage to escape the endosomes, while the non-targeted nanoparticles might be predominantly addressed in the rapidly-maturing endosomes ending up into late endosomes, thereby being degraded. Moreover, it was suggested that the presence of ligand affected the intracellular processing as RGD possess membrane destabilizing properties that can help the endosomal escape of the delivery system [33,34].

From the results obtained by RT-qPCR, it was possible to understand the lack of gene silencing of the non-targeted nanoparticles on the H1299 EGFP cells. Moreover, our results suggested that the concentration of nucleic acid is not the only parameter to optimize in order to obtain efficient gene silencing. A minimal local concentration of ligand and thus polymer is requested in order to achieve integrin-mediated uptake and efficient gene silencing on H1299 EGFP cells. A more widespread use

of such quantification method will certainly help the understanding of the small RNA delivery dynamic depending on the specific delivery carriers and the cell line.

We are currently examining the delivery potential of the $\alpha_v\beta_3$-targeted nanoparticles *in vivo*.

V. CONCLUSION

The novel stem loop RT-qPCR technique allowed for the quantification and comparison of the amount of the full-length DsiRNA antisense strand delivered into the cells by $\alpha_v\beta_3$-targeted chitosan-based nanoparticles (RGD NP and RGDp NP) and non-targeted nanoparticles. Our results demonstrate that the internalization behaviour of the $\alpha_v\beta_3$-targeted nanoparticles was dependent on the initial doses applied, suggesting that a minimum ligand concentration is required to induce $\alpha_v\beta_3$ integrin-mediated uptake. When this minimum concentration was reached, the $\alpha_v\beta_3$-targeted nanoparticles were internalized rapidly, in a higher amount than non-targeted nanoparticles and silenced EGFP expression up to 90% in H1299 EGFP cells without clear signs of toxicity. On the other hand, the non-targeted NP showed relatively low gene silencing efficiency, despite relatively high intracellular DsiRNA levels, hinting that these nanoparticles might end up in late endosomes or lysosomes without releasing their cargo to the cell cytoplasm. Thus, the silencing efficiency of the chitosan-based nanoparticles is strongly dependent on the uptake and the intracellular trafficking in H1299 EGFP cells. This study thus provides useful information about the siRNA delivery mechanisms of non-targeted and $\alpha_v\beta_3$-targeted chitosan-based nanoparticles. A better understanding of these mechanisms is mandatory for the future design of efficient siRNA delivery systems.

Acknowledgements

The authors gratefully acknowledge the Walloon Region (BioWin project), Wallonie Bruxelles International, the FNRS (mobility grant) for the financial support. Gaëlle Vandermeulen is a postdoctoral researcher of the Fonds de la Recherche Scientifique-FNRS. We are grateful to the Danish Agency for Science, Technology and Innovation, the Drug Research Academy (University of Copenhagen) and the Carlsberg Foundation for financial support for the Zetasizer Nano ZS, the Nanodrop 2000C spectrophotometer and the LightCycler® 480 system, respectively.

VI.REFERENCES

[1] F. Petrocca and J. Lieberman, Promise and challenge of RNA interference-based therapy for cancer, J. Clin. Oncol., 29 (2011) 747-754.

[2] H. Katas and H. O. Alpar, Development and characterisation of chitosan nanoparticles for siRNA delivery, J. Control Release, 115 (2006) 216-225.

[3] S. Mao, W. Sun, and T. Kissel, Chitosan-based formulations for delivery of DNA and siRNA, Adv. Drug Deliv. Rev., 62 (2010) 12-27.

[4] P. Baldrick, The safety of chitosan as a pharmaceutical excipient, Regul. Toxicol. Pharmacol., 56 (2010) 290-299.

[5] T. Kean and M. Thanou, Biodegradation, biodistribution and toxicity of chitosan, Adv. Drug Deliv. Rev, 62 (2010) 3-11.

[6] R. Riva, H. Ragelle, A. des Rieux, N. Duhem, C. Jérome, and V. +. Preat, Chitosan and Chitosan Derivatives in Drug Delivery and Tissue Engineering, in: R. Jayakumar, M. Prabaharan, and R. A. A. Muzzarelli (Eds.), Chitosan for Biomaterials II*,* Springer Berlin Heidelberg, 2011, pp. 19-44.

[7] T. H. Kim, S. I. Kim, T. Akaike, and C. S. Cho, Synergistic effect of poly(ethylenimine) on the transfection efficiency of galactosylated chitosan/DNA complexes, J. Control Release, 105 (2005) 354-366.

[8] W. F. Lai and M. C. Lin, Nucleic acid delivery with chitosan and its derivatives, J. Control Release, 134 (2009) 158-168.

[9] H. Ragelle, G. Vandermeulen, and V. Preat, Chitosan-based siRNA delivery systems, J Control Release, submitted (2013).

[10] H. Ragelle, R. Riva, G. Vandermeulen, B. Naeye, V. Pourcelle, C. S. Le Duff, C. D'haese, B. Nysten, K. Braeckmans, S. De Smedt, C. Jérôme, and V. Préat, Chitosan nanoparticles for siRNA delivery: optimizing formulation to increase stability and efficiency, to be submitted, (2013).

[11] G. C. Tucker, Integrins: molecular targets in cancer therapy, Curr. Oncol. Rep., 8 (2006) 96-103.

[12] F. Danhier, B. Vroman, N. Lecouturier, N. Crokart, V. Pourcelle, H. Freichels, C. Jerome, J. Marchand-Brynaert, O. Feron, and V. Preat, Targeting of tumor endothelium by RGD-grafted PLGA-nanoparticles loaded with paclitaxel, J Control Release, 140 (2009) 166-173.

[13] H. D. Han, L. S. Mangala, J. W. Lee, M. M. Shahzad, H. S. Kim, D. Shen, E. J. Nam, E. M. Mora, R. L. Stone, C. Lu, S. J. Lee, J. W. Roh, A. M. Nick, G. Lopez-Berestein, and A. K. Sood, Targeted gene silencing using RGD-labeled chitosan nanoparticles, Clin. Cancer Res., 16 (2010) 3910-3922.

[14] F. Danhier, B. A. Le, and V. Preat, RGD-based strategies to target alpha(v) beta(3) integrin in cancer therapy and diagnosis, Mol. Pharm., 9 (2012) 2961-2973.

[15] C. Chen, R. Tan, L. Wong, R. Fekete, and J. Halsey, Quantitation of microRNAs by real-time RT-qPCR, Methods Mol. Biol., 687 (2011) 113-134.

[16] A. Cheng, M. Li, Y. Liang, Y. Wang, L. Wong, C. Chen, A. V. Vlassov, and S. Magdaleno, Stem-loop RT-PCR quantification of siRNAs in vitro and in vivo, Oligonucleotides., 19 (2009) 203-208.

[17] S. Colombo, H. M. Nielsen, and C. Foged, Evaluation of carrier-mediated siRNA delivery: lessons for the design of a stem-loop qPCR-based approach for quantification of intracellular full-length siRNA, J. Control Release, 166 (2013) 220-226.

[18] S. D. Rose, D. H. Kim, M. Amarzguioui, J. D. Heidel, M. A. Collingwood, M. E. Davis, J. J. Rossi, and M. A. Behlke, Functional polarity is introduced by Dicer processing of short substrate RNAs, Nucleic Acids Res., 33 (2005) 4140-4156.

[19] V. Rerat, G. Dive, A. A. Cordi, G. C. Tucker, R. Bareille, J. Amedee, L. Bordenave, and J. Marchand-Brynaert, alphavbeta3 Integrin-targeting Arg-Gly-Asp (RGD) peptidomimetics containing oligoethylene glycol (OEG) spacers, J. Med. Chem., 52 (2009) 7029-7043.

[20] V. Rerat, S. Laurent, C. Burtea, B. Driesschaert, V. Pourcelle, E. L. Vander, R. N. Muller, and J. Marchand-Brynaert, Ultrasmall particle of iron oxide--RGD peptidomimetic conjugate: synthesis and characterisation, Bioorg. Med. Chem. Lett., 20 (2010) 1861-1865.

[21] V. Pourcelle, Le Duff C.S., Freichels F., Jérôme C., and Marchand-Brynaert J., Clickable PEG conjugate obtained by "clip" photochemistry: Synthesis and characterization by quantitative 19F NMR, Journal of Fluorine Chemistry, 140 (2012) 62-69.

[22] H. Katas and H. O. Alpar, Development and characterisation of chitosan nanoparticles for siRNA delivery, J. Control Release, 115 (2006) 216-225.

[23] D. M. Jensen, D. Cun, M. J. Maltesen, S. Frokjaer, H. M. Nielsen, and C. Foged, Spray drying of siRNA-containing PLGA nanoparticles intended for inhalation, J. Control Release, 142 (2010) 138-145.

[24] H. Freichels, V. Pourcelle, C. S. Le Duff, J. Marchand-Brynaert, and C. Jerome, "Clip" and "click" chemistries combination: toward easy PEGylation of degradable aliphatic polyesters, Macromol. Rapid Commun., 32 (2011) 616-621.

[25] A. Cheng, A. V. Vlassov, and S. Magdaleno, Quantification of siRNAs in vitro and in vivo, Methods Mol. Biol., 764 (2011) 183-197.

[26] Y. Landesman, N. Svrzikapa, A. Cognetta, III, X. Zhang, B. R. Bettencourt, S. Kuchimanchi, K. Dufault, S. Shaikh, M. Gioia, A. Akinc, R. Hutabarat, and R. Meyers, In vivo quantification of formulated and chemically modified small interfering RNA by heating-in-Triton quantitative reverse transcription polymerase chain reaction (HIT qRT-PCR), Silence., 1 (2010) 16.

[27] Y. Pei, P. J. Hancock, H. Zhang, R. Bartz, C. Cherrin, N. Innocent, C. J. Pomerantz, J. Seitzer, M. L. Koser, M. T. Abrams, Y. Xu, N. A. Kuklin, P. A. Burke, A. B. Sachs, L. Sepp-Lorenzino, and S. F. Barnett, Quantitative evaluation of siRNA delivery in vivo, RNA., 16 (2010) 2553-2563.

[28] S. Ouasti, P. J. Kingham, G. Terenghi, and N. Tirelli, The CD44/integrins interplay and the significance of receptor binding and re-presentation in the uptake of RGD-functionalized hyaluronic acid, Biomaterials, 33 (2012) 1120-1134.

[29] F. M. Mickler, Y. Vachutinsky, M. Oba, K. Miyata, N. Nishiyama, K. Kataoka, C. Brauchle, and N. Ruthardt, Effect of integrin targeting and PEG shielding on polyplex micelle internalization studied by live-cell imaging, J. Control Release, 156 (2011) 364-373.

[30] S. Hak, E. Helgesen, H. H. Hektoen, E. M. Huuse, P. A. Jarzyna, W. J. Mulder, O. Haraldseth, and C. L. Davies, The effect of nanoparticle polyethylene glycol surface density on ligand-directed tumor targeting studied in vivo by dual modality imaging, ACS Nano., 6 (2012) 5648-5658.

[31] K. L. Douglas, C. A. Piccirillo, and M. Tabrizian, Cell line-dependent internalization pathways and intracellular trafficking determine transfection efficiency of nanoparticle vectors, Eur. J. Pharm. Biopharm., 68 (2008) 676-687.

[32] M. Lakadamyali, M. J. Rust, and X. Zhuang, Ligands for clathrin-mediated endocytosis are differentially sorted into distinct populations of early endosomes, Cell, 124 (2006) 997-1009.

[33] I. J. Fang, I. I. Slowing, K. C. Wu, V. S. Lin, and B. G. Trewyn, Ligand conformation dictates membrane and endosomal trafficking of arginine-glycine-aspartate (RGD)-functionalized mesoporous silica nanoparticles, Chemistry, 18 (2012) 7787-7792.

[34] D. M. Shayakhmetov, A. M. Eberly, Z. Y. Li, and A. Lieber, Deletion of penton RGD motifs affects the efficiency of both the internalization and the endosome escape of viral particles containing adenovirus serotype 5 or 35 fiber knobs, J Virol., 79 (2005) 1053-1061.

CHAPTER V.
INFLUENCE OF THE RGDP CHEMICAL STRUCTURE AND THE METHOD OF GRAFTING ON THE ANTITUMORAL EFFICIENCY OF CHITOSAN-BASED SIRNA NANOPARTICLES

INFLUENCE OF THE RGDP CHARACTERISTICS AND THE METHOD OF GRAFTING ON THE ANTITUMORAL EFFICIENCY OF CHITOSAN-BASED SIRNA NANOPARTICLES

Ragelle H*., Corbet C*., Pourcelle V., Vanvarenberg K., Marchand-Brynaert J., Préat V#., Feron O#.

* These authors equally contribute to the work, #Corresponding co-authors

Article in preparation

The optimization of the chemical characteristics of the targeting ligand is a central issue when designing targeted nanoparticles (NPs). This is even more crucial for siRNA delivery systems, where the delivery of siRNA into the targeted cells is mandatory for activity. However, the development of targeted NPs that have been optimized in regard to the targeting ligand is generally underconsidered. Here, we developed chitosan-based siRNA delivery systems that target the $\alpha_v\beta_3$ integrins *via* a peptidomimetic of the RGD sequence (RGDp). The aim of the present study was to compare *in vitro* chitosan-based siRNA delivery systems equipped with different types of RGDp in order to determine the optimal characteristics of the RGDp that are required to achieve high gene silencing efficiency.Thus, various RGDp were designed that differed from (i) their chemical structure, (ii) the nature of the linker used for the grafting onto the PEG chains and (iii) the method of grafting. To investigate whether the aforementioned parameters impacted on the gene silencing efficiency of the NPs, two *in vitro* cell models that express the $\alpha_v\beta_3$ integrins were used. Moreover, in the perspective of future therapeutic application, the potential antitumor activity of the targeted NPs was evaluated through the silencing of two metabolic targets *i.e.* the glutamine transporter ASCT2 and the monocarboxylate transporter MCT1.

TABLE OF CONTENTS

I. INTRODUCTION

Inhibition of tumor growth by exploiting the RNA interference (RNAi) gene silencing pathway is a promising strategy for cancer therapy. Moreover, the specific delivery of siRNA to tumor cells by the grafting of targeting ligand on the nanoparticle (NP) surface increases the gene silencing efficiency mediated by the NPs. Although there are few studies describing the functionalization of NPs with targeting ligand and the biological evaluation of these NPs on tumor models, the optimization of the ligand characteristics is generally underappreciated [1]. Yet, the repartition of the targeting ligand on the NP surface as well as the potential interactions between the NP core and the ligand may affect the efficiency of the targeting strategy. For example, a study on targeted self-assembled NPs revealed that the solubility profile of the ligand had an influence on the composition of the NP surface and consequently on the targeting specificity [2].

In the present study, PEGylated-chitosan based NPs were functionalized with different types of peptidomimetics of the RGD sequence (RGDp) [3-5]. Chitosan is a natural polymer which is non-toxic, biodegradable and biocompatible. Because of its cationic nature, chitosan can complex siRNA into nanoparticles. Moreover, the chemical versatility of chitosan enables numerous chemical modifications, such as PEGylation in order to increase the water solubility, to improve the *in vivo* stability of the NPs, and to attach on the PEG chains the targeting ligands. The RGD peptide and RGDp are known to preferentially bind to $\alpha_v\beta_3$ integrins and other integrins such as $\alpha_V\beta_5$, $\alpha_5\beta_1$. The $\alpha_v\beta_3$ integrins are overexpressed both on endothelial cells lining tumor blood vessels and on some tumor cell types, thereby enabling a preferential tumor targeting following systemic administration of NP decorated with the RGD or RGDp ligands. The RGDp are more stable than the RGD because of the absence of easily cleavable peptidic link in their structure [6].

The aim of the present study was to compare the efficiency of chitosan-based siRNA delivery systems equipped with different types of RGDp in order to determine the characteristics of the RGDp that are required for an optimal effect. For that matter, various RGDp were designed. First, two different chemical structures of RGDp were investigated, *i.e.* an amino-pyridine and a naphthyridine structure. Secondly, the influence of the nature of the linker (hydrophilic *versus* lipophilic) used for the grafting of the RGDp on the PEG chain was evaluated. Finally, two methods of RGDp grafting on the PEG chains were used. The method of grafting impacted on the repartition of the RGDp along the PEG chain. While the traditional chain-end grafting enabled the RGDp to be selectively coupled at the end of the PEG, the clip photochemistry method resulted in the random repartition of the RGDp along the PEG chain [7,8]. The NPs coupled with the different types of RGDp were evaluated and compared on two different tumor cell models that expressed the $\alpha_v\beta_3$ integrins. Moreover, to evaluate the

antitumor potential of the targeted NPs, the glutamine transporter ASCT2 and the monocarboxylate transporter MCT1 were silenced. These two metabolic targets were selected in the perspective of future *in vivo* evaluation of the RGDp NPs. Indeed, since $\alpha_v\beta_3$ integrins are expressed both by tumor-associated endothelial cells and cancer cells, we reasoned that the optimal target(s) to be silenced should be proteins expressed by the two cell types and the expression of which being critical for their survival and/or proliferation. Based on our recent findings, lactate flux through the monocarboxylate transporter MCT1 [9-11] and glutamine transport through ASCT2 (unpublished data) represent two major sources of energy fuels to support the proliferation of angiogenic endothelial cells and tumor cells [10].

II. METHODS

II.1 MATERIALS

The chitosan (Kitozyme, Herstal, Belgium) used to synthesize the poly(ethylene glycol)-grafted-chitosan (PEG-chitosan, C_{PEG}) copolymers had a molecular weight of 90 kDa, based on intrinsic viscosity measurements, and a deacetylation degree of 81.3%. Branched poly(ethylene imine) (PEI, 25 kDa) and sodium tripolyphosphate (TPP) were purchased from Sigma-Aldrich (Diegem, Belgium).

The siRNA duplex directed against green fluorescent protein (GFP) and a control (CTRL) siRNA duplex were supplied by Eurogentec (Seraing, Belgium).The siRNAs had the following sequences and modification patterns: GFP sense 5'-pACCCUGAAGUUCAUCUGCACC-3', antisense 5'-UGCAGAUGAACUUCAGGGUCA-3', CTRL sense 5'- GAGCUCAUCGUUGCACUAUTT-3', antisense 5'-AUAGUGCAACGAUGAGCUCTT-3'.

The 2 siRNA antisense sequences targeting human SLC1A5 (ASCT2) in the siRNA pool were: 5'-CCGGUCCUGUACCGUCCUCAA-3' and 5'-UCGCUCAUACUCUACCACCUA-3' (Eurofins MWG Operon, Ebersberg, Germany). The siRNA antisense sequence against human SLC16A1 (MCT1) was 5'-AAGAGGCUGACUUUUCCAAAU-3'. A non-targeting control siRNA of a scrambled nucleotide sequence used as a negative control for nonspecific binding (siRNACont) was purchased from the same company: 5'-CAGGGUAUCGACGAUUACAAA-3'.

SiRNA labelled with Alexa647 (λ_{exc} = 650 nm and λ_{em} = 668 nm) at the 3'end of the sense strand was purchased from Qiagen (Venlo, the Netherlands). INTERFERin® was purchased from Polyplus transfection (Illkirch, France).

II.2 FORMULATION OF THE NANOPARTICLES

Unless otherwise stated, the solutions were prepared using RNAse-free water (Invitrogen™ by Life Technologies, Gent, Belgium) and filtered through 0.22 µm filters (VWR, Heverlee, Belgium). Throughout all experiments, RNase-free materials and conditions were carefully applied.

The nanoparticles were prepared by using the ionic gelation method. In brief, the negatively charged components, *i.e.* the siRNA (20, 50 or 100 µM), and TPP (1 mg/ml) were added to the positively charged components, i.e. the PEG-chitosan C_{PEG}, the RGD-grafted-PEG-chitosan $C_{PEG\ RGD}$ or the RGDp-grafted-PEG-chitosan $C_{PEG\ RGDp}$ (1 mg/ml in 0.2 M sodium acetate buffer, pH 5.7) and PEI (1 mg/ml in

RNAse-free water, pH 7.4) and vortexed for 30 s. The mixtures were incubated for 1 h at room temperature. The ratio between C_{PEG}, $C_{PEG\ RGD}$ or $C_{PEG\ RGDp}$ and PEI was 5/1 (w/w) in all formulations. The amount of siRNA in the formulations was kept constant and was 11.35 µg. The amount of TPP was optimized in order to obtain monodisperse nanoparticles. The copolymer:TPP ratio was 2.7/1 or 3.3/1 (w/w) depending on the copolymer.

The average size, the polydiversity index and the zeta potential of the nanoparticles were determined using a Nanosizer NanoZS (Malvern Instruments Ltd., Malvern, UK) by photon correlation spectroscopy and electrophoretic mobility, respectively. All samples were measured in triplicates in RNAse-free water.

II.3 CELL CULTURE

The human non-small cell lung carcinoma cell line H1299 expressing the destabilized enhanced green fluorescent protein (H1299 EGFP) was used for the *in vitro* tests as reported previously [12]. The H1299 EGFP cells were grown in RPMI 1640 medium (Invitrogen™ by Life Technologies, Gent, Belgium) supplemented with 10% heat-inactivated FBS (Invitrogen™ by Life Technologies, Gent, Belgium)

SiHa and HeLa cervix cancer cells were acquired from American Type Culture Collection (ATCC, Manassas, VA, USA) and were maintained in Dulbecco's modified Eagle's medium (DMEM ; Sigma-Aldrich, Diegem, Belgium) supplemented with 10% heat-inactivated FBS, 10 mM D-glucose, 2 mM L-glutamine and 1% penicillin-streptomycin, at 37°C, in 5% CO_2-humidified atmosphere. All media were prepared from DMEM based medium powder (Sigma-Aldrich, Diegem, Belgium). All cell lines were resuscitated from low passage with all experiments carried out with cells of passage number less than 20. Cells were passaged every 2-3 days to maintain exponential growth. Cells were monitored by microscopy and confirmed to maintain their original morphology. Cells were tested for mycoplasma contamination using the MycoAlert™ Mycoplasma Detection kit (Cambrex, Wiesbaden, Germany).

II.4 DETECTION OF INTEGRIN EXPRESSION

A number of $1x10^6$ cells were incubated with 10 µg of anti-$\alpha_v\beta_3$ antibody (mouse monoclonal BV3 against Integrin $\alpha_v\beta_3$, 0.1 mg/ml, GeneTex, Bio-Connect, Huissen, The Netherlands) or with 10 µg of isotype control FC antibody (APC Mouse IgG1, κ Isotype Ctrl (FC) Antibody, BioLegend) at 4°C for 30 min. The cells were rinsed twice with phosphate-buffered saline (PBS) and incubated with 2 µg of a

secondary antibody (Alexa647 goat–anti-mouse IgG1, 2 mg/mL, Molecular Probes) at 4°C for 30 min. As control, $1x10^6$ cells were incubated with 2 µg of the secondary antibody. The measurements were done on a FACS Calibur cytometer (BD Biosciences) in triplicates and the data were analyzed using FlowJo software. $2x10^4$ cells were analyzed in each measurement.

II.5 IN VITRO GENE SILENCING EFFICIENCY OF THE NANOPARTICLES

II.5.1 EGFP silencing on H1299 EGFP cells

The H1299 EGFP cells were seeded in 12-well plates at a density of $1x10^5$ cells per well 24 h prior to the experiment. The following day, the cells were transfected with the nanoparticles loaded with siRNA GFP or with CTRL siRNA for 4 h. Subsequently, the medium was replaced with fresh medium. After 24 or 48 h, the cells were washed with PBS, trypsinised and resuspended in 300 µl PBS prior to the flow cytometric analysis. The percentage of gene silencing was calculated by using the FL-1 median (median of the GFP fluorescence histogram). The cells transfected with nanoparticles loaded with the CTRL siRNA were used as negative control. A total number of $2x10^4$ cells were analysed per sample.

II.5.2 ASCT2 and MCT1 silencing in SiHa cells

For siRNA transfection, SiHa tumor cells were seeded in standard DMEM medium at 30% confluence in 96-well tissue culture plates (cell viability assays) or in 6-well plates (protein extraction). The next day, cells were transfected with the nanoparticles loaded with 100 nM siRNA for 4 h. Lipofectamine™ RNAiMAX transfection reagent (Invitrogen™ by Life Technologies, Gent, Belgium) was also used, as a transfection control, with 50 nM siRNA, following the manufacturer's instructions. Cell viability and protein expression were assessed after 72 h.

II.5.2.1 Western blot analysis

Subconfluent tumor cells were washed twice with ice-cold HEPES 50 mM pH 7.0, lysed and kept on ice 15 min in a buffer containing 50 mM Tris-HCl pH 7.4, 150 mM NaCl, 1 mM EDTA, 1% Triton X-100, 0.1% SDS, 1% sodium deoxycholate, supplemented with protease inhibitor cocktail (Sigma-Aldrich, Diegem, Belgium) and phosphatase inhibitor cocktail (Roche Applied Science, Vilvoorde, Belgium). Cells were then harvested with a rubber scraper, the lysates cleared by centrifugation (6000 x g, 10 min, 4°C), and the supernatants were collected. Protein concentration was determined using the BCA assay (Thermo Scientific, Erembodegem, Belgium) and samples were stored at -80°C until analysis. Whole cell lysates were then separated by SDS-PAGE under reducing conditions and

transferred onto PVDF membranes (Immobilon, Millipore, Overijse, Belgium). The membranes were blocked with 5% skimmed milk in TBS-0.1% Tween 20 (TBS-T) and subsequently immunoblotted with primary antibody for overnight incubation at 4°C. The membranes were probed with horseradish peroxidase-conjugated secondary antibody and reactive proteins were detected using Amersham ECL detection reagents (GE Healthcare Life Sciences, Diegem, Belgium). Anti-MCT1 (1/1000; home-made), anti-ASCT2 (1/1000; ABN73, Millipore, Overijse, Belgium) and anti-actin (1/10000; A5441, Sigma-Aldrich,Diegem, Belgium), used as an equiloading control, were diluted in 5% skimmed milk.

II.5.2.2 Cell viability

Cell viability was determined by using the Presto Blue cell viability reagent (Invitrogen™ by Life Technologies, Gent, Belgium), according to the manufacturer's instructions.

II.6 CELLULAR UPTAKE

Cellular uptake of nanoparticles was quantified by flow cytometry. H1299 EGFP cells were seeded in 12-well plates ($1.5x10^5$ cells/well), 24 h before experiment. Cells were incubated with nanoparticles for 1 h at a concentration of 100 nM Alexa 647-labelled siRNA. Cells were rinsed with PBS, trypsinized (0.25% trypsin) and diluted with medium. After centrifugation (250 xg, 5 min, 4°C), the cell pellet was resuspended in 200 µl PBS. The measurements were done on a FACS Calibur cytometer (BD Biosciences, Belgium) in triplicates and the data were analyzed using FlowJo software. A number of 2.10^4 cells were analyzed in each measurement.

II.7 FLUORESCENCE MICROSCOPY

The H1299 EGFP cells were seeded in 12-well plates (10^5 cells/well) containing a cover slip. After 24 h, the cells were incubated with the nanoparticles loaded with Alexa647-labelled siRNA (1 h at 100 nM), then fixed with fresh paraformaldehyde (2% (w/v) in PBS) and rinsed three times with PBS. In order to stain the nuclei, the cells were incubated with 4',6-diamidino-2-phenylindole DAPI (0.1 µg/ml) for 5 min and rinsed three times with PBS. The cells were incubated for 1 h with AlexaFluor488-conjugated Concanavalin A (5 µg/ml in PBS, Molecular Probes) to stain the cell membranes. After washing, the cover slips were placed on a slide using the Vectashield® mounting medium. The slides were imaged using a structured illumination AxioImager microscope equipped by an Apotome module (Zeiss, Germany, magnification 40x).

II.8 STATISTICS

The experiments were performed in triplicate, unless otherwise stated. Values are given as means ± standard deviations (SD). Statistically significant differences were assessed by an analysis of variance (ANOVA) at a 0.05 significance level and followed by Tukey´s post-hoc test or by two-way ANOVA followed by Bonferroni's post-hoc test, by using the GraphPad Prism 5.01 software (La Jolla, CA, USA). * $p < 0.05$, ** $p < 0.01$, *** $p < 0.001$ or **** $p < 0.0001$ were considered to be statistically significant.

III. RESULTS AND DISCUSSION

III.1 GRAFTING OF RGDP ON THE PEG CHAINS

Different types of RGDp grafted on the PEG chains were investigated and their characteristics are summarized in Table I. The first method of RGDp grafting was the clip photochemistry method that resulted in the random distribution of RGDp along the PEG chains, at approximately 4 to 12 mol% grafting ratio [13]. The RGDp grafted by using this method are RGDp 85, 91 and 92. The second method was the chain-end coupling that allowed the RGDp to be selectively grafted at the end of the PEG chains, with grafting ratio ranging from 33 to 50 mol% (RGDp 93, 95, 96 and 97). The linker between the RGDp and the PEG was either a short oligoethyleneglycol moiety (OEG) which is hydrophilic (RGDp 91, 92, 96 and 97) or an aminocaproic acid unit which is lipophilic (RGDp 85, 93 and 95). Finally, RGDp with two different RGDp chemical structures *i.e* .R = naphthyridine (RGDp 85, 92, 93 and 96) or R = amino-pyridine (RGDp 91, 95, and 97) were used. The Gly-Arg-Gly-Asp-Ser commercial pentapeptide (Eurogentec) (RGD) was grafted on the PEG chains using the clip photochemistry method at 10 mol%. The RGDp NPs were compared to the RGD NPs.

Table I: Overview of different RGDp: structure, grafting method and RGDp/PEG grafting ratio The colours correspond to the type of linker: the blue colour represents the caproyl linker and the grey colour represents the OEG linker.

Grafting method	RGDp structure	
	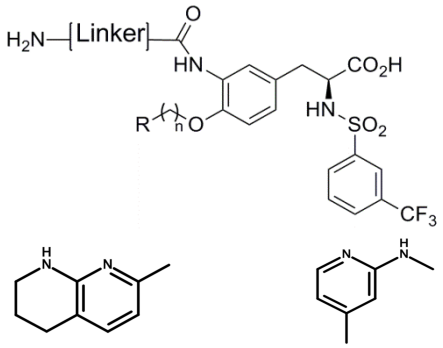	
	R=naphthyridine	R=amino-pyridine
Clip 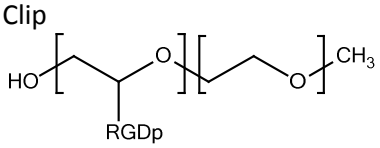	RGDp 85 (1/8)	/
	RGDp 92 (1/24)	RGDp 91 (1/14)
Chain-end 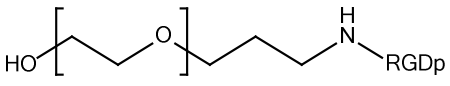	RGDp 93 (1/2.5)	RGDp 95 (1/2)
	RGDp 96 (1/3)	RGDp 97 (1/2)

III.2 PHYSICO-CHEMICAL CHARACTERISTICS OF THE NANOPARTICLES

The physicochemical characteristics of the nanoparticles are summarized in Table II. They presented a mean diameter between 239 and 467 nm. The RGDp 93 NPs presented a larger size in comparison to the other formulations ($p< 0.0001$). The polydispersity index (PDI) was below 0.26, suggesting that the nanoparticle populations were monodisperse. All types of nanoparticles presented a positive surface charge, but differences in the zeta potential values ($p< 0.0001$) can be observed depending on the amount of TPP in the formulation. The amount of TPP was optimized to obtain monodisperse NPs. Indeed, some of the formulations (NPs grafted with RGDp 85, 91, 92, 93 and 97) contained 75 µg of TPP while others (NP, RGD NPs, RGDp 95 NPs and RGDp 96 NPs) contained 50 µg TPP only. In the first case, the zeta potential was approximately 15 mV whereas it was increased to approximately 27 mV when the TPP amount in the formulation decreased.

Table II: Physicochemical characteristics of the nanoparticles (n=3)

	Size (nm)	PDI	Zeta potential (mV)
NP	239 ± 22	0.15 ± 0.02	27.8 ± 0.3
RGD NP	269 ± 18	0.16 ± 0.02	26.5 ± 1.1
RGDp 85 NP	244 ± 59	0.19 ± 0.06	13.6 ± 2.1
RGDp 91 NP	270 ± 25	0.14 ± 0.02	15.8 ± 1.0
RGDp 92 NP	334 ± 65	0.18 ± 0.04	16.3 ± 1.4
RGDp 93 NP	467 ± 130	0.26 ± 0.09	14.7 ± 0.0
RGDp 95 NP	250 ± 20	0.18 ± 0.02	27.3 ± 0.7
RGDp 96 NP	274 ± 23	0.21 ± 0.02	26.6 ± 1.9
RGDp 97 NP	285 ± 37	0.16 ± 0.01	18.3 ± 2.8

III.3 THE TARGETED NPS INDUCED EGFP SILENCING ON H1299 EGFP CELLS

The non-targeted and the $\alpha_v\beta_3$ targeted NPs were first evaluated for their ability to silence EGFP protein expression in H1299 EGFP cells after 48 h (Fig. 1). At 50 nM, no statistically significant differences in silencing were observed between the different types of nanoparticles. The EGFP silencing obtained by using the non-targeted NPs was below 25% irrespective of the applied doses of siRNA. However, at a siRNA concentration of 100 nM and above, the extent of EGFP silencing increased after transfection with the $\alpha_v\beta_3$ targeted nanoparticles grafted with the clip photochemistry method, in comparison to the non-targeted nanoparticles. Moreover, at this

concentration the $\alpha_v\beta_3$ targeted NPs grafted with the clip photochemistry method (Fig. 1A) were more efficient than their chain-end grafted counterparts (Fig. 1B): approximately 55 to 70% EGFP silencing was obtained with the clip-grafted NPs while only 22 to 40% was noticed by using the chain-end grafted NPs. However, at the highest dosage tested (150 nM) no statistically significant differences between the efficiency of the two grafting methods were observed: all the $\alpha_v\beta_3$ targeted NPs mediated approximately 70 to 80% EGFP silencing. The slight differences in the zeta potential values observed between the formulations (Table II) did not influence the gene silencing efficiency.

A

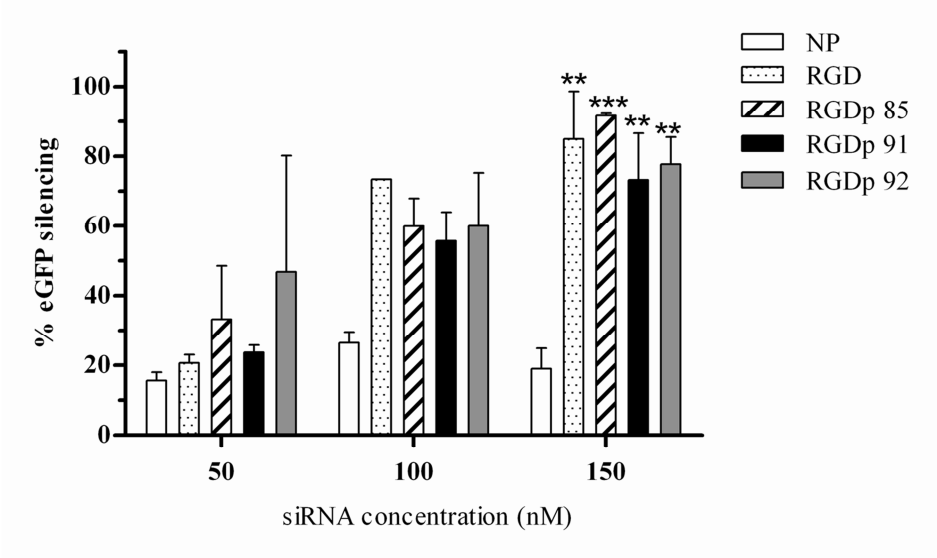

B

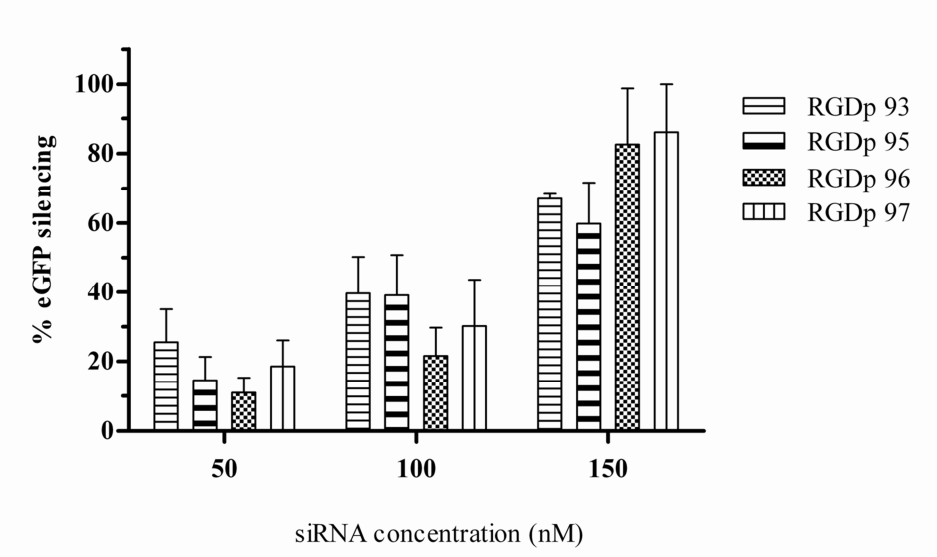

Figure 1: Percentage of EGFP silencing on H1299 EGFP cells 48 h after transfection with (A) EGFP siRNA loaded in non-targeted nanoparticles (NP) and $\alpha_v\beta_3$ targeted nanoparticles grafted using the clip method, (B) EGFP siRNA loaded in $\alpha_v\beta_3$ targeted nanoparticles grafted using the chain-end coupling method. Data represent mean values ± SD (n=3). Results significantly different from NP are indicated: **p < 0.01, ***p < 0.001.

Fluorescence microscopy revealed that the targeted NPs were efficiently internalized by H1299 EGFP cells after 1 h incubation (Fig. 2A-F). On the other hand, the non-targeted NPs were not internalized after 1 h incubation (data not shown), as it was previously observed (see Chapter IV). These results suggested that the non-targeted NPs are taken up in H1299 EGFP cells *via* an endocytosis mechanism that is different from the targeted NPs and that presented a slower kinetic of uptake.

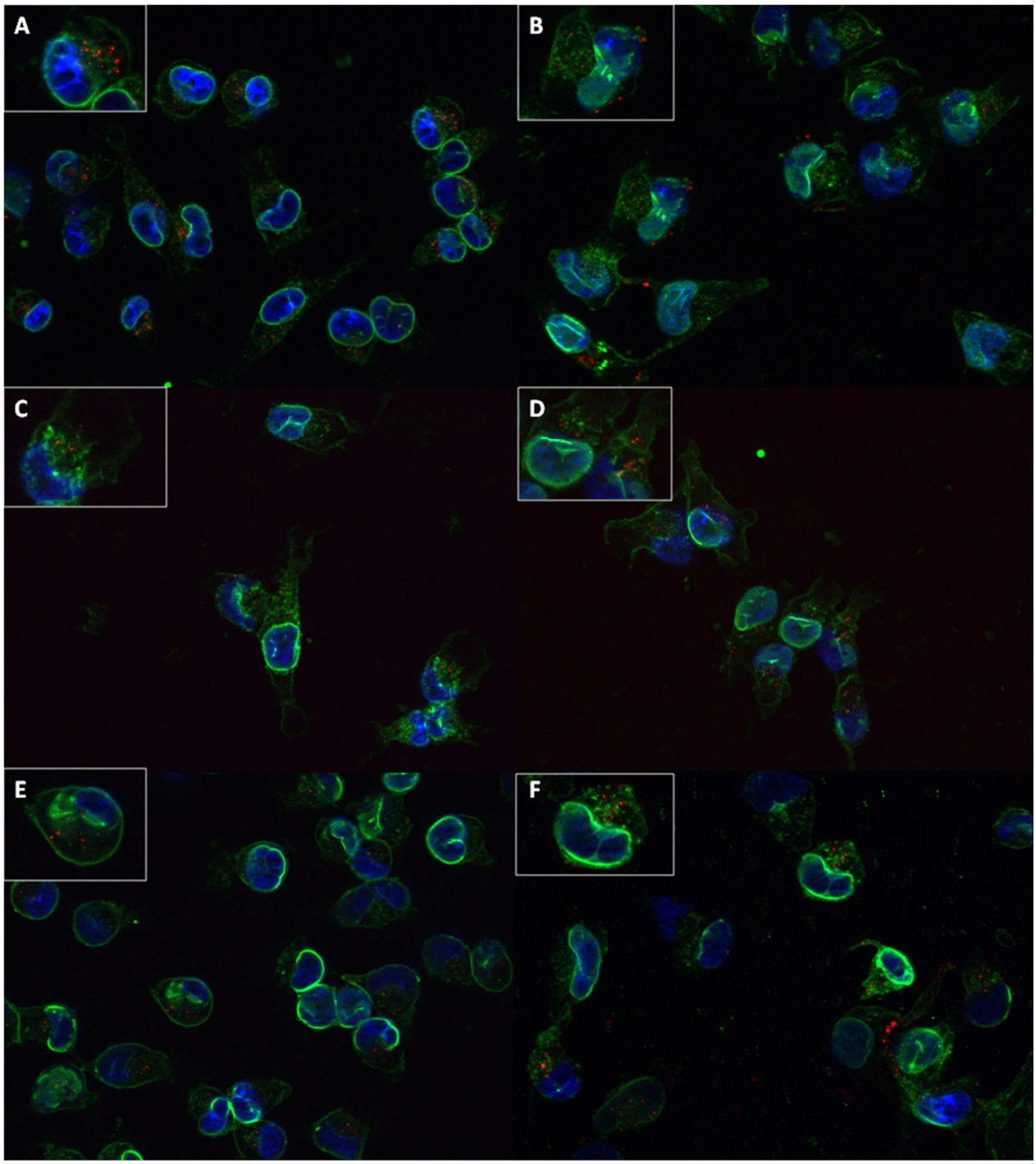

Figure 2: H1299 EGFP cells (blue: nuclei, green: cell membrane) transfected with (A) RGDp 85 NPs, (B) RGD NPs, (C) RGDp 91 NPs, (D) RGDp 92 NPs, (E) RGDp 95 NPs and (F) RGDp 96 NPs loaded with 100 nM Alexa647-siRNA (red) for 1 h. The magnification was 40x.

III.4 THE ENDOCYTOSIS OF TARGETED NPS IS MEDIATED BY THE A_VB_3 INTEGRINS

Both SiHa cells and H1299 EGFP cells express the $\alpha_v\beta_3$ integrins, but to a larger extent for SiHa cells as demonstrated in Fig. 3. The cellular uptake of the $\alpha_v\beta_3$ targeted NPs (RGD NPs and RGDp 85 NPs) and non-targeted NPs was assessed using fluorophore-conjugated siRNA on these two $\alpha_v\beta_3$ positive cell lines and on HeLa cells that do not express $\alpha_v\beta_3$ integrins or to a very low extent [14,15].

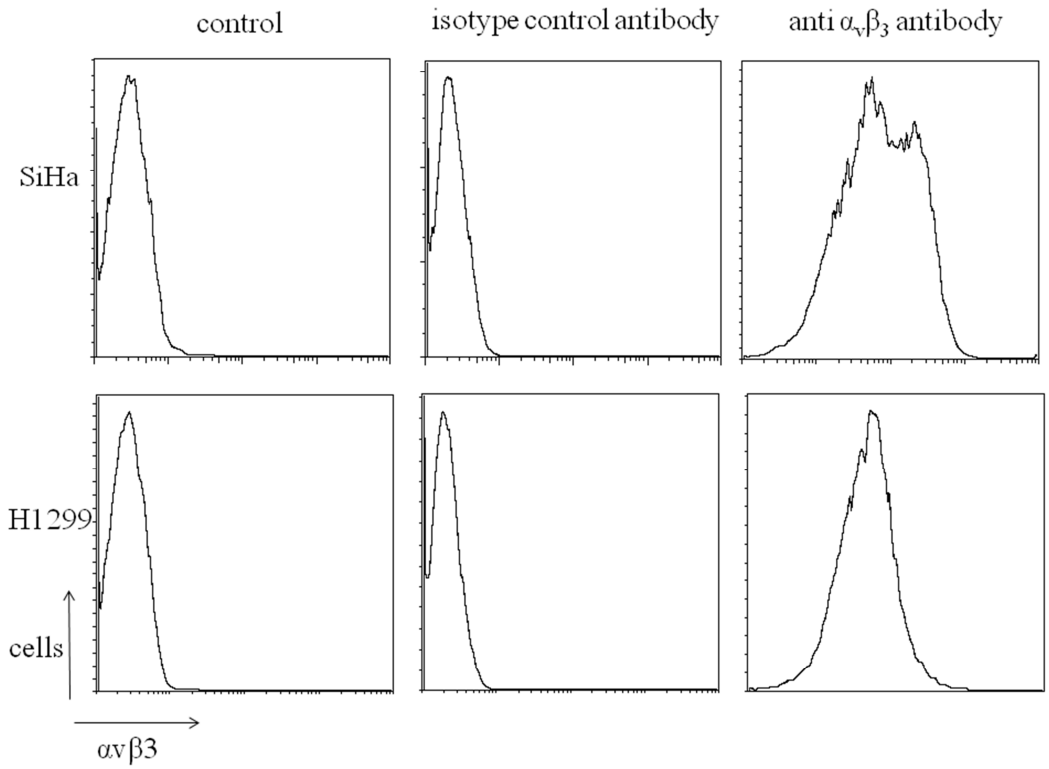

Figure 3: Detection of $\alpha_v\beta_3$ integrins on SiHa cells and H1299 EGFP cells using an Alexa 647 secondary antibody. Fluorescence histograms of flow cytometric analysis (A): control, (B): incubation with the isotype control FC antibody (C): incubation with the anti-$\alpha_v\beta_3$ antibody.

The cellular uptake of the RGD NPs and the RGDp 85 NPs (loaded with Alexa647-labelled siRNA) was increased in both $\alpha_v\beta_3$ positive cells. Moreover, the amount of RGD NPs internalized by the SiHa cells was higher in comparison with the RGDp 85 NPs. On the other hand, the non-targeted NPs showed the same internalization profiles in the three cell lines (Fig. 4). This suggests that both $\alpha_v\beta_3$ receptor – dependent and –independent endocytosis of NPs can occur: while non-targeted NPs only enter cells through the latter, endocytosis of RGD NPs and RGDp 85 NPs in SiHa and H1299 EGFP cells results from the combination of both mechanisms.

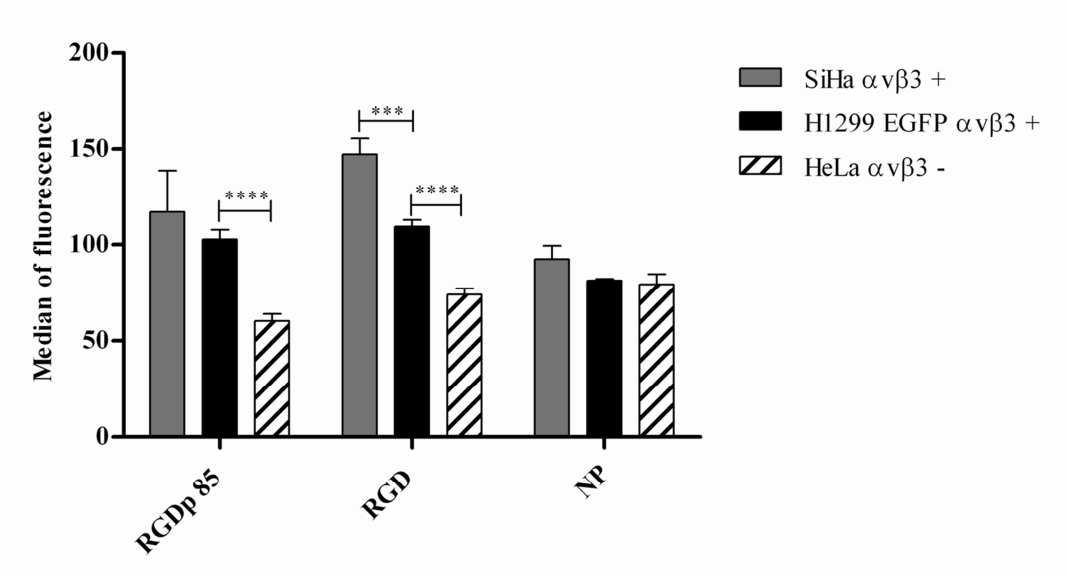

Figure 4: Cellular uptake of RGDp85 NPs, RGD NPs and NPs loaded with 100 nM Alexa647 siRNA, for 1 h, on SiHa cells, H1299 EGFP cells and HeLa cells. Data represent mean values ± SD (n=3). Results significantly different are indicated: ***p < 0.001, ****p<0.0001.

III.5 IN VITRO THERAPEUTIC EFFICACY OF THE TARGETED RGDP-NPS ON SIHA CELLS

III.5.1 The targeted NPs efficiently silenced MCT1 and ASCT2

To determine the potential therapeutic efficacy of gene silencing, we next chose to target ASCT2 and MCT1 proteins which support the high energy-demand metabolism of tumor cells (and of tumor-associated endothelial cells), by mediating glutamine and lactate flux, respectively. SiHa cells were selected for these experiments because they exhibit an exacerbated glutamine and lactate metabolism and express high levels of $\alpha_v\beta_3$ integrins (see Fig. 3). The in vitro silencing experiments were performed at a siRNA concentration of 100 nM, as this concentration optimally enabled the discrimination between the different targeted formulations (see Fig. 1).

First, the efficiency of the silencing of MCT1 (Fig. 5A) and of ASCT2 (Fig. 5B) by using the non-targeted and the $\alpha_v\beta_3$ targeted nanoparticles was evaluated. To estimate the gene silencing efficiency, densitometry analysis was performed (data not shown). Approximately 40% to 70% MCT1 silencing were obtained after transfection with the $\alpha_v\beta_3$ targeted NPs, except for the RGDp 91 NPs that showed a relatively low silencing efficiency (<10%). Regarding ASCT2, similar levels of silencing (40% to 60%) were achieved after transfection with the $\alpha_v\beta_3$ targeted NPs, except for RGDp 92 NPs (< 30%). On the other hand, the non-targeted NPs were unable to silence any of the targets (< 1%).

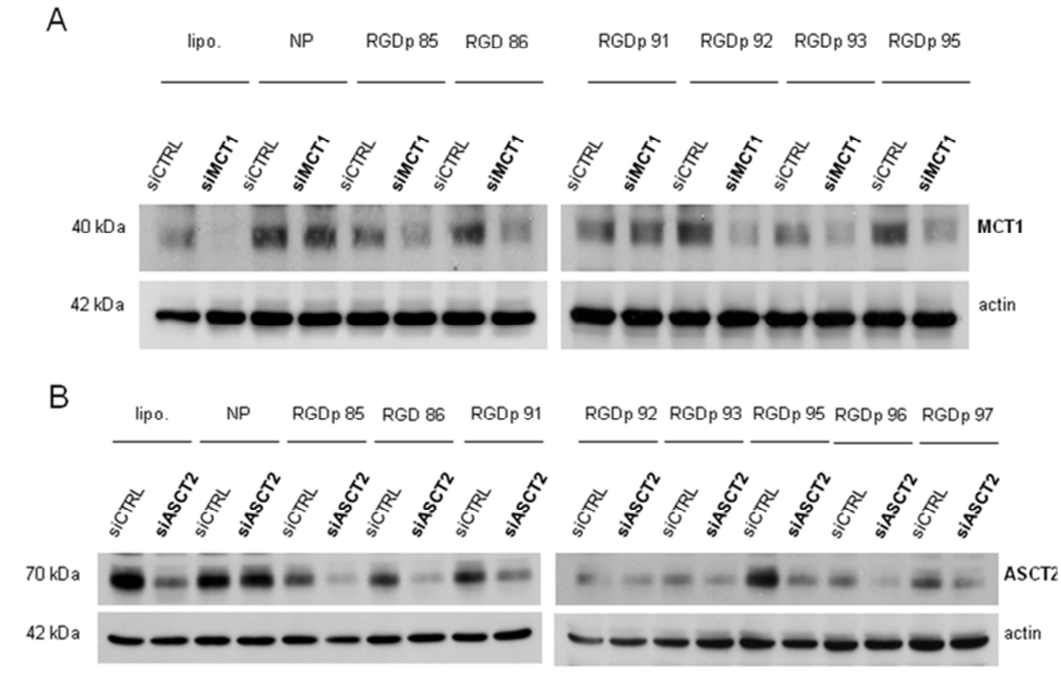

Figure 5: Western Blot analysis for (A) MCT1 and (B) ASCT2 silencing mediated by lipofectamine, non-targeted NPs and targeted NPs at 72 h. The concentration of siRNA used was 50 nM for the Lipofectamine and 100 nM for the NPs.

III.5.2 The silencing of MCT1 and ASCT2 resulted in an antiproliferative effect

To investigate whether the silencing of MCT1 induced an antiproliferative effect, the SiHa cells were incubated with the NPs loaded with anti-MCT1 siRNA in lactate containing medium and the cell viability was measured 72 h after transfection (Fig. 6A). In these transfection conditions, the lactate represented the main energetic substrate for the cells. Thus, an efficient MCT1 silencing results in significant cell death, as the cells are deprived of their metabolic fuel. As observed in Fig. 6, the use of non-targeted NPs loaded with anti-MCT1 siRNA did not lead to tumor cell death in agreement with the lack of MCT1 silencing observed in Fig. 5A. By contrast, when anti-MCT1 siRNA were delivered using targeted NPs, 20 to 65% cell death were observed according to the targeting moieties. The RGDp 85 NPs and the RGD NPs were the most efficient formulations, inducing up to 50-65% cell death whereas the RGDp 91 NPs and the RGDp 92 NPs showed limited antitumor effect (approximately 20% cell death). The poor efficiency of the RGDp 91 NPs and the RGDp 92 NPs could be explained by their low ligand density (7 and 4 mol% respectively) in comparison to the lipophilic RGDp 85 NPs (12.5 mol%). On the opposite, no influence of the linker nature on the silencing efficiency could be observed for the chain-end grafted NPs: approximately 40% cell death was obtained irrespective of the linker nature.

As a control of the specificity of the MCT1 targeting (and thus of the innocuity of the formulations), we next verified that formulations did not induce cell death when the SiHa cells where cultured in medium containing glutamine and glucose instead of lactate (Fig. 6B).

A

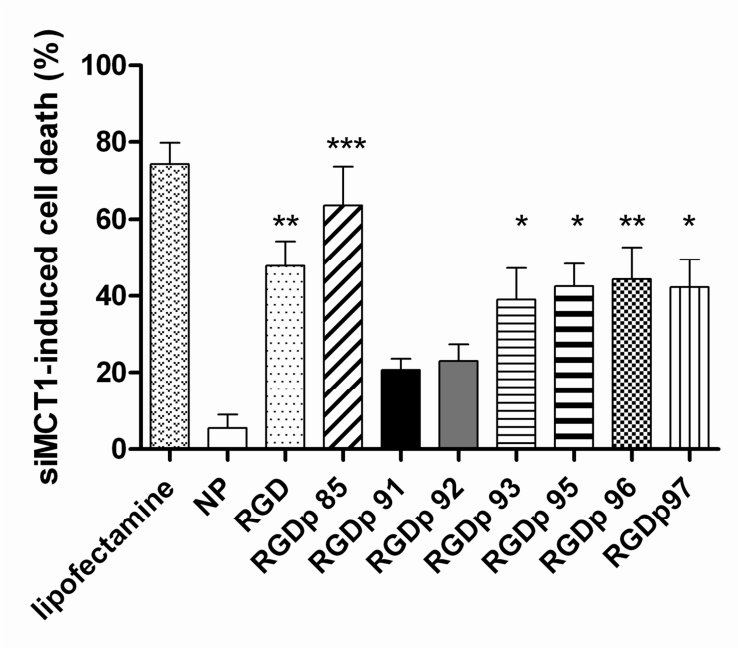

B

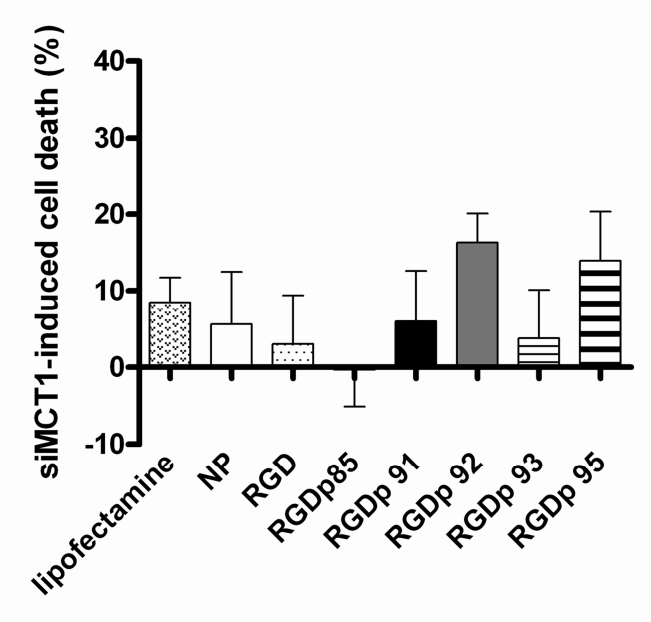

Figure 6: (A) Antitumoral effect of MCT1 silencing (% of cell death) in SiHa cells in DMEM 10% Fp171BS containing 10 mM L-lactate 72 h after transfection by using the non-targeted and the targeted NPs. (B) Effect of the non-targeted and the targeted NPs on the viability of SiHa cells cultivated in DMEM 10% FBS containing 10 mM D-glucose and 2 mM L-glutamine. Data represent mean values ± SD (n=8).

To evaluate the *in vitro* antitumor effects resulting from ASCT2 silencing, SiHa placed in medium containing glucose and glutamine were transfected with the different formulations and evaluated as described above for anti-MCT1 siRNA. The cell viability was measured at 72 h (Fig. 7A). The RGD NPs, the RGDp 85 NPs and the RGDp 95 NPs were the most efficient formulations to induce cell death. No significant differences were observed between the non-targeted NPs, RGDp 91 NPs, RGDp 92 NPs and RGDp 93 NPs. These results confirmed the lowest efficiency of RGDp 91 NPs and RGDp 92 NPs observed previously (Fig. 6).

Similar experiment was performed in SiHa cells resulting from a clonal selection aiming to select cells endowed with a largest dependence towards glutamine (*vs.* glucose) (Fig. 7B). In these cells, the NPs induced an overall higher antitumor effect in comparison to what was observed in non-selected SiHa cells (Fig 7A, further validating the glutamine transporter ASCT2 as an interesting therapeutic target.

A

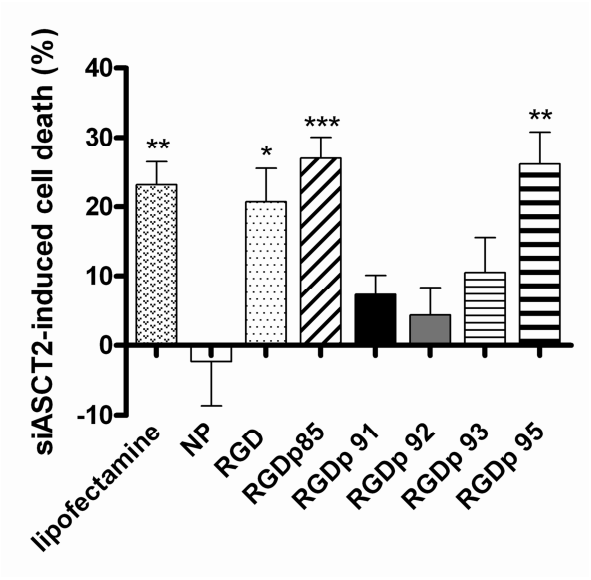

B

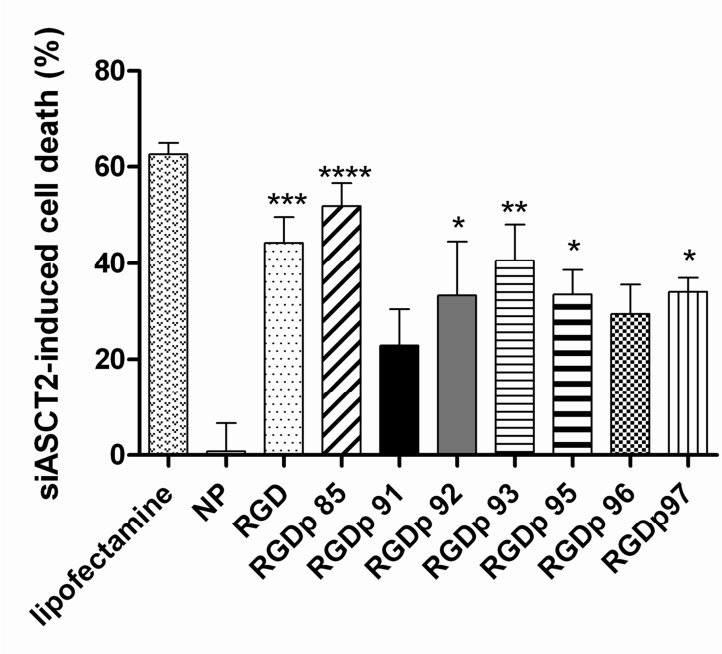

Figure 7: Antitumoral effect of ASCT2 silencing by using the non-targeted and the targeted NPs (A) in SiHa cells in DMEM 10% FBS containing 2 mM L-glutamine and 10 mM D-glucose and (B) in low pH-adapted SiHa cells in DMEM 10% FBS pH 6.5. Data represent mean values ± SD (n=8). Results significantly different from NP are indicated: * $p < 0.05$, ** $p < 0.01$, *** $p < 0.001$ and **** $p < 0.0001$.

IV. CONCLUSION

In this work, several RGDp that differed from (i) their chemical structure, (ii) the nature of the linker used for the grafting of the RGDp onto the PEG and (iii) the method of grafting, were evaluated for their ability to silence EGFP and two therapeutic targets *i.e.* MCT1 and ASCT2 in H1299 EGFP cells and in SiHa cells, respectively, both cell models being $\alpha_v\beta_3$ positive.

The targeted NPs were more efficient than the non-targeted NPs on both cell models. The RGDp 85 NPs induced the highest levels of MCT1 and ASCT2 silencing resulting in great anti-proliferative effects and presented similar efficiency than the RGD NPs. In contrast, the RGDp 91 NPs and the RGDp 92 NPs showed the lowest efficiency. Thus, the combination of a hydrophilic linker with the clip grafting method was not optimal. Interestingly, the clip photochemistry method of grafting (RGDp 85 NPs) was more efficient than the traditional chain-end coupling (RGDp 93 NPs), despite the lower ligand density obtained by using the clip grafting. Finally, the gene silencing efficiency of the chain-end grafted NPs was less prone to the influence of the linker nature and of the chemical structure of the RGDp.

Further characterization and biological evaluation of the $\alpha_v\beta_3$ targeted NPs are needed to better understand these results. Moreover, the antitumor effect of the targeted NPs loaded with MCT1 and/or ASCT2 will be assessed *in vivo* after intratumoral and systemic injection on SiHa tumor bearing mice. The combination of both MCT1 and ASCT2 siRNA within the same NP will be particularly suited to oppose tumor metabolism plasticity (which describes the capacity of tumor cells to adapt themselves in order to use an alternate metabolic route when another pathway is blocked). More generally, the tumor heterogeneity is known to lead to the co-existence within a same tumor, of regions more dependent on lactate or instead on glucose and/or glutamine. This offers an additional rationale to exploit cocktails of siRNA simultaneously targeting several metabolic paths in order to reach the largest proportion of cancer cells.

Finally, our *in vitro* results indicate that besides the ability of RGDp to preferentially address the NP into $\alpha_v\beta_3$-expressing tumor tissues following systemic administration, these ligands confer a net advantage in terms of NP endocytosis (*vs.* non-targeted NP). In this context, the use of *in vivo* models of tumor xenografts resulting from cancer cells expressing or not the $\alpha_v\beta_3$ integrin, will offer the opportunity to discriminate between the effects of NP delivering their payload only to the $\alpha_v\beta_3$-expressing endothelial cells lining tumor blood vessels or to both endothelial and cancer cells.

V. REFERENCES

[1] H. D. Han, L. S. Mangala, J. W. Lee, M. M. Shahzad, H. S. Kim, D. Shen, E. J. Nam, E. M. Mora, R. L. Stone, C. Lu, S. J. Lee, J. W. Roh, A. M. Nick, G. Lopez-Berestein, and A. K. Sood, Targeted gene silencing using RGD-labeled chitosan nanoparticles, Clin. Cancer Res., 16 (2010) 3910-3922.

[2] P. M. Valencia, M. H. Hanewich-Hollatz, W. Gao, F. Karim, R. Langer, R. Karnik, and O. C. Farokhzad, Effects of ligands with different water solubilities on self-assembly and properties of targeted nanoparticles, Biomaterials, 32 (2011) 6226-6233.

[3] S. Biltresse, M. Attolini, G. Dive, A. Cordi, G. C. Tucker, and J. Marchand-Brynaert, Novel RGD-like molecules based on the tyrosine template: design, synthesis, and biological evaluation on isolated integrins alphaVbeta3/alphaIIbbeta3 and in cellular adhesion tests, Bioorg. Med Chem., 12 (2004) 5379-5393.

[4] V. Rerat, G. Dive, A. A. Cordi, G. C. Tucker, R. Bareille, J. Amedee, L. Bordenave, and J. Marchand-Brynaert, alphavbeta3 Integrin-targeting Arg-Gly-Asp (RGD) peptidomimetics containing oligoethylene glycol (OEG) spacers, J Med Chem., 52 (2009) 7029-7043.

[5] V. Rerat, S. Laurent, C. Burtea, B. Driesschaert, V. Pourcelle, E. L. Vander, R. N. Muller, and J. Marchand-Brynaert, Ultrasmall particle of iron oxide--RGD peptidomimetic conjugate: synthesis and characterisation, Bioorg. Med Chem. Lett., 20 (2010) 1861-1865.

[6] F. Danhier, B. A. Le, and V. Preat, RGD-based strategies to target alpha(v) beta(3) integrin in cancer therapy and diagnosis, Mol. Pharm., 9 (2012) 2961-2973.

[7] M. Garinot, V. Fievez, V. Pourcelle, F. Stoffelbach, R. A. des, L. Plapied, I. Theate, H. Freichels, C. Jerome, J. Marchand-Brynaert, Y. J. Schneider, and V. Preat, PEGylated PLGA-based nanoparticles targeting M cells for oral vaccination, J Control Release, 120 (2007) 195-204.

[8] V. Pourcelle, H. Freichels, F. Stoffelbach, R. Auzely-Velty, C. Jerome, and J. Marchand-Brynaert, Light induced functionalization of PCL-PEG block copolymers for the covalent immobilization of biomolecules, Biomacromolecules., 10 (2009) 966-974.

[9] R. Boidot, F. Vegran, A. Meulle, B. A. Le, C. Dessy, P. Sonveaux, S. Lizard-Nacol, and O. Feron, Regulation of monocarboxylate transporter MCT1 expression by p53 mediates inward and outward lactate fluxes in tumors, Cancer Res, 72 (2012) 939-948.

[10] P. Sonveaux, F. Vegran, T. Schroeder, M. C. Wergin, J. Verrax, Z. N. Rabbani, C. J. De Saedeleer, K. M. Kennedy, C. Diepart, B. F. Jordan, M. J. Kelley, B. Gallez, M. L. Wahl, O. Feron, and M. W. Dewhirst, Targeting lactate-fueled respiration selectively kills hypoxic tumor cells in mice, J Clin. Invest, 118 (2008) 3930-3942.

[11] F. Vegran, R. Boidot, C. Michiels, P. Sonveaux, and O. Feron, Lactate influx through the endothelial cell monocarboxylate transporter MCT1 supports an NF-kappaB/IL-8 pathway that drives tumor angiogenesis, Cancer Res, 71 (2011) 2550-2560.

[12] D. M. Jensen, D. Cun, M. J. Maltesen, S. Frokjaer, H. M. Nielsen, and C. Foged, Spray drying of siRNA-containing PLGA nanoparticles intended for inhalation, J Control Release, 142 (2010) 138-145.

[13] H. Freichels, V. Pourcelle, C. S. Le Duff, J. Marchand-Brynaert, and C. Jerome, "Clip" and "click" chemistries combination: toward easy PEGylation of degradable aliphatic polyesters, Macromol. Rapid Commun., 32 (2011) 616-621.

[14] L. L. Cai, P. Liu, X. Li, X. Huang, Y. Q. Ye, F. Y. Chen, H. Yuan, F. Q. Hu, and Y. Z. Du, RGD peptide-mediated chitosan-based polymeric micelles targeting delivery for integrin-overexpressing tumor cells, Int J Nanomedicine., 6 (2011) 3499-3508.

[15] Q. Xu, Y. Liu, S. Su, W. Li, C. Chen, and Y. Wu, Anti-tumor activity of paclitaxel through dual-targeting carrier of cyclic RGD and transferrin conjugated hyperbranched copolymer nanoparticles, Biomaterials, 33 (2012) 1627-1639.

CHAPTER VI.
DISCUSSION AND PERSPECTIVES

TABLE OF CONTENTS

I. CONTRIBUTION TO THE FIELD

RNA interference represents a powerful approach to treat diseases in which specific proteins are upregulated and offers great promise for cancer treatment because of the high specificity of the RNAi mediators, *i.e.*, the siRNA. In addition, siRNAs can theoretically silence any gene, thereby extending the druggable targets to the entire genome. The sequencing of the human genome and the screening of the genetic characteristics of tumors have identified numerous genes implicated in cancer progression, all of them representing possible targets for siRNAs [1].

Like all drugs, siRNAs presents side-effects, which include the possible activation of an immune-response and the potential induction of off-target effects. Moreover, their susceptibility to nucleases is a severe disadvantage in their *in vivo* administration. However, advances in siRNA design have allowed the emergence of chemical modifications that are highly efficient in preventing an immune response and increasing siRNA stability [2]. Moreover, algorithms can predict the off-target effects mediated by a specific siRNA sequence. Although one of the first siRNAs evaluated in clinical trials induced a strong immune response, the siRNAs currently being investigated in clinical trials present good safety profiles.

Thus, siRNA therapeutic exploitation is entirely dependent on the development of delivery systems that can overcome the numerous barriers to the cytoplasmic delivery of siRNAs. The requirements of the delivery system are (i) the complexation of siRNAs into non-toxic, biocompatible, biodegradable and monodisperse nanoparticles (NPs) that present (ii) a good stability in blood, (iii) that are internalized by the targeted cells and (iv) that release their siRNA cargo in the cell cytoplasm. This is particularly crucial for cancer therapy, in which tumor cells are disseminated throughout the body. Moreover, gene silencing must theoretically occur in all tumor cells to produce tumor regression [1].

In this work, we aimed at elucidating the parameters governing the design of an efficient chitosan-based siRNA delivery system considering the biological barriers to siRNA delivery.

I.1. IS CHITOSAN A GOOD MATERIAL FOR SIRNA DELIVERY?

The successful development of siRNA delivery systems depends largely on the choice of a good building material. Cationic compounds are highly favorable to efficiently complex siRNA. In contrast, the use of neutral or anionic materials can result in an inefficient siRNA encapsulation. Compared with cationic lipids, cationic polymers are generally easier to manufacture and to handle. Synthetic cationic polymers such as PEI or PLL and natural cationic polymers such as chitosan have both been investigated *in vivo* and offer plenty of possibilities for chemical modifications and surface functionalization. In comparison with chitosan, synthetic polymers possess higher charge density that is responsible for their important transfection efficiency on the one hand and their cellular toxicity on the other hand [3,4]. Polycation-based materials activate the complement system in a charge density-dependent manner [5]. Thus, the development of synthetic polymers such as PEI has been slow because of their toxicity. In contrast, chitosan possesses the advantage of being biodegradable and biocompatible, characteristics that are highly desired in a drug delivery system.

Polymers often present a polydisperse MW distribution and a heterogeneous distribution of isomers. As a result, the synthesis of precise polymers has been proposed, especially for PEI and polyamidoamine (PAMAM) dendrimers, the latter being the more developed to date [6]. The term 'precise polymers' refers to the synthesis of low polydispersity polymers with a defined charge number. For synthetic polymers, this is made possible using improved polymerization technologies to avoid random polymerization. Because chitosan is a natural polymer, the extraction procedure and the variability of the starting material (*i.e.*, crustacean shells or fungi walls) can influence the final chitosan characteristics and are more difficult to control than synthetic polymer processes. Chitosan can present a heterogeneous MW distribution, depending on the manufacturer [7]. Moreover, deacetylation processes occur randomly, resulting in the chemical polydispersity of the DD value, and can be accompanied by the degradation of the polymeric chains [8]. Thus, the DD and the MW might vary from batch to batch, while the formation of NPs comprising chitosan and siRNAs is based upon a fine charge equilibrium. Even slight modifications to the polymer structure can disrupt this balance, affecting the NP formation, physicochemical characteristics and biological activity, resulting in the discrepancies that are often observed from one publication to another.

When chemical modifications such as PEGylation or the addition of functional groups such as targeting ligands are imparted to chitosan, their grafting must be controlled to obtain a homogenous siRNA delivery system. This is even more crucial when these modifications are made to the chemical groups that are responsible for siRNA binding. In our study, the first PEGylation method (PEG of

1,000 Da) implemented was performed on the chitosan hydroxyl groups and led to random chitosan chain degradation during the de-protection step *(Chapter III)*. The PEG chains (PEG 5,000 Da) were then grafted onto the amino groups of the chitosan *(Chapter IV and following)*. Thus, for a given batch, depending on the percentage PEGylation obtained, the number of free amines available for siRNA binding might vary, thereby modifying the formulation composition and potentially affecting the stability of the NPs and/or their efficiency. Polymer variability among batches is not acceptable in clinical development, where a homogenous product is mandatory. Furthermore, in addition to the need to synthesize defined polymers, the development of appropriate and reliable analytical methods must be developed to precisely characterize the polymers.

The development of chitosan and its derivatives has made considerable progress, although it remains challenging to obtain good reproducibility between batches. Solving this issue will definitely lead to the emergence of powerful chitosan delivery systems with clinical applications.

I.2. HOW TO DEVELOP EFFICIENT AND STABLE SIRNA CHITOSAN-BASED NANOPARTICLES?

In regard to the barriers for siRNA delivery, the two main limitations of chitosan are first its poor buffering capacity that may result in poor endosomal escape and subsequently in an inefficient release of siRNA in the cell cytoplasm. The other issue when using chitosan as siRNA delivery system is its low water solubility at physiological pH, which may be problematic for the NP stability and thus the *in vivo* administration of siRNA.

I.2.1. Mediating endosomal release is required

In our hands, the simple complexation method did not result in the formation of NPs, most likely because the interactions between the chitosan and the siRNAs were too weak. However, the ionic gelation method using TPP as a cross-linking agent allowed the formation of NPs in the 200 nm range that were monodisperse and positively charged because of the excess of chitosan in the formulation. To obtain NPs, the amount of TPP in the formulation was varied while the other components were kept constant. Regardless of the chitosan characteristics (MW, origin), these NPs were not effective in silencing the luciferase on a murine melanoma B16F10 luc cell model. Interestingly, differences in the biological activity of chitosan/siRNA NPs are observed in the literature depending on the cell model or the transfection protocol.

We hypothesized that the lack of effectiveness of the NPs was related to the poor buffering capacity of chitosan, as mentioned by other groups [9-12]. Thus, polymers that displayed high buffering capacities (PEI, PLR or methacrylic acid copolymer Eudragit®) were included in the formulation to

promote endosomal escape [13]. Among them, PEI exhibited the best transfection results without toxicity (70% luciferase silencing) at a chitosan/PEI ratio of 5/1 (w/w) and was chosen for the rest of the work.

I.2.2. The addition of PEG and hyaluronic acid improve stability in plasma

Stability of the delivery system in blood is crucial first for preventing NP dissociation and siRNA release and secondly to avoiding NP aggregation and toxicity. Using fluorescence correlation spectroscopy, we were able to monitor the behavior of the NPs in plasma. The non-PEGylated NPs fell apart rapidly in plasma, resulting in the release of the siRNA. This instability could be due to the deprotonation of some of the chitosan amino groups at physiological pH, rendering the binding of siRNA less efficient. In addition, instability could arise due to competition for chitosan binding between the siRNA and anionic blood components such as proteins or fibrinogen, leading to the disassembly of the chitosan/siRNA NPs [14].

With the inclusion of C_{PEG} in the formulation, the NPs displayed good stability, with 100% siRNA complexation achieved following a 2 h incubation in plasma. The PEG shielding repelled blood proteins, reducing their interactions with chitosan. Furthermore, by comparing NPs containing different amounts of C_{PEG} (*i.e.,* CC_{PEG} PEI NPs and C_{PEG} PEI NPs) using single particle tracking, we determined that the less the NPs were PEGylated, the more prone they were to aggregation. Thus, the amount of PEG in the nanoparticles was a key factor in achieving stability by reducing interparticle aggregation. The structure of the C_{PEG} PEI NP surface was investigated using ^{1}H NMR, and it was confirmed that the NPs displayed a PEG corona. Moreover, they presented a solid chitosan core collapsed around the TPP, siRNA and PEI segments that appeared to be situated both inside and outside of the NPs. This was in agreement with the slightly positive zeta potential of the C_{PEG} PEI NPs (5.8 ± 8.0 mV) due to both the shielding effect of the PEG and the partial contact of water with the chitosan and PEI.

Furthermore, with the inclusion of hyaluronic acid, the size distribution of the NPs did not change in plasma. Hyaluronic acid has been described as an alternative to PEG for NP shielding, and its shielding effect combined with its long polymeric chains may reinforce NP stability [15,16]. Moreover, the hyaluronic acid containing NPs were negatively charged (- 15.6 ± 2.5 mV) and therefore less susceptible to interactions with the anionic blood components. Although their surface charges were negative, these NPs were taken up in a similar manner to the positive NPs and induced an approximately 60% luciferase inhibition.

I.3. HOW TO DELIVER SIRNA TO TUMOR CELLS?

$\alpha_v\beta_3$ integrins are cell adhesion receptors that are overexpressed both on endothelial cells lining tumor blood vessels and on some tumor cell types but not on normal cells. Delivery systems grafted with RGD or non peptide RGD mimics (RGD peptidomimetics, RGDp) have been shown to increase the treatment efficacy due to the tumor targeting properties of the ligands to integrins, as compared to their non-targeted counterparts. Moreover, RGDp-grafted systems have a longer half-life and a higher bioavailability than RGD-grafted systems because of the absence of a peptide bond in their structure [17].

I.3.1. The ligand influences the siRNA delivery modalities

The tumor targeting strategy developed in this study was to graft RGD or RGDp onto C_{PEG} to specifically target $\alpha_v\beta_3$ integrins. The rationale behind using targeted NPs is based on their ability to deliver higher amount of drugs to the targeted cells [18]. Although analytical techniques are available to quantify the majority of the drugs, siRNA delivery is currently assessed mainly by microscopy or flow cytometry, allowing, respectively, the visualization of the fluorescently labeled siRNA in the cells or a quick estimation of the cellular fluorescence intensity. Both techniques are not fully quantitative and detect the fluorophore associated with the siRNA and not the siRNA itself. Thus, an innovative stem loop RT-qPCR method developed for the quantification of the intracellular amount of the full-length antisense strand of DsiRNA, which was 25/27 nt length and exhibited similar efficacy to siRNAs, was used. This technique allowed the comparison of the delivery efficiency of the $\alpha_v\beta_3$ targeted NPs and the non-targeted NPs [19].

Different internalization behaviors were noticed between the non-targeted NPs and the $\alpha_v\beta_3$ targeted NPs. First, the $\alpha_v\beta_3$ targeted NPs were taken up more rapidly than the non-targeted ones due to the high turnover rate of integrins. Secondly, they delivered approximately 2-fold more intracellular siRNA than the non-targeted NPs. However, this occurred for specific concentrations, starting from 100 nM DsiRNA (corresponding to 30 µg of copolymer), and resulted in 90% EGFP silencing in H1299 EGFP cells. Based on these results, it appeared that the local ligand concentration should be high enough to activate $\alpha_v\beta_3$ integrin-mediated endocytosis. Below this threshold, non-specific interactions between the NPs and the cells occurred, resulting in non-specific endocytosis [20]. Regardless of the applied dose, the non-targeted NPs were not effective in silencing EGFP (only 20-30% EGFP silencing), despite relatively elevated levels of DsiRNA detected in the cells; however, the DsiRNA was not released in the cell cytoplasm. Targeted and non-targeted NPs likely travelled to different vesicles in the H1299 cells. Thus, the internalization pathway strongly influenced the final

efficiency of the delivery system. Moreover, the NP trafficking was cell-line dependent. Indeed, in the B16F10 luc model used in *Chapter III*, the non-targeted NPs (C_{PEG} PEI a) induced approximately 70% of luciferase silencing.

Preliminary biodistribution studies revealed an accumulation of the targeted NPs in tumor tissue, suggesting that the targeting strategy is effective *in vivo*.

I.3.2. The RGDp characteristics can impact NP efficiency

The interactions between a targeting ligand and its receptor are complex and may change when the ligand is present on NPs. First, fine balance has to be found between the amount of targeting ligand to induce an effective targeting and the PEG shielding to avoid the detection of the NPs by the immune system. Moreover, the effectiveness of a targeting strategy is not only dependent on the receptor density on the targeted cells but also on the NP properties, which may impact the ligand availability on the NP surface. A study on PLGA-PEG NPs underlined the importance of the solubility profiles of the NP core and the targeting ligand for the uptake efficiency [21]. The authors demonstrated that a hydrophilic ligand, such as RGD (> 50 mg/mL at neutral pH), was more available at the surface of hydrophobic PLGA NPs than a folate ligand, which presents a relatively poor water solubility (0.0016 mg/mL at neutral pH) and tended to interact with the NP core. As a result, the folate targeting efficiency was reduced. With this type of amphiphilic copolymer, the lipophilic and hydrophilic domains are clearly separated, rendering such a study possible. However, with chitosan it is more difficult to predict the ligand partition, as the copolymer exhibits partial water solubility.

Here, we attempted to investigate whether (i) the grafting method (*i.e.*, clip photochemistry versus chain-end grafting), (ii) the nature of the linker between the PEG chains and the RGDp (*i.e.*, hydrophilic *versus* lipophilic) or (iii) the RGDp chemical structure (*i.e.*, naphthyridine *versus* amino pyridine) exerts an influence on the gene silencing efficiency of the targeted NPs.

The first method of RGDp grafting, namely the clip photochemistry method, resulted in the random distribution of RGDp along the PEG chains at approximately 4 to 12 mol%. On the other hand, the chain-end coupling allowed the RGDp to be selectively grafted at the end of the PEG chains with higher grafting ratios ranging from 33 to 50 mol%. For further clinical development the chain-end coupling is most likely more suitable, as the grafting occurred at a specific reaction site and thus was predictable. Regarding the gene silencing efficiency in H1299 EGFP cells however, the clip grafting method was more efficient at 100 nM (55 to 70% EGFP silencing) than chain-end grafting (22 to 40%), although the latter presented a higher percentage of RGDp. At 150 nM, however, the gene silencing

efficiency was similar for all ligands. Interestingly, the particular topology of the clip-grafted RGDp appeared to be efficient at lower doses than the traditional chain-end coupling.

However, using the H1299 EGFP cell model did not allow a precise distinction between the different RGDp, with all of them inducing significant EGFP inhibition. The NPs were then tested on SiHa cells to silence two metabolic targets *i.e.* the glutamine transporter ASCT2 and the monocarboxylate transporter MCT1. The SiHa cells express higher levels of $\alpha_v\beta_3$ integrins than the H1299 EGFP cells and enabled the discrimination between the RGDp.

Two different linkers, namely an oligoethyleneglycol moitie, which is hydrophilic, and an aminocaproic acid unit, which is lipophilic, were investigated. Interestingly, RGDp grafted by the clip photochemistry method and presenting the hydrophilic linker (*i.e.*, RGDp 91 and 92) exhibited the lowest gene silencing efficiency in SiHa cells. The grafting of RGDp with hydrophilic linkers on the PEG chains appeared less efficient, resulting in a lower percentage of RGDp grafting (4 to 7 mol%) compared with the aminocaproic acid unit grafted counterpart (RGDp 85, 12.5 mol%). This difference between the linkers was not observed for chain-end coupling, most likely because the percentages of RGDp grafting obtained using this method were more important. The other ligands (RGD, RGDp 85, 93, 95, 96 and 97) efficiently silenced both ASCT2 and MCT1. Moreover, when the cells were grown in a medium containing lactate or glutamine, the gene silencing exerted an antitumor effect with significant cell death (20 to 65%).

Previous work done in the laboratory on the affinity of single RGDp for $\alpha_v\beta_3$ integrins demonstrated a higher efficiency for RGDp presenting a naphthyridine structure compared with RGDp presenting an amino-pyridine. In this study, we noticed a net superior efficiency of RGDp 85, which presents the naphthyridine structure. The RGDp 85 NPs exhibited similar gene silencing efficiency than the RGD NPs. Finally, the RGDp grafted with the chain-end method demonstrated relatively good activity as well, and their efficiency *in vitro* appeared to be less dependent on the RGDp structure and the linker properties.

In conclusion, the siRNA chitosan-based delivery systems developed in this project mediated high gene silencing efficiency *in vitro* in different cell lines and for different gene targets. Furthermore, the formulation parameters required to obtain good stability of the NPs in plasma were established. The $\alpha_v\beta_3$ targeting strategy was found to be highly efficient, allowing an enhanced and more rapid uptake of the NPs. Moreover, several RGDp exhibited good efficiency and are possible candidates for further *in vivo* studies. However, more work is needed to further investigate the effect of the ligand nature on the efficiency of the NPs and to evaluate the NPs *in vivo*.

II. PERSPECTIVES

Systemic siRNA administration is a complex multi-stage process which has to end up with the delivery of siRNA in the cell cytoplasm to achieve gene silencing. Slight inefficiencies at any step will impact on the final efficiency of the siRNA delivery system. This work provides some solutions and formulation improvements of chitosan-based delivery systems in regards to the multiple *in vivo* barriers for siRNA delivery. However, more studies are needed in order to obtain a precisely engineered delivery system. A key challenge remains the development of targeted NPs that can be reproducibly synthesized and that present optimized and well-characterized surface composition.

Thus, deeper analysis and characterization of the RGDp repartition on the NPs and the effect of this repartition on the targeting efficiency of the delivery system would be helpful to determine the optimal RGDp characteristics. In addition, further *in vivo* biodistribution studies would provide more information about the efficiency of the targeting approach on tumor-bearing mice. Finally, antitumor efficiency *in vivo* has to be performed to evaluate whether the delivery system is efficient or requires more optimization.

II.1. EVALUATION OF THE LIGAND CHARACTERISTICS AND THEIR IMPACT

The investigation of the different types of RGDp-grafted NPs *in vitro* was only based on their gene silencing efficiency. To further evaluate the ligand characteristics and their influence, it would be interesting to use additional analytical techniques. First, to observe whether the properties of the RGDp affect its repartition on the NP surface, NMR analysis could be employed. ^{1}H NMR has been successfully applied to characterize the non-targeted NPs, and ^{19}F NMR analysis could be used to detect the presence of the RGDp on the NP surface because fluor atoms are present in the structure of the RGDp [22]. The stem-loop RT-qPCR method could also be highly advantageous, allowing a comparison of the different RGDp NPs in terms of their intracellular siRNA delivery.

II.2. *IN VIVO* ANTITUMOR EFFICIENCY

The efficiency of the $\alpha_v\beta_3$ targeting approach for delivering siRNAs was demonstrated *in vitro* in two different cell models. Moreover, the silencing of ASCT2 and MCT1 mediated by the targeted NPs, led to a significant anti-proliferative effect *in vitro*. Furthermore, the formulation parameters required to maintain NP stability *in vivo* were defined. Thus, further work will investigate the *in vivo* antitumor efficiency of the NPs after intra-tumoral and systemic injection.

Based on the results obtained in Chapter IV, new batches of polymers are currently being synthesized for future experiments. The ASCT2 and MCT1 siRNAs will be evaluated separately and in combination, to oppose tumor metabolism plasticity. Moreover, the glucose transporter will be considered as a potential target as well. Finally, the use of *in vivo* models of tumor xenografts resulting from cancer cells expressing or not the $\alpha_v\beta_3$ integrins, will offer the opportunity to discriminate between the effects of the targeted NPs delivering their payload only to the $\alpha_v\beta_3$-expressing endothelial cells lining tumor blood vessels or to both endothelial and cancer cells.

II.3. *IN VIVO* BIODISTRIBUTION STUDY

Preliminary biodistribution studies after I.V. injection of RGD NPs and RGDp 85 NPs using a fluorescently labeled siRNA allowed the detection of the nucleic acid in most of the organs, including the tumor (Fig 1A-B). Moreover, fluorescence was observed in the kidneys. This could be explained by the partial destabilization of the nanoparticles upon injection, and the release of a part of the encapsulated siRNA from the nanoparticles.

A

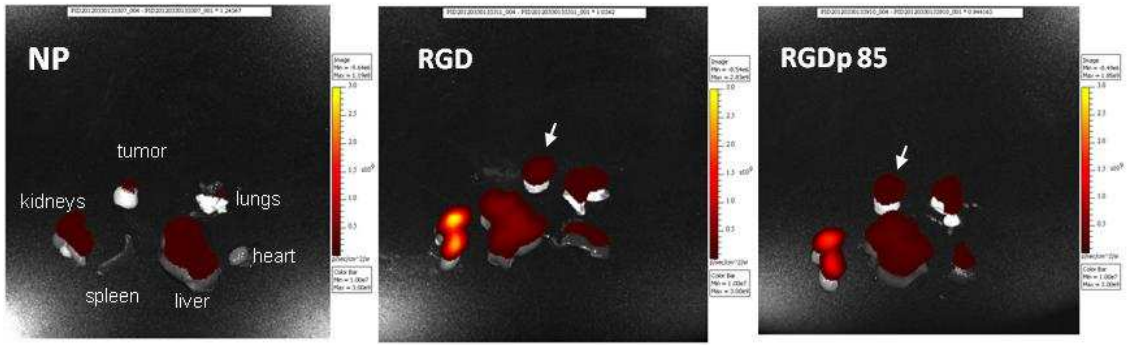

B

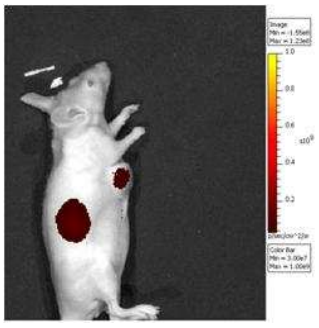

Figure 1 A: Biodistribution of NP, RGD NP and RGDp 85 NP in the different organs of the mice bearing MDA-MB231 human breast cancer 1 h after I.V. injection B: Accumulation of RGDp 85 NP 1 h Steafter I.V. injection in mice bearing MDA-MB231 human breast cancer.

Further biodistribution studies are required to confirm the results obtained in the preliminary studies. Moreover, the *in vivo* targeting efficiency of the most efficient ligands (RGDp 85, RGD and two chain-end grafted RGDp) could be compared by using this method. Furthermore, it would be interesting to evaluate the biodistribution of the copolymer as well. For this purpose, radiolabeling of the siRNA and the copolymer could be considered. Moreover, it would then be possible to quantify the amount of the products distributed in the various organs.

In the study with the targeted NPs, we have decided not to include hyaluronic acid in the formulation, given that hyaluronic acid acts as a shield for the NPs and could then affect the targeting efficiency by hindering and/or masking the ligand. Moreover, the PEGylated NPs without hyaluronic acid did not release siRNA in plasma *(see Chapter III)*. Nevertheless, depending of the results of the *in vivo* biodistribution studies, the optimized addition of hyaluronic acid could represent an interesting solution to avoid the partial destabilization of the NPs, to decrease the possible liver uptake of the NPs and to potentially increase the circulation time of the NPs.

Finally, chemical modifications could be imparted to the siRNA in order to increase its *in vivo* stability by conferring resistance to the nucleases.

II.4. PERSPECTIVES FOR A POTENTIAL TRANSLATIONAL DEVELOPMENT

Overall, the I.V. administration of siRNA requires a multifunctional delivery system to (i) complex siRNA, (ii) provide stability, (iii) target the desired organ and (iv) promote endosomal disruption. The synthesis of a material compiling all of these properties remains highly challenging and multiple components are thus usually included in the same delivery system. From the perspective of a translational development, such delivery system will require a complex level of technical testing and characterization as well as regulatory documentation. Indeed, the biological effect of every single component of the delivery system should be examined, as well as their biodistribution, toxicity etc rendering the development process of such system highly challenging. In addition, the identification of appropriate analytical techniques is essential [23].

In regards to the delivery system developed in this work, besides the lack of reproducibility of the synthesis and/or characterization of the copolymer – which represents a major drawback for an eventual translational development, another important limitation remains the lack of data about the safety of the components of the delivery system after I.V. administration. Sodium TPP, PEG >1 kDa and HA are listed in the inactive ingredients database of the FDA, but for other administration routes than I.V. More precisely, sodium TPP is indexed for oral route, PEG >1 kDa is listed for oral, mucosal,

intramuscular or subcutaneous administration while HA is filed for intramuscular, intra-arterial, topical or intravitreal routes. Chitosan as food additive has been recognized as GRAS but no information about I.V. administration is currently available. In addition, no mention of PEI could be found in the FDA database.

The development of polymeric delivery systems for I.V. administration is still is early stage and less advanced than the lipidic systems, thus relatively few safety data are available. The development of polymeric devices such as CALAA-01 for siRNA delivery will hopefully provide more information in the near future.

III. REFERENCES

[1] F. Petrocca and J. Lieberman, Promise and challenge of RNA interference-based therapy for cancer, J. Clin. Oncol., 29 (2011) 747-754.

[2] R. L. Kanasty, K. A. Whitehead, A. J. Vegas, and D. G. Anderson, Action and reaction: the biological response to siRNA and its delivery vehicles, Mol. Ther., 20 (2012) 513-524.

[3] D. Fischer, Y. Li, B. Ahlemeyer, J. Krieglstein, and T. Kissel, In vitro cytotoxicity testing of polycations: influence of polymer structure on cell viability and hemolysis, Biomaterials, 24 (2003) 1121-1131.

[4] Y. K. Oh and T. G. Park, siRNA delivery systems for cancer treatment, Adv. Drug Deliv. Rev., 61 (2009) 850-862.

[5] B. Ballarin-Gonzalez and K. A. Howard, Polycation-based nanoparticle delivery of RNAi therapeutics: adverse effects and solutions, Adv. Drug Deliv. Rev., 64 (2012) 1717-1729.

[6] C. Troiber and E. Wagner, Nucleic acid carriers based on precise polymer conjugates, Bioconjug. Chem., 22 (2011) 1737-1752.

[7] S. Nguyen, S. Hisiger, M. Jolicoeur, F. M. Winnik, and M. D. Buschmann, Fractionation and characterization of chitosan by analytical SEC and 1H NMR after semi-preparative SEC, Carbohydrate Polymers, 75 (2009) 636-645.

[8] Aranaz, Inmaculada, Mengibar, Marian, Harris, Ruth, Panos, Ines, Miralles, Beatriz, Acosta, Niuris, Galed, Gemma, and Heras, Angeles. Functional Characterization of Chitin and Chitosan. Current Chemical Biology 3[2], 203-230.

[9] T. H. Kim, S. I. Kim, T. Akaike, and C. S. Cho, Synergistic effect of poly(ethylenimine) on the transfection efficiency of galactosylated chitosan/DNA complexes, J. Control Release, 105 (2005) 354-366.

[10] D. Jere, H. L. Jiang, Y. K. Kim, R. Arote, Y. J. Choi, C. H. Yun, M. H. Cho, and C. S. Cho, Chitosan-graft-polyethylenimine for Akt1 siRNA delivery to lung cancer cells, Int. J. Pharm., 378 (2009) 194-200.

[11] A. K. Varkouhi, R. J. Verheul, R. M. Schiffelers, T. Lammers, G. Storm, and W. E. Hennink, Gene silencing activity of siRNA polyplexes based on thiolated N,N,N-trimethylated chitosan, Bioconjug. Chem., 21 (2010) 2339-2346.

[12] Y. K. Kim, A. Minai-Tehrani, J. H. Lee, C. S. Cho, M. H. Cho, and H. L. Jiang, Therapeutic efficiency of folated poly(ethylene glycol)-chitosan-graft-polyethylenimine-Pdcd4 complexes in H-ras12V mice with liver cancer, Int. J. Nanomedicine., 8 (2013) 1489-1498.

[13] V. Dehousse, N. Garbacki, A. Colige, and B. Evrard, Development of pH-responsive nanocarriers using trimethylchitosans and methacrylic acid copolymer for siRNA delivery, Biomaterials, 31 (2010) 1839-1849.

[14] K. Buyens, S. C. De Smedt, K. Braeckmans, J. Demeester, L. Peeters, L. A. van Grunsven, d. J. de Mollerat, X, R. Sawant, V. Torchilin, K. Farkasova, M. Ogris, and N. N. Sanders, Liposome based systems for systemic siRNA delivery: stability in blood sets the requirements for optimal carrier design, J Control Release, 158 (2012) 362-370.

[15] D'Sa Raechelle A and R. J. P. B. K. a. M. B. J. Dickinson Peter J, Inhibition of lens epithelial cell growth via immobilisation of hyaluronic acid on atmospheric pressure plasma modified polystyrene, Soft Matter, 7 (2010) 608-617.

[16] M. Ravina, E. Cubillo, D. Olmeda, R. Novoa-Carballal, E. Fernandez-Megia, R. Riguera, A. Sanchez, A. Cano, and M. J. Alonso, Hyaluronic acid/chitosan-g-poly(ethylene glycol) nanoparticles for gene therapy: an application for pDNA and siRNA delivery, Pharm. Res., 27 (2010) 2544-2555.

[17] F. Danhier, B. A. Le, and V. Preat, RGD-based strategies to target alpha(v) beta(3) integrin in cancer therapy and diagnosis, Mol. Pharm., 9 (2012) 2961-2973.

[18] F. Danhier, B. Vroman, N. Lecouturier, N. Crokart, V. Pourcelle, H. Freichels, C. Jerome, J. Marchand-Brynaert, O. Feron, and V. Preat, Targeting of tumor endothelium by RGD-grafted PLGA-nanoparticles loaded with paclitaxel, J Control Release, 140 (2009) 166-173.

[19] S. Colombo, H. M. Nielsen, and C. Foged, Evaluation of carrier-mediated siRNA delivery: lessons for the design of a stem-loop qPCR-based approach for quantification of intracellular full-length siRNA, J. Control Release, 166 (2013) 220-226.

[20] F. M. Mickler, Y. Vachutinsky, M. Oba, K. Miyata, N. Nishiyama, K. Kataoka, C. Brauchle, and N. Ruthardt, Effect of integrin targeting and PEG shielding on polyplex micelle internalization studied by live-cell imaging, J. Control Release, 156 (2011) 364-373.

[21] P. M. Valencia, M. H. Hanewich-Hollatz, W. Gao, F. Karim, R. Langer, R. Karnik, and O. C. Farokhzad, Effects of ligands with different water solubilities on self-assembly and properties of targeted nanoparticles, Biomaterials, 32 (2011) 6226-6233.

[22] H. Freichels, V. Pourcelle, C. S. Le Duff, J. Marchand-Brynaert, and C. Jerome, "Clip" and "click" chemistries combination: toward easy PEGylation of degradable aliphatic polyesters, Macromol. Rapid Commun., 32 (2011) 616-621.

[23] N. Desai, Challenges in development of nanoparticle-based therapeutics, AAPS. J, 14 (2012) 282-295.